Understanding LHC searches for new physics with simplified models

Ursula Laa

Communauté
UNIVERSITÉ Grenoble Alpes

THÈSE

Pour obtenir le grade de

DOCTEUR DE LA COMMUNAUTÉ UNIVERSITÉ GRENOBLE ALPES

Spécialité : **Physique Subatomique et Astroparticules**

Arrêté ministériel : 25 mai 2016

Présentée par

Ursula LAA

Thèse dirigée par **Sabine KRAML et Genevieve BELANGER**

préparée au sein du
Laboratoire de Physique Subatomique et Cosmologie
et de **l'École Doctorale de Physique de Grenoble**

Interpreter les recherches de nouvelle physique au LHC à l'aide de modèles simplifiés

Understanding LHC Searches for New Physics with Simplified Models

Thèse soutenue publiquement le **15 Septembre 2017**,
devant le jury composé de :

Benjamin FUKS
Professeur, Université Pierre et Marie Curie, Président
Michael KRÄMER
Professeur, Université RWTH Aachen - Allemagne, Rapporteur
Veronica SANZ
Maître de conférences, Université de Sussex - Grande Bretagne, Rapporteur
Ulrich ELLWANGER
Professeur, Université Paris-Sud, Examinateur
Marie-Hélène GENEST
Chargé de recherche, CNRS Delegation Alpes, Examinatrice

Acknowledgements
First and foremost I thank my supervisors, Sabine and Geneviève, for providing me the opportunity to come to Grenoble for my thesis, as well as countless more opportunities throughout these last three years. Your expertise and motivation have been inspiring, and discussions with you have always been fruitful and clarifying. Sabine, I am sincerely grateful for your support in all aspects of my PhD studies, the freedom you gave me in my research, while at the same time applying the right amount of pressure to push me to do my best work. Geneviève, it was always a pleasure to work with you, and I greatly appreciate your clear and direct approach, and your valuable comments.
This thesis is the result of many fruitful collaborations, and I am grateful to all my collaborators on the various projects presented here. I am particularly greatful to all members of the SModelS collaboration, for the constructive teamwork as well as their friendship. I wish to thank Wolfgang who first introduced me to the subject and collaboration, Andre and Suchita from whom I have learned so much over the years, and the many students that I have worked with closely, in particular also Jory and Federico. I can honestly say that it has been pleasant to work with all of you, and that I hope to continue doing so.
I thank the members of the LPSC theory group and its many visitors for the shared lunches, dinners, hikes and cakes that have been an important part of my stay in Grenoble. In particular I want to thank Christopher, Ingo, Olek, Kentarou, Dipan, Josselin, Jérémy, Kseniia, Selim and Mohammad as well as Kimiko and Juhi. I also thank the members of LAPTh who have always been welcoming during my visits to Annecy. I am grateful to the administrative staff of LPSC and LAPTh for the smooth handling of all my missions as well as any problems that came up, in particular Sonia Benaissa, Christine Servoz-Gavin, Colette Deslorieux and Véronique Jonnery, and to those who have supported me during the completion of the label RES, Olivier Méplan, Guillaume Pignol, Laurent Derome, Mourad Ramdhane and Johann Collot.
Special thanks go to my jury. Veronica Sanz and Michael Krämer, thank you for promptly accepting to review this thesis and to come to Grenoble for my defence, and Benjamin Fuks, Ulrich Ellwanger and Marie-Hélène Genest for being part of my jury.
Last but not least I want to thank my family, who made me believe that I can achieve anything I wanted to, and supported me in all my decisions that led me here. And to Jérémy who was here for me through all of it, who has helped me so much, and without whom this experience would not have been the same.

CONTENTS

CHAPTER

ONE

INTRODUCTION

Our Standard Model (SM) of particle physics, describing the physics of fundamental particles and interactions, is built on a long history of fruitful interplay between experimental and theoretical physics. Starting out from the simple idea that there exist elementary particles that compose all matter, and aiming to describe nature by one consistent theoretical model, the SM was gradually built up. New experimental results often challenged our understanding, leading us to develop new models that describe all observations. It is clear that any such new model should make predictions that allow us to test it experimentally. Therefore, as experimental results guide the development of more complete theories, theoretical predictions also guide the development and interpretation of new experiments. It is this interplay that deepens our understanding of nature. While there exists a multitude of examples in particle physics alone, a notable one is the development of the theory of electroweak interactions. In this intoductory Chapter we will introduce the SM and its construction in this context. Discussing how it was tested and thus established as the standard description of particle physics will then highlight the success of the interplay between theory and experiment. Many of the concepts that were vital in the development of the SM description also motivate us to consider possible extensions. We will first list a few shortcomings of the SM relevant to the following discussion, and then give an overview of some extended models, discussing how they can overcome these shortcomings. We will focus in particular on supersymmetric models, that will be studied in detail in this thesis.

The aim of this thesis is then to examine how we can retain the close connection between theoretical and experimental particle physics. In fact it is becoming more obscured as experimental techniques become more sophisticated, while theorists consider highly complex models with a potentially large number of free parameters (to address shortcomings of the SM without violating experimental observations that are in agreement with SM predictions to a high level in accuracy). Given these developments it is important to develop also sophisticated methods and tools that can facilitate relating the model parameters and the results from experimental tests and searches. In particular, this work will be dedicated to discussing how we can test extended models of particle physics in high energy collisions at the Large Hadron Collider (LHC) in the context of so-called simplified model interpretations (or simplified model spectra, SMS). The concept of SMS has been developed with the aim of maximal model independence, while capturing the main features relevant to the detection at collider experiments. As a consequence they can guide the development of search strategies without introducing large “theory prejudice”. On the other hand, limits obtained in this con-

text can be interpreted in a number of generic models in a straightforward way, thus allowing to understand the impact of experimental observations in an efficient manner.
The remainder of this thesis is structured as follows. We will first discuss the strategy and interpretation of LHC searches in Chapter 2, where the concept of simplified model interpretations will be introduced in some detail. Moreover, different approaches to the reinterpretation of LHC searches and the neccessary tools will be listed. Chapter 3 will then focus on SModelS, a reinterpretation tool based on the SMS concept. In Chapter 4 we discuss the assumptions that allow us to translate simplified model interpretations to generic models, and show that they are valid for some specific cases of particular interest. We then proceed to discuss how we can use SModelS to constrain generic models in Chapter 5. While the major part of this work will focus on SMS that are inspired by supersymmetric models we will give an example of a more minimal simplified model description for dark matter searches in Chapter 6. Finally some concluding remarks will be presented in Chapter 7.

1.1. A Standard Model of Particle Physics

We will start our discussion by reviewing how the theory of weak interaction was developed, eventually leading to a unified description of electroweak interactions. We then formulate the SM of particle physics in Section 1.1.2, again focussing mainly on the electroweak interactions. This in turn will allow us to discuss experimental tests and measurements, establishing the SM description, in Section 1.1.3.

1.1.1. From Beta Decay to Electroweak Unification

Let us first recall some major steps in the development of the theory of weak interactions and its unification with the theory of electromagnetic interactions.[1] We can trace the development of the theory of weak interactions back to 1914 when James Chadwick measured the energy spectrum of electrons in beta decays [2]. Rather than a well defined value he observed a continuous spectrum, inconsistent with the assumption that only an electron is emitted in the decay. To explain energy conservation in the beta decay, Wolfgang Pauli postulated an additional neutral particle in 1930, today known as the neutrino. The idea was picked up by Enrico Fermi, who in 1933 proposed a theoretical framework for the description of the beta decay ("Fermi's interaction") [3]. The theory describes a four-fermion contact interaction and can be considered an effective theory of the electroweak interaction. It is described by an effective coupling that today can be defined as

$$G_F = \frac{\sqrt{2}}{8}\frac{g^2}{m_W^2} \tag{1.1}$$

where g is the coupling constant of the weak interaction and m_W the mass of the W boson. While Fermi initially proposed a scalar interaction, the most general form of the four-fermion interaction Lagrangian is

$$\mathcal{L} = \sum_{i=1}^{5} g_i \{\bar{\psi}_1 \mathcal{O}^i \psi_2\}\{\bar{\psi}_3 \mathcal{O}_i \psi_4\} \tag{1.2}$$

where the operator $\mathcal{O}_i = (1, \gamma_\mu, \sigma_{\mu\nu}, i\gamma_5\gamma_\mu, \gamma_5)$ (referred to as scalar (S), vector (V), tensor (T), axial vector (A) and pseudoscalar (P) respectively), and ψ_i are the fermion fields.

[1] A more detailed account can be found e.g. in [1].

Careful analysis of experimental data (in particular from studying angular distributions) led to the conclusion that the weak interaction is best described by a V−A theory [4, 5]. This theory could accurately describe interactions at low energies, but it failed at high energies, notably above $O(100\ \text{GeV})$, thus hinting at an important new scale in particle physics (the "weak scale"). This shortcoming signalled a cut-off scale for the Fermi interaction and the requirement of new exchange particles mediating the interaction, to accurately describe weak interactions at higher energies. In parallel, the theory of quantum electrodynamics (QED) based on the principle of invariance under a local $U(1)_{em}$ gauge transformation was well established in the 1950s. It was in excellent agreement with experimental data, thus considered as a blueprint for building a consistent theory to describe weak interaction in terms of massive mediators. Moreover, this also stimulated speculations of a unified theory describing both electromagnetic and weak interactions. In 1961 efforts to construct a unified gauge theory of electroweak interactions were advanced by Sheldon Lee Glashow [6], who recognised that a total of 4 vector bosons are required to describe both the parity conserving electromagnetic interaction as well as the parity violating weak interactions. This is possible in a $SU(2)\times U(1)$ gauge theory because a mixing between the two neutral bosons can generate one parity conserving boson (the photon).[2] An additional neutral boson (Z boson) as well as the charged bosons ($W^{\pm}$) then violate parity. However, in that theory all gauge bosons are necessarily massless, adding an explicit mass terms for the $W^{\pm}$ and the Z boson would yield the theory unrenomalizable. A way out seemed to be spontaneous symmetry breaking, that would allow the generation of mass terms. However, according to the Goldstone theorem it would always imply additional massless bosons ("Goldstone bosons") [7]. This was unacceptable as they had not been observed experimentally. Upon further inspection of the problem it turned out that the Goldstone theorem does not hold for gauge theories, where the massless Goldstone boson is not physical, but instead can be combined with the massless gauge boson to give a massive gauge boson, as described by the Higgs mechanism [8–11]. In the following a unified electroweak gauge theory incorporating the notion of spontaneous symmetry breaking was formulated [12] and proven to be renormalizable [13].

In parallel, a gauge theory of strong interactions (quantum chromodynamics, QCD) was developed, based on an $SU(3)$ gauge group [14,15], where strong interaction between quarks (carrying so-called color charge) is described via the exchange of color octet vector bosons, the gluons [16]. In contrast to the electroweak gauge theory the $SU(3)$ symmetry is unbroken, and the gluons are massless. Moreover, only color singlets appear in nature, a consequence of confinement. However at high energies interactions are weaker, and this so-called asymptotic freedom allows the use of perturbation theory to describe interactions between quarks and gluons. Factorisation then allows to calculate the perturbative contributions at high energies, and combine them with non-perturbative low energy contributions in a defined way [17].

1.1.2. Description of the Standard Model

We consider the $SU(3)_C \times SU(2)_L \times U(1)_Y$ gauge group, and associate the coupling strengths (g_s, g, g') to the respective corresponding gauge couplings. $SU(3)_C$ describes the strong interaction, the subscript C indicates that we describe the interactions in terms of color charges. The quarks are color-triplets, while the leptons are singlets and thus do not feel the strong interaction. The mediators are massless vector bosons, so-called gluons. The $SU(2)_L \times U(1)_Y$ gauge group describes the electroweak interactions. The subscript L

[2] Where $U(1)$ is a newly introduced gauge group different from $U(1)_{em}$.

Name	Symbol	$SU(3)_C, SU(2)_L, U(1)_Y$
Quarks	$Q = (u_L\ d_L)^T$	$(\mathbf{3}, \mathbf{2}, \frac{1}{6})$
	u_R	$(\mathbf{3}, \mathbf{1}, \frac{2}{3})$
	d_R	$(\mathbf{3}, \mathbf{1}, -\frac{1}{3})$
Leptons	$L = (\nu_L\ e_L)$	$(\mathbf{1}, \mathbf{2}, -\frac{1}{2})$
	e_R	$(\mathbf{1}, \mathbf{1}, -1)$
Gluon	G	$(\mathbf{8}, \mathbf{1}, 0)$
W boson	$(W^1\ W^2\ W^3)^T$	$(\mathbf{1}, \mathbf{3}, 0)$
B boson	B	$(\mathbf{1}, \mathbf{1}, 0)$
Higgs	$H = (\phi^+ \phi^0)^T$	$(\mathbf{1}, \mathbf{2}, \frac{1}{2})$

Table 1.1.: Field content of the Standard Model and their gauge quantum numbers. There are 3 copies (families) of quarks and leptons, differing by their mass.

implies that only left-chiral fermions are involved in $SU(2)_L$ gauge interactions. Left-chiral fermions are described via the projection

$$P_L = \frac{1 - \gamma_5}{2}, \tag{1.3}$$

thus the left-chiral nature of this interaction is equivalent to the V−A description discussed above. Left-chiral quarks and leptons are doublets under $SU(2)_L$, while the right-chiral counterparts are singlets.[3] The hypercharge Y of each multiplet can be calculated from the relation $Q = T_3 + Y$, where Q is the electric charge in units of the positron charge, and T_3 the third component of the weak isospin. We also add a complex scalar field H (the Higgs field) to the description. H is an $SU(2)_L$ doublet and color singlet and will give rise to the spontaneous breaking of the electroweak symmetry. The field content of the SM is summarized in Table 1.1.

We can now write the gauge invariant, renormalizable Lagrangian of the SM as

$$\mathcal{L} = -\frac{1}{4} F^a_{\mu\nu} F^{a\ \mu\nu} + i\bar{\chi} \not{D} \chi + |D_\mu H|^2 + \mathcal{L}_{Yukawa} - V(H). \tag{1.4}$$

The first term describes the propagation and self-interaction of gauge bosons, written in terms of the field-strength tensors $F^a_{\mu\nu}$. The second term is a kinetic term for all fermions (quarks and leptons as listed in Table 1.1). We denote χ the Dirac spinors for each fermion species and generation, and the sum over all species and generations is implicit. Similarly we write a kinetic term for the Higgs fields H. Gauge invariance is ensured via the covariant derivative

$$D_\mu = \partial_\mu - i\frac{g'}{2} Y B_\mu - i\frac{g}{2} \sigma_j W^j_\mu - i\frac{g_s}{2} \lambda_\alpha G^\alpha_\mu, \tag{1.5}$$

where $\sigma_j, j = 1, 2, 3$ the Pauli matrices and $\lambda_\alpha, \alpha = 1...8$ the Gell-Mann matrices. These gauge invariant kinetic terms therefore give rise to the gauge interactions of the fermion and

[3] A commonly used short hand notation identifies left-chiral fileds as left-handed (LH) fields, and right-chiral fields as right-handed (RH) fields. While chirality and helicity are not stricly speaking equivalent for massive particles, this notation is often used for simplicity.

Higgs fields. In addition to the kinetic terms we introduce the Yukawa interactions, coupling the fermion and Higgs fields. They are defined as

$$\mathcal{L}_{Yukawa} = -\mathbf{y_e}\bar{L}\cdot He_R - \mathbf{y_d}\bar{Q}\cdot Hd_R - \mathbf{y_u}\epsilon^{ab}\bar{Q}_a H_b^\dagger u_R + h.c. \tag{1.6}$$

where ϵ^{ab} is the completely antisymmetric $SU(2)$ tensor ($\epsilon = i\sigma_2$). Here we have suppressed the flavor indices of the fermions, generically the Yukawa couplings $\mathbf{y_e}, \mathbf{y_d}, \mathbf{y_u}$ are 3×3 matrices in flavor space. The last term is the Higgs potential

$$V(H) = \mu^2 H^\dagger H + \lambda (H^\dagger H)^2. \tag{1.7}$$

μ is the only dimensionful parameter in the SM, and potentially a mass term (if $\mu^2 > 0$). However, to realize the Higgs mechanism we require $\mu^2 < 0$ and $\lambda > 0$, thus there is no explicit mass term in the SM. In this configuration the minimum of $V(H)$ is not at the origin, instead we find a continuum of minima at $H^\dagger H = \frac{\mu^2}{2\lambda} \equiv \frac{v}{2}$, where we define v as the vacuum expectation value (vev) of the Higgs field. As a consequence the vacuum state of the Higgs field is no longer invariant under $SU(2)_L \times U(1)_Y$ and thus breaks the electroweak symmetry. To describe the system as fluctuations around the minimum we shift the Higgs field to

$$H(x) = \frac{1}{\sqrt{2}}\begin{pmatrix} \theta_2 + i\theta_1 \\ v + h(x) - i\theta_3 \end{pmatrix}. \tag{1.8}$$

Now all fields θ_i and h have a zero vev. By gauge transformation into unitary gauge we find that only h is physical, while the θ_i can be transformed away. Considering now the gauge invariant kinetic term for the Higgs field we find that we have generated mass terms for three of the electroweak gauge bosons, the charged $W^\pm$ and a linear combination of the neutral W^3 and B that we call Z, with

$$M_W^2 = \frac{g^2 v^2}{4}, \quad M_Z^2 = \frac{(g^2 + g'^2)v^2}{4} = \frac{M_W^2}{\cos^2\theta_W}, \tag{1.9}$$

where θ_W is the Weinberg angle parametrizing the mixing.Similarly we obtain fermion mass terms from $\mathcal{L}_{Yukawa}$ after the electroweak symmetry is broken. Diagonalizing the y_{ij} matrix we find

$$m_{f,i} = \frac{y_i v}{\sqrt{2}}, \tag{1.10}$$

where $f = u, d, e$ labels the fermion species, and $i = 1, 2, 3$ the generation. The up and down type quark mass matrices are diagonalized by two distinct sets of unitary matrices $V^i_{L,R}, i = u, d$. The mismatch between these matrices gives rise to a flavor changing nature of the charged-current interactions, described by the Cabbibo-Kobayashi-Maskawa (CKM) matrix $V_{CKM} = V_L^u V_L^{d\dagger}$. On the other hand, flavor changing neutral currents are highly suppressed in the SM. Finally we note that the SM does not include a right-chiral neutrino, thus it cannot describe neutrino masses.

1.1.3. Establishing the Standard Model Description of Particle Physics

Given the SM description of particle physics the next step was to test the predictions of the theory, and eventually measure its free parameters. One important prediction was the existence of neutral weak currents, mediated by the Z boson. Indeed in 1973 a first observation

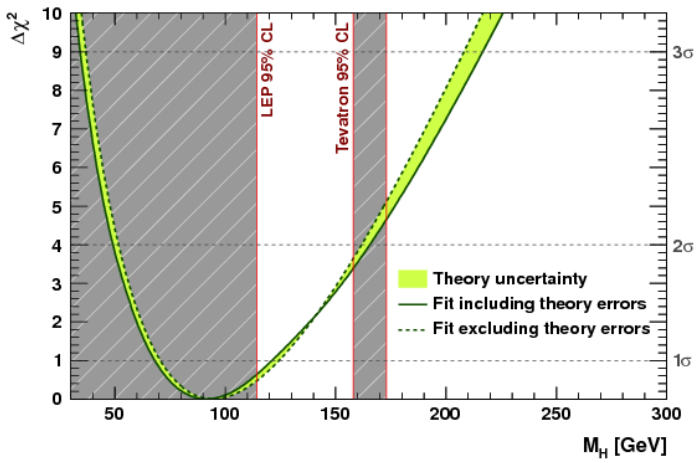

Figure 1.1.: Indirect determination of the Higgs boson mass from gFitter [26].

of neutral current induced processes, neutrino-hadron scattering without charged leptons, was reported [18], and in 1983 the W and Z particles were observed [19, 20]. Moreover, the thrid generation of fermiones, postulated in 1973 to explain observed CP violations [21][4] was confirmed with the observation of the tau lepton [22] and the bottom quark [23], and completed in 1995 with the discovery of the top quark [24, 25]. In the thus established electroweak theory the Higgs mass was the last free parameter that remained to be measured.

Nevertheless, even before its discovery one could place bounds on the allowed mass range by considering loop contributions to electroweak precision observables (as well as from theoretical considerations). For example the gFitter group evaluated the allowed mass range [26] from fitting a number of electroweak precision observables, which depend in particular on the top quark and Higgs boson mass, see Figure 1.1. On the other hand, the mass being the only undetermined parameter, one could predict the production cross section as well as the decay branching ratios as a function of the mass, thus allowing experimentalists to pinpoint the search strategies [27]. Indeed a Higgs boson was finally observed by the LHC experiments in 2012 [28,29], with a mass of 125 GeV, i.e. in the expected range, and with properties consistent with predictions. This discovery thus allowed to complete the description of the electroweak interactions.

However, while the standard description of the electroweak theory is now self-consistent and valid up to large energy scales, we might also conclude that we do not yet have the complete picture. For one we have seen that loop contributions are vital to the theoretical description, and as such we should also consider loop corrections to the Higgs mass. Such considerations would lead us to expect that the Higgs should be much heavier than what we observed. The successful unification of the electromagnetic and weak interaction further encourages us to consider that all interactions can be unified at a higher scale. However, such a grand unified theory would require new physics, not described by the SM. Moreover, as we have already noted, neutrino masses are not described in the SM, since they might be generated in a fundamentally different way than the other fermion mass terms. These open questions will be discussed in somewhat more detailes in the next Section.

[4] CP symmetry is an invariance under the combination of charge (C) and parity (P) transformations.

1.2. Going Beyond

1.2.1. Hierarchies, Masses and Unification

In contrast to e.g. the Fermi interaction, the SM is a consistent model, and potentially valid up to high energies. Indeed there is no imperative argument that points to a new mass scale below the Planck mass $M_P \approx 10^{19}$ GeV (where perturbativity of a quantum theory of gravity breaks down). However, it raises the question of why there is such a large hierarchy between the weak force and gravity.

It is instructive to study the SM as a low-energy effective theory of a unified description, which is also motivated in the context of unified theories. Similar to the electroweak theory predicting the mass of the $W^{\pm}$ and Z boson in terms of the fundamental couplings and the Higgs vev, we expect that the free parameters of the SM should be predicted by such a unified theory. As we will see, requiring that the Higgs mass is predicted in a natural way (i.e. without the need for fine-tuned cancellations) indeed points to a scale much below M_P at which new physics should appear. Moreover, generating the large hierarchies observed between various fermion masses can also guide us when constructing theories beyond the SM (BSM). Finally, we will see that unification of all gauge couplings cannot be achieved in the SM, thus pointing for example to supersymmetric extensions.

Hierarchy Problem and the Higgs Mass We assume that the SM is valid up to a high cut-off scale $\Lambda_{SM} \approx M_P$. The free parameters, in particular also the Higgs mass, should be determined by the physics at Λ_{SM}, and we consider that the SM is an effective description at lower scales. The Higgs mass is of special interest, since the relevant operator in the Lagrangian is in fact the only SM operator of mass dimension $d = 2$. Following the discussion in [30], in the context of an effective field theory description we are led to assume that it should in fact be enhanced by the squared cut-off scale

$$c\Lambda_{SM}^2 H^\dagger H. \tag{1.11}$$

We can further understand this by considering loop corrections to the Higgs propagator, and integrating the contributions up to Λ_{SM}. We split the corrections as

$$m_H^2 = \delta_{SM} m_H^2 + \delta_{BSM} m_H^2 \tag{1.12}$$

and from estimating top quark, electroweak gauge boson and Higgs loop contributions we get

$$\delta_{SM} m_H^2 = \frac{3y_t^2}{8\pi^2}\Lambda_{SM}^2 - \frac{3g_W^2}{8\pi^2}(\frac{1}{4} + \frac{1}{8\cos^2\theta_W})\Lambda_{SM}^2 - \frac{3\lambda}{8\pi^2}\Lambda_{SM}^2. \tag{1.13}$$

We see that $\delta_{SM} m_H^2$ will be large if the cut-off scale Λ_{SM} is large. In that case the observed light Higgs mass implies that the two contributions $\delta_{SM} m_H^2$ and $\delta_{BSM} m_H^2$ cancel to very high accuracy, despite emerging from separate energy scales. Such a cancellation implies a fine-tuning between unrelated terms, that we can quantify e.g. via the fine-tuning parameter Δ as

$$\Delta \leq \frac{\delta_{SM} m_H^2}{m_H^2} \approx \frac{3y_t^2}{8\pi^2}(\frac{\Lambda_{SM}}{m_H})^2. \tag{1.14}$$

We note that we have formulated the naturalness problem in terms of cut-off regularisation, such that the scale dependence is manifest. However, it remains problematic in any regularisation scheme, as the accurate cancellation of high-energy parameters is always required.

Fermion Masses In the SM the fermion masses (i.e. their Yukawa couplings) are free parameters, to be measured by experiments. However, there are large hierarchies between the different masses. Considering in particular the extreme ends of the spectrum, it is interesting to ask why neutrinos are so light, and why top quarks are so heavy. Let us first discuss neutrino masses.

Neutrinos are fundamentally different from all other SM fermions, because a right-chiral neutrino does not have any gauge interaction. Moreover, while the electroweak interactions are lepton number (L) conserving, L is violated by neutrino oscillation. In the SM we generally consider only left-chiral neutrinos, while the sterile neutrinos are absent (by choice), and therefore neutrinos are massless in the SM description. We could generate neutrino-masses by adding the non-renormalizable dimension five operator (known as the Weinberg operator)

$$\frac{\lambda_{ij}}{M}(L_i H)^T (L_j H), \quad i,j = e,\mu,\tau \tag{1.15}$$

with H the Higgs doublet, λ_{ij} dimensionless couplings and M the cut-off scale. We see that this will give mass terms after electroweak symmetry breaking, and will break lepton number by $\Delta L = 2$. Considering couplings $O(1)$ one finds that with a cut-off scale $M \sim 10^{14}$ GeV, the Weinberg operator can account for the observed mass and lepton number violation [31]. However, this is not very satisfactory, and we would like to understand the origin of this operator. The simplest realization consists in adding right-chiral neutrinos to the SM. We can then generate a mass term in the same way as for all other fermions, via a Yukawa coupling. In addition, as the right-chiral neutrino is a SM singlet, we can also write down a Majorana mass term

$$M_R \nu_R^T \nu_R^C + h.c. \tag{1.16}$$

Similar to our discussion of the Higgs mass, we are led to assume that M_R is naturally very large, and in particular much larger than the Dirac mass m_D from the Yukawa coupling. Diagonalizing the mass matrix we find that a large hierarchy is generated, the heavy state will have a mass close to M_R, while the mass of the light state will be suppressed as $\frac{m_D}{M_R}$. The Yukawa interaction can then generate the Weinberg operator when integrating out the heavy ν_R. This minimal scenario is called the Seesaw I mechanism. For a more detailed discussion and non-minimal scenarios, see [32].

On the other end of the spectrum, the top quark is the heaviest particle in the SM, with a mass at the electroweak scale. On the one hand his means that it drives considerations about fine-tuning in the SM, see Eq. (1.14). On the other hand we might consider that the large Yukawa coupling arises from a deeper connection with the mechanism of electroweak symmetry breaking, we will discuss this possibility in Section 1.4.1.

Unification Inspired by the unified description of electroweak interactions, a unified description of all SM interactions was proposed in 1974 [33]. A first observation was that the electromagnetic and weak interaction were not truly unified, as the theory based on the $SU(2)_L \times U(1)$ gauge group still contains two independent coupling constants. Moreover, the assignment of electric charge (controlled by the hypercharge in the SM description, and thus not necessarily quantised) appears to be arbitrary, and the exact cancellation between electron and proton charge is not explained in the SM. The quantisation of electric charge and the necessary cancellation can be achieved when considering a so-called "Grand Unified Theory" (GUT), that is described by a single (non-abelian) gauge group. The simplest realisations containing the SM gauge group are the initially proposed $SU(5)$ or an $SO(10)$

gauge group.

A necessary condition for realising a GUT description is that it requires all gauge couplings to unify at some energy scale (thus defining the GUT scale). Such unification of all three SM gauge couplings is not achieved at any scale in the SM description. However, considering supersymmetric extensions (introduced in Section 1.3) we find that the couplings might indeed unify at an energy scale around 10^{16} GeV, i.e. a scale similar to the one we had found for the description of neutrino masses. This is sketched in Figure 1.2, where we compare the values of $\alpha_i = g_i^2/4\pi$ for the three SM gauge couplings. Note that as indicated above, due to its abelian nature the $U(1)$ gauge coupling is not fixed in the SM. On the other hand it is fixed in an $SU(5)$ GUT description as $g' = \sqrt{\frac{3}{5}} g_1$, and we use $g_2 = g$ and $g_3 = g_s$. The energy dependence of the gauge couplings is described by the Renormalization Group Equations (RGEs), and we compare in Figure 1.2 the evolution in the SM and in its minimal supersymmetric extension (MSSM).

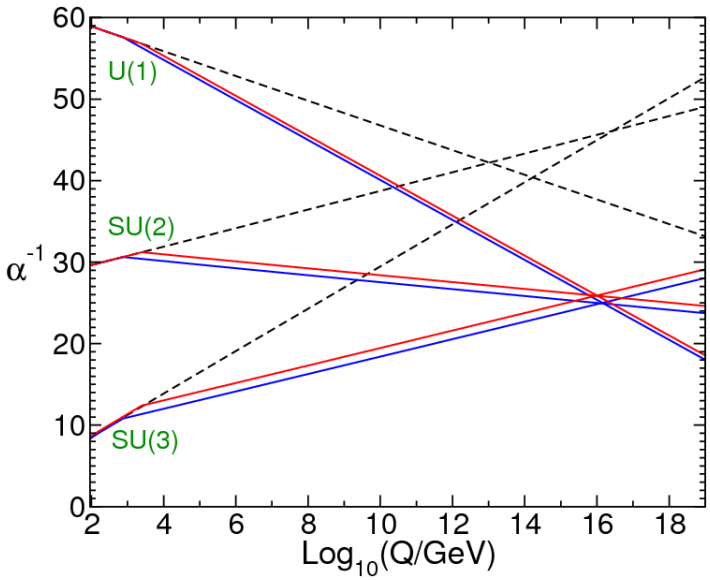

Figure 1.2.: Two-loop renormalization group evolution of the SM gauge couplings, from [34]. The dashed lines show the evolution as given in the SM, the solid lines correspond to MSSM scenarios with a common sparticle mass threshold of 500 GeV (blue) or 1.5 TeV (red).

1.2.2. Dark Matter

Since Fritz Zwicky first suggested the existence of Dark Matter (DM) to explain the velocity of galaxies in clusters in 1933 [35] numerous observations have corroborated its necessity. We will quickly review the evidence for DM and then discuss the particularly appealing scenario of thermal DM and give a brief overview of direct and indirect detection experiments. LHC signatures will be discussed in the dedicated Chapter 2, and the interpreation of LHC searches in Chapter 6.

Evidence for Dark Matter

The problem of DM became manifest in the 1970s through detailed studies of galactic rotation curves. For example it was shown that the velocity of stars in the galaxy is nearly

constant far from the center [36], despite the expectation that it should fall off as $\frac{1}{\sqrt{r}}$ with growing distance r from the galactic center. This observation implied the existence of a large DM halo. Other observations such as measurements of gravitational lensing, or comparing the mass to light ratio in clusters as derived by different methods further emphasized the need for DM. A review of the observational evidence for DM was given in [37]. This type of observational evidence tells us very little about the nature of DM, and we might imagine that it could be explained by SM physics of very cold and neutral particles. There is however a different class of observations that give somewhat more insight. In particular measurements of the power spectrum of the Cosmic Microwave Background (CMB) is a powerful tool in determining the DM density in the universe. This is because both the baryonic and the total matter density enter the power spectrum, and we can thus determine the amount of non-baryonic matter in the early universe. A precise measurement (from fitting the standard cosmological model ΛCDM[5] to various measurements) was recently presented by the Planck collaboration [38], finding a dark matter relic density of

$$\Omega h^2 = 0.1188 \pm 0.0010 \tag{1.17}$$

where h is the Hubble constant in units $100\mathrm{km}/(\mathrm{s}\cdot\mathrm{Mpc})$, and Ω is the DM density in units of the critical density of the universe, $\Omega = \rho_{DM}/\rho_c$.

While we do know the abundance of DM in the universe we note here that all existing evidence for DM is gravitational, and most properties of DM are unknown. We know that it should be stable (or at least very long-lived), not charged, not strongly self-interacting and cold (i.e. non relativistic at ∼keV temperatures, so as not to affect structure formation). On the other hand a wide mass range, from 10^{-22} eV up to the Planck mass, could be imagined, and we can imagine a large number of different models that could describe DM. One particularly compelling scenario is however that of thermal DM that will be described in the next Section.

Note that while we have restricted our discussion to particle DM, as suggested e.g. by observations of the Bullet Cluster [39], alternative explanations such as modified Newton dynamics [40] are still discussed. For example the recent proposal of emergent gravity by Verlinde [41] suggests that the effects attributed to particle DM may arise from an interplay between ordinary matter and dark energy. Verlindes proposal has received considerable attention, however it appears to be in tension with observations [42, 43].

WIMP Dark Matter

If massive DM particles can couple to SM particles through some weak interaction they are referred to as Weakly Interacting Massive Particles (WIMPs). We imagine that WIMPs could have been in thermal equilibrium with the SM particles in the early universe. As the universe cools off the production of the heavy DM particles is no longer possible, and we might expect that all DM particles annihilate into SM particles. However, as the universe expands the distance between two DM particles grows and annihilation is no longer possible. This is called the freeze-out, at this point the DM density is stable. If the WIMP describes the full DM content of the universe the DM density at this point should match the measured relic density, see Eq. (1.17). For a given model we can calculate the relic density at freeze-out by

[5] The ΛCDM model is a parametrization of the Big Bang cosmological model in particular in terms of a cosmological constant Λ associated with dark energy, and cold dark matter (CDM).

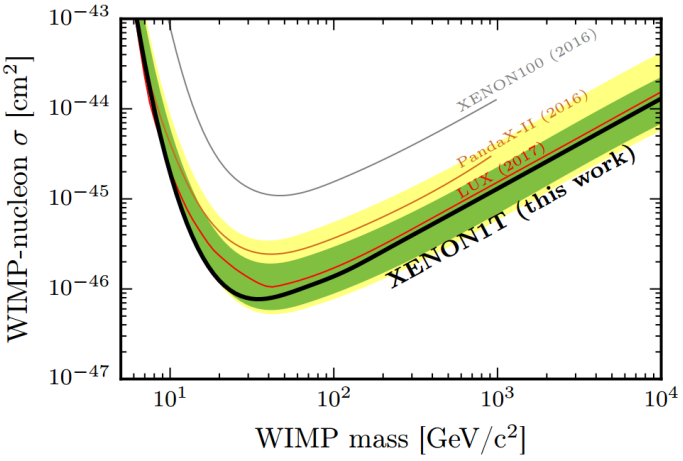

Figure 1.3.: Recent 90% CL limits on the spin-independent scattering cross section as a function of the WIMP mass, taken from [49].

considering the rate equation

$$\frac{\mathrm{d}n}{\mathrm{d}t} = -3Hn - \langle\sigma_{ann}v\rangle(n^2 - n_{eq}^2), \tag{1.18}$$

with n the DM number density, H the Hubble constant, $\langle\sigma_{ann}v\rangle$ the thermally averaged annihilation cross section and n_{eq} the WIMP equilibrium number density. In fact it turns out that for candidates with mass and cross sections around the weak scale, the predicted relic density can match the measured value, which is often referred to as the "WIMP miracle". The relic density in a generic model can be calculated numerically, as is done e.g. in `micrOMEGAs` [44] or MadDM [45]. Moreover, the relic density in superymmetric models can be calculated in DarkSUSY [46] and SuperIso Relic [47].

Direct and Indirect DM Detection

If DM is indeed a WIMP it could be detected through its interaction with SM particles, either by scattering with nuclei (direct detection experiments) or by detection of its annihilation products (indirect detection). Direct detection experiments aim to measure the recoil energy when a WIMP scatters with nuclei. The interaction can generally be split into spin independent and spin dependent interactions. The advantage of spin independent measurements is that protons and neutrons contribute equally and the total amplitude grows as the number of nuclei. As the interaction cross sections are typically very low, large detectors using heavy elements as the target nuclei have been designed to reach good sensitivity. The most recent limits on the spin-independent scattering cross section are summarized in Figure 1.3. A detailed review of direct detection experiments was presented in [48].

Compared to direct detection experiments, indirect detection experiments typically have much higher uncertainties as the results depend for example on the modeling of DM halos and the propagation of charged particles through the Galaxy. An exception is the observation of photons from dwarf spheroidal galaxies [50], giving robust constraints for light WIMPs with masses up to about 100 GeV. Therefore, we use only those limits in the following. For a recent review of indirect searches for DM see [51].

Predictions for both direct and indirect detection rates can be obtained within `micrOMEGAs`, see [52, 53]. Direct detection cross sections can also be calculated in MadDM [54].

1.3. Supersymmetry

Supersymmetry (SUSY) denotes an invariance under generalized spacetime transformations connecting fermions and bosons. SUSY transformations are described by anticommuting spinor generators that transform bosons and fermions into one another. This symmetry protects the Higgs mass from receiving large corrections as each fermionic (bosonic) contribution gets cancelled by a contribution with opposite sign from the corresponding bosonic (fermionic) degrees of freedom. This cancellation is exact in unbroken SUSY, but as we will see even so-called "softly broken" SUSY allows to address the hierarchy problem. Moreover, we have already seen that the unification of gauge couplings can be achieved in supersymmetric theories, see Figure 1.2. Finally, to suppress proton decays, it is reasonable to introduce a new type of parity ("R parity") that should be conserved. This R parity conservation has the consequence that SUSY models naturally provide a DM candidate. Thus the concept of SUSY can address a number of open questions in particle physics, and has therefore been studied extensively, notably since the 1980s when it was discovered that it provides a potential solution to the hierarchy problem [55].

Here we first introduce general concepts and notations important to the discussion, concrete descriptions are then given for the simplest supersymmetric version of the Standard Model, the Minimal Supersymmetric Standard Model (MSSM). Finally we will also introduce different extensions of this minimal setup, that will be studied in the following.

1.3.1. Constructing Supersymmetric Theories

Supersymmetric Lagrangian

To construct a supersymmetric Lagrangian it is first necessary to define the superfield formalism. A superfield should conveniently describe bosonic and fermionic fields as components of a single entity. This can be done using the superspace coordinates (x, θ), where θ is a Majorana spinor with components $\theta_a, a = 1, 2, 3, 4$ that are anticommuting Grassmann numbers. Thus we can think of θ as fermionic coordinates. A superfield $\hat{\mathcal{S}}(x, \theta)$ is a function of four commuting spacetime coordinates x^μ and four anticommuting coordinates θ_a. In the following we will adopt the notation of [56] and describe fermionic fields in terms of 4-component Majorana spinors, i.e.

$$\psi = \begin{pmatrix} \chi_L \\ -i\sigma_2 \chi_L^* \end{pmatrix} \tag{1.19}$$

where χ_L is a left-handed two component Weyl spinor, and $-i\sigma_2\chi_L^*$ transforms as a right-handed spinor, thus we have constructed a 4-component spinor from one Weyl spinor. As usual we then define $\psi_{L,R} = P_{L,R}\psi$. A generic Dirac spinor can then be obtained as a combination of two such Majorana spinors.

Two types of superfields will be relevant here. First, so-called "chiral superfields", that can describe matter and Higgs fields. A left-chiral superfield contains a complex scalar field $\mathcal{S}$, a fermion field ψ_L and an auxiliary field $\mathcal{F}$. Defining $\hat{x}_\mu = x_\mu + \frac{i}{2}\bar{\theta}\gamma_5\gamma_\mu\theta$ we can express the superfield as

$$\hat{\mathcal{S}}_L(x, \theta) = \mathcal{S}(\hat{x}) + i\sqrt{2}\bar{\theta}\psi_L(\hat{x}) + i\bar{\theta}\theta_L\mathcal{F}(\hat{x}) \tag{1.20}$$

The auxiliary field is not physical, i.e. it is not propagating. However, it allows us to conve-

niently describe SUSY transformations and invariants.[6] From the chiral superfields we can construct the function $\mathcal{W}$, the so-called "super-potential". It describes the interaction between the chiral superfields. As a product of left-chiral superfields only, the super-potential is again described as a left-chiral superfield. The contribution to the Lagrangian from the superpotential are those that change by a total derivative under SUSY transformations, thus yielding a SUSY invariant action. This is true for the $\bar{\theta}\theta_L$ component of a left-chiral superfields. We thus refer to the superpotential contributions as F-term contributions to the Lagrangian.

Gauge fields are promoted to gauge superfields. In the Wess-Zumino gauge we can write a gauge superfield containing a vector field V^μ, a fermion field λ (the so-called "gaugino") and the auxiliary field $\mathcal{D}$ as

$$\hat{\Phi}_A = \frac{1}{2}(\bar{\theta}\gamma_5\gamma_\mu\theta)V_A^\mu + i\bar{\theta}\gamma_5\theta\bar{\theta}\lambda_A - \frac{1}{4}(\bar{\theta}\gamma_5\theta)^2\mathcal{D}_A. \tag{1.21}$$

Supersymmetric gauge kinetic terms can be described defining a curl superfield, that will give rise to gauge-invariant kinetic terms for the fermion field λ as well as the kinetic terms for the vector fields in terms of the field strength tensor $F_{\mu\nu}$.

Gauge invariant kinetic terms of the chiral superfields are obtained via the Kähler potential

$$K = \hat{\mathcal{S}}_L^\dagger e^{-2gt_A\hat{\Phi}_A}\hat{\mathcal{S}}_L. \tag{1.22}$$

The resulting supersymmetric contributions to the Lagrangian are the $(\bar{\theta}\gamma_5\theta)^2$ components of K. They give rise to the gauge invariant kinetic terms for the scalar and fermionic fields of the superfield. In addition we get interaction terms between the gauginos and the scalar and fermionic components of the chiral superfields that are determined by the corresponding gauge couplings. Finally there are also contributions to the scalar potential, deriving from the elimination of the auxiliary field $\mathcal{D}$. Because of their origin these are typically called D-term contributions, and they are proportional to the gauge coupling g.

Softly Broken Supersymmetry

If SUSY is exact, every bosonic state must have a corresponding fermionic partner with exactly the same mass and vice versa (i.e. the components of one superfield, that transform into one another under SUSY transformations). This situation is excluded experimentally, and we must therefore consider broken supersymmetry. Considering only SUSY breaking terms that do not reintroduce quadratic divergences, such that SUSY remains a viable solution to address the hierarchy problem, is referred to as soft SUSY breaking. Linear, bilinear and trilinear scalar interactions, and scalar and gaugino mass terms break SUSY softly.

It is particularly compelling to assume that SUSY is broken spontaneously. However, no convincing theory of SUSY breaking has been found, and we therefore parametrize the effects of SUSY breaking by adding all possible soft SUSY breaking terms to the Lagrangian, as is done e.g. in the MSSM. On the other hand, specific patterns in the soft SUSY breaking parameters arise when considering that SUSY is broken in an unknown "hidden sector", and studying how the low energy phenomenology depends on how this breaking is mediated to the observable sector. This is in particular interesting as we can predict the large number of possible SUSY breaking terms from a much smaller set of free parameters. We will return

[6] Auxiliary fields are simply eliminated via their algebraic equations of motion when working out the Lagrangian for the dynamically independent fields.

Superfield	Spin-0	Spin-1/2	$SU(3)_C, SU(2)_L, U(1)_Y$
$\hat{Q} = (\hat{u}_L\ \hat{d}_L)^T$	$(\tilde{u}_L\ \tilde{d}_L)^T$	$(\psi_{uL}\ \psi_{dL})^T$	$(\mathbf{3}, \mathbf{2}, \frac{1}{6})$
$\hat{U}^c$	$\tilde{u}_R^\dagger$	ψ_{U^cL}	$(\mathbf{3}^*, \mathbf{1}, -\frac{2}{3})$
$\hat{D}^c$	$\tilde{d}_R^\dagger$	ψ_{D^cL}	$(\mathbf{3}^*, \mathbf{1}, \frac{1}{3})$
$\hat{L} = (\hat{\nu}_L\ \hat{e}_L)^T$	$(\tilde{\nu}\ \tilde{e}_L)^T$	$(\psi_{eL}\ \psi_{\nu L})^T$	$(\mathbf{1}, \mathbf{2}, -\frac{1}{2})$
$\hat{E}^c$	$\tilde{e}_R^\dagger$	ψ_{E^cL}	$(\mathbf{1}, \mathbf{1}, 1)$
$\hat{H}_u = (\hat{h}_u^+\ \hat{h}_u^0)^T$	$(h_u^+\ h_u^0)^T$	$(\psi_{h_u^+}\ \psi_{h_u^0})$	$(\mathbf{1}, \mathbf{2}, \frac{1}{2})$
$\hat{H}_d = (\hat{h}_d^-\ \hat{h}_d^0)^T$	$(h_d^-\ h_d^0)$	$(\psi_{h_d^-}\ \psi_{h_d^0})$	$(\mathbf{1}, \mathbf{2}^*, -\frac{1}{2})$

Table 1.2.: Chiral superfield content of the MSSM with gauge transformation properties and weak hypercharge.

Spin-1/2	Spin-1	$SU(3)_C, SU(2)_L, U(1)_Y$
gluino $\tilde{g}$	gluon g	$(\mathbf{8}, \mathbf{1}, 0)$
wino $\tilde{W}^\pm, \tilde{W}^0$	W boson $W^\pm, W^0$	$(\mathbf{1}, \mathbf{3}, 0)$
bino $\tilde{B}^0$	B boson B	$(\mathbf{1}, \mathbf{1}, 0)$

Table 1.3.: Gauge supermultiplet content of the MSSM.

to this idea after specifying the MSSM.

1.3.2. The Minimal Supersymmetric Standard Model

The MSSM can be considered a direct supersymmetrization of the SM, containing the minimal number of new particle states needed. The matter content consists of left-chiral scalar superfields corresponding to the SM matter fields. To give mass to all fermions two Higgs doublet fields of opposite hypercharge have to be introduced. They are also described by left-chiral superfields. The chiral superfields, their components and their quantum numbers are summarized in Table 1.2.The fermionic fields are written in terms of Majorana spinors defined in Eq. (1.19), the Dirac fields can be obtained as e.g. $e = P_L\psi_e + P_R\psi_{E^c}$. In contrast to Table 1.1 we now defined the field content in terms of left-handed fields only, such that we can directly construct the superpotential from these fields.

Similarly the SM gauge bosons are promoted to gauge superfields, the components of the gauge supermultiplets are summarized in Table 1.3.

The superpotential of the MSSM is

$$\mathcal{W} = \mu\hat{H}_u\hat{H}_d + \mathbf{y_u}\epsilon_{ab}\hat{Q}^a\hat{H}_u^b\hat{U}^c + \mathbf{y_d}\hat{Q}\hat{H}_d\hat{D}^c + \mathbf{y_e}\hat{L}\hat{H}_d\hat{E}^c \tag{1.23}$$

where the chiral superfields are given in Table 1.2, $\mathbf{y_u}, \mathbf{y_d}, \mathbf{y_e}$ are 3×3 matrices in family space, and μ a mass parameter for the Higgs superfield, determining in particular also the higgsino mass. Here we have added explicitly the $SU(2)$ indices in the second term, reflecting that the antisymmetric combination corresponds to an $SU(2)$ singlet.

We note here that in principle baryon (B) and lepton (L) number violating terms are allowed by both the SM gauge symmetries as well as supersymmetry. They have not been included in the superpotential defined in Eq. (1.23), as they are strongly constrained by ex-

periments (in particular through the non-observation of proton decay). These terms can be forbidden by introducing a new discrete symmetry, R-parity. It can be defined as

$$R = (-1)^{3(B-L)+2s} \tag{1.24}$$

with s the particle spin. It follows that all SM particles and the Higgs bosons are even ($R = 1$) while their superpartners are odd ($R = -1$) under the new parity. This has important phenomenological consequences as the superpartners can thus only interact in pairs, and in particular the lightest supersymmetric particle (LSP) is stable. If the LSP is electrically and color neutral it is an excellent dark matter candidate.

Following Section 1.3.1 we further introduce the soft supersymmetry breaking terms[7]

$$\begin{aligned}\mathcal{L}_{soft} = & -\frac{1}{2}(M_3\tilde{g}\tilde{g} + M_2\tilde{W}\tilde{W} + M_1\tilde{B}\tilde{B} + h.c.) \\ & + (\mathbf{a_u}\epsilon_{ab}\tilde{Q}^a H_u^b \tilde{u}_R^\dagger + \mathbf{a_d}\tilde{Q}H_d\tilde{d}_R^\dagger - \mathbf{a_e}\tilde{L}H_d\tilde{e}_R^\dagger + h.c.) \\ & - \tilde{Q}^\dagger \mathbf{m_Q^2}\tilde{Q} - \tilde{L}^\dagger \mathbf{m_L^2}\tilde{L} - \tilde{u}_R^\dagger \mathbf{m_U^2}\tilde{u}_R - \tilde{d}_R^\dagger \mathbf{m_D^2}\tilde{d}_R - \tilde{e}_R^\dagger \mathbf{m_E^2}\tilde{e}_R \\ & - m_{H_u}^2 H_u^* H_u - m_{H_d}^2 H_d^* H_d + (bH_u H_d + h.c.)\end{aligned} \tag{1.25}$$

where we have introduced gluino, wino and bino masses M_3, M_2 and M_1, and the trilinear couplings $\mathbf{a_i}$ and scalar masses $\mathbf{m_i}$ for the various fermion species that are in general 3×3 matrices in flavor space. We have now fully specified the MSSM Lagrangian and can discuss the physical implications, in particular for electroweak symmetry breaking, particle masses and supersymmetric DM. We will then conclude our discussion of the MSSM by considering how the large number of free parameters, introduced in particular by the generic soft-SUSY breaking Lagrangian, can be reduced, either by studying specific models of SUSY breaking mediation, or from phenomenological considerations.

Electroweak symmetry breaking

The Higgs potential now contains as free parameters $|\mu|^2, m_{H_u}^2, m_{H_d}^2$ and b. These parameters need to fulfil a non-trivial condition in order to facilitate electroweak symmetry breaking. Writing the vevs of the neutral fields as

$$v_u = \langle h_u^0 \rangle, \quad v_d = \langle h_d^0 \rangle \tag{1.26}$$

such that

$$v_u^2 + v_d^2 = v^2 = 2m_Z^2/(g^2 + g'^2) \tag{1.27}$$

and introducing

$$\tan\beta = \frac{v_u}{v_d} \tag{1.28}$$

we can write the conditions for electroweak symmetry breaking as

$$b\mu = \frac{(m_{H_u}^2 + m_{H_d}^2 + 2\mu^2)\sin 2\beta}{2}, \tag{1.29}$$

$$\mu^2 = \frac{m_{H_d}^2 - m_{H_u}^2 \tan^2\beta}{\tan^2\beta - 1} - \frac{M_Z^2}{2}. \tag{1.30}$$

[7] Here we follow sign conventions as used e.g. in [56], note that different conventions are used e.g. in [34] and in the SLHA format [57].

We see that either all parameters should take values around the electroweak scale, or a significant accidental cancellation is needed. This is often referred to as the "μ problem", since all other terms can have a common origin (they are SUSY breaking parameters), while the μ term in the superpotential is SUSY conserving, and a priori independent. Naturally we would expect it to be either very small or very large compared to the electroweak scale.

Starting from a total of eight degrees of freedom in the Higgs sector, we are left with five physical states after electroweak symmetry breaking. They are commonly denoted as h, H (CP-even neutral states, sorted by mass), $H^{\pm}$ (charged Higgs bosons) and A (CP-odd neutral state). Commonly the four free parameters are traded for $\mu, m_A, \tan\beta$ and v.

(S)particle Masses

Gauge boson masses By setting $v^2 = v_u^2 + v_d^2$ we recover the $W^{\pm}$ and Z boson mass relations from the SM description, see Eq. (1.9).

Matter fermions The fermion masses now depend on v, the Yukawa couplings y_i, but also on $\tan\beta$. At tree level they are given as

$$m_t = y_t v \sin\beta, \quad m_b = y_b v \cos\beta, \quad m_\tau = y_\tau v \cos\beta. \tag{1.31}$$

Higgs boson masses The mass of the physical pseudoscalar boson and the charged Higgs bosons are given as

$$m_A^2 = B\mu(\cot\beta + \tan\beta), \tag{1.32}$$

$$m_{H^\pm}^2 = B\mu(\cot\beta + \tan\beta) + M_W^2. \tag{1.33}$$

Finally the real, neutral components give two physical states with masses

$$m_{h,H}^2 = \frac{1}{2}[(m_A^2 + M_Z^2) \mp \sqrt{(m_A^2 + M_Z^2)^2 - 4m_A^2 M_Z^2 \cos^2 2\beta}]. \tag{1.34}$$

In particular at tree level we have $m_h \leq M_Z|\cos 2\beta|$, and therefore large loop contributions are required to reproduce the observed Higgs mass ($m_h \approx 125$ GeV) in the MSSM.

Gluino mass Because of the unbroken $SU(3)_C$ the gluino cannot mix with any other fermion. At tree level the mass can therefore simply be read-off from the soft SUSY breaking mass term, and $m_{\tilde{g}} = |M_3|$.

Chargino and Neutralino masses On the other hand, the breaking of electroweak symmetry implies that all states with the same electric charge, color and spin will mix. In the MSSM this means that electroweak gauginos and higgsinos will mix and are generically referred to as electroweakinos. The resulting mass eigenstates are referred to as neutralinos (neutral mass eignestates) and charginos (charged mass eigenstates). In the gauge-eigenstate basis $(\tilde{B}, \tilde{W}^0, \psi_{h_d^0}, \psi_{h_u^0})$ the neutralino mass matrix can be written as

$$M_{\tilde{\chi}^0} = \begin{pmatrix} M_1 & 0 & -g'v_d/\sqrt{2} & g'v_u/\sqrt{2} \\ 0 & M_2 & gv_d/\sqrt{2} & -gv_u/\sqrt{2} \\ -g'v_d/\sqrt{2} & gv_d/\sqrt{2} & 0 & \mu \\ g'v_u/\sqrt{2} & -gv_u/\sqrt{2} & \mu & 0 \end{pmatrix}. \tag{1.35}$$

The mass matrix is diagonalised by a unitary matrix V_n as $V_n^\dagger M_{\tilde{\chi}^0} V_n = M_{diag}$. The gauge eigenstates are therefore related to the mass eigenstates as

$$\begin{pmatrix} \tilde{B} \\ \tilde{W}^0 \\ \psi_{h_d^0} \\ \psi_{h_u^0} \end{pmatrix} = V_n \begin{pmatrix} \tilde{\chi}_1^0 \\ \tilde{\chi}_2^0 \\ \tilde{\chi}_3^0 \\ \tilde{\chi}_4^0 \end{pmatrix}, \tag{1.36}$$

where we denote the mass eigenstates as $\tilde{\chi}_i^0$, and $i = 1, 2, 3, 4$ sorts the neutralinos by increasing mass. Effectively the mixing is often assumed to be only a small perturbation, and we speak of "bino-like", "wino-like" and "higgsino-like" mass eigenstates, with masses determined primarily by M_1, M_2 and $|\mu|$ respectively. This happens when M_1, M_2 and $|\mu|$ are very different and is not the case for the well-tempered neutralino scenarios described below.

Similarly for charginos the mass matrix reads (in wino-higgsino basis)

$$M_{\tilde{\chi}^\pm} = \begin{pmatrix} M_2 & -gv_d \\ -gv_u & -\mu \end{pmatrix}. \tag{1.37}$$

The chargino mass eigenstates are denoted $\tilde{\chi}_i^\pm$, with $i = 1, 2$ sorted again by increasing mass.

Sfermion masses Here we restrict the discussion to the mass of the top squark. Other sfermion mass eigenstates can be obtained in a similar fashion. After electroweak symmetry breaking there are four different sources of stop mass terms. Below we list them in the $(\tilde{t}_L, \tilde{t}_R)$ basis.

- Superpotential terms: the sfermion receives the same mass contribution as the corresponding fermion (Yukawa mass) that is diagonal, as well as an off-diagonal mixing term that is also proportional to the Yukawa coupling ($m_t \mu \cot \beta$).[8]
- SUSY breaking scalar mass: diagonal contribution that can be read off from the soft breaking Lagrangian ($m^2_{\tilde{t}_L}, m^2_{\tilde{t}_R}$). These terms are present independent of electroweak symmetry breaking, therefore there is only one mass parameter for each generation of left-handed squarks.
- SUSY breaking trilinear term: off-diagonal contribution to the stop mass matrix that is present after electroweak symmetry breaking. The contribution is commonly written proportional to the fermion mass by substituting a_t by $A_t y_t$.
- D-term contributions: the D-terms also give rise to diagonal contributions to the mass matrix after electroweak symmetry breaking, arising from squark-Higgs boson cross terms. Due to their origin they depend on the sfermion charges.

Combining all contributions we can write the squared stop mass matrix as

$$M^2_{\tilde{t}} = \begin{pmatrix} m^2_{\tilde{t}_L} + m_t^2 + D(\tilde{t}_L) & m_t(-A_t + \mu \cot \beta) \\ m_t(-A_t + \mu \cot \beta) & m^2_{\tilde{t}_R} + m_t^2 + D(\tilde{t}_R) \end{pmatrix} \tag{1.38}$$

where generically

$$D = M_Z^2 \cos 2\beta (T_3 - Q \sin^2 \theta_W). \tag{1.39}$$

[8] For down-type sfermions this mixing scales as $\mu \tan \beta$ instead of $\mu \cot \beta$.

We see that the stop mixing, being proportional to m_t, can be large. We can parametrize it by a mixing angle θ_t as

$$\begin{pmatrix} \tilde{t}_1 \\ \tilde{t}_2 \end{pmatrix} = \begin{pmatrix} \cos\theta_t & \sin\theta_t \\ -\sin\theta_t & \cos\theta_t \end{pmatrix} \begin{pmatrix} \tilde{t}_L \\ \tilde{t}_R \end{pmatrix}, \tag{1.40}$$

such that $\tilde{t}_1$ is lighter than $\tilde{t}_2$. On the other hand, as the off-diagonal terms scale with the fermion mass, we conclude that the mixing is negligible for 1st and 2nd generation sfermions.

Dark Matter in the MSSM

A priori the MSSM contains two possible DM candidates, the sneutrino or the lightest neutralino. However, the sneutrino of the MSSM is excluded as a DM candidate because it has a non-zero hypercharge: its couplings to the Z boson makes it annihilate too efficiently in the early Universe, and hence its final relic abundance is lower than the measured value of $\Omega_{\rm DM}h^2$, see Eq. (1.17). Very stringent limits come moreover from direct DM detection experiments: the $\tilde{\nu}_L$ scattering off nuclei is mediated by t-channel Z boson exchange, giving a spin-independent (SI) cross section of order 10^{-39}cm^2 — a value excluded already a decade ago for DM particles heavier than 10 GeV. A light $\tilde{\nu}_L$ with mass below $m_Z/2$ is also excluded by the Z invisible width.

On the other hand the lightest neutralino can be a very compelling candidate, reproducing the observed relic density and in compliance with limits from direct detection experiments. For example a mixed neutralino LSP can reproduce the observed relic density by appropriately tuning the admixtures, the so-called well-tempered neutralino [58]. Note that a pure bino neutralino is typically overabundant while higgsino and wino neutralinos are underabundant if they are lighter than $\approx 1 - 1.5$ TeV. For a detailed general review of SUSY DM see [59], for a recent review of viable neutralino DM scenarios see [60].

Models of SUSY Breaking Mediation

We have now formulated the MSSM writing the most general soft-SUSY breaking Lagrangian. Despite our ignorance of the origin of SUSY breaking, we can study the relation of the various free parameters by considering how SUSY breaking in an unknown hidden sector is mediated to the observable sector (described by the MSSM). Here we list some ideas of how the SUSY breaking is mediated, and what they predict for the parameters.

Gravity-mediated SUSY Breaking We consider that the hidden sector communicates with the MSSM only via gravitational interactions. The SUSY breaking in the hidden sector gives rise to a mass term for the gravitino (the superpartner of the graviton), which then generates soft SUSY breaking mass terms through radiative corrections. The minimal version is called mSUGRA (minimal supergravity) or cMSSM (constrained MSSM), and is fully determined by 4 free parameters that are defined at the GUT scale, and the sign of μ. The free parameters are

- m_0, common mass parameter for all scalars (sleptons, squarks, Higgs bosons)
- $m_{1/2}$, common mass parameter for gauginos and higgsinos
- A_0, common trilinear coupling

- $\tan\beta$
- sign(μ).

The MSSM parameters at the weak scale are then determined by considering their RGEs. In particular we find that the gaugino masses are related as $M_1 : M_2 : M_3 \approx 1 : 2 : 6$, the third generation squarks are the lightest squarks because of their large Yukawa coupling, and sleptons are generally lighter than squarks because they do not have strong interaction loop contributions that considerably increase the masses of the squarks.

Anomaly-mediated SUSY Breaking MSSM soft terms could further be generated through anomalous violation of a local superconformal invariance (an extension of scale invariance), such models are referred to as anomaly-mediated SUSY breaking (AMSB). The minimal version (mAMSB) is characterized by 3 parameters (scalar mass m_0, gravitino mass $m_{3/2}$, $\tan\beta$) defined at the GUT scale and the sign of μ. This type of SUSY breaking mediation leads to different gaugino mass hierarchies at the weak scale. Notably $M_1/M_2 \approx 3$, so the winos are lighter than the bino in these scenarios.

Gauge-mediated SUSY breaking Assuming that SUSY breaking is communicated to the MSSM via SM gauge interactions is called gauge-mediated SUSY breaking (GMSB). We consider that so-called messenger fields, that are charged under SM gauge interactions, couple also to the hidden sector. The messenger particles will generate SUSY breaking masses via their gauge couplings (at loop level). In contrast to SUGRA and AMSB scenarios, GMSB predicts a light gravitino, which is thus the LSP, giving rise to very different phenomenology.

pMSSM

Without considering a particular mechanism of SUSY breaking mediation, we can still significantly restrict the parameter space by phenomenological observations, this is commonly referred to as the phenomenological MSSM (pMSSM). While the generic MSSM contains more than 100 free parameters, experiments tell us that many of them should be related or very small. The resulting assumptions were summarized in [61] as

- No new source of CP-violation (eliminating all phases in the soft-SUSY breaking potential)
- No flavor changing neutral currents (the sfermion mass and trilinear coupling matrices are taken to be diagonal in flavor space)
- First and second generation universality

Taking into account in addition the conditions for electroweak symmetry breaking, this leaves us with 19 free parameters in addition to the SM parameters, namely

- Higgs sector: $\tan\beta$, M_A, μ
- Gaugino masses: M_1, M_2, M_3
- Universal first/second generation sfermion mass terms: $m_{\tilde{q}}$, $m_{\tilde{u}_R}$, $m_{\tilde{d}_R}$, $m_{\tilde{l}}$, $m_{\tilde{e}_R}$
- Third generation sfermion mass terms: $m_{\tilde{Q}}$, $m_{\tilde{t}_R}$, $m_{\tilde{b}_R}$, $m_{\tilde{L}}$, $m_{\tilde{\tau}_R}$
- Third generation trilinear couplings: A_t, A_b, A_τ

Natural SUSY

Fine-tuning considerations in the context of the MSSM may allow us to estimate the masses of particles related to the Higgs sector [62,63]. SUSY scenarios with low fine-tuning are referred to as natural SUSY scenarios. In particular the higgsinos has be light, below about 700 GeV. Moreover the stop mass and the gluino mass (giving important contributions to the running of the stop mass) should not be much heavier than about 1 TeV. For example a 1.5 TeV gluino is associated with about 1% fine-tuning, and a 1.5 TeV stop with about 10% fine-tuning [63]. Note that these values depend on the specific definition of the fine tuning measure, and on the details of the model. Nevertheless they give a useful estimate of the mass scales expected in natural SUSY scenarios.

1.3.3. MSSM+RN

We have seen that the sneutrino is not a viable DM candidate in the MSSM because of its non-zero hypercharge. The picture changes dramatically if we include in the MSSM a RH neutrino superfield which gives rise to Dirac neutrino masses. Besides the RH neutrino, the superfield also contains a scalar field, the RH sneutrino $\tilde{N}$ (strictly speaking this is a right-chiral field, but we use the RH notation for simplicity). This field, if at the TeV scale, can mix with the LH partner $\tilde{\nu}_L$ and yield a mostly RH sneutrino LSP as a viable thermal DM candidate. We denote this extension, first defined in [64,65], as MSSM+RN.[9]

In the following we adopt the notation used in [71,72], that differs only slightly from the notation used in Section 1.3.2. The superpotential for the Dirac RH neutrino superfield is given by

$$W = \epsilon_{ij}(\mu \hat{H}_i^u \hat{H}_j^d - Y_l^{IJ} \hat{H}_i^d \hat{L}_j^I \hat{R}^J + Y_\nu^{IJ} \hat{H}_i^u \hat{L}_j^I \hat{N}^J)\,, \tag{1.41}$$

where Y_ν^{IJ} is a matrix in flavor space (which we choose to be real and diagonal), from which the mass of neutrinos are obtained as $m_D^I = v_u Y_\nu^{II}$. Note that lepton-number violating terms are absent in this scheme. The additional scalar fields contribute with new terms in the soft-breaking potential

$$V_{\rm soft} = (M_L^2)^{IJ}\, \tilde{L}_i^{I*} \tilde{L}_i^J + (M_N^2)^{IJ}\, \tilde{N}^{I*} \tilde{N}^J - [\epsilon_{ij}(\Lambda_l^{IJ} H_i^d \tilde{L}_j^I \tilde{R}^J + \Lambda_\nu^{IJ} H_i^u \tilde{L}_j^I \tilde{N}^J) + \text{h.c.}]\,, \tag{1.42}$$

where both matrices M_N^2 and Λ_ν^{IJ} are real and diagonal, $M_N^2 = \text{diag}(m_{N^k}^2)$ and $\Lambda_\nu^{IJ} = \text{diag}(A_{\tilde{\nu}}^k)$, with $k = e, \mu, \tau$ being the flavor index. In the sneutrino interaction basis, defined by the vector $\Phi^\dagger = (\tilde{\nu}_L^*,\, \tilde{N}^*)$, the sneutrino mass potential is

$$V_{\rm mass}^k = \frac{1}{2}\, \Phi_{LR}^\dagger\, \mathcal{M}_{LR}^2\, \Phi_{LR}\,, \tag{1.43}$$

with the squared–mass matrix $\mathcal{M}_{LR}^2$

$$\mathcal{M}_{LR}^2 = \begin{pmatrix} m_{L^k}^2 + \frac{1}{2} m_Z^2 \cos(2\beta) + m_D^2 & \frac{1}{\sqrt{2}} A_{\tilde{\nu}}^k v \sin\beta - \mu m_D / \tan\beta \\ \frac{1}{\sqrt{2}} A_{\tilde{\nu}}^k v \sin\beta - \mu m_D / \tan\beta & m_{N^k}^2 + m_D^2 \end{pmatrix}. \tag{1.44}$$

[9] Pure RH sterile sneutrinos can also be viable (non-thermal, depending on the model) DM candidates, as discussed e.g. in [66–70]. In particular, if the RH neutrino is charged under an extended gauge group, it can also be a DM candidate. An example for such a scenario, with an additonal $U(1)$ gauge group, will be introduced in Section 1.3.5.

Here, $m^2_{L^k}$ are the soft mass terms for the three SU(2) leptonic doublets. The Dirac neutrino mass m_D is small and can be safely neglected.

The off-diagonal term determines the mixing of the LH and RH fields. If $A^k_{\tilde{\nu}} = \eta Y_\nu$, that is if the trilinear term is aligned to the neutrino Yukawa, this term is certainly very small as compared to the diagonal entries and is therefore negligible. However, $A^k_{\tilde{\nu}}$ can in general be a free parameter and may naturally be of the order of the other entries of the matrix [64, 65], thus inducing a sizable mixing among the interaction eigenstates. The sneutrino mass eigenstates are then given by

$$\begin{pmatrix} \tilde{\nu}_{k_1} \\ \tilde{\nu}_{k_2} \end{pmatrix} = \begin{pmatrix} -\sin\theta^k_{\tilde{\nu}} & \cos\theta^k_{\tilde{\nu}} \\ \cos\theta^k_{\tilde{\nu}} & \sin\theta^k_{\tilde{\nu}} \end{pmatrix} \begin{pmatrix} \tilde{\nu}^k_L \\ \tilde{N}^k \end{pmatrix} . \tag{1.45}$$

The relevant parameters at the electroweak scale for the sneutrino sector are the two mass eigenvalues $m_{\tilde{\nu}_{k_1}}$ and $m_{\tilde{\nu}_{k_2}}$ and the mixing angle $\theta^k_{\tilde{\nu}}$, related to the $A^k_{\tilde{\nu}}$ term via

$$\sin 2\theta^k_{\tilde{\nu}} = \sqrt{2}\frac{A^k_{\tilde{\nu}}\, v \sin\beta}{(m^2_{\tilde{\nu}_{k2}} - m^2_{\tilde{\nu}_{k1}})} . \tag{1.46}$$

The sneutrino coupling to the Z boson, which does not couple to the singlet fields, is now controlled by the mixing angle. This has a relevant impact on the sneutrino phenomenology, as discussed e.g. in [64, 71, 73–75].

In the following we consider a common scalar mass and trilinear coupling for all sneutrino families at the GUT scale. By neglecting all lepton Yukawas but Y_τ in the running of the masses we find that at the electroweak scale the sneutrino tau, $\tilde{\nu}_{\tau_1}$, is the lightest one among the three sneutrino flavors and hence the LSP, while $\tilde{\nu}_{e_1} = \tilde{\nu}_{\mu_1}$.[10] Note that in this setup the mass splitting between $\tilde{\nu}_{\tau_1}$ and $\tilde{\nu}_{e_1,\mu_1}$ is generally very small, which means that regarding collider phenomenology they are practically degenerate.

1.3.4. NMSSM

Another simple addition to the MSSM would be a minimal extension of the Higgs sector. As we have seen the condition for electroweak symmetry breaking in the MSSM gives rise to the "μ problem". That is, there is no reason why the SUSY conserving μ term should be connected to the SUSY breaking mechanism and scale. This is amended if the μ term is in fact induced by SUSY breaking terms, similar to the Yukawa mass terms of fermions. This is the case in the simplest possible extension of the MSSM, where a SM singlet chiral superfield $\hat{S}$, containing the complex scalar field S, and its fermionic partner, the singlino $\tilde{S}$ is added. This model is called the Next-to-Minimal Supersymmetric Standard Model (NMSSM). After electroweak symmetry breaking the components of the singlet S will mix with H_u and H_d to three CP-even and two CP-odd neutral scalars. Similarly, the singlino $\tilde{S}$ will mix with the higgsinos and gauginos to give five neutralino mass eigenstates.

In the simplest NMSSM scenario with a $\mathbb{Z}_3$ symmetry we can add to the superpotential the terms

$$\mathcal{W}_{\hat{S}} = \lambda \hat{S}\hat{H}_u \cdot \hat{H}_d + \frac{\kappa}{3}\hat{S}^3 \tag{1.47}$$

[10] In the following we consider only MSSM+RN scenarios where the sneutrino is lighter than the lightest neutralino, and hence the LSP.

and thus a vev s of $\hat{S}$ will generate an effective μ-term with

$$\mu_{eff} = \lambda s. \tag{1.48}$$

The vev s is naturally related to the SUSY breaking scale, thus resolving the μ problem. Moreover, the fine-tuning is reduced as there are additional tree level contributions to the light Higgs mass. The phenomenology can be significantly altered with respect to the MSSM, it is in particular interesting to consider the possibility of a singlino-like neutralino as the LSP. A doublet-singlet mixing can also modify significantly the tree-level couplings of the light Higgs.

In the following we will not be considering the NMSSM but rather a further extension by an additional $U(1)$ gauge group introduced in the next section. For details about the NMSSM we refer the reader to [76].

1.3.5. UMSSM

A less minimal extension, that retains some of the good features of the NMSSM, consists in adding a new $U(1)$ gauge group to the MSSM, denoted "UMSSM" in the following. Contributions from U(1) D-terms in addition to those from the superpotential present in the NMSSM, can further increase the light Higgs mass [77,78] reaching easily 125 GeV without a very large contribution from the stop sector. Furthermore, because the singlet mass is driven by the mass of the new gauge boson which is strongly constrained by LHC searches to be above the TeV scale [79, 80][11], the tree-level couplings of the light Higgs are expected to be SM-like, in agreement with results from ATLAS and CMS [82, 83]. Another nice feature of the UMSSM (as the NMSSM) is that the μ parameter, generated from the vev of the singlet field responsible for the breaking of the U(1) symmetry, is naturally at the weak scale. Finally, this model is well motivated within the context of superstring models [84–88] and grand unified theories [89, 90].

The symmetry group of the model is $SU(3)_c \times SU(2)_L \times U(1)_Y \times U(1)'$. Following the description in [91,92] we assume that the UMSSM is derived from an underlying E_6 model. In this case the $U(1)'$ charges of each field F of the model are parameterized by an angle θ_{E_6} as

$$\mathcal{Q}'_F = \cos\theta_{E_6}\mathcal{Q}'_\chi + \sin\theta_{E_6}\mathcal{Q}'_\psi, \tag{1.49}$$

where $\theta_{E_6} \in [-\pi/2, \pi/2]$ and the charges $\mathcal{Q}'_\chi$ and $\mathcal{Q}'_\psi$ are given in Table 1.4 for all fermionic fields that we will consider [93, 94]. The dependence on θ_{E_6} of the $U(1)'$ charge of some matter fields is shown in Figure 1.4.

The matter sector of the E_6 model contains, in addition to the chiral supermultiplets of the SM fermions, three families of new particles, each family containing : a RH neutrino, two Higgs doublets (H_u, H_d), a singlet, and a colour $SU(3)_c$ (anti)triplet. While the complete matter sector is needed for anomaly cancellations, for simplicity we will assume that all exotic fields, with the exception of three RH neutrinos, two Higgs doublets and one singlet, are above a few TeV's and can be neglected. Similarly in addition to the MSSM chiral multiplets we will only consider the chiral multiplets corresponding to these fields, that is the multiplet with a singlet S and the singlino $\tilde{S}$ and another multiplet with RH neutrinos ν_{iR} $(i \in \{e, \mu, \tau\})$ and their supersymmetric partners, the sneutrinos, $\tilde{\nu}_{iR}$.

Finally the UMSSM model contains a new vector multiplet, with a new boson B' and the corresponding gaugino $\tilde{B}'$. The superpotential is the same as in the MSSM with $\mu = 0$ but

[11] In this work we concentrate on a Z' above the electroweak scale, for scenarios with light Z' see [81].

	$\mathcal{Q}'_Q$	$\mathcal{Q}'_u$	$\mathcal{Q}'_d$	$\mathcal{Q}'_L$	$\mathcal{Q}'_\nu$	$\mathcal{Q}'_e$	$\mathcal{Q}'_{H_u}$	$\mathcal{Q}'_{H_d}$	$\mathcal{Q}'_S$
$\sqrt{40}\mathcal{Q}'_\chi$	-1	-1	3	3	-5	-1	2	-2	0
$\sqrt{24}\mathcal{Q}'_\psi$	1	1	1	1	1	1	-2	-2	4

Table 1.4.: $U(1)'$ charges of all matter fields considered.

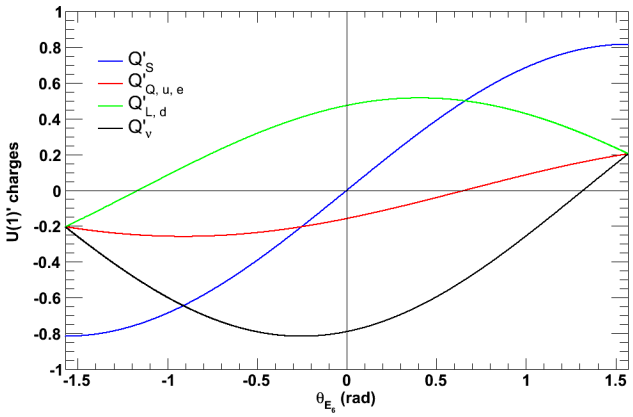

Figure 1.4.: $U(1)'$ charges of some matter fields in the UMSSM as a function of θ_{E_6}.

has additional terms involving the singlet,[12]

$$\mathcal{W}_{\rm UMSSM} = \mathcal{W}_{\rm MSSM}|_{\mu=0} + \lambda \hat{S}\hat{H}_u\hat{H}_d + \mathbf{y}_\nu \hat{L}\hat{H}_u\hat{\nu}^c_R + \mathcal{O}(\text{TeVs}) \tag{1.50}$$

where $\mathbf{y}_\nu$ is the neutrino Yukawa matrix. The vev of S, $\langle S\rangle = \frac{v_s}{\sqrt{2}}$ breaks the $U(1)'$ symmetry and induces a μ term

$$\mu = \lambda\frac{v_s}{\sqrt{2}}. \tag{1.51}$$

Note that for $\theta_{E_6} = 0$ the $U(1)'$ symmetry cannot be broken by the singlet field since $\mathcal{Q}'_S = 0$. Note also that the invariance of the superpotential under $U(1)'$ imposes a condition on the Higgs sector, namely $\mathcal{Q}'_{H_u} + \mathcal{Q}'_{H_d} + \mathcal{Q}'_S = 0$. The soft-breaking Lagrangian of the UMSSM is

$$\begin{aligned}\mathscr{L}^{\rm soft}_{\rm UMSSM} = \mathscr{L}^{\rm soft}_{\rm MSSM}|_{b=0} - \left(\frac{1}{2}M'_1\tilde{B}'\tilde{B}' + \tilde{\nu}^*_R\mathbf{a}_\nu\tilde{L}H_u + \text{h.c.}\right) - \tilde{\nu}^*_R\mathbf{m}^{\mathbf{2}}_{\tilde{\nu}_\mathbf{R}}\tilde{\nu}_R \\ - m^2_S|S|^2 - (\lambda A_\lambda S H_u H_d + \text{h.c.}) + \mathcal{O}(\text{TeVs}),\end{aligned} \tag{1.52}$$

with the trilinear coupling A_λ, the $\tilde{B}'$ mass term M'_1, and the singlet mass term m_S. The soft sneutrino mass term matrices $\mathbf{a}_\nu$ and $\mathbf{m}^{\mathbf{2}}_{\tilde{\nu}_\mathbf{R}}$ are taken to be diagonal in the family space. We now describe briefly the sectors of the model that will play a role in the considered observables.

[12] Here we follow conventions from [91, 92, 95].

Gauge bosons

The two neutral massive gauge bosons, Z^0 and $Z' = B'$ can mix through both mass and kinetic mixing [96, 97]. In the following we will neglect the kinetic mixing for simplicity.[13] The electroweak and $U(1)'$ symmetries are broken respectively by the vev's of the doublets, $v_u/\sqrt{2} = \langle H_u \rangle$, $v_d/\sqrt{2} = \langle H_d \rangle$ and singlet, $v_s/\sqrt{2} = \langle S \rangle$. The mass matrix reads

$$M_Z^2 = \begin{pmatrix} M_{Z^0}^2 & \Delta_Z^2 \\ \Delta_Z^2 & M_{Z'}^2 \end{pmatrix}, \tag{1.53}$$

where

$$\begin{aligned} M_{Z^0}^2 &= \frac{1}{4}\frac{g_2^2}{c_W^2}(v_u^2 + v_d^2) \\ M_{Z'}^2 &= g_1'^2(\mathcal{Q}'_{H_d}{}^2 v_d^2 + \mathcal{Q}'_{H_u}{}^2 v_u^2 + \mathcal{Q}'^2_S v_s^2) \end{aligned} \tag{1.54}$$

$$\Delta_Z^2 = \frac{g_2 g_1'}{2c_W}(\mathcal{Q}'_{H_u} v_u^2 - \mathcal{Q}'_{H_d} v_d^2) \tag{1.55}$$

with $g_2 = e/s_W$, $g_1' = \sqrt{5/3}g_1$, $g_1 = e/c_W$ and c_W (s_W) is the cosinus (sinus) of the Weinberg angle. Diagonalisation of the mass matrix leads to two eigenstates

$$\begin{aligned} Z_1 &= \cos\alpha_Z Z^0 + \sin\alpha_Z Z' \\ Z_2 &= -\sin\alpha_Z Z^0 + \cos\alpha_Z Z' \end{aligned} \tag{1.56}$$

where the mixing angle is defined as

$$\sin 2\alpha_Z = \frac{2\Delta_Z^2}{M_{Z_2}^2 - M_{Z_1}^2} \tag{1.57}$$

and the masses of the physical fields are

$$M_{Z_1,Z_2}^2 = \frac{1}{2}\left(M_{Z^0}^2 + M_{Z'}^2 \mp \sqrt{\left(M_{Z^0}^2 + M_{Z'}^2\right)^2 + 4\Delta_Z^4}\right). \tag{1.58}$$

Precision measurements at the Z^0-pole and from low energy neutral currents provide stringent constraints on the $Z^0 - Z'$ mixing angle. Depending on the model parameters the constraints are below a few 10^{-3} [102, 103]. The new gauge boson Z_2 will therefore have approximately the same properties as the Z'. As input parameters we choose the physical masses, $M_{Z_1} = 91.187$ GeV, M_{Z_2} and the mixing angle, α_Z. From these together with the coupling constants, we extract both the value of $\tan\beta = v_u/v_d$ and the value of v_s. Note that as in [104] we adopt the convention where both λ and $\tan\beta$ are positive while μ (and then v_s) and A_λ can have both signs. From Eqs. (1.55) and (1.57),

$$\cos^2\beta = \frac{1}{\mathcal{Q}'_{H_d} + \mathcal{Q}'_{H_u}}\left(\frac{\sin 2\alpha_Z (M_{Z_1}^2 - M_{Z_2}^2) c_W}{v^2 g_1' g_2} + \mathcal{Q}'_{H_u}\right), \tag{1.59}$$

where $v^2 = v_u^2 + v_d^2$.

For each $U(1)'$ model the value of $\tan\beta$ can be strongly constrained as a consequence

[13] The impact of the kinetic mixing on the Higgs boson mass and on the Z' and DM phenomenology was examined in the $U(1)_{B-L}$ extension of the MSSM in [98–100] and recently for the UMSSM in [101].

of the requirement $0 \leq \cos^2\beta \leq 1$. For example for the $U(1)_\psi$ case with $\sin\alpha_Z > 0$ and $M_{Z_2} \gg M_{Z_1}$ the value of $\tan\beta$ has to be below 1. The reason is that for this choice of θ_{E_6} we have

$$\Delta_Z^2 = \frac{g_2 g_1'}{c_W\sqrt{24}}(\tan^2\beta - 1)v_d^2 < 0. \tag{1.60}$$

For other choices of parameters the value of $\tan\beta$ can be very large, $\mathcal{O}(100)$. Another interesting relation is found for the case of small mass mixing between Z^0 and Z' namely $\alpha_Z \ll \frac{v^2}{M_{Z_2}^2}$. In this limit β is determined from the $U(1)'$ charges only,

$$\cos^2\beta \simeq \frac{\mathcal{Q}'_{H_u}}{\mathcal{Q}'_{H_d} + \mathcal{Q}'_{H_u}}. \tag{1.61}$$

One might think that small values of $\tan\beta$ are problematic for the Higgs boson mass since the MSSM-type tree-level contribution becomes very small. However, as we will see below, additional terms to the light Higgs mass and especially their dependence on α_Z can help raise its value to 125 GeV.

Sfermions

The important new feature in the sfermion sector is that the $U(1)'$ symmetry induces new D-term contributions to the sfermion masses. These are added to the diagonal part of the usual MSSM sfermion matrix, and read

$$\Delta_F = \frac{1}{2}{g_1'}^2\mathcal{Q}'_F\left(\mathcal{Q}'_{H_d}v_d^2 + \mathcal{Q}'_{H_u}v_u^2 + \mathcal{Q}'_S v_s^2\right), \tag{1.62}$$

where $F \in \{Q, u, d, L, e, \nu\}$.

For large values of v_s the new D-term contribution can completely dominate the sfermion mass. Moreover this term can induce negative mass corrections, even driving the charged sfermion to be the LSP. Thus the requirement that the LSP be neutral (either the lightest neutralino or RH sneutrino) constrains the values of θ_{E_6} (unless one allows large soft masses for the sfermions). For example, for $-\tan^{-1}(3\sqrt{3/5}) < \theta_{E_6} < 0$, the corrections to the d-squark and to LH slepton masses are negative, while for $0 < \theta_{E_6} < \tan^{-1}(\sqrt{3/5})$ the corrections to the u-squark and RH slepton masses are negative. The latter implies that the u-type squarks (and in particular the lightest top squark) and the RH sleptons can be the Next-to-LSP (NLSP). Interestingly for $\theta_{E_6} = -\tan^{-1}(3\sqrt{3/5}) \approx -1.16$ the LH smuon/sneutrino can be sufficiently light to contribute significantly to the the anomalous magnetic moment of the muon and bring it in agreement with the data [105, 106].

Neutralinos

In the UMSSM the neutralino mass matrix in the basis $(\tilde{B}, \tilde{W}^3, \tilde{H}_d, \tilde{H}_u, \tilde{S}, \tilde{B}')$ reads ($c_\beta = \cos\beta$ and $s_\beta = \sin\beta$)

$$\mathbf{M}_{\tilde{\chi}^0} = \begin{pmatrix} M_1 & 0 & -M_{Z^0} c_\beta s_W & M_{Z^0} s_\beta s_W & 0 & 0 \\ 0 & M_2 & M_{Z^0} c_\beta c_W & -M_{Z^0} s_\beta c_W & 0 & 0 \\ -M_{Z^0} c_\beta s_W & M_{Z^0} c_\beta c_W & 0 & -\mu & -\lambda \frac{v_u}{\sqrt{2}} & \mathcal{Q}'_{H_d} g'_1 v_d \\ M_{Z^0} s_\beta s_W & -M_{Z^0} s_\beta c_W & -\mu & 0 & -\lambda \frac{v_d}{\sqrt{2}} & \mathcal{Q}'_{H_u} g'_1 v_u \\ 0 & 0 & -\lambda \frac{v_u}{\sqrt{2}} & -\lambda \frac{v_d}{\sqrt{2}} & 0 & \mathcal{Q}'_S g'_1 v_s \\ 0 & 0 & \mathcal{Q}'_{H_d} g'_1 v_d & \mathcal{Q}'_{H_u} g'_1 v_u & \mathcal{Q}'_S g'_1 v_s & M'_1 \end{pmatrix}. \tag{1.63}$$

Diagonalisation by a 6×6 unitary matrix $\mathbf{Z_n}$ leads to the neutralino mass eigenstates :

$$\tilde{\chi}^0_i = Z_{nij} \psi^0_j, \qquad i,j \in \{1,2,3,4,5,6\}. \tag{1.64}$$

The chargino sector is identical to that of the MSSM.

The LSP could be any combination of bino/higgsino/wino/singlino and bino'. However, as will be discussed in Section 5.3.2, the LSP is never pure bino', the pure bino and singlino tend to be overabundant while pure higgsino and wino lead to under abundance of DM.

The Higgs Sector

The Higgs sector of the UMSSM consists of three CP-even Higgs bosons $h_i, i \in \{1,2,3\}$, two charged Higgs bosons $H^\pm$ and one CP-odd Higgs boson A^0. Details about the Higgs potential, minimization conditions and mass matrices can be found in the Appendix A. The lightest Higgs is usually SM like but can be heavier than in the MSSM. Indeed the tree-level lightest Higgs boson mass squared, which can be approximated by [107]

$$\begin{aligned} m^2_{h_1,\,\text{tree}} \simeq\; & M^2_{Z^0} \cos^2 2\beta + \frac{1}{2}\lambda^2 v^2 \sin^2 2\beta + g'^2_1 v^2 \left(\mathcal{Q}'_{H_d} \cos^2\beta + \mathcal{Q}'_{H_u} \sin^2\beta\right)^2 \\ & - \frac{\lambda^4 v^2}{g'^2_1 \mathcal{Q}'^2_S} \left(1 - \frac{A_\lambda \sin^2 2\beta}{2\mu} + \frac{g'^2_1}{\lambda^2}\left(\mathcal{Q}'_{H_d} \cos^2\beta + \mathcal{Q}'_{H_u} \sin^2\beta\right) \mathcal{Q}'_S\right)^2, \end{aligned} \tag{1.65}$$

receives three types of additional contributions as compared to the MSSM. The first one proportional to λ is also found in the NMSSM, the second one comes from the additional U(1) gauge coupling g'_1 and the last arises from a combination of pure UMSSM and NMSSM terms. The first term is not expected to play as important a role as in the NMSSM since λ is small. This is because λ is inversely proportional to the vev of the singlet Higgs field which is in turn related to the mass of the new gauge boson, see Eqs. (1.51) and (1.54). The strong dependence of the latter two terms on the $U(1)'$ charges means that the size of the tree-level contribution to the Higgs mass will mostly depend on the value of θ_{E_6}.

Typically the Higgs spectrum will consist of a standard model like light Higgs, a heavy mostly doublet scalar which is almost degenerate with the pseudoscalar and the charged Higgs, and a predominantly singlet Higgs boson. The latter can be either h_2 or h_3, depending on the values of the free parameters of the model, in particular M_{Z_2} and A_λ. The singlet Higgs is never h_1 because its mass depends on v_s which is large due to the lower bound on M_{Z_2}.

1.4. Other Extensions of the Standard Model

An alternative, non-supersymmetric, way of addressing the hierarchy problem is the idea that the Higgs boson is in fact a composite state, arising from a new, strongly interacting sector. The picture is dual to scenarios of warped extra dimensions, and we will introduce both the concept and consequences of composite Higgs and extra dimension scenarios.

1.4.1. Composite Higgs

We consider a new composite sector that interacts weakly with the elementary sector (fermions and gauge bosons of the SM), and is described by an exact symmetry group $\mathcal{G}$ (containing $SU(2)_L \times U(1)_Y$). If spontaneous breaking of $\mathcal{G}$ to a subgroup $\mathcal{H}$ gives rise to at least four Goldstone bosons that can be arranged in a complex $SU(2)_L$ doublet, they can be identified with the Higgs doublet. In addition the interaction with the elementary sector can give rise to an explicit breaking of $\mathcal{G}$, and the now pseudo Goldstone bosons will develop a potential, thus enabling electroweak symmetry breaking. As the Higgs is now described as a pseudo Goldstone boson, it can be naturally light (and in particular lighter than other new bound states).

Moreover, fermion masses can be described as a result of partial compositeness, i.e. the physical states are linear superpositions of elementary and composite degrees of freedom [108]. The mass of the so-called partners arises from the confinement in the strong sector, and as a consequence they must be "vector-like", i.e. have the same quantum numbers for both chiralities, such that a Dirac mass term is allowed. We can then describe the hierarchy in quark masses as a consequence of partial compositeness, the light quark masses are explained by a tiny compositeness fraction, while a larger fraction gives rise to large Yukawa couplings for the top quark. In these scenarios the Higgs mass is related to the mass of the heavy resonances, which thus allows us to put an upper bound on the mass of the partners. While the exact bound will depend on the specific model, typically the top partner should have a mass $\lesssim 1$ TeV [109]. For a detailed introduction to composite Higgs models see [30]. LHC constraints on composite Higgs scenarios were recently summarized in [110].

1.4.2. Extra Dimensions

In models with extra dimensions the Planck scale M_P is in fact not a fundamental scale, but can arise from the electroweak scale by considering that gravity propagates in n additional, compactified extra dimensions. In the ADD model of large extra dimensions [111] we can relate the fundamental scale (i.e. the Planck scale in $4+n$ dimensions) to the 4 dimensional Planck scale via the radius R of the compactified dimensions as

$$M_P^2 \sim M_{P(4+n)}^{2+n} R^n. \tag{1.66}$$

The fundamental scale can be around the weak scale for large radius or number of extra dimensions. The most stringent constraints on ADD models come from astrophysical observations, and require $n \geq 4$ to solve the hierarchy problem [112].

An alternative approach is the Randall-Sundrum model of warped extra dimensions [113]. If the four-dimensional metric is scaled by a "warp" factor that rapidly changes as function of an additional dimension, we can address the hierarchy problem with a single, small extra

dimension. The metric is defined as

$$ds^2 = e^{-2kr_c\phi}\eta_{\mu\nu}dx^\mu dx^\nu + r_c^2 d\phi^2, \tag{1.67}$$

where k is a scale of order the Planck scale, x^μ the four-dimensional coordinates and $0 \leq \phi \leq \pi$ the coordinate of the extra dimension, and finally r_c the finite size of the extra dimension. ϕ is therfore an angular coordinate parametrizing the compactified fifth dimension. We assume that at the fixed points $\phi = 0, \pi$ branes supporting $(3+1)$-dimensional field theories are located. In this setup the observed 4-dimensional Planck scale M_P is related to the fundamental parameters as

$$M_P^2 = \frac{M^3}{k}[1 - e^{-2kr_c\pi}] \tag{1.68}$$

with M the fundamental Planck scale. Here the reduced 4-dimensional Planck scale shows only a weak dependence on r_c. On the other hand the observed symmetry-breaking scale v as well as masses are described as

$$m \equiv e^{-kr_c\pi}m_0. \tag{1.69}$$

Thus if $e^{kr_c\pi} \sim 10^{15}$ this mechanism produces TeV physical mass scales from fundamental mass parameters at the Planck scale. Moreover, we can explain the mass hierarchies observed between the different SM fermions, by considering different localization of the corresponding fields in the 5-dimensional bulk, see e.g. [114]. This class of models are typically referred to as bulk-RS models.

In models of warped extra dimensions the tensor and scalar fluctuations of the metric describe a graviton and radion field. The KK graviton $G_{\mu\nu}$ and the radion r can couple to a SM field (or a DM field) i via its energy-momentum tensor $T_i^{\mu\nu}$ (and its trace T_i), and in 4 dimensions the effective Lagrangian reads [115]

$$\mathcal{L}_{KK} = -\frac{c_i^G}{\Lambda}G_{\mu\nu}T_i^{\mu\nu} + \frac{c_i^r}{\sqrt{6}\Lambda}rT_i, \tag{1.70}$$

with Λ the compactification scale determined by the geometry. The coefficient $c_i^{G,r}$ is the overlap of wave functions in the bulk, and thus depends on the localization of the field i. Such models can be constrained by searching for resonances in collider experiments. A phenomenological study of the LHC constraints in a universal coupling scenario will be discussed in Chapter 6. Finally it is interesting to note that we can relate models of warped extra dimensions with strongly coupled conformal theories, see e.g. [116, 117].

A third class of models that is interesting here are models of Universal Extra Dimensions (UED) [118], where all SM fields can propagate in the bulk, and will give rise to so-called Kaluza-Klein resonances (or KK excited states). The momentum in each dimension is quantized and we can describe it by a new quantum number (KK number $j_i, i = 1, ..., \delta$, δ the number of extra dimensions). Momentum conservation in the extra dimensions then implies a conservation of the KK number. Similar to R-parity in SUSY this implies that KK excitations are produced only in pairs, and decay to a lightest KK excited state, which is thus a dark matter candidate. Generically the KK excitations at each level will be degenerate, with a mass given by $M_j = \frac{p_j}{R}$, where $p_j^2 = j_1^2 + ... + j_\delta^2$. However, loop corrections give rise to a mass splitting depending on the specific model description. Finally we note that while the 0-mode fermions are chiral, all KK excitations are vector-like. LHC constraints on the

Minimal UED Model were studied recently in [119, 120].

CHAPTER

TWO

LHC SEARCHES AND THEIR INTERPRETATION

In the introduction we have seen several models that can address open questions in particle physics, in particular supersymmetric models. We next want to study how we can test their predictions experimentally. Here we focus on direct searches in high-energy collision experiments, in particular at hadron colliders. For constraints from electroweak precision observables we refer the reader to [121], for constraints from flavor observables see e.g. [122].

We start by giving an overview of potential SUSY signals in a hadron collider, i.e. describing the main production and decay channels and the resulting signatures in Section 2.1. As a consequence of R-parity superpartners are always produced in pairs, and then cascade decay to the LSP. Due to their strong interaction, colored superpartners are expected to be produced abundantly in hadron collisions if they are light. Electroweak production can also be relevant, but only if the colored superpartners are much heavier. Therefore the decay chains of the originally produced particles typically lead to signatures with several hard jets and/or leptons, while the LSP is stable and escaping the detection.

We then briefly review different seach strategies in Section 2.2, in particular differentiating between resonance searches and searches with missing transverse momentum from new invisible particles, i.e. DM candidates. The interpretation of SUSY searches is discussed in detail in Section 2.3. As we will see, so-called simplified models are a particluarly useful tool in the interpretation of SUSY searches, and we will introduce them in some detail. A short review of the current experimental status from LHC search results will be given in Section 2.4.

Finally Section 2.5 gives an overview of methods for the reinterpretation of the search results in generic models, introducing in particular the toolchain required for reinterpretation based on event simulation. Moreover, alternative methods, that allow for a faster evaluation of collider constraints, are also described. They are based either on simplified model results, generally giving a conservative estimate of the constraints, or on machine learning techniques. Note that reinterpretation based on simplified model results will be introduced in detail in Chapter 3, where the tool SModelS is presented.

The interpretation of DM searches will be disucssed in the dedicated Chapter 6.

2.1. SUSY at Hadron Colliders

As the main focus of this work lies on SUSY phenomenology at the LHC we here give a short overview of sparticle prodcution and decay channels. We base our discussion on the MSSM, differences in extended models will be discussed explicitly in the dedicated sections.

2.1.1. Sparticle Production

We consider here the cross sections in hadron collisions in the parton model framework. The fractional longitudinal momentum x_a of a parton a (constituent of hadron A) is described by the parton distribution function (PDF), and will depend on the the squared four-momentum transfer Q^2 of the underlying elementary process. The PDF is thus a function $f_{a/A}(x_a, Q^2)$ and we can obtain a final cross section by convoluting the subprocess production cross section $d\hat{\sigma}$ with the parton distribution function,

$$d\sigma(AB \to cdX) = \sum_{a,b} \int_0^1 dx_a \int_0^1 dX_b f_{a/A}(x_a, Q^2) f_{b/B}(x_b, Q^2) d\hat{\sigma}(ab \to cd) \tag{2.1}$$

where A, B are the initial hadrons, c, d the produced superparteners and X any hadronic debris. The sum over a, b includes all initial partons producing a final state $c+d$. The PDFs are universal (they do not depend on the hard process considered) and can be obtained from fitting data from deep inelastic scattering experiments and then evolving them to higher scales. This QCD evolution of parton densities is described by the splitting equations introduced by Dokshitzer [123], Gribov and Lipatov [124], and Altarelli and Parisi [125], the so-called DGLAP evolution. Various PDF descriptions (using different datasets and approximations for the fits) are available, a standardised access is provided via the Les Houches Accord PDF (LHAPDF) library [126]. The hard scattering cross section $d\hat{\sigma}$ can be obtained via a phase space integral over the matrix element, that can be calculated from the Feynman diagrams. In the following we will only schematically discuss the main production processes and compare their cross sections in $\sqrt{s} = 13$ TeV proton-proton collisions. A detailed discussion, including Feynman diagrams and explicit calculations can be found in, e.g., [56].

Strong Production

If squarks and/or gluinos are light, the dominant production channels in hadron collisions are from strong production processes. The relevant reactions are

$$gg \to \tilde{g}\tilde{g}, \tilde{q}_i\tilde{q}_j^*, \tag{2.2}$$

$$gq \to \tilde{g}\tilde{q}_i, \tag{2.3}$$

$$q\bar{q} \to \tilde{g}\tilde{g}, \tilde{q}_i\tilde{q}_j^*, \tag{2.4}$$

$$qq \to \tilde{q}_i\tilde{q}_j. \tag{2.5}$$

Gluon fusion gives rise to gluino pair production either through t-channel exchange of a gluino or an s-channel gluon. Moreover, gluinos pairs are produced from $q\bar{q}$ either via an s-channel gluon or a t-channel (or u-channel) squark exchange. Similarly squark-antisquark pairs are produced via s-channel gluons from gluon or $q\bar{q}$ initial states, by the exchange of a t-channel squark (gluino) from a gluon ($q\bar{q}$) initial states, and from a 4-point gluon-squark interaction. In additon squark-squark pairs are produced from qq initial states through t-channel exchange of a gluino. Feynman diagrams for squark-(anti)squark production are shown in Figure 4.1, see also Figure 4.2 for the specific case of top squark production. Since the top quark PDFs are negligible, only stop-antistop production is relevant. Finally gluino-squark production from gluon-squark initial states is also possible, either through t-channel squark or gluino, or via an s-channel quark.

Note that in general all cross sections depend on both gluino and squark masses, as e.g.

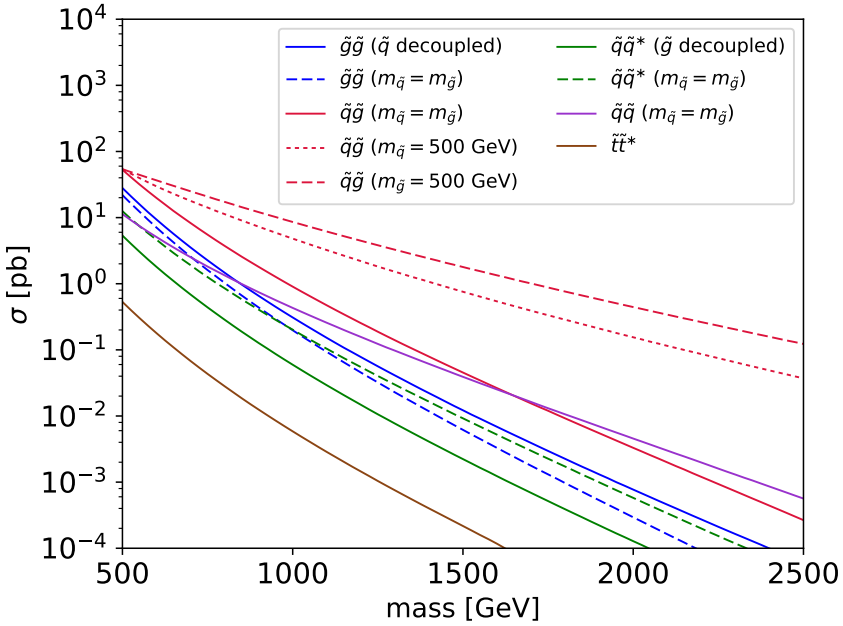

Figure 2.1.: Strong production cross secions at the LHC at $\sqrt{s} = 13$ TeV, obtained with NLLfast [127–134] and NNPDF [135] PDFs. The notation $\tilde{q}$ includes all squarks except stop.

t-channel squark exchange can be important in gluino pair production. An exception is the production of top squarks that at leading order depends only on the mass of the produced particle. A comparison of the various production cross sections is shown in Figure 2.1. While the gluino pair production cross section slightly drops if squarks are also light due to interference in the $q\bar{q}$ initiated production, the squark-antisquark production cross section is siginificantly increased profiting from enhancement of $q\bar{q}$ induced production in the presence of a light gluino. Moreover squark-squark and gluino-squark production are possible if both the gluino and the first generation squarks are light, significantly increasing the total SUSY cross section. Direct stop production is dominant only if other squarks and the gluino are much heavier, in particular because of the smaller number of degrees of freedom. Here all cross sections have been calculated at NLO+NLL (Next-to Leading Order + Next-to Leading-Log), and we note that K factors can be quite large. For example the correction from Leading Order (LO) to NLO gives K factors $K = \sigma_{NLO}/\sigma_{LO}$ up to a factor two for the processes considered in [128] and the K factor is further increased when adding NLL contributions [131] and NNLL contributions [136].

Elektroweak Production

Electroweakino pairs are produced in the following electroweak processes:

$$q\bar{q} \rightarrow \tilde{\chi}_i^+ \tilde{\chi}_j^-, \tilde{\chi}_k^0 \tilde{\chi}_l^0, \tag{2.6}$$

$$u\bar{d} \rightarrow \tilde{\chi}_i^+ \tilde{\chi}_k^0, \quad d\bar{u} \rightarrow \tilde{\chi}_i^- \tilde{\chi}_k^0, \tag{2.7}$$

where $i, j = 1, 2$ and $k, l = 1...4$ enumerates the charginos and neutralinos as a function of increasing mass. Chargino and neutralino pair production proceeds via Drell-Yan type scat-

tering, charginos are produced via virtual photons or Z bosons, neutralinos via Z bosons.[1] In addition t-channel exchange of squarks also contributes to chargino and neutralino pair production from $q\bar{q}$ initial states. Similarly chargino-neutralino production proceeds via $W^{\pm}$ bosons or t-channel squark exchange.

The direct production of bino-like neutralinos is typically negligible, because the production via Z boson is possible only via the higgsino admixture, and production via t-channel squark is also supressed because of the hypercharge coupling and potentially also by a large squark mass. On the other hand the direct production of winos or higgsinos can be important if they are much lighter than colored superpartners, as they couple to the electroweak gauge bosons. In particular wino production profits from the large isotriplet coupling to the $W^{\pm}$ bosons.

Similarly, sleptons are also produced in electroweak processes as

$$q\bar{q} \to \tilde{l}_i^+ \tilde{l}_j^-, \tilde{\nu}_l \tilde{\nu}_l^* \tag{2.8}$$

and

$$u\bar{d} \to \tilde{l}_L^+ \tilde{\nu}_l, \quad d\bar{u} \to \tilde{l}_L^- \tilde{\nu}_l^*. \tag{2.9}$$

Note that $i, j = 1, 2$ for mixed stau mass eigenstates, but only like-type (L or R) slepton pairs can be produced for the first two generations. Charged slepton pairs are produced via a virtual photon or a Z boson, sneutrino pairs via Z bosons, while $\tilde{l}_L^{\pm}\tilde{\nu}_l$ production proceeds via $W^{\pm}$.

We compare the cross sections in $\sqrt{s} = 13$ TeV proton-proton collisions in Figure 2.2, taken from [137]. All cross sections are calculated at NLO+NLL order. Weakino production cross sections are calculated according to [138, 139] and using CTEQ6.6 [140] and MSTW2008nlo90cl [141] PDFs, slepton production cross sections are calculated according to [142] using NLO CT10 [143] PDFs.

2.1.2. Sparticle Decays

We now summarise qualitatively the decay patterns in the R-parity conserving MSSM with a neutralino LSP $\tilde{\chi}_1^0$. In practice decay widths and branching ratios are calculated numerically using tools like SOFTSUSY [144] or SPheno [145].

Gluino Decays

Gluino decays proceed exclusively via squarks. If at least one squark is lighter than the gluino the two-body decay

$$\tilde{g} \to q\tilde{q} \tag{2.10}$$

is dominant. On the other hand, if squarks are heavier, the decay will generally proceed through off-shell squarks, resulting in the effective three-body decays

$$\tilde{g} \to q\bar{q}\tilde{\chi}_i^0, qq'\tilde{\chi}_j^{\pm}, \tag{2.11}$$

where $i = 1...4$ and $j = 1, 2$. The preferred channels are determined by the available phase space and by the couplings involved in the decay. For example third generation final states can be strongly favoured if the stop is the lightest squark and/or when the decay to

[1] Note that only the higgsino components couple the neutralinos to the Z boson, and consequently neutralino pair production via this process is relevant mainly for higgsino-like neutralinos.

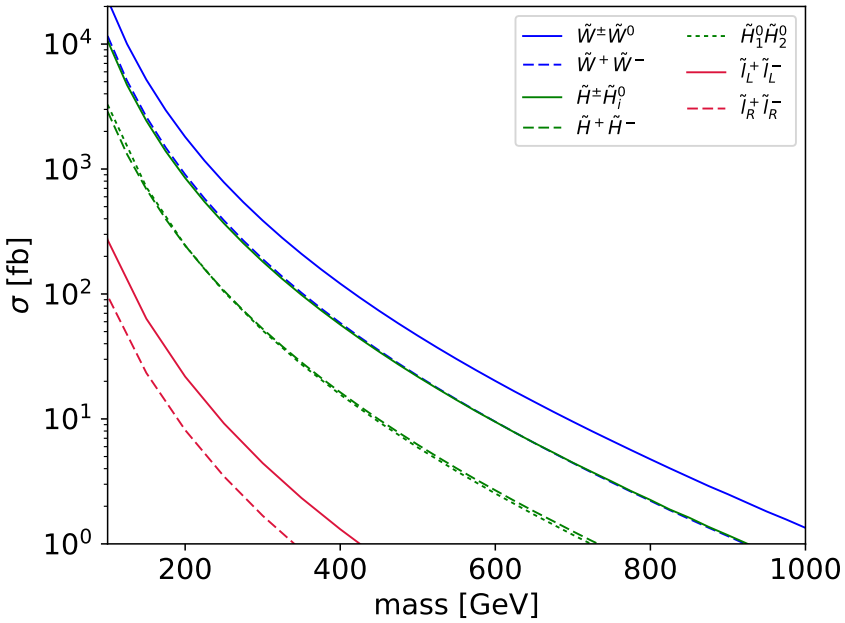

Figure 2.2.: Electroweak production cross secions at the LHC at $\sqrt{s} = 13$ TeV. H_i^0 includes the sum over $H_1^0 + H_2^0$, slepton cross sections are for one species of left- or right-handed sleptons.

a higgsino-like neutralino is kinematically allowed. Finally in a compressed scenario the radiative decay through a quark-squark loop is also relevant, i.e. $\tilde{g} \to g\tilde{\chi}_i^0$. Long-lived gluinos may appear in particular in split-SUSY type scenarios where sfermions are much heavier than the gauginos [146].

Sfermion Decays

Sfermions can decay via their gauge and Yukawa couplings as

$$\tilde{f} \to f\tilde{\chi}_i^0, \quad \tilde{f} \to f'\tilde{\chi}_j^{\pm}, \tag{2.12}$$

where $i = 1...4$, $j = 1, 2$, $f = l, \nu, q$, and the chargino couples up-type to down-type (s)quarks, and (s)leptons to (s)neutrinos. If the LSP is bino-like, decays to intermediat wino- or higgsino-like neutralinos/charginos are typically preferred when open. In particular left-handed sferminos strongly prefer decays into wino-like neutralinos and charginos because of the large gauge coupling, and third generation sferminos can have relevant branching fractions into higgsino-like states due to their sizable Yukawa couplings. Note that the prefered squark decay channel will impact also the gluino decay branching ratios via off-shell squarks. Moreover, if the gluino is lighter than the squark, the dominant squark decay is typically via strong interaction,

$$\tilde{q} \to q\tilde{g}. \tag{2.13}$$

For third generation squarks more complicated decay patterns are generally possible. For example a bottom squark can decay to a top squark and a W boson. Finally in scenarios with small mass difference between stop and LSP the flavor supressed decay $\tilde{t} \to c\tilde{\chi}_1^0$ or the four-body decay $\tilde{t} \to bff'\tilde{\chi}_1^0$ can be dominant.

Chargino and Neutralino Decays

We restrict the discussion to two-body decay modes. Three body decays via virtual bosons are relevant only if two-body decay modes are supressed or forbidden. We further assume that only the SM-like Higgs h is light enough to appear in the decays. Electroweakino decays can then be summarised as

$$\tilde{\chi}_i^0 \to Z\tilde{\chi}_k^0, W\tilde{\chi}_j^\pm, h\tilde{\chi}_k^0, l\tilde{l}, \nu\tilde{\nu}, q\tilde{q}, \tag{2.14}$$

$$\tilde{\chi}_j^\pm \to W\tilde{\chi}_l^0, Z\tilde{\chi}_1^\pm, h\tilde{\chi}_1^\pm, l\tilde{\nu}, \nu\tilde{l}, q\tilde{q}', \tag{2.15}$$

where $i = 2, 3, 4$, $j = 1, 2$, $k = 1, 2, 3$ ($k < i$) and $l = 1...4$. The relative importance of each decay channel will depend both on the mass spectrum and on the mixing patterns. In particular wino-like states typically decay via their weak coupling to LH sfermions if this decay is kinematically accessible, while higgsino-like states favor decays via third generation sfermions.[2] Decays via Higgs bosons are relevant mainly in decays involving a higgsino-like and a gaugino-like state. Finally decays via Z boson are important if one of the electroweakinos is largely higgsino-like, and decays via W if one of the electroweakinos is wino-like. Note that especially in a wino-like LSP scenario the mass difference between $\tilde{\chi}_1^\pm$ and $\tilde{\chi}_1^0$ can be very small, resulting in a long-lived chargino.

2.1.3. Signatures

We have seen that if gluinos and/or squarks are light they will be the dominant production channel. Moreover there are a large number of decay cascades that can be constructed. The relative importance of each channel will depend on the mass spectrum, as well as the mixing patterns. In general we expect SUSY events to be characterised by a number of hard jets and possibly leptons, and the invisible neutralino LSP escaping the detector. If the 3rd generation squarks are light (as we would expect from naturalness arguments) we further expect a number of b-tagged jets in the final state. Other signatures could include boosted top quarks or same-sign leptons. Qualitatively different signatures can arise in scenarios with non-prompt decays, leading e.g. to charged tracks of new heavy particles or displaced vertices. Experimentally most challenging are compressed scenarios, where for example the gluino is only slightly heavier than the LSP, thus all final state quarks will be very soft [147].

2.2. Searching for New Physics

One of the main objectives of the LHC experiments is the search for BSM physics. In particular the ATLAS and CMS experiments have an extensive program of so-called SUSY and Exotics searches. Here we roughly classify these searches into the following categories:

- Resonance searches
- Missing energy searches (SUSY and DM searches)
- Searches for displaced vertices or heavy stable charged particles (HSCP)

and we give a short introduction and example for each of these categories. Note that a number of searches do not fall in any of the above categories, for example searches for R

[2] In particular decays into stops are prefered, and for large $\tan\beta$ also decays into staus and sbottoms.

parity violating SUSY or searches for pair produced vector-like quarks decaying into SM particles. They are not relevant to the discussion in this thesis, and we refer the reader to [148] for a comprehensive summary of non-SUSY BSM searches at the LHC.

Resonance Searches

Resonance searches usually target the visible SM final states of a promptly decaying new state produced in the s-channel. Note that decays into additonal new states are not included here, in particular mediator decays into DM particles. The mass of the new state can be reconstructed by calculating the invariant mass of the decay products. A new resonance with narrow width will thus appear as a sharp peak in the invariant mass spectrum of the final state particles. A good example are the Higgs boson searches, e.g. we can observe the peak from the Higgs resonance in the di-photon invariant mass spectrum. Given the data and a background hypothesis, i.e. the invariant mass distribution expected in the SM, a statistical procedure such as the BUMPHUNTER algorithm [149] can assign a confidence level (CL) for the background only hypothesis, or for a given signal+background hypothesis. If the invariant mass distribution is in agreement with the SM prediction, the result thus constrains the maximum allowed signal strength of a considered new particle at a selected CL.

Particularly challenging is the search for a dijet resonance in the low mass region, since the jets are typically not hard enought to trigger event recording. However, new techniques have recently been developed to enable such searches. For example in [150] additional radiation from the initial state (initial state radiation, ISR), either an energetic jet or photon, produced in association with the new resonance, is used for triggering, and [151] is searching for light dijet resonances in the boosted regime using jet substructure techniques as well as ISR jets.

One might also construct a search for a new resonance decaying partly into invisible final states (i.e. neutrinos), by considering quantities sensitive to the resonance mass. The transverse momentum of a single invisible particle in a recorded event can be reconstruced, since initially the momentum in the transverse direction of the beams is essentially zero in LHC collisions. It is characterized by the so-called "missing transverse energy" E_T^{miss}, defined as the magnitude of the negative vector sum of all transverse momenta p_T observed in the event

$$\vec{p}_T^{\,miss} = -\sum_i \vec{p}_T^{\,i}, \tag{2.16}$$

where the sum i runs over all reconstructed particles in the event. We can further include the missing momentum in the definition of the transverse mass

$$m_T^2 = (\sum_j E_T^j)^2 - (\sum_j \vec{p}_T^{\,j})^2, \tag{2.17}$$

where now j sums over all considered reconstructed final states plus the missing momentum. The distribution of the m_T observable will then show a peak at the mass of the new particle.

Missing Energy Searches

Searching for models with a DM candidate implies that the new stable, invisible state will escape the detector, and similar to a neutrino final state, can be measured via the resulting transverse momentum imbalance, i.e. the E_T^{miss} observable. As described in Section 2.1, SUSY events typically have hard jets and/or leptons from the cascade decays of the initially produced superpartners, as well as E_T^{miss} from the escaping neutralinos. On the other hand

searching for DM that is directly produced, assuming either an effective contact interaction, or production via a new mediator particle is substantially different, as there are no cascade decay products in the events. We therefore further devide the missing energy searches into SUSY searches and DM searches.

Dark Matter Searches It is not obvious to search for DM direct prodcution at the LHC, since there are no visible final states, and therefore we can no longer construct the E_T^{miss} observable. However, this can be resolved if we consider DM production with an extra hard jet or electroweak boson, that might be emitted in particular from the initial state. These types of searches are generally referred to as "mono-X" searches. Here we take the example of the mono-jet search, relying on one (or more) hard jets that are produced in association with the DM production. Such additional jets are typically radiated from an initial state quark or gluon. If at least one of those jets has a large transverse momentum we can employ the E_T^{miss} variable, and we expect that signal events (i.e. DM+jets production) should have a high E_T^{miss}. On the contrary events with large E_T^{miss} and no lepton in the final state are rare in the SM, and we can define an event selection that supresses the SM background, but selects potential signal events with a high efficiency. In each of the so constructed signal regions (SRs) we can then compare the SM expectation to the number of experimentally observed events to make a statement about a possible DM signal. Due to the typically low number of expected background events, a dedicated statistical procedure, the so-called CL_s prescription, is generally used for limit setting in E_T^{miss} searches. A short description of the method is given in the Appendix B.

SUSY Searches R-parity conservation implies that superpartners can only be produced in pairs, followed by a cascade decay to the LSP. Assuming that all superpartners decay promptly, the signal events are typically characterised by multiple SM final state particles plus E_T^{miss} from the neutralinos escaping the detector. Signatures with non-prompt decays are quite distinct, as they would lead to either dispalced vertices or charged tracks of heavy new particles. We further specify that R-parity violating SUSY scenarios lead to very different signatures, since there is no new source of E_T^{miss} in the events. On the other hand the term "SUSY searches" can be misleading, as we can consider other BSM scenarios that will resemble SUSY scenarios (i.e. pair production followed by a cascade decay to a DM candidate). Thus while this class of searches was initially motivated by SUSY, their results apply to a more general class of models, for example also to UED scenarios.

Both ATLAS and CMS have designed a large number of SUSY searches, targeting different final states, and employing different strategies to supress SM background with respect to the considered SUSY signal. Typically these searches employ a "cut and count" strategy, where SRs are defined by a set of cuts on relevant kinematical variables, and in each SR we can compare the observed event number to the predicted number of SM background events. An important example, motivated in particular by naturalness, is the search for top squarks. In a minimal setup a $\tilde{t}\tilde{t}^*$ pair is produced, followed by a prompt decay of each stop into a top quark and a neutralino. The resulting $t\bar{t} + E_T^{\text{miss}}$ signature can be searched for in various final states, classified by the number of leptons, and using various variables in the SR definition. This example will be discussed in further detail in Section 4.2.

Non-prompt Decays

A new particle with a lifetime of the order of the detector scale would decay while traversing the detector, thus giving rise to a displaced vertex signature. Such scenarios can for example arise in the MSSM when the LSP is close in mass to the NLSP, e.g. the lightest chargino. On the other hand, if the lifetime is much larger than the detector scale the new particle will traverse the entire detector. If electrically charged, this new particle will thus resemble a heavy muon in the measured event. The situation is somewhat more complicated in the case of long-lived new particles with color charge, e.g. the gluino in the split SUSY scenarios [146]. The initially produced gluino will hadronise, forming charged or neutral "R-hadrons". The fraction of charged R-hadrons strongly depends on the unknown hadronisation model, and can have a strong impact on the interpreation of a search.

We note here that these types of searches have typically very low SM background, thus despite being experimentally very challenging they give strong constraints on scenarios with non-prompt decays. However, while the (re)interpretation is fairly straightforward for electrically charged particles traversing the full detector, it is delicate to (re)interpret searches for displaced vertices or R-hadrons.

2.3. Interpretation of SUSY Searches

As long as width and interference effects are not important, the interpretation of resonance searches is generally relatively straightforward and model independent. In contrast the situation is much more complex for DM or SUSY searches. For example the collider signatures of an MSSM scenario depend on a large number of free parameters. The number of parameters can be reduced when considering specific (minimal) SUSY breaking scenarios, that generally only have a small set of free parameters. Notably, the first LHC SUSY search results were interpreted in the cMSSM. However, in this way model specific patterns, e.g. fixing mass correlations between various particles, are introduced. Such an interpretation cannot be translated to alternative scenarios. Moreover, optimizing searches to test one such scenario implies that large parts of the more general MSSM parameter space will remain untested, even if they can in principle be constrained by the available data. To avoid theory prejudice in the design and interpretation of SUSY searches the notion of simplified models (or Simplified Model Spectra, SMS) has been introduced. In this section the underlying idea and the implementation of SMS for SUSY searches are presented. A similar approach for DM searches, so-called DM simplified models, will be discussed in Chapter 6.

2.3.1. On-Shell Effective Theories and Simplified Models

The general idea of SMS descriptions was proposed in the context of so-called On-Shell Effective Theories (OSETs) [152], motivated by the fact that SUSY searches should be sensitive in particular to the mass spectrum of the new particles responsible for a signal. An OSET is determined by the masses and gauge quantum numbers of the new particles, their production cross sections and their decay branching ratios into SM and new particles. An OSET can be illustrated as a set of Feynman-like diagrams where every particle is on-shell. The assumption is that the OSET description can describe the essential phenomenology of new physics in terms of only a few free variables that dominate the kinematic structure. While in general model specifics need to be known to accurately calculate the matrix element, in

particular to capture angluar distrubutions, it is assumed that the production is characterized only by a rate, this is indicated by a "blob" in the Feynman-like diagram.

Following the OSET idea the SMS description was developed [153–156] as a model independent approach to the interpretation of SUSY searches. The simplified models could be either described as OSETs, or based on an underlying Lagrangian description. In practice an underlying MSSM description has been commonly used. It is then assumed that only a few of the new particles are light, i.e. relevant to the experimental signature, and the masses and decay channels of these light new particles will determine the detector signature. This can be understood intuitively. For example in gluino pair production followed by a direct decay into quark pairs and the LSP, a large mass difference between the gluino and the LSP leads to very hard jets and large E_T^{miss} in the final state, making such signal events easy to detect. As the spectrum gets more compressed, signal events are more challenging to detect, as the final states will generally be soft. Moreover, the number of (b-tagged) jets and leptons in the final state will depend on the initially produced particles and their dominant decay channel.

Thus, instead of characterising the new physics model by a small set of high scale parameters, and introducing large model dependence, it is assumed that the signal can be parametrized it in terms of weak scale simplified models, where the masses and decay branching ratios are the free parameters. In addition to the decreased model dependence, the SMS description has the advantage that there is a clear relation between the free parameters and the detector signatures. In practice the decay branching ratios are often fixed to 100%, leaving only the masses as free parameters. A main advantage from an experimental point of view is that SMS allow to efficiently design and tune search strategies. Moreover the interpretation is straightforward and allows and easy comparison of different results.

A first set of simplified models relevant to the LHC searches was worked out in [157], and the approach was quickly adopted by the ATLAS [158] and CMS [159] collaborations. Moreover, as pointed out in [155], such a generic interpretation with minimal number of free parameters would be useful for the first characterization of a SUSY-like signal at the LHC. Otherwise, in the absence of any signal, the limits set on the SMS production cross sections (times branching ratio) can be used to constrain generic models predicting the same signature.

Simplified models have become a standard tool, allowing an efficient comunication between the experimental and theoretical physics community. On the one hand, they allow the experiments to design new searches inspired by a given theoretical model in a more generic fashion while presenting and comparing the results in a clear way. On the other hand they provide an efficient method for the theoretical community to understand the impact of a result on the parameter space of a given generic model without need for computationally expensive simulations or detailed understanding of each experimental analysis.

2.3.2. Simplified Models for SUSY Searches

We next give a more detailed description of SUSY-like simplified model interpretations for the example of top squark searches, i.e. the interpretation of a $t\bar{t} + E_T^{\text{miss}}$ search. The simplest SMS interpretation assumes that only the lighter top squark and the neutralino are important to the interpretation, while all other new particles are assumed to be irrelevant for the interpretation and are decoupled.[3] The main SUSY production channel is then stop

[3] They are assumed to be too heavy to be relevant at the given collision energy, both in the sense that they will not be produced or appear as on-shell states in the decay chain, and that they should not contribute to the production via t-channel exchange.

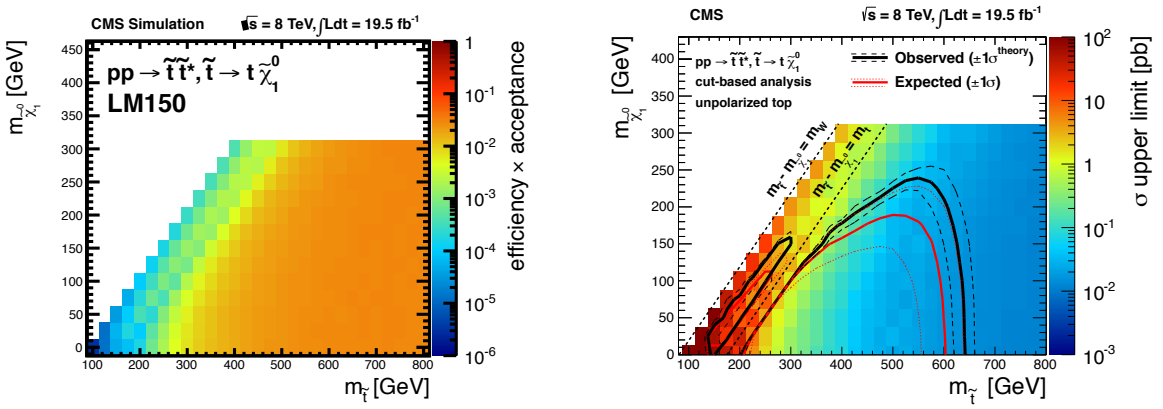

Figure 2.3.: Signal selection efficiency for the LM150 signal region (left) and $\sigma \times \mathcal{B}$ upper limit from the full cut-based analsyis (right) for the stop-neutralino simplified model interpretation of the CMS stop search [160].

pair production, and the only open decay channel for the stop will be $t\tilde{\chi}_1^0$. In the following we refer to this topology as the stop-neutralino simplified model. To first order the event kinematics will be determined by the masses of the stop and the LSP and the underlying MSSM structure.[4]

Assuming that the experimental observation is compatible with the predicted SM background, the result can be interpreted in terms of SMS cross section upper limits. For the simple example of a cut+count analysis the first step is the evaluation of the "signal selection efficiency",[5] i.e. the probablility for a signal event to pass all selection cuts, and therefore enter the count of a given signal region. In the stop-neutralino SMS the efficiencies are a function of only 2 free parameters, the stop and neutralino masses. For illustration Figure 2.3 (left), shows the efficiency in one of the SRs of the CMS search [160] as color code in the mass-vs-mass plane. Given the efficiency in this plane an upper limit on the signal cross section σ, or rather $\sigma \times \mathcal{B}$ with $\mathcal{B}$ the branching ratio into the considered final states, is evaluated using the CL_s prescription, see Appendix B. Limits are typically set at 95% CL. The limits from the cut-based analysis of [160] are shown as the color code of Figure 2.3 (right). For the simplified model with 100% $\mathcal{B}$ into this final state, this translates directly to a limit on the masses of the new particles, indicated by the "exclusion line" in Figure 2.3 (right).

However, the limit on $\sigma \times \mathcal{B}$ is valid in a more general setup, e.g. allowing for alternative decay channels of the stop, and will in general give a conservative estimate of the true exclusion. The reason for this is that the different simplified models (i.e. decay cannels) will likely contribute to the same signal region, increasing the total signal prediction. For the example of the $t\bar{t} + E_T^{\text{miss}}$ searche, if one chargino is lighter than the initially produced top squark the decay via an on-shell chargino will in general yield the same decay products as the direct decay to the neutralino LSP, but the selection efficiencies for this SMS depend on a third parameter, the chargino mass. The two simplified models are illustrated in Figure 2.4. The overall limit then depends on the two efficiencies, and on the relative branching ratio into the two allowed decay channels. Thus a more accurate estimate of the exclusion is obtained

[4] In fact the polarization of the top quark final state also affects the event kinematics, introducing a dependence on the stop and neutralino mixing matrix, see Section 4.2.1.

[5] This corresponds to $A \times \epsilon$, "Acceptance × Efficiency" in the language of ATLAS and CMS. In this work only the overall selection efficieny is important and we omit this additional distinction.

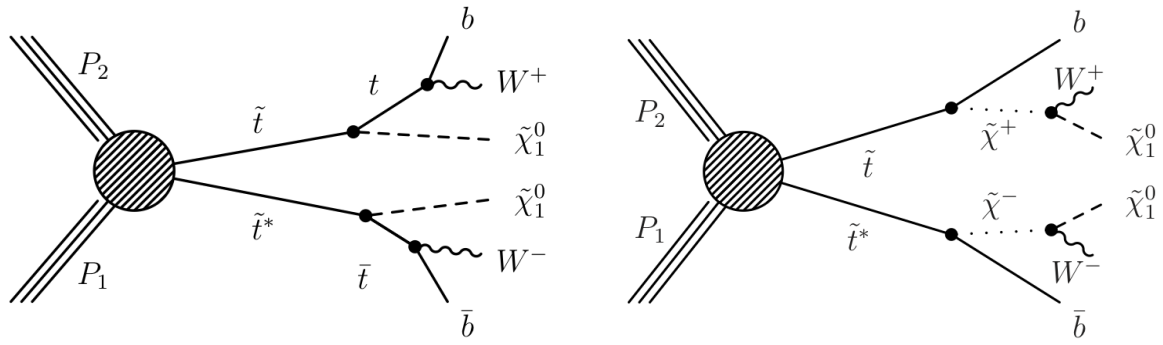

Figure 2.4.: Simplified model topologies from stop production followed by direct decay to neutralino (left) or via an intermedate chargino (right), taken from [160].

when considering the various relevant SMS at the same time, evaluating the appropriate efficiency for each component, and adding the individual signal predictions before comparing against a total limit on the number of signal events in the corresponding signal region. We will discuss this further in the following Chapters.

In the spirit of the original OSET proposal, the argument that the particle masses are the most relevant parameter can be extended, omitting also the dependence on the underlying MSSM Lagrangian description. Then the limits obtained in the SMS context should be a good approximation also in alternative scenarios leading to the same final state, for example the UED scenarios mentioned above. Thus under a set of assumptions a single SMS result can be used to constrain a broad class of generic models. These assumptions are further specified and exploited in Chapter 3, and some explicit tests are presented in Chapter 4.

2.4. Experimental Status

The current LHC results as presented at Moriond, March 2017, place strong bounds on superpartner masses in the SMS interpretations. In particular we can consider the mass bounds in the context of simplified models. The latest ATLAS results are summarized in Figure 2.5, taken from [161]. For scenarios with a light neutralino LSP, gluino masses up to about 2 TeV are already excluded, the exact limit depends on the specific SMS under consideration. Stop masses of about 1 TeV can be excluded in the stop-neutralino SMS. However, limits are less severe in more compressed regions of parameter space. As an example we show in Figure 2.6 some limits from CMS in the mass-vs-mass plane, taken from [162]. On the left limits for the stop-neutralino SMS are shown, where pair-produced top squarks decay directly into a neutralino LSP. On the right limits for a gluino-neutralino SMS are shown, where gluino pair production is followed by a three-body decay of each gluino into two light quarks and a neutralino LSP, and assuming that all squarks are heavy. We see in particular that limits on the stop mass in the stop-neutralino SMS vanish for neutralino masses above 500 GeV, and that the very compressed region ($\Delta(m) < 20$ GeV) was not tested for the gluino-neutralino SMS. Note however that this region might still be constrained, as discussed e.g. in the context of the radiative gluino decay in [163].

Finally we show in Figure 2.7 recent limits on non-promt decay scenarios. Over a large range of lifetimes chargino masses up to around 600 GeV can be excluded, see Figure 2.7 (left). It is also interesting to note that the limits on the gluino mass depend strongly on the modelling of the hadronisation, see blue triangles in Figure 2.7 (right). Nevertheless the mass limits do not strongly depend on it, and gluino masses up to about 1.5 TeV can be

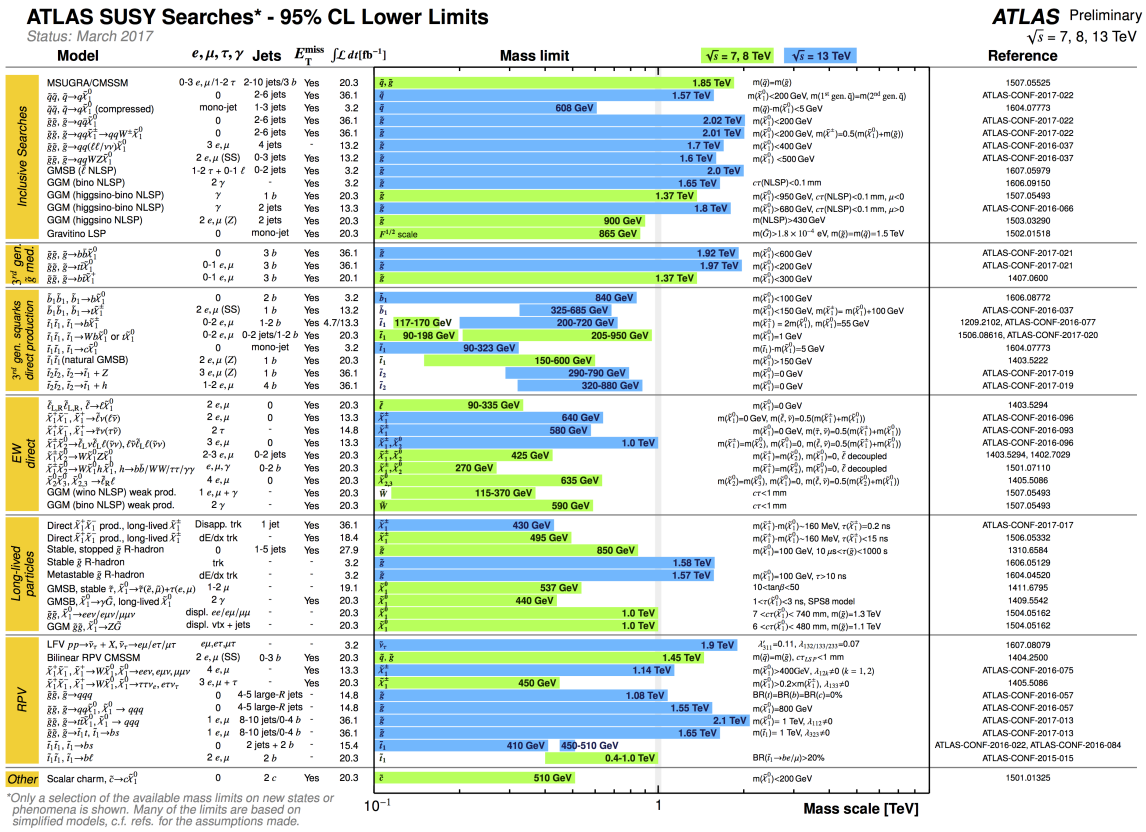

Figure 2.5.: Summary of ATLAS mass limits in the context of constrained or Simplified Model SUSY scenarios.

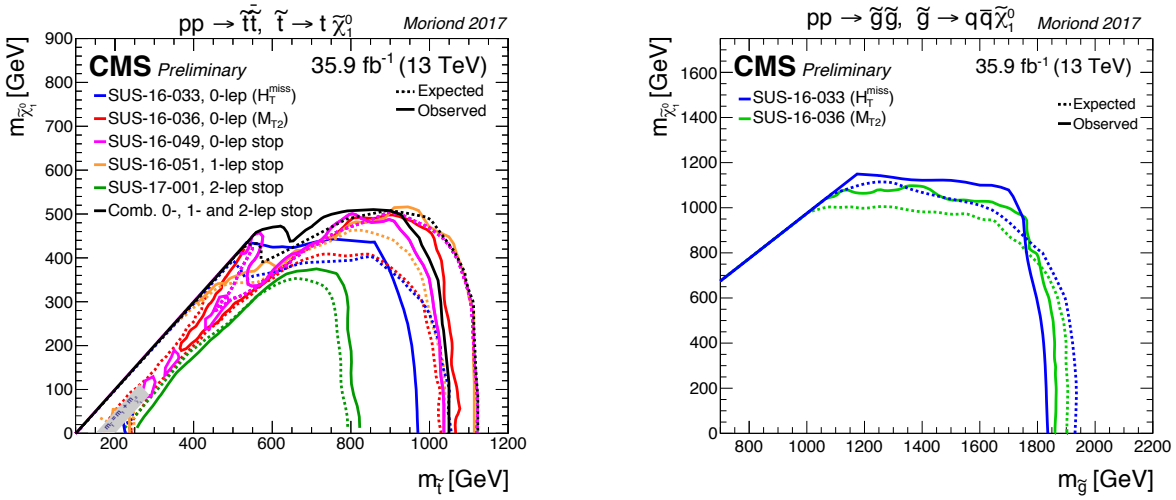

Figure 2.6.: Summary of CMS mass limits in the mass-vs-mass plane, in the context of stop (left) and gluino (right) simplified models.

excluded. This is in agreement with limits from ATLAS, see Figure 2.5. Note however that these limits rely on the gluino forming charged R-hadrons.

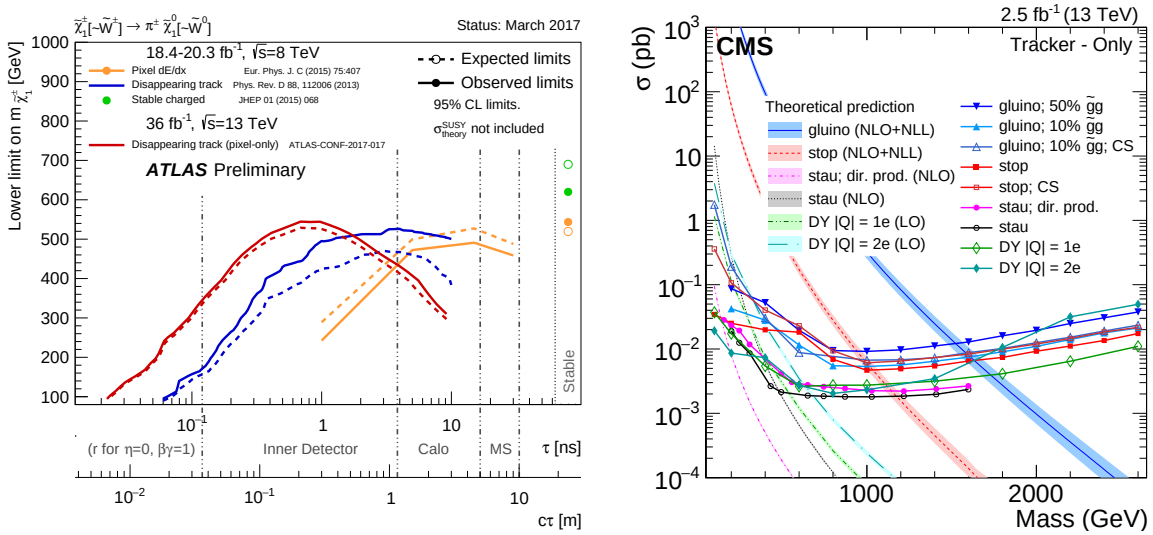

Figure 2.7.: Recent results from disappearing and charged track searches. Left: limits on the chargino mass as a function of its lifetime, taken from [161]. Right: limits on various scenarios, assuming the long-lived particle traverses the full detector, taken from [164].

2.5. Reinterpretation of Searches

Up to now none of the LHC searches for new physics observe any convincing evidence for a BSM signal. As a consequence the parameter spaces of many weak-scale BSM scenarios are already highly constrained. Some examples of current superpartner mass limits, in the context of simplified models, were given in Section 2.4. However, these mass limits are model dependent; they generally illustrate the maximum reach but may be significantly weaker in more generic scenarios.[6] Phenomenological studies are required to interpret the experimental results in such generic models, to identify the allowed parameter space and potential future probes. In practice such studies rely heavily on sophisticated software tools, which allow the computation of observables, and test them against experimental results.

Different approaches exist, the most comprehensive being a full modeling of the signal events and detector response. The detector objects can then be used to calculate the signal selection efficiency by applying the signal selection cuts used by the experimental analysis. Note that this limits the approach to cut-based analysis techniques, while for example multivariate analysis techniques [165] cannot be reproduced with the currently provided information. An overview of the required steps and some available tools for event simulation based reinterpretation is given in Section 2.5.1. The drawback of this approach is that it is very CPU-time consuming, and therefore not always suitable (in particular when studying large parameter spaces). Alternatively simplified model results typically provided by the experiments can also be used for reinterpretation. Decomposing a generic model into SMS components allows to directly use signal selection efficiencies or cross section upper limits to constrain the corresponding signature in the model. This is much faster, however it will generally give more conservative constraints, as it is limited by the availability of the required SMS results. We will only briefly discuss this in Section 2.5.2, as a more detailed description

[6] The reach may also extend beyond the SMS mass limits in alternative scenarios with increased cross section. Squark mass limits extend much further if the gluino is also light and mass limits on fermionic quark partners generally extend well above the limits on squark masses, see Section 4.1 and Section 4.2.

will be given in the context of the tool SModelS in Chapter 3. Finally, new approaches for fast evaluation of LHC constraints in large parameter spaces are being developped based on machine learning techniques, see Section 2.5.3.

Note that besides direct searches for new particles, precise SM measurements also provide important constraints on BSM scenarios. For example the recently presented CONTOUR framework [166], based on existing Rivet [167] implementations of SM measurements, allows systematic tests agains a large number of LHC measurements. Since the focus of this thesis is on BSM searches, we will not consider this approach here.

2.5.1. Recasting based on Event Simulation

Fully studying the collider pheonomenology of a given model (i.e. a Lagrangian description with a set of free parameters) requires the prediction of the visible signal as a function of the free parameters. Thus it is necessary to calculate both the total signal cross section and the signal selection efficiency. Modern tools allow to study the collider phenomenology of a generic model starting from the Lagrangian description, up to the evaluation of signal selection efficiencies, in an automatised fashion. Given the complexity of the problem, each tool focuses on solving only a specific task. The full picture is then obtained by linking them appropriately. This linking is facilitated in a straightforward fashion owing to standardised formats, allowing to easily pass information from one step to the next. We briefly summarise this toolchain below, giving also some of the relevant tools and standard formats needed for each step.

- The Lagrangian can be implemented using e.g. LanHEP [168], FeynRules [169], or SARAH [170]. These tools will return model files in a standardised format (such as the in UFO format [171]), containing the particles and their quantum numbers (spin, color, electric charge, ...), the free parameters (masses, coupling constants, ...) and an explicit description of the interactions in terms of vertex descriptions. A large database of existing model implementations can be found at [172].

- Specialised tools for the calculation of mass spectra and decay tables from the free input parameters can be useful if high precision is important, for example SOFTSUSY [173], SuSpect [174] and SPheno [145] for SUSY models. These tools return parameter files in the standardised SLHA format [57].

- The Monte Carlo (MC) event generator MadGraph5 [175] takes UFO model files and automatically generates matrix elements for a given process in any BSM model. Other tools follow a similar approach, in particular CalcHEP [176] is used inside `micrOMEGAs`. Note however that CalcHEP is limited to LO calculations, while NLO calculations are also possible in MadGraph5. The tools then calculate the cross sections and simulate events for a given set of input parameters, specified either in a tool specific parameter card, or in SLHA format. Events are simulated at parton level, employing a selected implementation of the PDFs, typically via the LHAPDF interface [126]. The standardised format for parton level events is called LHE [177].

- Higher order inclusive cross sections have been calculated and tabulated for processes of particular interest, e.g. gluino and squark production cross sections at NLO+NLL accuracy can be obtained from NLLfast [127–134], and recently also at next-to-NLL accuracy (NNLL) via NNLLfast [136]. It is often assumed that the kinematic distributions are not significantly altered by the higher order corrections, and we can

rescale LO cross sections with a global k-factor from inclusive higher order calculations. While this is generally a valid approximation in the context of analysis reinterpretations, higher order event simulations may be necessary in precision studies, see for example [178].

- To get realistic full events from the parton level simulations, parton showering, hadronisation and particle decays have to be modeled, using tools like PYTHIA [179] or HERWIG [180]. Moreover it might be neccesary to simulate events with a variable number of additional hard jets, e.g. from initial state radiations. The hard jets are best simulated at matrix element level, while soft radiation is best modeled through parton shower algorithms. Dedicated algorithms have been developed to merge the different samples and add parton showering on top without double counting. A comparative study of various algorithms was presented in [181]. Hadronised events are typically stored in the STDHEP [182] or HEPMC [183] format.

- Analysis objects (jets, leptons, E_T^{miss},...) are obtained by simulating the detector response, using for example the fast detector simulation framework DELPHES [184] and clustering of jets. A number of jet finding algorithms are implemented in FASTJET [185]. Given the analysis objects, analysis cuts can be applied to the simulated signal events to obtain the corresponding signal selection efficiency. Several tools are available to facilitate the implementation of analysis object selection and analysis cuts, e.g. CHECKMATE [186, 187], MADANALYSIS5 [188, 189] or RIVET [167]. Both CHECKMATE and MADANALYSIS5 use the DELPHES framework for detector simulation. RIVET originally collected only unfolded data that can be directly compared to simulated events.[7] From version 2.5 onwards it also allows the user to include detector effects through smearing and efficiency functions. These analysis recasting tools generally come with a database of already implemented analyses that is readily extendible, see [189, 190].

Running this toolchain will provide the user with the number of predicted signal events, the expected signal yield n_{signal}, calculated as the product of total cross section, signal selection efficiency, and the integrated luminosity analysed by the considered search. Moreover the number of expected (SM background) and observed events, as well as the error on the number of expected events are provided by the experimental collaboration. It is thus up to the user to apply a statistical procedure to interpret the result An implementation of the standard CL_s procedure is included in CHECKMATE and MADANALYSIS5, and limits are typically evaluated at the 95% CL. Commonly the ratio $r = \frac{n_{signal}}{n_{UL}^{95}}$ is quoted, where n_{UL}^{95} is the 95% CL upper limit on the number of signal events, as evaluated with the CL_s method. Thus if $r > 1$ the parameter point can be considered excluded at 95% CL.

While a number of tools are required when studying the collider phenomenology through this event simulation based recasting approach, we note that this is in fact more and more opaque to the user. The latest CHECKMATE version [187] integrates event simulation in MADGRAPH5 and PYTHIA as well as the DELPHES detector simulation. Similarly, MADANALYSIS5 includes an interface to the DELPHES detector simulation, and can be accessed from inside MADGRAPH5. Thus it suffices to supply the UFO and parameter (or SLHA) files to run the remaining toolchain through a single interface.

[7] SM measurements are typically unfolded, and the results can therefore be compared directly to simulated events, without any detector simulation. This is however not viable in BSM searches.

2.5.2. Reinterpretation with Simplified Models

The experiments provide an interpretation of most SUSY searches in the context of simplified models, publishing in particular also efficiency and/or upper limit maps in the mass-vs-mass plane of the considered SMS (see Figure 2.3). In Section 2.3.2 we argued that these efficiencies or upper limits to good approximation remain valid in a generic model predicting the same signature as the simplified model, and $\sigma \times \mathcal{B}$ into this topology can be compared directly to the upper limit found for the given mass combination. Alternatively efficiency maps may be used to directly compute the visible cross section, and thus the predicted yield, without any event and detector simulations.

This simple idea gets quickly complicated in realistic models with a multitude of relevant production and decay channels. Therefore specialised tools have been developed to systematically decompose generic models into SMS components, keeping track of the BSM masses and $\sigma \times \mathcal{B}$ for each topology, and comparing them to the experimental limits. This type of procedure has been implemented for the interpretation of generic $\mathbb{Z}_2$ symmetric BSM scenarios in SModelS [191, 192], for MSSM scenarios in FastLim [193], and for scenarios with extra heavy quarks in XQCAT [194]. A detailed description of the relevant concepts and general working principle used inside SModelS will be given in the next Chapter.

2.5.3. Alternative Approaches

Alternative ideas for the fast evaluation of collider constraints on BSM parameter spaces relying on machine learning techniques have been proposed recently. While the training and testing of these methods require considerable CPU time, single points can afterwards be tested within a few milliseconds.

Several highly efficient methods have been presented. For example SUSY-AI identifies points as excluded/allowed in the 19-parameter pMSSM [195], based on a neural network trained on a large number of parameter points tested against ATLAS SUSY searches in [196]. In [197] a method for the prediction of signal region selection efficiencies was presented in the context of natural SUSY. SCYNet [198] is using a neural network to predict a profile likelihood ratio (χ^2) from the model parameters, and the 11-parameter pMSSM was studied as a showcase.

Note that in general these tools rely on MSSM input parameters and cannot be used to constrain alternative models. An exception is SCYNet, that also considers a method to first re-parametrise the model parameters in terms of model-independent objects directly related to the signature. Similar to the simplified model approach the new physics model is then characterised through production cross sections, particle masses and decay branching ratios. The run time is somewhat longer in this case, in particular since cross section calculations have to be performed. The resulting neural network can then be used to test a wider class of new physics models. This generic application is however somewhat limited, as in general the most relevant regions of the re-parametrised parameter space may not be covered after training the network on a different model.

CHAPTER

THREE

SMODELS

Various approaches to the reinterpretation of LHC search results have been introduced in Section 2.5, in particular also the reinterpretation based on simplified models. It allows a fast, but conservative, evaluation of constraints from collider searches, and is therefore particularly interesting for the identification of allowed and excluded regions of large parameter spaces, or to quickly discard excluded parameter points before performing more detailed studies. Moreover it allows to easily identify the most relevant searches and signatures, and may even point to relevant signatures not yet considered by the experiments. Another advantage is the availability of a large number of SMS results, as they are the primary interpretation of ATLAS and CMS SUSY searches.

When describing simplified models in a generic fashion, they can be used to test a large class of BSM models (not restricted to SUSY models). In particular the tool SModelS provides a generic decomposition procedure, matching full models (for example an MSSM parameter point) onto generalised simplified models without any explicit model dependence, and can be used for any BSM model with a $\mathbb{Z}_2$ symmetry. In addition to the decomposition procedure, SModelS provides an automated matching of the SMS components to the relevant constraints in the included database. Moreover, it provides detailed information of relevant topologies that are not covered by any result in the database.

In this Chapter we first introduce the main concepts relevant to the SModelS description in Section 3.1. In particular the SModelS language to describe SMS topologies in a model independent fashion is introduced, and the different types of results (efficiency and upper limit map type results) are described. The decomposition procedure and the matching to the experimental result database work is then presented in Section 3.2. A short summary of how to run SModelS, via the executable *runSModelS.py* or through an interface to `micrOMEGAs` , is given in Section 3.3, including a short description of the SModelS output. Note that detailed instructions and descriptions of the main run parameters can be found in the Appendix C. Finally some concluding remarks are presented in Section 3.4.

3.1. General Concepts

SModelS maps a given BSM model onto SMS topologies via a generic decomposition procedure. The concept is completely general, but for the time being the procedure is limited to BSM models with a $\mathbb{Z}_2$ symmetry. In order not to restrict the procedure to the MSSM a generalised SMS description is used, omitting any implicit model dependence. The decomposition procedure as well as the mapping to a model independent description rely on

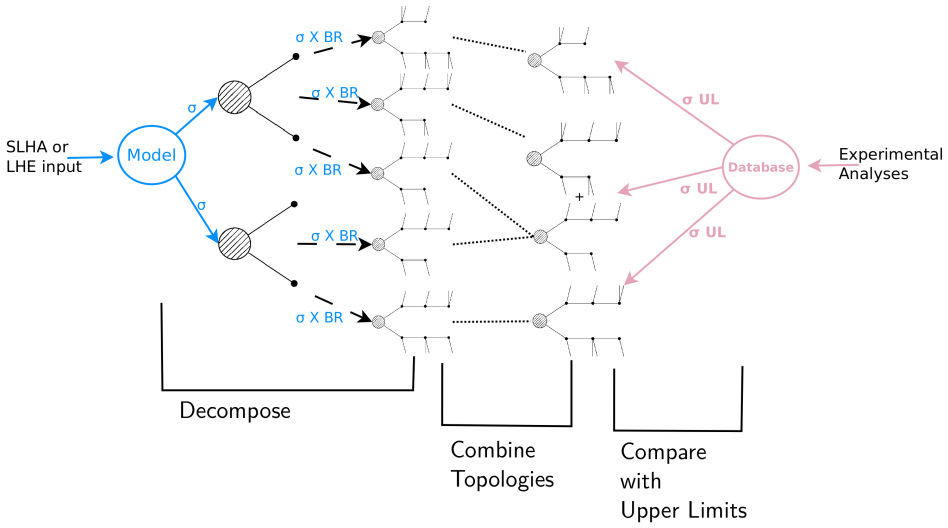

Figure 3.1.: SModelS working principle for testing against cross section upper limits.

a set of generalisations, that are assumed to hold to good approximation for the purpose of calculating signal selection efficiencies. In the following we will refer to this concept as the "SMS assumption".

The relevant generalisations have been introduced in Section 2.3, and can be summarised as follows. First, the production process is not taken into account, and only on-shell particles are considered in cascade decays. Virtual particles are replaced by an effective vertex, where only the on-shell decay products are specified. Additionally, new states are described only by their mass, neglecting all other quantum numbers. The validity of these generalisations will depend on the concrete model under consideration, as well as details of the experimental search. In particular, an inclusive cut-and-count search should be less sensitive to the SMS assumption than a shape-based analysis or a multivariate analysis.[1] Finally it should be noted that the SMS approach is only valid within the narrow width approximation. Generally, it is the responsibility of the user to apply SModelS only to models and experimental results for which the SMS assumption is approximately valid. The validity has been studied for several topologies and alternative scenarios, see Chapter 4.

Under the SMS assumption the BSM model properties are reduced to its mass spectrum, production cross sections (σ) and decay branching ratios ($\mathcal{B}$). With this knowledge we can decompose the full BSM signal in a series of independent signal topologies with their specific weights given by the corresponding production cross section times branching ratio ($\sigma \times \mathcal{B}$). Such a decomposition is extremely helpful to cast the theoretical predictions of a specific BSM model in a model-independent framework, which can then be compared against the experimental limit on this $\sigma \times \mathcal{B}$. A schematic view of the working principle is given in Figure 3.1, for the example of testing model predictions against cross section upper limits. When using efficiency maps the appropriate efficiencies have to be multiplied before combining topologies.

The first step is to compute all signal topologies appearing in the full model and their respective weights, $\sigma \times \mathcal{B}$. Since here we only consider models with a $\mathbb{Z}_2$ symmetry the possible signal topologies will always arise from pair production of new $\mathbb{Z}_2$-odd particles, which decay as $P \to P' + \mathrm{SM}$ particles, where P and P' are the parent and daughter BSM

[1] The analyses used when running SModelS can be selected via the parameter file described in the Appendix C.1. It is up to the user to select only analyses that apply to the given scenario.

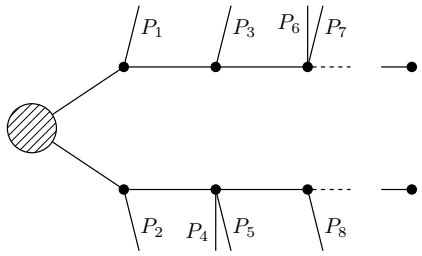

Figure 3.2.: The general type of SMS topology considered in SMODELS. The P_i label the SM final state particles. The end of each decay chain is always the lightest $\mathbb{Z}_2$-odd particle which is stable.

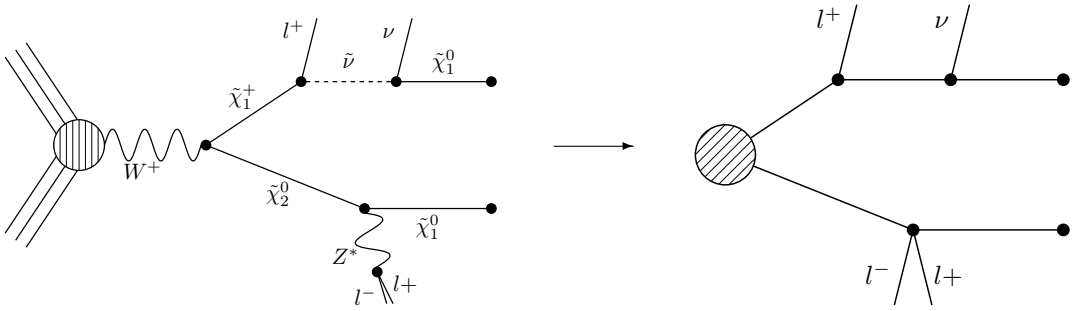

Figure 3.3.: A full model diagram (left) and its SMS equivalent topology (right).

particles, respectively. Hence all topologies will be of the form represented in Figure 3.2, which shows the production of the initial pair of BSM states (represented by a circle with two outgoing legs) and their subsequent cascade decays, where all particles appearing in the SMS topology, both $\mathbb{Z}_2$-even and $\mathbb{Z}_2$-odd, are on-shell. The case of off-shell decays is always included as 3-body decays, with no mention to the off-shell states. Therefore all the relevant information (in the SMS framework) of such a diagram can be reduced to three main objects:

- the diagram topology: number of vertices and SM final state particles in each vertex;
- the masses (mass vector) of the $\mathbb{Z}_2$-odd BSM particles appearing in the diagram;
- the diagram weight ($\sigma \times \mathcal{B}$).

Non-SM $\mathbb{Z}_2$-even particles are also considered as final states, but the corresponding topologies will not be constrained as there are no applicable results in the SMODELS database. The reduction of a particular process to its equivalent SMS topology is illustrated in Figure 3.3.

The next and more involved step is to confront the theoretical predictions obtained from the decomposition with the experimental constraints. For that it is necessary to map the signal topologies produced in the decomposition to the SMS topologies constrained by data. For some experimental analyses this is a trivial matter, since they provide an upper limit for a single topology cross section as a function of the relevant BSM mass vector. Examples are constraints on squark pair production, with $\tilde{q} \to q + \tilde{\chi}_1^0$, which give an upper limit on $\sigma \times \mathcal{B}$ as a function of $(m_{\tilde{q}}, m_{\tilde{\chi}_1^0})$, or gluino pair production, with $\tilde{g} \to t\bar{t} + \tilde{\chi}_1^0$, which limit $\sigma \times \mathcal{B}$ as a function of $(m_{\tilde{g}}, m_{\tilde{\chi}_1^0})$. However it is often the case that the experimental analysis does not constrain a single topology but rather a sum of several topologies, assuming a specific relative contribution from each of them. As an example, consider the slepton pair

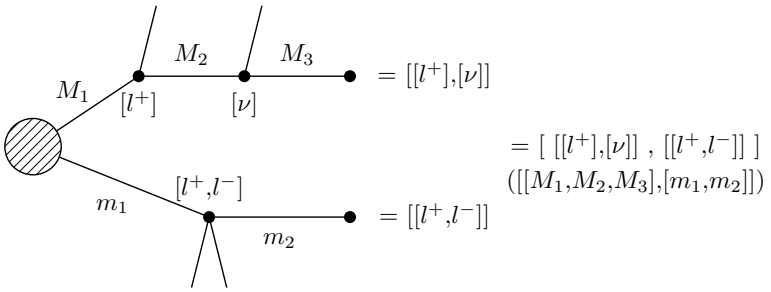

Figure 3.4.: The element labeling scheme adopted in SModelS applied to an example diagram. In parenthesis we show the respective mass vector for the diagram.

production limits, where the interpretation constrains the sum over final state lepton flavors (e's and μ's) under the assumption that each flavor contributes 50% to the signal and that selectrons and smuons are mass degenerate, $(m_{\tilde{e}}, m_{\tilde{\chi}_1^0}) = (m_{\tilde{\mu}}, m_{\tilde{\chi}_1^0})$. In order to apply this experimental constraint to the signal topologies obtained from the decomposition, it is necessary to combine all topologies with a single lepton being emitted in each branch and which have the same mass vector. Moreover, in order for the experimental constraint to be valid, it is necessary to verify the analysis conditions: topologies with e's and μ's contribute equally to the final theoretical prediction ($\sigma \times \mathcal{B}$). Finally when all signal topologies are combined according to the assumptions of each experimental result, the resulting theoretical predictions for the cross sections of the combined topologies can be directly compared to the experimental upper limits. Thus it can be decided whether a particular parameter point (a particular BSM spectrum) is excluded or not by the available SMS results.

3.1.1. Element Description

For an automatised decomposition procedure, we describe topologies in a text based language. We choose to represent the topology structure through nested brackets. Because of the assumed $\mathbb{Z}_2$ symmetry each topology will be described by two branches, each branch describing the cascade decay of one of the initially produced particles. The two branches are arranged in a so-called element in a first bracket, [branch1, branch2]. The branches are sorted according to their size, i.e. by the number of vertices and by the number of outgoing final state particles in each vertex. Each branch is described by a number of vertices, where each vertex describes the decay of a $\mathbb{Z}_2$-odd state into $\mathbb{Z}_2$-even particles (the final state particles) and another $\mathbb{Z}_2$-odd particle (either an intermediate state or if it is stable and neutral it is considered a E_T^{miss} final state). The vertex structure of one branch is again described via nested brackets, e.g. branch1 = [vertex1, vertex2] = [[final state particles in vertex1],[final state particles in vertex2]], where each vertex contains a list of all outgoing $\mathbb{Z}_2$-even particles in that vertex. Vertices are ordered according to the decay topology, final state particles are sorted alphabetically. Note that the E_T^{miss} final state in the last decay vertex is always implied and not listed explicitly in this description. The intermediate states are described by their mass, and in addition to the vertex information, an element contains the mass vectors of the two branches. An illustrative example is shown in Figure 3.4. Finally an element may also holds information about its corresponding weight, i.e. cross section times branching ratio.[2]

[2] An element from the decomposition holds mass vector and weight information. The element description is also used to describe database entries, in that case it does not hold mass and weight informations.

We further define the notion of "topologies" as the element topology, a description in terms of vertex structure only, i.e. the number of vertices and the number of outgoing final state particles in each vertex. Inside SModelS elements are grouped according to their topology.

3.1.2. Database Definitions

The SModelS database collects experimental results of SUSY searches from both ATLAS and CMS. Starting with version 1.1, the SModelS database includes two types of experimental constraints:

- Upper Limit (UL) constraints: based on ($\sigma \times \mathcal{B}$) limits for the simplified models provided by the experimental collaborations;
- Efficiency Map (EM) constraints: constrains the total visible signal ($\sum \sigma \times \mathcal{B} \times \epsilon$) in a specific signal region. Here ϵ denotes the signal selection efficiency as defined in Section 2.3.2. These are either provided by the experimental collaborations or computed by theory groups.

Upper Limit Type Results

UL experimental results contain the experimental constraints on the cross section times branching ratio ($\sigma \times \mathcal{B}$) from simplified model interpretations from a specific experimental publication or preliminary result. These constraints are typically given in the format of Upper Limit maps, which correspond to 95% CL upper limit values on ($\sigma \times \mathcal{B}$) as a function of the BSM masses.[3] An example is shown in Figure 2.3 (right).

The UL values usually assume the best signal region (for a given point in parameter space), a combination of signal regions or more involved limits from other methods. Hence, for UL results from one analysis there is a single UL map for each simplified model considered in the analysis. The simplified model is specified as an upper limit constraint, i.e. an element or a sum of elements. The sum of elements indicates that the sum of the weights of the respective elements is constrained by the result. Note that the sum can be over particle charges, flavors or more complex combinations of elements. However, almost all experimental results sum only over elements sharing a common topology.

In some cases the UL constraints assume specific contributions from each element. When applying these constraints to general models, one must also verify if these conditions are satisfied. For example, leptonic searches often assume equal branching ratio into electrons and muon. Muons typically have higher selection efficiencies, thus the resulting limit is only valid if they contribute at least half of the cross section in the general model. On the other hand if the muon contribution is dominant the limit gives a conservative estimate and can be used to constrain the model. In several cases it is desirable to relax the analysis conditions, so the analysis upper limits can be applied to a broader spectrum of models. The departure from the exact condition can then be properly quantified and one can decide whether the analysis upper limits are applicable or not to the model being considered. Concretely, SModelS computes for each condition a number between 0 and 1, where 0 means the condition is exactly satisfied and 1 means it is maximally violated. Allowing for a 20% violation of a condition corresponds approximately to a "condition violation value" (or simply condition value) of 0.2.

[3] SMS results are typically presented in mass-vs-mass planes. Results for topologies with more than two mass parameters can be used if interpolation between several planes is possible.

Efficiency Map Type Results

Unlike UL-type results, the main information held by EM results are the efficiencies for simplified models, see Figure 2.3 (left). These may be provided by the experimental collaborations or independently computed by theory groups. An EM lists the signal selection efficiency in one SR as a function of the BSM masses. Additional information, such as the luminosity, number of observed and expected events, etc is also stored in an EM-type result. An important difference between UL-type results and EM-type results is the existence of several signal regions, which in SModelS are mapped to data sets. While UL-type results contain a single data set, EM results hold several data sets, one for each signal region. Each data set contains one or more efficiency maps, one for each element or sum of elements. In order to use a language similar to the one used in UL-type results, the element (or elements) to which the efficiencies correspond to are still called constraint.

TxName Convention

Since using the bracket notation to describe the simplified models appearing in the upper limit or efficiency maps can be rather lengthy, it is useful to define a shorthand notation for the constraints. SModelS adopts a notation based on the CMS SMS conventions, where each specific constraint is labeled as *T<constraint name>*, which we refer as *TxName*. A complete list of TxNames and their translation to SModelS bracket notation, as well as graphical representation, can be found in [199].

3.2. Detailed Description

3.2.1. Input Files

The main input for SModelS is the model definition, which can be given in the two following forms:

- SLHA file containing masses, branching ratios and cross sections for the BSM states
- LHE file containing parton level events

The SLHA format is usually more compact and best suited for supersymmetric models. On the other hand, an LHE file can always be generated for any BSM model (through the use of your favorite MC generator).[4] In this case, however, the precision of the results is limited to the MC statistics used to generate the file.

For an SLHA input the production cross sections for the BSM states also have to be included in the file as SLHA blocks, according to the SLHA cross section format [201]. For the MSSM and some of its extensions, they may be calculated automatically using Pythia [202, 203] and NLLfast [127–134] through a SModelS interface.

For an LHE input the total production cross section as well as the center-of-mass energy should be listed according to the standard LHE format [177]. Moreover, all the $\mathbb{Z}_2$-even particles should be set as stable, since in SModelS they are effectively considered as final states. As mentioned above this also includes any non-SM $\mathbb{Z}_2$-even particle. When generating the events it is also important to ensure that no mass smearing is applied, so the mass values for a given particle are the same throughout the LHE file.

[4] Generic models may also be described in an SLHA-type format, as done for example in SLHAplus [200].

Besides information about the masses and branching ratios, the user must also define which particles are $\mathbb{Z}_2$-odd and even states. These definitions must be given in the `particles.py` file, where some default values (for SM and MSSM particles) are already loaded. An example is given in the Appendix C.1.

If the user wants to check the SLHA input file for possible errors, it is also necessary to define some of the particle's quantum numbers, as illustrated in the `particles.py` file. SModelS can then check for charged LSP, displaced visible decays and long-lived charged particles. Such scenarios are not currently tested by SModelS and can be skipped automatically when the corresponding test is enabled. This is the default behaviour when using the commandline tool `runSModelS.py`. In addition some consistency checks can be performed, in particular checking that all decay blocks are present, and all decays are on-shell, as required for the SModelS description.

3.2.2. Decomposition into Simplified Models

Given an input model, the first task of SModelS is to decompose the full model into a sum of simplified models (i.e. elements). Based on the input format, two distinct (but similar) decomposition methods are applied: the SLHA-based or the LHE-based decomposition.

SLHA-based Decomposition

The SLHA file describing the input model is required to contain the masses of all the BSM states as well as their production cross sections and decay branching ratios. All the above information must follow the guidelines of the SLHA format.

The production cross sections are read from the input file and all the cross sections for production of two $\mathbb{Z}_2$-odd states are stored and serve as the initial step for the decomposition. Starting from these primary mothers, all the possible decays are generated according to the information contained in the DECAY blocks. Each of the possible cascade decays for each mother corresponds to a branch. In order to finally generate elements, all the branches are combined in pairs according to the production cross sections. Each of the elements generated according to the procedure just described will also store its weight, which equals its production cross section times all the branching ratios appearing in it.

Some models contain a large number of new states and each may have a large number of possible decays. As a result, long cascade decays are possible and the number of elements generated by the decomposition process may become too large, and the computing time too long. For most practical purposes, however, elements with extremely small weights can be discarded, since they will fall well below the experimental limits. Therefore, during the SLHA decomposition, whenever an element is generated with a weight below some minimum value, this element (and all elements derived from it) is ignored. The minimum weight is a free input parameter ("sigmacut") and is easily adjustable.[5] The final output of the SLHA decomposition is a list of topologies, where each topology contains a list of the elements generated during the decomposition.

[5] When computing the theory predictions, the weight of several elements can be combined together. Hence it is recommended to set the value of sigmacut approximately one order of magnitude below the minimum signal cross sections the experimental data can constrain.

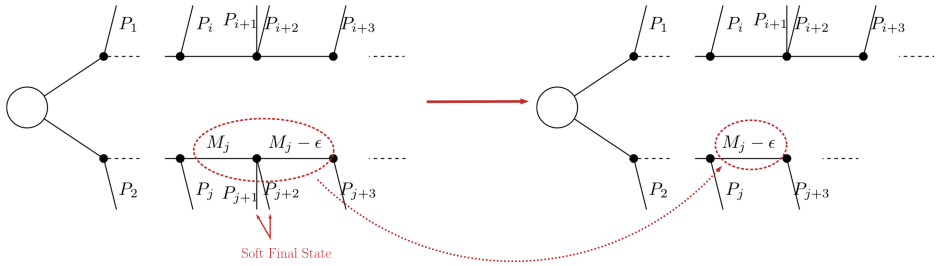

Figure 3.5.: Schematic representation of "mass compression" performed by SModelS to deal with soft final states.

LHE-based Decomposition

More general models can be input through an LHE event file containing parton-level events, including the production of the primary mothers and their cascade decays.[6] Each event can then be directly mapped to an element with the element weight corresponding to the event weight. Finally, identical elements can be combined together (adding their weights). Notice that, for the LHE decomposition, the elements generated are restricted to the events in the input file. Hence, the uncertainties on the elements weights (and which elements are actually generated by the model) are fully dependent on the Monte Carlo statistics used to generate the LHE file.

Element Compression

During the decomposition process it is possible to perform several simplifications on the elements generated. In both the LHE and SLHA-based decompositions, two useful simplifications are possible: mass compression and invisible compression. The main advantage of performing these compressions is that the simplified element is always shorter (has fewer cascade decay steps), which makes it more likely to be constrained by experimental results. The details behind the compression methods are as follows.

Mass Compression In case of small mass differences, the decay of an intermediate state to a nearly degenerate one will in most cases produce soft final states, which can not be experimentally detected. Consequently, it is a good approximation to neglect the soft final states and compress the respective decay, as shown in Figure 3.5.

After the compression, only the lightest of the two near-degenerate masses are kept in the element. The main parameter which controls the compression is called "minmassgap", and corresponds to the maximum value of ϵ in Figure 3.5 to which the compression is performed. Note that the compression is an approximation since the final states, depending on the boost of the parent state, may not always be soft. It is recommended to choose values of minmassgap of 1–10 GeV; the default value is 5 GeV.

Invisible Compression Another type of compression is possible when the final states of the last decay are invisible. The most common example is

$$A \to \nu + B$$

[6] As noted above, input via a generalised SLHA-type input is also possible.

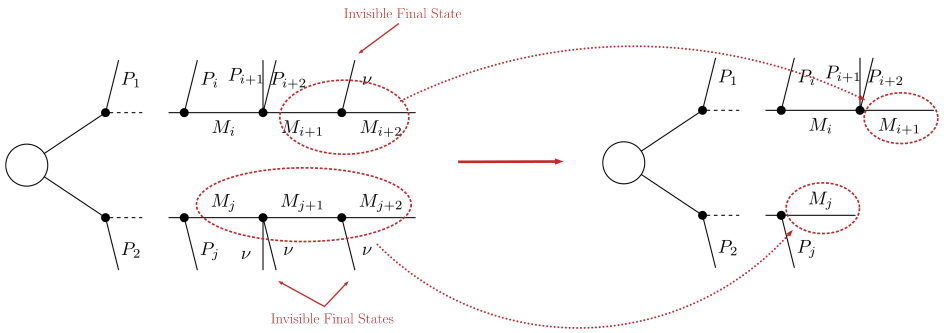

Figure 3.6.: A schematic representation of "invisible compression" as performed by SMODELS to deal with the emission of invisible particles in the final steps of the cascade decay.

as the last step of the decay chain, where B is an invisible particle leading to a E_T^{miss} signature. Since both the neutrino and B are invisible, for all experimental purposes the effective E_T^{miss} object is $B + \nu = A$. Hence it is possible to omit the last step in the cascade decay, resulting in a compressed element. This compression can be applied consecutively to several steps of the cascade decay if all of them contain only invisible final states, as illustrated in Figure 3.6. Moreover, invisible compression may become possible after performing mass compression. Note however that invisible compression is possible only for the final step of a cascade decay, as the full mass and vertex information is required in topologies where an invisible decay is followed by a visible on. In the example of Figure 3.6 this means that the decays to P_1 and P_2 cannot be invisible compressed (independent of the SM final states in the vertex) if any of the later decays, e.g. to P_i, P_j are visible (i.e. they cannot be invisible or mass compressed).

Mass and invisible compression can be turned on independently when setting the SMODELS run parameters, see Section C.1.

3.2.3. Theory Predictions

The decomposition of the input model as a sum of elements is the first step for confronting the model with the experimental limits. The next step consists of computing the relevant signal cross sections (or theory predictions) for comparison with the experimental limits. Below we describe the procedure for the computation of the theory predictions after the model has been decomposed.

UL-type results constrain the weight ($\sigma \times \mathcal{B}$) of one element or sum of elements. Therefore SMODELS must compute the theoretical value of ($\sigma \times \mathcal{B}$) summing only over the elements appearing in the respective constraint. This value can then be compared with the respective 95% CL upper limit extracted from the UL map.

On the other hand, EM-type results constrain the total signal ($\sum \sigma \times \mathcal{B} \times \epsilon$) in a given signal region (a data set in SMODELS language). Consequently, in this case SMODELS must compute $\sigma \times \mathcal{B} \times \epsilon$ for each element, using the efficiency maps for the corresponding data set and constraint. The final theoretical prediction is the sum over all elements with a non-zero value of $\sigma \times \mathcal{B} \times \epsilon$. This value can then be compared with the signal upper limit for the respective data set. The procedure can always be divided in two main steps: element selection and element clustering.

For UL-type results the selection is a simple check if the element appears in the constraint.

The clustering is somewhat more involved. The selected elements usually differ in their masses[7] and the experimental limit assumes that all the elements appearing in the constraint have the same mass. As a result, the selected elements must be grouped into clusters of equal masses. When grouping the elements, however, one must allow for small mass differences, since the experimental efficiencies should not be strongly sensitive to small mass differences. Unfortunately there is no way to unambiguously define "similar masses" and the definition should depend on the experimental result, since different results will be more or less sensitive to mass differences. SModelS uses an UL map-dependent measure of the distance between two element masses, defined in the following way:

$$\begin{aligned}
&\text{Element } A\ (M_A = [[M1, M2, ...], [m1, m2, ...]]) \rightarrow \text{ Upper Limit}(M_A) = x \\
&\text{Element } B\ (M_B = [[M1', M2', ...], [m1', m2', ...]]) \rightarrow \text{ Upper Limit}(M_B) = y \\
&\qquad \Rightarrow \text{mass distance}(A, B) = \frac{|x - y|}{(x + y)/2}
\end{aligned}$$

where M_A, M_B (x, y) are the mass arrays (upper limits) for the elements A and B, respectively. If two of the selected elements have a mass distance smaller than a maximum value, they are grouped in the same mass cluster. Once all the elements have been clustered, their weights can finally be added together and compared against the experimental upper limit.
Notice that the above definition of mass distance quantifies the experimental analysis sensitivity to mass differences, which is the relevant parameter when clustering elements. In addition, a check is performed to ensure that masses with very distinct values but similar upper limits are not clustered together.

The element selection for the case of an EM-type result consists of rescaling all the elements weights by their efficiencies, according to the efficiency map of the considered data set. The efficiency for a given data set depends both on the element mass and on its topology and particle content. In practice the efficiencies for most of the elements will be extremely small (or zero), hence only a subset effectively contributes after the element selection.[8] The clustering is trivial in this case, as we have already used the appropriate efficiency for each element with a given mass vector and we can directly sum up all elements.

3.2.4. Confronting Predictions with Experimental Limits

Once the relevant signal cross sections (i.e. the theory predictions) have been computed for the input model, they must be compared to the respective upper limits. The upper limits for the signal are stored in the SModelS database and depend on the type of experimental result.

In the case of an UL-type result, the theory predictions typically consist of a list of signal cross sections for the single data set, one for each cluster. Each theory prediction must then be compared to its corresponding upper limit. This limit is simply the cross section upper limit provided by the experimental publication or preliminary result and is extracted from the corresponding UL map.

[7] When referring to an element mass, we mean all the intermediate state masses appearing in the element (or the element mass array). Two elements are considered to have identical masses if their mass arrays are identical.

[8] The number of elements passing the selection also depends on the availability of efficiency maps for the elements generated by the decomposition. Whenever there are no efficiencies available for a element, the efficiency is taken to be zero.

For EM-type results there is a single cluster for each data set, and hence a single signal cross section value. This value must be compared to the upper limit for the corresponding signal region. This upper limit is easily computed using the number of observed and expected events and their uncertainties, and it is typically stored in the database. Since most EM-type results have several signal regions, there will be one theory prediction/upper limit for each data set. By default SModelS keeps only the best data set, i.e. the one with the largest ratio (theory prediction)/(expected limit). Thus each EM-type result will have a single theory prediction/upper limit, corresponding to the best data set, based on the expected limit.

The procedure described above can be applied to all the experimental results in the database, resulting in a list of theory predictions and upper limits for each experimental result. A model can then be considered excluded by the experimental results if, for one or more predictions, we have theory prediction $>$ upper limit.[9] Additional information (expected limit and likelihood computation) is available for EM-type results only.

3.2.5. Coverage by Simplified Model Results

In addition to comparing theory predictions against matching experimental limits, SModelS also returns information about the coverage of the input model by simplified model results. Given the decomposition output (i.e. the list of elements), as well as the database information, it finds and classifies the elements which are not tested by any of the experimental results in the database. These elements are grouped into the following classes:

- *missingTopos*: elements which are not tested by any of the experimental results in the database (independent of the element mass). The missing topologies are further classified as:
  - *longCascade*: elements with long cascade decays (more than one intermediate particle in one of the branches);
  - *asymmetricBranches*: elements where the first branch differs from the second branch (but that are not considered as long cascade decays).
- *outsideGrid*: elements which could be tested by one or more experimental result, but are not constrained because the mass array is outside the available mass grid.

Usually the list of missing or outsideGrid elements is very long. Hence, to compress this list, all elements differing only by their masses (with the same final states) or electric charges are combined. Moreover, by default, electrons and muons are combined to light leptons (denoted "l"); gluons and light quarks are combined into jets. Missing topologies are further classified (if applicable) into long cascade decay or asymmetric branch topologies. This classification is done keeping track of the initially produced mother particles without reference to the element description.

Thus the topologies for each of the four categories are then grouped according to the final state (for the missingTopos and outsideGrid classes) or according to the PDG ids of the mother partiles (for the longCascade and asymmetricBranches classes). Note that to avoid double counting only the most compressed elements are considered when evaluating the topology coverage.

[9] The statistical significance of the exclusion statement is difficult to quantify exactly since the model is being tested by a large number of results simultaneously.

3.3. Running SModelS

Running SModelS via the standard interface requires three input files, the SLHA or LHE input, the `particles.py` defining the new particles, and a parameter file for conveniently setting run parameters and output options. Here we only give a brief usage example of the comman-line tool `runSModelS.py`, in particular to describe the SModelS output. Details about the arguments, as well as a description of the `particles.py` and parameter file are given in the Appendix C.1 and in [204].

runSModelS A convenient way of using SModelS is via the executable `runSModelS.py`, which covers several different applications, with the option of turning various features on or off, as well as setting the basic parameters through a parameter file. These functionalities include detailed checks of input SLHA files, running the decomposition, evaluating the theory predictions and comparing them to the experimental limits available in the database, determining missing topologies and printing the output in several available formats. It can process a single input file or a whole folder containing a set of SLHA or LHE files, and it supports parallelization when processing an input folder.

A typical usage example is:

```
runSModelS.py -f inputFiles/slha/gluino_squarks.slha
-p parameters.ini -o ./ -v warning
```

The resulting output will be generated in the current folder, according to the printer options set in the parameters file.

Output The output will be written in the specified output formats, as an example we show below the human-readable summary text file output. The output file is written in terms of the following blocks:

- information about the basic input parameters and the status of the run:

```
Input status: 1
Decomposition output status: 1 #decomposition was successful
# Input File inputFiles/slha/gluino_squarks.slha
# maxcond = 0.2
# minmassgap = 5.
# ncpus = 1
# sigmacut = 0.03
# Database version: 1.1.1pre1
```

- a list of all the theory predictions obtained and the corresponding experimental result upper limit. If expandedSummary is set to False in the parameter file only the most constraining experimental result is printed. For each theory prediction entry, the corresponding experimental result id, the signal region used (only for EM-type results) and the experimental result $\sqrt{s}$ is printed. In general the signal region naming follows that assigned by the corresponding experimental analysis. Furthermore, the txnames contributing to the signal cross section, the theory cross section (Theory_Value), the observed upper limit (Exp_limit), the (theory cross section)/(observed upper limit) ratio (r) and, when available, the (theory cross section)/(expected upper limit) ratio (r_expected) are also printed. For UL-type results the condition violation is also included. Note that results failing the condition requirements are not included here, the

listed condition violation is therefore always smaller than the value selected for the maxcond parameter. Finally, if computeStatistics is set to True in the parameter file, the χ^2 and likelihood values (for EM-type results) are printed:

```
#Analysis Sqrts Cond_Violation Theory_Value(fb) Exp_limit(fb) r r_expected

CMS-SUS-13-019  8.00E+00  0.0  1.773E+00  3.760E+00  4.716E-01  N/A
 Signal Region:  (UL)
 Txnames:  T2
--------------------------------------------------------------------------
ATLAS-SUSY-2013-02  8.00E+00   0.0  6.617E+00  1.718E+01  3.851E-01  N/A
 Signal Region:  (UL)
 Txnames:  T6WW
--------------------------------------------------------------------------
ATLAS-SUSY-2013-02  8.00E+00  0.0  5.525E-01  1.818E+00  3.039E-01  3.653E-01
 Signal Region:  SR2jt
 Txnames:  T1, T2
 Chi2, Likelihood =  4.185E-02  2.542E-02
--------------------------------------------------------------------------
```

- the maximum value for the (theory cross section)/(observed upper limit) ratio. If this value is higher than 1 the input model is likely excluded by one of the experimental results

```
==========================================================================
The highest r value is = 0.471627309932
```

- summary information about the missing topologies, if testCoverage is set to True in the parameter file. The total missing topology cross section corresponds to the sum of all elements cross sections which are not tested by any experimental result, see Section 3.2.5. Element that could be tested, but with a mass outside the efficiency or upper limit grids, are included in the total cross section outside the grid. Finally, the elements which contribute to the total missing topology cross section are subdivided into elements with long decays or with asymmetric branches

```
Total missing topology cross section (fb):  2.767E+02
Total cross section where we are outside the mass grid (fb):  1.760E-01
Total cross section in long cascade decays (fb):  1.096E+02
Total cross section in decays with asymmetric branches (fb):  1.630E+02
```

- detailed information about the missing topologies with highest cross sections. The element cross section (weight) as well as its description in bracket notation is included. By default up to 10 missing topologies are printed and missing topologies are evaluated at the highest $\sqrt{s}$ available in the input cross sections.

```
==========================================================================
Missing topologies with the highest cross-sections (up to 10):
Sqrts (TeV)   Weight (fb)        Element description
  8.0  1.601E+01    #                [[[jet],[W]],[[jet,jet],[W]]]
  8.0  1.395E+01    #       [[[jet],[jet,jet],[W]],[[jet,jet],[W]]]
```

- detailed information about the topologies which are outside the experimental results grid:

```
================================================================================
Contributions outside the mass grid (up to 10):
Sqrts (TeV)   Weight (fb)        Element description
  8.0  1.440E-01    #                              [[[jet]],[[t,t]]]
  8.0  3.203E-02    #                          [[[t],[W]],[[t],[W]]]
```

- information about the missing topologies with long cascade decays. The long cascade decays are classified by the initially produced mother particles. If more than one pair of mothers are contributing to the same class of elements, the full list is given in the comment. For definiteness all lists are sorted by increasing PDG ids.

```
================================================================================
Missing topos: long cascade decays (up to 10 entries), sqrts = 8 TeV:
Mother1 Mother2 Weight (fb)  # allMothers
1000021 2000002  3.743E+01 # [[1000021, 2000002]]
1000002 1000021  1.626E+01 # [[1000002, 1000021]]
...
1000002 2000001  2.600E+00 # [[1000002, 2000001], [1000002, 2000003]]
```

- information about the missing topologies with asymmetric decays, in the same format as the long cascade decay description:

```
================================================================================
Missing topos: asymmetric branches (w/o long cascades, up to 10), sqrts = 8 TeV
Mother1 Mother2 Weight (fb) # allMothers
1000002 1000021  4.725E+01 # [[1000002, 1000021]]
1000021 1000021  4.324E+01 # [[1000021, 1000021]]
```

Gluino pair production gives rise to asymmetric branches when several decay channels are open. In this example no one decay is dominant, and of an overall gluino pair production cross section of 59 fb there are 43 fb in asymmetric branch topologies not constrained by any result in the database.

For more detailed instructions on running SModelS and different output formats see [204].

Interface to micrOMEGAs SModelS can also be called from inside `micrOMEGAs` via the interface presented in [205]. For a given $\mathbb{Z}_2$ symmetric model and parameter point `micrOMEGAs` writes the necessary input files, i.e. an SLHA-type input containing masses, decays and cross sections as well as the `particles.py` defining the model content. The interface uses the `runSModelS.py` functionalities and by default writes an SLHA-type output file that can easily be read in `micrOMEGAs` for further processing. The usage and output are described in the Appendix C.2.

3.4. Concluding Remarks

SModelS is an automatised tool for interpreting simplified model results from the LHC. It can decompose the signatures of any BSM model containing a $\mathbb{Z}_2$ symmetry into its SMS topologies and compare them to the existing LHC constraints from a large database of experimental results. The recent version 1.1 of the code presented here includes several new features, most importantly the inclusion of efficiency maps. Efficiency maps allow to combine the results from different topologies and should thus improve the constraining power of the tool. Moreover, extensive information is provided on the topology coverage.

The database of experimental results, version 1.1.0 Silvester 2016, contains 133 results (94 upper limit type results and 39 efficiency map type results) from 25 ATLAS and 23 CMS SUSY searches [206], covering 35 simplified models.[10] Most of the results are for Run 1 at 8 TeV; for the early 13 TeV data, there are currently three results: two upper limit maps from CMS and one from ATLAS. FASTLIM-1.0 [193] efficiency maps converted to SMODELS format are also available; they cover another 16 simplified models. An update of the database with more 13 TeV results is in preparation and will be released soon, as will be new 'home-grown' efficiency maps for testing topologies currently absent in the SMODELS database.

The program so far only deals with $\mathbb{Z}_2$-symmetric models leading to $E_T^{\rm miss}$ final states — extending the formalism to account for non-$E_T^{\rm miss}$ final states will be one of the major improvements for upcoming versions of the code. For example an interpretation of searches for long-lived charged particles in terms of SMS was presented in [207] and will be included in future versions of SMODELS. Moreover, the inclusion of resonance searches is also foreseen.

SMODELS relies on the SMS assumption, as detailed in Section 3.1. This assumption might not always be valid when using it to study generic models. In particular extensions of the MSSM or non-SUSY BSM scenarios might predict the same signatures, but for which the selection efficiencies differ significantly. In the next Chapter we will review existing tests of the validity of the SMS assumption, for the interpretation of dijet, $t\bar{t}$ and dilepton plus $E_T^{\rm miss}$ searches. Applications of SMODELS to the MSSM and some extensions (defined in Section 1.3) will then be discussed in Chapter 5.

[10] This is *not* counting preliminary results (CMS-PAS or ATLAS-CONF notes) which are present in the database but have been superseded by published data and are thus not used with default SMODELS settings.

CHAPTER

FOUR

VALIDITY OF THE SIMPLIFIED MODEL APPROACH

Under the SMS assumption inspired by the OSET description and outlined in Section 2.3.2 and Section 3.1 SModelS can be used to constrain generic models predicting the same topologies as those constrained by the SUSY searches. For example we can constrain generic MSSM scenarios, extended supersymmetric models and also UED scenarios that generally predict SUSY like signal topologies differing only in the spin of the BSM states.

In this Chapter we present tests of the SMS assumptions for a few simple final states and topologies. We first discuss in Section 4.1 the dijet $+E_T^{\text{miss}}$ final state and its interpretation in a squark-neutralino simplified model, considering both the dependence on the production channel and the dependence on the spin structure. The t-channel exchange of a gluino can be an important contribution in the production of first generation squarks if the gluino is not decoupled. This contribution is not considered in the typical SMS interpretation of squark searches, and if the kinematics of such events are significantly altered with respect to the typical squark-antisquark production, the application of SMS upper limits might not be valid to constrain the same SMS topology in such light gluino scenarios. To test the dependence on the spin structure we compare the squark-neutralino simplified model results to those obtained in a UED scenario where KK quarks are produced in pairs and decay to a bosonic DM candidate and quarks, thus giving rise to the same signal topology.

In Section 4.2 we study the spin dependence in the interpretation of $t\bar{t} + E_T^{\text{miss}}$ searches, considering either a stop-neutralino simplified model, or a fermionic top partner decaying to a scalar or vector DM candidate, and keeping track of the final state top polarisation. Searches with zero, one or two lepton final states are considered. The discussion is largely based on [208], published in JHEP in November 2016.

Finally, Section 4.3 contains a study of the spin dependence in the dilepton $+E_T^{\text{miss}}$ final state, comparing a chargino-sneutrino simplified model to the standard slepton-neutralino simplified model in the MSSM. The former occures in models with a sneutrino LSP, e.g. in the MSSM+RN model described in Section 1.3.3, when chargino pair-production is followed by a decay into a lepton and a sneutrino LSP.

4.1. Simplified Model Interpretations for Dijet + E_T^{miss} Searches

The standard SMS interpretation of dijet + E_T^{miss} searches is for a squark-neutralino simplified model, considering that only the first and second generation squarks and the neutralino

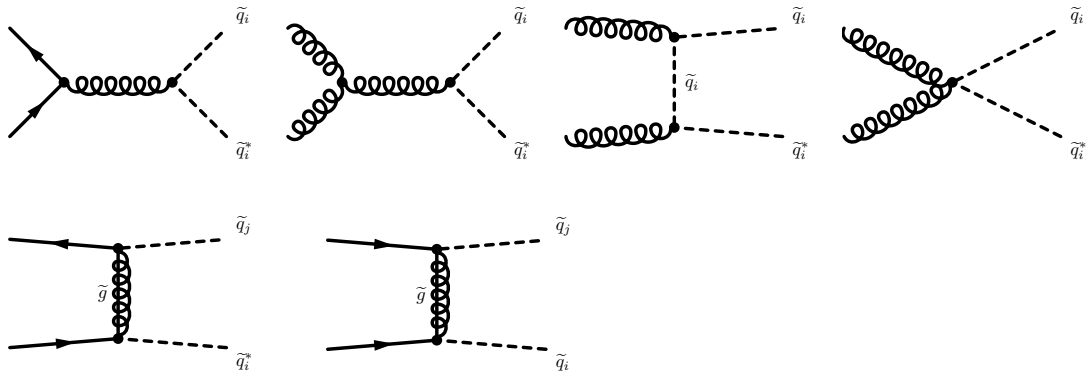

Figure 4.1.: Feynman diagrams for squark-(anti)squark production in hadronic collisions, taken from [209].

LSP are light. This means that only squark-antisquark pairs are produced via their couplings to gluons, see top row of Figure 4.1. The pair production is followed by a direct decay of the squark to a light quark and the neutralino. If in addition the gluino is also light, new production processes are relevant, in particular also squark pair production, see bottom row of Figure 4.1. For light gluinos the t-channel gluino exchange is in fact the most important contribution to the overall squark production cross section (compare Figure 2.1).

Alternatively, UED scenarios where fermionic quark partners (the KK-quarks) are produced in pairs and decay to a bosonic DM candidate (the lightest KK excitation, "LKP") and light quarks, predict the same signature as the SUSY scenario.

The uncertainties introduced when applying the standard squark-neutralino SMS limits to these two variations were considered in [209, 210]. Here we review briefly the results, and give a small update for the non-decoupled gluino scenario.

4.1.1. Non-decoupled Gluino

The case of non-decoupled gluinos was studied in [209]. Here we summarize the main results from this analysis, and present some updated results based on a new analysis with a few benchmark points (BPs).

In [209] the effect on the efficiency and mass exclusion was studied, comparing the results found for the decoupled gluino scenario to those found for heavy, but non-decoupled, gluino scenarios ($m_{\tilde{g}}/m_{\tilde{q}} = 2$ or 4). Two 8 TeV CMS searches were considered, employing the hadronic α_T variable [211] or the hadronic activity H_T [212].

It was found that over most of the parameter space the differences in efficencies are small, typically below 20%, and thus comparable to other sources of uncertainty in the interpretation of LHC searches. As a consequence the mass limits derived using efficiencies obtained in the decoupled gluino simplified model are very similar to the actual mass limits in the full simulation. Larger differences (up to 70% in extreme cases) were observed in the compressed region, and in particular when the squark mass is large. However, since this region is not constrained by the experimental analysis, these large differences are not important for limit setting.

It is further noted that the efficiencies for the two scenarios are even closer if the ratio $m_{\tilde{g}}/m_{\tilde{q}}$ is smaller than 2 or larger than 4. However, we note that if the gluino mass is similar or smaller than the squark mass it would make sense to extend the simplified model to

BP	$m_{\tilde{\chi}_1^0}$	$m_{\tilde{q}}$	$m_{\tilde{g}}$	best SR	ε_{T2}	$\varepsilon_{generic}$	$\delta(\varepsilon)$	σ_{T2}^{UL}	$\sigma_{generic}^{UL}$
1	100	600	1200	SR01_b.2jm	0.11	0.12	+0.09	0.038	0.034
2	100	1200	2400	SR02_3j	0.13	0.097	−0.24	0.0034	0.0045
3	100	1200	1500	SR02_3j	0.13	0.097	−0.24	0.0034	0.0045
4	900	1000	2000	SR01_c.2jt	0.0066	0.0059	−0.12	0.27	0.30

Table 4.1.: Comparison of selection efficiencies and cross section upper limits in the most sensitive SR, for selected benchmark points. Masses are given in GeV, cross section limits in pb.

consider at the same time gluino-pair, squark-pair and gluino-squark associated production. Note further that depending on the spectrum the gluino (squark) will most likely not decay to the LSP directly but via an intermediate squark (gluino), hence leading to a different topology.

To investigate further the effect of a light gluino and update the results found in [209] we consider an inclusive ATLAS 2-6 jet search [213], that has previously been implemented in CHECKMATE2 [187] for [214]. The analysis cuts require 2-6 hard jets, and employ different observables to supress the SM background. The signal regions are defined in particular by the number of jets required and by the effective mass m_{eff}, defined as the scalar sum of the transverse momentum of all jets with $p_T > 40$ GeV and E_T^{miss}. For a few selected BPs defined in Table 4.1, di-squark production is simulated in MADGRAPH5 [175], with up to 1 extra matrix element jet, either for generic production (including t-channel gluino), or explicitly excluding all diagrams with gluinos. 100k events are simulated using NNPDF [135], hadron-level signal samples are generated by using the tree-level matrix-element plus parton-shower (ME+PS) merging procedure. In practice, we make use of the shower-k_T scheme [215], implemented in MADGRAPH5 [175] with PYTHIA6 [202]. Squark decays are also simulated in PYTHIA6 [202]. We then use CHECKMATE2 [187] to calculate efficiencies.

The considered benchmark points and results are summarized in Table 4.1. We define ε_{T2} the efficiency in the decoupled gluino scenario, $\varepsilon_{generic}$ the efficiency when t-channel gluinos are relevant in the production and $\delta(\varepsilon) = (\varepsilon_{generic} - \varepsilon_{T2})/\varepsilon_{T2}$ as the relative difference. For each BP the same SR is most sensitive for both scenarios, and is also listed in Table 4.1.

We observe that for the light squark scenario, BP 1, and for the compressed scenario, BP 4, the most sensitive signal region is one selecting 2 signal jets. The SR SR01_c.2jt requires larger m_{eff} and is thus relevant at higher squark masses. In those points the differences are around 10%. We note that the E_T^{miss} requirement cuts more events in the generic scenario, while in turn the m_{eff} requriement cuts more events in the decoupled gluino scenario. Overall the selection efficiency is somewhat higher for the generic scenario.

On the other hand for points with heavy squarks and light neutralino (BP 2 and 3) we find that SR02_3j is actually most sensitive, requiring 3 signal jets. We thus expect a higher sensitivity to the production channel (and initial state), and indeed we find 24% difference, both if the gluino mass is $2 * m_{\tilde{q}}$ or just slightly larger than the squark mass (BP 3). Efficiencies are higher in the decoupled gluino scenario, where gluon initiated production is more important.

Finally we also list the 95% CL upper limits on the cross sections σ^{UL} in Table 4.1. We see that the differences in efficiencies translate to $10-30\%$ differences in cross section limits. In most points the limits will be overestimated when considering the efficiencies obtained for the decoupled gluino SMS, but the differences are of the same order as other uncertainties in the interpretation.

4.1.2. Fermionic Quark Partner

The dependence on the spin structure was studied in [210], for the 8 TeV CMS searches using the α_T variable [211] and the hadronic activity H_T [212]. A scalar quark partner scenario (SUSY) and a fermionic quark partner scenario (UED) are compared, again studying the topology where pair production of the quark partner is followed by a direct decay to a light quark and a DM candidate. For simplicity the gluino/KK-gluon is considered to be decoupled.[1] Again it was found that the differences in efficiencies can be large in regions with lower efficiencies (i.e. mostly in the compressed region), with differences up to $\approx 60\%$. However, in most of the parameter space, differences were found to be around 25% or below, resulting in differences in the mass limit around 10%.

Depending on the search strategies limits can be overestimated ($\not{H}_T$ selection) or underestimated (α_T selection). Overall we conclude that the SMS approach can be used to estimate limits in the same spin scenario, the additionally introduced uncertainty is similar to other uncertainties generally associated with any fast reinterpretation method.

4.2. Simplified Model Interpretations for $t\bar{t} + E_T^{miss}$ Searches

Searches for light top partners are particularly well motivated in the context of naturalness. Scalar top partners are predicted by SUSY models, and typically R-parity conserving models are considered where pair produced stops decay to SM particles and a neutralino LSP. On the other hand, fermionic top partners appear in composite Higgs and extra dimension scenarios. Searches for fermionic top partners (or any extra quarks XQs) typically consider XQ decays into SM particles only. However, scenarios with XQs that are odd under some $\mathbb{Z}_2$ symmetry and decay exclusively to a DM candidate are also possible. This occurs for instance in UED [118,216–219], Little Higgs models with T-parity [220–225], or generically any model with extra matter and a $\mathbb{Z}_2$ parity under which the SM particles are even and (part of) the new states are odd.

Thus while the blueprint model for the interpretation of $t\bar{t} + E_T^{\text{miss}}$ searches is a stop-neutralino simplified model, the same signature is predicted in scenarios with $\mathbb{Z}_2$-odd fermionic top partners decaying to a top quark and a scalar or vector DM candidate. To understand how the concrete collider signatures change for such a same-spin scenario, we compare constraints on the pair production of scalar (SUSY) and fermionic (XQ) top partners with charge 2/3, which decay into $t+\text{DM}$, thus leading to a $t\bar{t}+E_T^{\text{miss}}$ final state. Concretely, we consider the processes

$$\begin{aligned} \text{Top partner with spin 0:} \quad & pp \to \tilde{t}\,\tilde{t}^* \to t\bar{t} + \tilde{\chi}^0\tilde{\chi}^0 \\ \text{Top partner with spin 1/2:} \quad & pp \to T\bar{T} \to t\bar{t} + \{S^0S^0 \text{ or } V^0V^0\} \end{aligned}$$

where $\tilde{\chi}^0$, S^0 and V^0 represent fermionic, scalar, and vectorial DM candidates respectively. Recasting a number of ATLAS and CMS searches for stops [160, 226–228] from Run 1 of the LHC, as well as a generic search for gluinos and squarks [213] by means of CHECKMATE [186] and MADANALYSIS 5 [188,189], we compare the efficiencies of these searches for the processes above.

Related studies exist in the literature. In particular, a re-interpretation of a few ATLAS and

[1] Recall that this is a simplified model description, and not a realistic model.

CMS SUSY searches at 7 TeV in terms of UED signatures was done in [229], using among others a simplified scenario with top-partners decaying to DM and light quarks. Recently 13 TeV searches were also re-interpreted in UED scenarios in [119]. A study of constraints and LHC signatures of a scenario with a vector-like top partner decaying to a top quark and scalar DM has been performed in [230]. Here we compare in detail the selection efficiencies and upper limits for the opposite-spin and same-spin scenario, applying up-to-date recasting tools. This work was published in [208].

This section is organised as follows. In Section 4.2.1, we describe the simplified models we use for the SUSY and XQ scenarios and define the benchmark points we consider for our analysis. The tools we use and the processes we consider are described in Section 4.2.2, together with selected kinematical distributions at generator level which are useful for a better understanding of our results. Section 4.2.3 provides detailed descriptions of the experimental analyses and the effects found for our benchmark points. The results are then summarized in the top-partner versus DM mass plane in Section 4.2.4. Section 4.2.5 contains our conclusions.

4.2.1. Benchmark Scenarios

The SUSY case: stop–neutralino simplified model

The prototype for the $t\bar{t} + E_T^{\text{miss}}$ signature in the SUSY context is a stop–neutralino simplified model. This assumes that the lighter stop, $\tilde{t}_1$, and the lightest neutralino, $\tilde{\chi}_1^0$, taken to be the lightest SUSY particle and the DM candidate, are the only accessible sparticles — all other sparticles are assumed to be heavy. In this case, direct stop pair production is the only relevant SUSY production mechanism. Moreover, for large enough mass difference, the $\tilde{t}_1$ decays to 100% into $t + \tilde{\chi}_1^0$. Thus the process we consider is

$$pp \to \tilde{t}_1 \tilde{t}_1^* \to t\bar{t}\tilde{\chi}_1^0\tilde{\chi}_1^0 \,. \tag{4.1}$$

Following the notation of [231], the top–stop–neutralino interaction is given by ($i = 1, 2$; $k = 1, ..., 4$)

$$\begin{aligned} \mathcal{L}_{t\tilde{t}\tilde{\chi}^0} &= g\,\bar{t}\,(f_{Lk}^{\tilde{t}} P_R + h_{Lk}^{\tilde{t}} P_L)\,\tilde{\chi}_k^0\,\tilde{t}_L + g\,\bar{t}\,(h_{Rk}^{\tilde{t}} P_R + f_{Rk}^{\tilde{t}} P_L)\,\tilde{\chi}_k^0\,\tilde{t}_R + \text{h.c.} \\ &= g\,\bar{t}\,(a_{ik}^{\tilde{t}} P_R + b_{ik}^{\tilde{t}} P_L)\,\tilde{\chi}_k^0\,\tilde{t}_i + \text{h.c.} \end{aligned} \tag{4.2}$$

where $P_{R,L} = \frac{1}{2}(1 \pm \gamma_5)$ are the right and left projection operators, and

$$\begin{aligned} a_{ik}^{\tilde{t}} &= f_{Lk}^{\tilde{t}}\, R_{i1}^{\tilde{t}} + h_{Rk}^{\tilde{t}}\, R_{i2}^{\tilde{t}} \,, \\ b_{ik}^{\tilde{t}} &= h_{Lk}^{\tilde{t}}\, R_{i1}^{\tilde{t}} + f_{Rk}^{\tilde{t}}\, R_{i2}^{\tilde{t}} \,. \end{aligned} \tag{4.3}$$

The $f_{L,R}^{\tilde{t}}$ and $h_{L,R}^{\tilde{t}}$ couplings are

$$\begin{aligned} f_{Lk}^{\tilde{t}} &= -\tfrac{1}{\sqrt{2}}\,(N_{k2} + \tfrac{1}{3}\tan\theta_W N_{k1}) \,, \\ f_{Rk}^{\tilde{t}} &= \tfrac{2\sqrt{2}}{3}\,\tan\theta_W N_{k1} \,, \qquad\qquad h_{Rk}^{\tilde{t}} = -y_t\, N_{k4} = h_{Lk}^{\tilde{t}*} \,, \end{aligned} \tag{4.4}$$

with N the neutralino mixing matrix and $y_t = m_t/(\sqrt{2} m_W \sin\beta)$ the top Yukawa coupling in the MSSM. Finally, R is the stop mixing matrix. All this follows SLHA [57] conventions.

Under the assumption that all other neutralinos besides the $\tilde{\chi}_1^0$ and the charginos are heavy,

the $\tilde{\chi}_1^0$ is dominantly a bino. Neglecting the wino and higgsino components N_{12} and N_{14}, the $t\tilde{t}_1\tilde{\chi}_1^0$ interaction from Eq. (4.2) simplifies to

$$\mathcal{L}_{t\tilde{t}_1\tilde{\chi}_1^0} \approx -\frac{g}{3\sqrt{2}} \tan\theta_W N_{11}\, \bar{t}\,(\cos\theta_{\tilde{t}}\, P_R - 4\sin\theta_{\tilde{t}}\, P_L)\, \tilde{\chi}_1^0\, \tilde{t}_1 + \text{h.c.}\,. \tag{4.5}$$

While in practice one never has a *pure* bino, this approximation shows that the polarisation of the tops originating from the $\tilde{t}_1 \to t\tilde{\chi}_1^0$ decays will reflect the chirality of the $\tilde{t}_1$. The wino interaction also preserves the chirality, while the higgsino one flips it. This will be relevant for defining XQ benchmark scenarios analogous to SUSY ones, since the p_T and angular distributions of the top decay products somewhat depend on the top polarisation [232–242].

The extra quark scenario: conventions and Lagrangian terms

As the XQ analogue of the SUSY case above, we consider a minimal extension of the SM with one extra quark state and one DM state, assuming that the XQ mediates the interaction between the DM and the SM quarks of the third generation. Interactions between the XQ, DM and lighter quarks are neglected. The most general Lagrangian terms depend on the representation of the DM and of the XQ. We label XQ singlet states as T (with charge $+2/3$) or B (with charge $-1/3$) and XQ doublet states as Ψ_Y, where Y corresponds to the weak hypercharge of the doublet in the convention $Q = T_3 + Y$, with Q the electric charge and T_3 the weak isospin. The doublets can then be $\Psi_{1/6} = \binom{T}{B}$ or states which contain exotic components $\Psi_{7/6} = \binom{X_{5/3}}{T}$ and $\Psi_{-5/6} = \binom{B}{Y_{-4/3}}$. The DM states are labelled as S^0_{DM} if scalar singlets or $V^{0\mu}_{\text{DM}}$ if vector singlets; if the DM belongs to a doublet representation, the multiplet is labelled as $\Sigma_{\text{DM}} = \binom{S^+}{S^0_{\text{DM}}}$ (with the charge conjugate $\Sigma^c_{\text{DM}} = \binom{S^0_{\text{DM}}}{-S^-}$) if scalar or $\mathcal{V}_{\text{DM}} = \binom{V^+}{V^0_{\text{DM}}}$ (with the charge conjugate $\mathcal{V}^c_{\text{DM}} = \binom{V^0_{\text{DM}}}{V^-_{\text{DM}}}$) if vector. The couplings between the XQ, the DM and the SM quarks are denoted as λ^q_{ij} if the DM is scalar, or g^q_{ij} if the DM is vector. The labels $\{i,j\} = 1,2$ indicate the representations of the XQ and DM respectively (1 for singlet, 2 for doublet), while $q = t, b$ identifies which SM quark the new states are coupled with, in case of ambiguity. We classify below the Lagrangian terms for the minimal SM extensions with one XQ and one DM representation (singlets and doublets) but we anticipate that in the following, for simplicity, we will only consider scenarios with a DM singlet.

- Lagrangian terms for a *DM singlet*. A DM singlet can couple either with a XQ singlet or with a XQ doublet $\Psi_{1/6} = \binom{T}{B}$.

$$\mathcal{L}_1^S = \left[\lambda^t_{11}\bar{T}P_R t + \lambda^b_{11}\bar{B}P_R b + \lambda_{21}\overline{\Psi}_{1/6}P_L\begin{pmatrix}t\\b\end{pmatrix}\right] S^0_{\text{DM}} + \text{h.c.} \tag{4.6}$$

$$\mathcal{L}_1^V = \left[g^t_{11}\bar{T}\gamma_\mu P_R t + g^b_{11}\bar{B}\gamma_\mu P_R b + g_{21}\overline{\Psi}_{1/6}\gamma_\mu P_L\begin{pmatrix}t\\b\end{pmatrix}\right] V^{0\mu}_{\text{DM}} + \text{h.c.} \tag{4.7}$$

- Lagrangian terms for a *DM doublet*. A DM doublet can couple with XQ singlets or

doublets with different hypercharges.

$$\begin{aligned}\mathcal{L}_2^S &= \left[\lambda_{12}^b \bar{B} P_L \begin{pmatrix} t \\ b \end{pmatrix} + \lambda_{22}^b \overline{\Psi}_{1/6} P_R b + (\lambda_{22}^t)' \overline{\Psi}_{5/6} P_R t\right] \Sigma_{\mathrm{DM}} \\ &+ \left[\lambda_{12}^t \bar{T} P_L \begin{pmatrix} t \\ b \end{pmatrix} + \lambda_{22}^t \overline{\Psi}_{1/6} P_R t + (\lambda_{22}^b)' \overline{\Psi}_{-1/6} P_R b\right] \Sigma_{\mathrm{DM}}^c \qquad (4.8) \\ \mathcal{L}_2^V &= \left[g_{12}^b \bar{B} \gamma_\mu P_L \begin{pmatrix} t \\ b \end{pmatrix} + g_{22}^b \overline{\Psi}_{1/6} \gamma_\mu P_R b + (g_{22}^t)' \overline{\Psi}_{5/6} \gamma_\mu P_R t\right] \mathcal{V}_{\mathrm{DM}}^\mu \\ &+ \left[g_{12}^t \bar{T} \gamma_\mu P_L \begin{pmatrix} t \\ b \end{pmatrix} + g_{22}^t \overline{\Psi}_{1/6} \gamma_\mu P_R t + (g_{22}^b)' \overline{\Psi}_{-1/6} \gamma_\mu P_R b\right] \mathcal{V}_{\mathrm{DM}}^{c,\mu} \qquad (4.9)\end{aligned}$$

However, in scenarios with a DM doublet, there are always additional exotic states besides the XQ partners of the SM quarks and the DM state, namely charged scalars or vectors and quarks with charges $5/3$ or $4/3$. As mentioned above, in order to stick to a minimal extension of the SM containing a partner of the top quark and the DM candidate as the only new states, in the following we consider only the Lagrangian terms of Eqs. (4.6) or (4.7), depending on the spin of the DM. It is also worth noticing that in the considered scenarios the XQs do not mix with SM states because they have a different quantum number under the $\mathbb{Z}_2$ symmetry. Moreover, to focus only on top partners, we set $\lambda_{11}^b = g_{11}^b = 0$. Depending on the representation of the XQ, one can then identify some limiting cases:

- *Vector-like XQ (VLQ).* If the XQ is vector-like, the left-handed and right-handed projections belong to the same $SU(2)$ representation. Therefore if the VLQ is a singlet, only couplings with SM singlets are allowed, and $\lambda_{21} = 0$ or $g_{21} = 0$. On the other hand, if the VLQ is a doublet, $\lambda_{11} = 0$ or $g_{11} = 0$. Unlike cases where VLQs mix with the SM quarks through Yukawa couplings via the Higgs boson, couplings for the opposite chiralities are not just suppressed, they are identically zero. The mass term for a VLQ can be written in a gauge-invariant way as:

$$\mathcal{L}_{\mathrm{VLQ}} = -M_{T_{\mathrm{VLQ}}} \bar{T} T \qquad (4.10)$$

  where $M_{T_{\mathrm{VLQ}}}$ is a new physics mass scale not necessarily related to a Higgs-like mechanism for mass generation.

- *Chiral XQ (ChQ).* If the XQ is chiral, all the couplings of Eqs. (4.6) or (4.7) can be allowed at the same time. ChQs can acquire mass in a gauge invariant way via the Higgs mechanism, analogously to SM quarks:

$$\begin{aligned}\mathcal{L}_{\mathrm{ChQ}} = &- y_{\mathrm{XQ}}^B \bar{\Psi}_{1/6} H B - y_{\mathrm{XQ}}^T \bar{\Psi}_{1/6} H^c T + \mathrm{h.c.} \\ &\Longrightarrow \; -M_{T_{\mathrm{ChQ}}} \bar{T} T - M_{B_{\mathrm{ChQ}}} \bar{B} B \qquad (4.11)\end{aligned}$$

  where $M_{\{T,B\}_{\mathrm{ChQ}}} = y_{\mathrm{XQ}}^{\{T,B\}} v/\sqrt{2}$ and v is the Higgs vev. At this point it has to be mentioned that the contribution of the new ChQ to Higgs production and decay processes, even if different from scenarios where a 4$^{\text{th}}$ chiral generation mixes with the SM quarks, can be used to pose constraints on the coupling between the XQ and the Higgs boson, and as a consequence, on the maximum mass the ChQ can acquire through the Higgs mechanism. Of course, ChQs can still acquire mass by some different new physics mechanism (for example by interacting with a heavier scalar which develops

	(600, 10)L		(600, 300)L	
$\tilde{t}_1 \sim \tilde{t}_L$	$a^{\tilde{t}}_{11} = -8.3649\ 10^{-2}$	$b^{\tilde{t}}_{11} = 1.5406\ 10^{-3}$	$a^{\tilde{t}}_{11} = -8.3638\ 10^{-2}$	$b^{\tilde{t}}_{11} = 2.5811\ 10^{-3}$
XQ + $S^0_{\rm DM}$	$\lambda^t_{21} = -8.3649\ 10^{-2}$	$\lambda^t_{11} = 1.5406\ 10^{-3}$	$\lambda^t_{21} = -8.3638\ 10^{-2}$	$\lambda^t_{11} = 2.5811\ 10^{-3}$
XQ + $V^0_{\rm DM}$	$g^t_{21} = -8.3649\ 10^{-3}$	$g^t_{11} = 1.5406\ 10^{-4}$	$g^t_{21} = -8.3638\ 10^{-3}$	$g^t_{11} = 2.5811\ 10^{-4}$
	(600, 10)R		**(600, 300)R**	
$\tilde{t}_1 \sim \tilde{t}_R$	$a^{\tilde{t}}_{11} = 1.1425\ 10^{-3}$	$b^{\tilde{t}}_{11} = 3.3467\ 10^{-1}$	$a^{\tilde{t}}_{11} = 2.1823\ 10^{-3}$	$b^{\tilde{t}}_{11} = 3.3466\ 10^{-1}$
XQ + $S^0_{\rm DM}$	$\lambda^t_{21} = 1.1425\ 10^{-3}$	$\lambda^t_{11} = 3.3467\ 10^{-1}$	$\lambda^t_{21} = 2.1823\ 10^{-3}$	$\lambda^t_{11} = 3.3466\ 10^{-1}$
XQ + $V^0_{\rm DM}$	$g^t_{21} = 1.1425\ 10^{-4}$	$g^t_{11} = 3.3467\ 10^{-2}$	$g^t_{21} = 2.1823\ 10^{-4}$	$g^t_{11} = 3.3466\ 10^{-2}$

Table 4.2.: Benchmark points for the SUSY and XQ scenarios.

a vev). For this reason we can consider the ChQ mass as a free parameter in the following analysis.

Benchmark Points

In order to compare the XQ and SUSY scenarios, it is useful to consider benchmark points with the same top-partner and DM masses as well as the same left and right couplings (leading to t_L or t_R in the final state) for the two models. To this end, we start from the stop–neutralino simplified model and choose two mass combinations: $(m_{\tilde{t}_1},\, m_{\tilde{\chi}^0_1}) = (600,\, 10)$ GeV and $(m_{\tilde{t}_1},\, m_{\tilde{\chi}^0_1}) = (600,\, 300)$ GeV. The first one is excluded by the 8 TeV searches, while the second one lies a bit outside the 8 TeV bounds [160, 212, 243–245].[2] Moreover, since the searches for $\tilde{t}_1 \to t\tilde{\chi}^0_1$ exhibit a small dependence on the top polarisation [227], we consider the two cases $\tilde{t}_1 \sim \tilde{t}_R$ and $\tilde{t}_1 \sim \tilde{t}_L$.[3] The results for arbitrary stop mixing (or top polarisation) will then always lie between these two extreme cases. This leads to four benchmark scenarios, which we denote by

$$(600,\, 10)\mathrm{L}\,; \quad (600,\, 10)\mathrm{R}\,; \quad (600,\, 300)\mathrm{L}\,; \quad (600,\, 300)\mathrm{R}\,.$$

The strategy then is to use the same mass combinations $(m_T,\, m_{\rm DM})$ and left/right couplings for the XQ case. For the scalar DM case we directly use $\lambda^t_{11} = b^{\tilde{t}}_{11}$ and $\lambda^t_{21} = a^{\tilde{t}}_{11}$. For the vector DM case, however, the width of the XQ would be too large if we were using the same parameters as in the SUSY or scalar DM case; to preserve the narrow width approximation, we therefore reduce the couplings by a factor 10, i.e. $g^t_{11} = b^{\tilde{t}}_{11}/10$ and $g^t_{21} = a^{\tilde{t}}_{11}/10$. The concrete values for the different benchmark scenarios are listed in Table 4.2.

The alert reader will notice that in Table 4.2, although there is a strong hierarchy between the left and right couplings, both of them are non-zero. Moreover, the couplings for the (600, 300)L case are not the same as for the (600, 10)L case; the same is true for (600, 300)R vs. (600, 10)R. The reason for this is as follows. The pure left or pure right case, $\tilde{t}_1 \equiv \tilde{t}_L$ or $\tilde{t}_R$, would require that the off-diagonal entry in the stop mixing matrix is exactly zero, that is $A_t \equiv \mu/\tan\beta$, where A_t is the trilinear stop-Higgs coupling, μ is the higgsino mass parameter and $\tan\beta = v_2/v_1$ is the ratio of the Higgs vacuum expectation values. To avoid such tuning, and also because the $\tilde{\chi}^0_1$ will never be a 100% pure bino even if the winos and higgsinos are very heavy, we refrain from using the approximation of Eq. (4.5) with $N_{11} = 1$ and $\cos\theta_{\tilde{t}} = 1$ or 0. Instead, we choose the masses of the benchmark points as

[2] The $(m_{\tilde{t}_1},\, m_{\tilde{\chi}^0_1}) = (600,\, 300)$ GeV mass combination actually lies just on the edge of the new 13 TeV bounds presented by CMS [246] at the Moriond 2016 conference.

[3] Strictly speaking, because of SU(2), a $\tilde{t}_1 \sim \tilde{t}_L$ should be accompanied by a $\tilde{b}_L$ of similar mass; with no other 2-body decay being kinematically open, the sbottom would however decay to 100% into $b\tilde{\chi}^0_1$and thus not contribute to the $t\bar{t} + E_T^{\rm miss}$signature.

desired by appropriately adjusting the relevant soft terms while setting all other soft masses to 3–5 TeV. From this we then compute the stop and neutralino mixing matrices and the full $\tilde{\chi}_1^0 \tilde{t}_1 t$ couplings $a_{11}^{\tilde{t}}$ and $b_{11}^{\tilde{t}}$ of of Eq. (4.2), using SUSPECT v2.41 [174]. The resulting values are $N_{11} \simeq 1$, $\cos\theta_{\tilde{t}} \simeq 1$ (or $\sin\theta_{\tilde{t}} \simeq 1$) to sub-permil precision, but nonetheless this leads to a small non-zero value for the sub-dominant coupling, and to a slight dependence on the $\tilde{\chi}_1^0$ mass. An interesting consequence is that our comparison between SUSY and XQ is effectively between SUSY and ChQ scenarios. A comparison between SUSY and VLQ scenarios would require $\tilde{t}_1 \equiv \tilde{t}_L$ or $\tilde{t}_1 \equiv \tilde{t}_R$. Our conclusions however do not depend on this.

4.2.2. Monte Carlo Event Generation

Setup and Tools

For the Monte Carlo analysis, we simulate the $2 \to 6$ process

$$pp \to t\,\bar{t}\,\mathrm{DM}\,\mathrm{DM} \to (W^+b)(W^-\bar{b})\,\mathrm{DM}\,\mathrm{DM}$$

with MADGRAPH 5 [175, 247], where DM is the neutralino in the SUSY scenario or the scalar/vector boson in the XQ scenario. This preserves the spin correlations in the $t \to Wb$ decay. Events are then passed to PYTHIA 6 [202], which takes care of the decay $W \to 2f$ as well as hadronisation and parton showering.[4]

For the SUSY scenarios we make use of the MSSM model file in MADGRAPH, while for the XQ simulation we implemented the model in FEYNRULES [169] to obtain the UFO model format to be used inside MADGRAPH. For the PDFs we employ the cteq6l1 set [249]. To analyse and compare the effects of various ATLAS and CMS 8 TeV analyses, we employ CHECKMATE [186] as well as MADANALYSIS 5 [188]. Both frameworks use DELPHES 3 [184] for the emulation of detector effects.

The Feynman diagrams relevant for the SUSY and XQ processes are shown in Figure 4.2. We observe that besides the difference in the spin of the mediator and DM, in the SUSY case there is a topology which is not present in the XQ case, namely the 4-leg diagram initiated by two gluons. The $pp \to \tilde{t}_1\tilde{t}_1^*$ and $pp \to T\bar{T}$ production cross-sections at $\sqrt{s} = 8$ TeV are compared in Figure 4.3. The comparison is done at the highest available order for each scenario, i.e. at NLO+NLL for SUSY [127–134] and at NLO+NNLL for XQ [250]. We see that, for the same mass, the XQ cross-section is about a factor 5–10 larger than the SUSY cross-section. The same experimental analysis targeting $t\bar{t} + E_T^{\mathrm{miss}}$ will therefore have a significantly higher reach in fermionic (XQ) than in scalar (SUSY) top partner masses. For instance, an excluded cross-section of 20 fb corresponds to $m_{\tilde{t}_1} \gtrsim 620$ GeV in the SUSY case but $m_T \gtrsim 800$ GeV in the XQ case. The precise reach will, of course, depend on the specific cut acceptances in the different models.

Generator-level Distributions

As a first check whether we can expect specific differences in the cut efficiencies between the SUSY and XQ models, it is instructive to consider some basic parton-level distributions,

[4] In [248] it was argued that certain kinematic distributions show sizeable differences between LO and NLO, which can be ameliorated by including initial state radiation of extra jets. We tested this but did not find any relevant differences with and without simulating extra jets for the analyses we consider in this paper. We therefore conclude that LO matrix element plus parton showering is sufficient for the scope of this study, in particular as it saves a lot of CPU time.

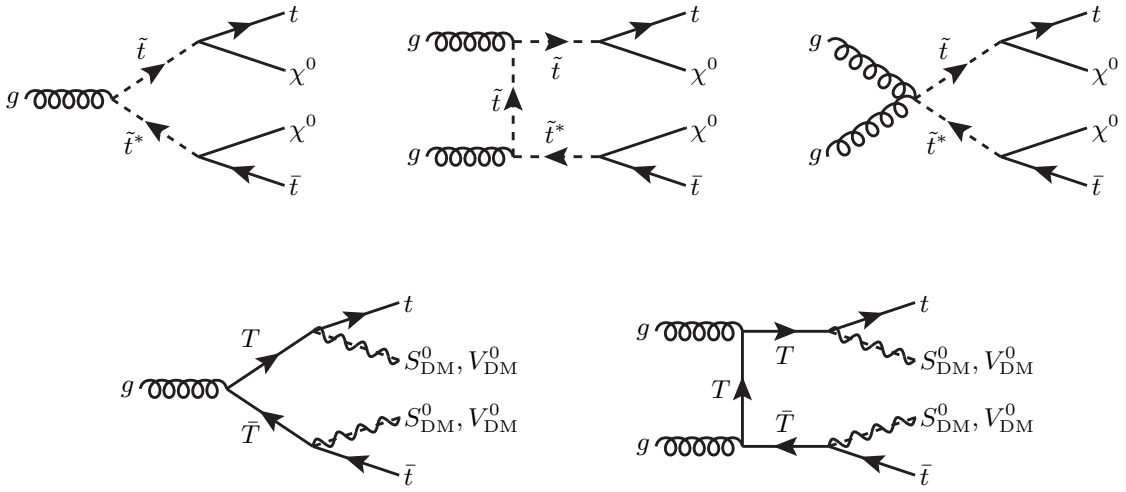

Figure 4.2.: Feynman diagrams for the production of $t\bar{t} + E_T^{\rm miss}$ in the SUSY and XQ scenarios. We have omitted for simplicity the gg and $q\bar{q}$ initial states which are common for the s-channel gluon topologies.

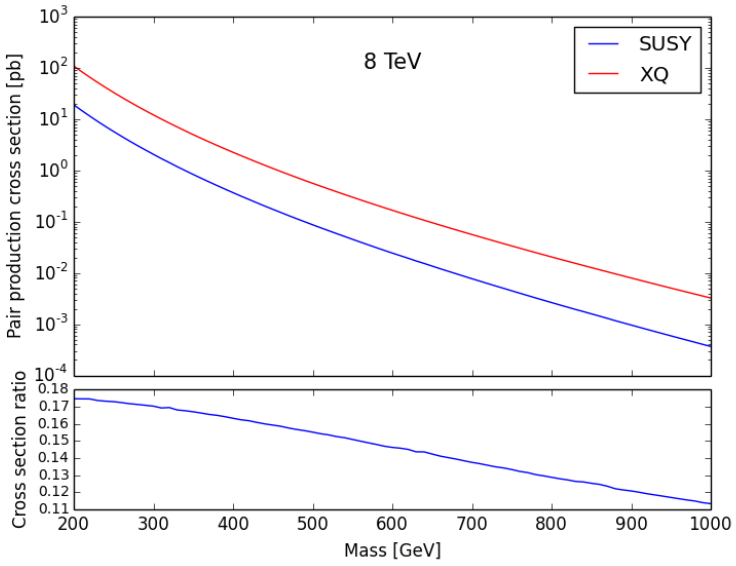

Figure 4.3.: Production cross-sections for SUSY and XQ top partners at $\sqrt{s} = 8$ TeV.

as shown in Figure 4.4 for the (600, 10) mass combination. These distributions have been obtained using MADANALYSIS 5 and considering the showered and hadronised event files from PYTHIA; jets have been processed through FASTJET [185, 251] using the anti-kt algorithm with minimum $p_T = 5$ GeV and cone radius $R = 0.5$. We see that the SUSY events tend to have more jets and a slightly harder $E_T^{\rm miss}$ spectrum. Moreover, the leading and subleading jets tend to be somewhat harder in the SUSY than in the XQ cases. Overall, these differences are however rather small and will likely not lead to any significant differences in the cut efficiencies.

Regarding the lepton p_T, the small difference that appears is between the L and R cases rather than between SUSY and XQ: all the (600, 10)R scenarios exhibit somewhat harder $p_T(l)$ than the (600, 10)L scenarios. This comes from the fact that the top polarisation influences the p_T of the top decay products. These features persist for smaller top-partner–DM

mass difference, see Figure 4.5.

Polarisation effects in stop decays were studied in detail in [232–242]. Sizeable effects were found in kinematic distributions of the final-state leptons and b-quarks, and in particular in their angular correlations. While this might help to constrain the relevant mixing angles in precision studies of a positive signal [235,236,238–241] and possibly to characterise the spin of the top-partner mediators and of the DM states through the structure of their coupling [234, 236, 237], as we will see, the current experimental analyses are not very sensitive to these effects.

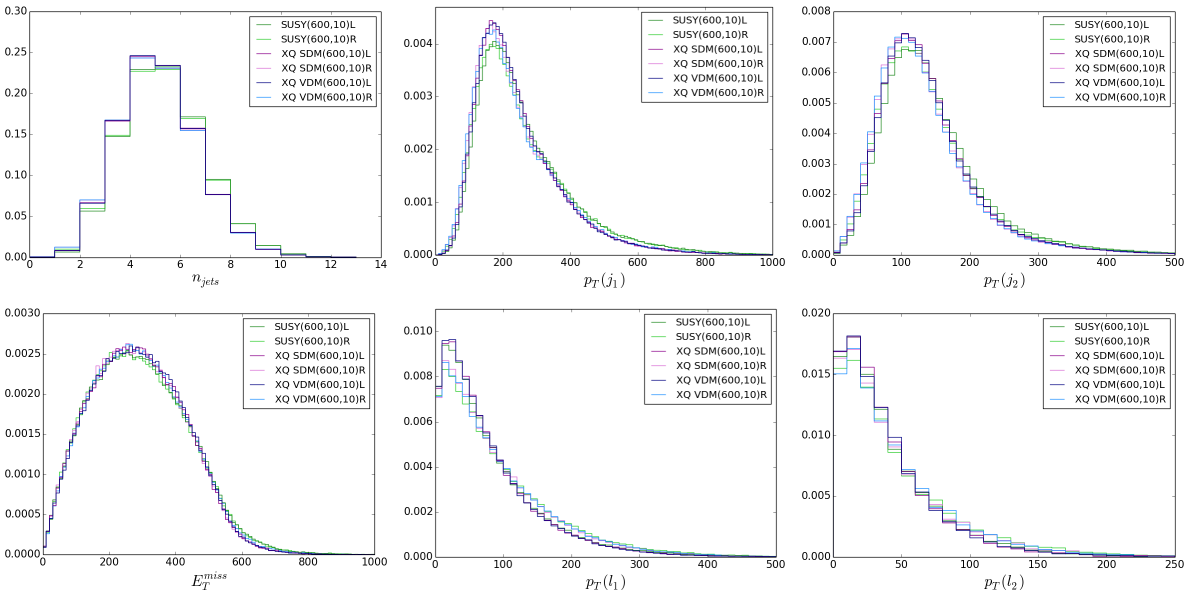

Figure 4.4.: Differential distributions (normalized to one) of jet multiplicity n_{jets}, transverse momentum of the leading and sub-leading jet $p_T(j_1)$ and $p_T(j_2)$, missing transverse energy E_T^{miss}, and p_T of the leading and sub-leading lepton $p_T(l_1)$ and $p_T(l_2)$ for the mass combination $(600,\ 10)$.

4.2.3. Effects in existing 8 TeV Analyses

Let us now analyse how the cut acceptances of existing 8 TeV analyses compare for the SUSY and XQ scenarios. To this end, we consider the following ATLAS and CMS analyses implemented in CHECKMATE [186] or the MADANALYSIS 5 Public Analysis Database (MA5 PAD) [189]:

- Fully hadronic stop search: ATLAS-CONF-2013-024 [226] implemented in CHECKMATE
- Stop searches in the single lepton mode from ATLAS [227] (CHECKMATE) and CMS [160] (MA5 PAD, recast code [252])
- The stop search with 2 leptons from ATLAS [228] implemented in CHECKMATE
- The generic gluino/squark search in the 2–6 jets plus missing energy channel from ATLAS [213] (MA5 PAD, recast code [253])

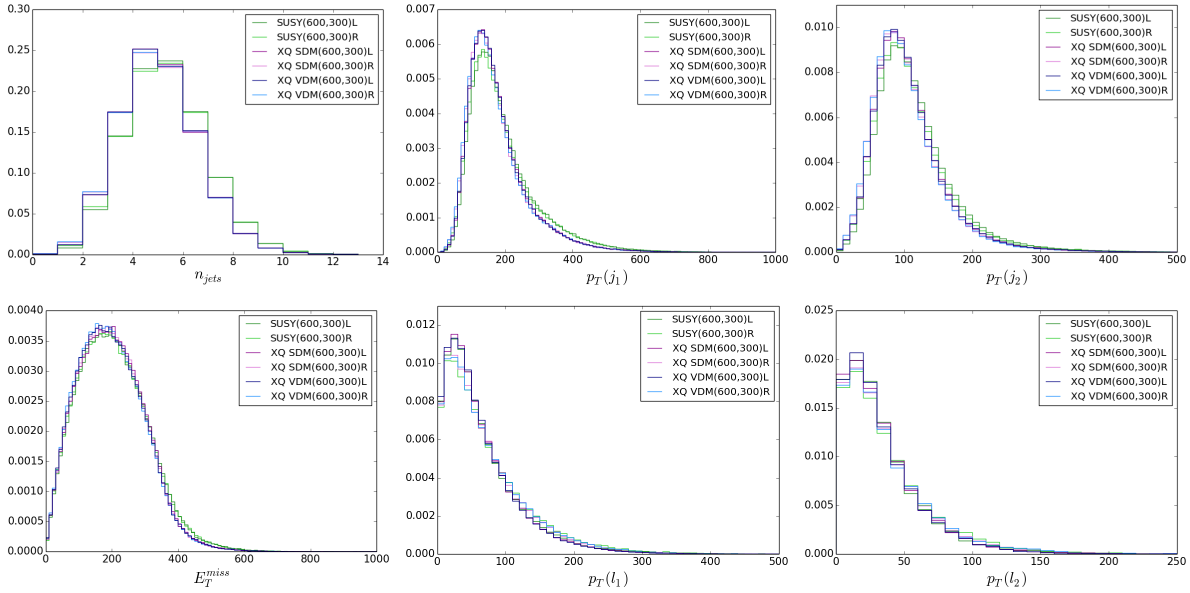

Figure 4.5.: Same as Figure 4.4 but for the $(600,\ 300)$ mass combination.

Fully hadronic stop search

The ATLAS analysis [226] implemented in CHECKMATE targets stop-pair production followed by stop decays into a top quark and the lightest neutralino, $pp \to \tilde{t}_1\tilde{t}_1^* \to t\bar{t}\tilde{\chi}_1^0\tilde{\chi}_1^0$ in the fully-hadronic top final state, $t \to bW \to bq\bar{q}$. The search is thus conducted in events with large missing transverse momentum and six or more jets, of which at least 2 must have been b-tagged. The two leading jets are required to have $p_T > 80$ GeV with the remaining jets having $p_T > 35$ GeV. Pre-selected electrons or muons, as well as taus are vetoed. Further requirements are imposed on azimuthal angle ($\Delta\phi$) and transverse mass (m_T) variables and on two 3-jet systems. Then three overlapping signal regions (SRs) are defined by requirements on E_T^{miss}, SR1: $E_T^{\text{miss}} \geq 200$ GeV, SR2: $E_T^{\text{miss}} \geq 300$ GeV and SR3: $E_T^{\text{miss}} \geq 350$ GeV.[5]

The effect of the various cuts is illustrated in Table 4.3 for the example of Point (600, 10)L. We observe that most preselection cuts have very similar efficiencies[6] when comparing SUSY and XQ cases. Small differences, of the level of few percent, occur only in the requirement of at least six jets (cf. Figure 4.4) and the condition on "3 closest jets" and "second closest jets", but these differences tend to compensate each other. Finally, the effect of the E_T^{miss} cuts that define the three SRs is almost the same for the SUSY and XQ scenarios. Consequently, the final numbers of events in each of the SRs agree within $\lesssim 5\%$ for the SUSY

[5] We note that the conference note [226] was superseded by the paper publication [254], which has six SRs targeting the $\tilde{t}_1 \to t\tilde{\chi}_1^0$ decay instead of three. Four of these, SRA1–4, are for "fully resolved" events with ≥ 6 jets and a stacked E_T^{miss} cut of 150, 250, 300 and 350 GeV. This is similar to the conference note. Two more SRs, SRB1–2, are for "partially resolved" events with 4 or 5 jets and higher E_T^{miss}, designed to target high stop masses. Moreover, the paper considers three SRs, SRC1–3, optimized for stop decays into charginos. The limit is then set from a combination of SRA+B or SRA+C. Since this cannot be reproduced without a prescription of how to combine the SRs, we keep using the CHECKMATE implementation of the conference note to test the efficiencies of the hadronic stop search for our benchmark points. This is also justified by the fact that we are not primarily interested in the absolute limit but in potential differences in selection efficiencies between scalar and fermionic top partners.

[6] Here and in the following, we use the term "efficiency" for the percentage of events remaining after one or more cuts. Strictly speaking this is the quantity acceptance$\times$efficiency, $A\epsilon$.

	SUSY	XQ-SDM	XQ-VDM
Initial no. of events	200000	200000	200000
$E_T^{\rm miss} > 80$ GeV (Trigger)	187834 (-6.08 %)	187872 (-6.06 %)	188358 (-5.82 %)
muon veto ($p_T > 10$ GeV)	154643 (-17.67 %)	153946 (-18.06 %)	154710 (-17.86 %)
electron veto ($p_T > 10$ GeV)	123420 (-20.19 %)	122439 (-20.47 %)	123247 (-20.34 %)
$E_T^{\rm miss} > 130$ GeV	113638 (-7.93 %)	112808 (-7.87 %)	113620 (-7.81 %)
≥ 6 jets, $p_T > 80, 80, 35$ GeV	33044 (-70.92 %)	27987 (-75.19 %)	28285 (-75.11 %)
reconstr. $E_T^{\rm miss,track} > 30$ GeV	32564 (-1.45 %)	27563 (-1.51 %)	27901 (-1.36 %)
$\Delta\phi(E_T^{\rm miss}, E_T^{\rm miss,track}) < \pi/3$	31200 (-4.19 %)	26583 (-3.56 %)	26939 (-3.45 %)
$\Delta\phi(E_T^{\rm miss}$, 3 hdst jets) > 0.2π	26276 (-15.78 %)	22795 (-14.25 %)	23129 (-14.14 %)
tau veto	22880 (-12.92 %)	19967 (-12.41 %)	20354 (-12.00 %)
2 b jets	9668 (-57.74 %)	8510 (-57.38 %)	8660 (-57.45 %)
$m_T(b\,\text{jets}) > 175$ GeV	7202 (-25.51 %)	6447 (-24.24 %)	6579 (-24.03 %)
3 closest jets 80–270 GeV	6437 (-10.62 %)	5877 (-8.84 %)	5929 (-9.88 %)
same for second closest jets	3272 (-49.17 %)	3186 (-45.79 %)	3351 (-43.48 %)
$E_T^{\rm miss} \geq 150$ GeV	3230 (-1.28 %)	3156 (-0.94 %)	3312 (-1.16 %)
$E_T^{\rm miss} \geq 200$ GeV (SR1)	3067 (-5.05 %)	3000 (-4.94 %)	3161 (-4.56 %)
$E_T^{\rm miss} \geq 250$ GeV	2795 (-8.87 %)	2732 (-8.93 %)	2867 (-9.30 %)
$E_T^{\rm miss} \geq 300$ GeV (SR2)	2413 (-13.67 %)	2373 (-13.14 %)	2490 (-13.15 %)
$E_T^{\rm miss} \geq 350$ GeV (SR3)	1948 (-19.27 %)	1926 (-18.84 %)	2010 (-19.28 %)

Table 4.3.: Cut-flow of the hadronic stop analysis of ATLAS for Point (600, 10)L, derived with CHECKMATE.

and XQ scenarios.

The total efficiencies in the three SRs, cross-section excluded at 95% CL and corresponding top-partner mass limits in GeV are compared in Table 4.4 for all four benchmark scenarios.[7] We see that for a specific mass combination, the total efficiencies and hence the upper limit on the cross-section are very similar for the SUSY and XQ hypotheses. The derived lower limit on the top-partner mass of course depends on the input cross-section (whether it is assumed SUSY-like or XQ-like), and is thus higher for the XQ interpretation than for the SUSY interpretation. However, the differences in the mass limits arising from applying SUSY, XQ-SDM or XQ-VDM efficiencies are generally small. Indeed for the (600, 10) scenarios, i.e. large mass splitting, they are only 2–4 GeV, which is totally negligible. For smaller mass splittings, represented by the (600, 300) scenarios, they reach about 10–20 GeV, which is still negligible. Finally, note that the effect on the mass limit from considering L vs. R polarised tops is of comparable size.

Stop search in the single lepton final state

Stops are also searched for in final states with a single lepton, jets and $E_T^{\rm miss}$, arising from one W decaying leptonically while the other one decays hadronically. The ATLAS analysis [227] for this channel is implemented in CHECKMATE, while the (cut-based version of) the corresponding CMS analysis [160] is implemented in the MA5 PAD.

In the CMS analysis [160], events are required to contain one isolated electron (muon) with $p_T > 30$ (25) GeV, no additional isolated track or hadronic τ candidate, at least four jets with $p_T > 30$ GeV at least one of which must be b-tagged, $E_T^{\rm miss} > 100$ GeV and $M_T > 120$ GeV. The analysis further makes use of the quantity $M_{\rm T2}^W$,[8] a hadronic top χ^2 ensuring that three of the jets in the event be consistent with the $t \to bW \to bq\bar{q}$ decay,

[7] Given the upper limit on the cross-section together with the cross-section prediction as a function of the top-partner mass one can estimate the 95% CL mass limit under the assumption that the efficiency is flat. While this kind of extrapolation is not a substitute for determining the true limit through a scan over the masses, it does give an indication of i) the impact of the differences in the excluded cross-section and ii) the higher reach in XQ as compared to SUSY. As we will see, this extrapolation works reasonably well for the stop searches but not for analyses that involve cuts which are directly sensitive to the overall mass scale.

[8] Based on the m_{T2} ("stransverse mass") variable [255, 256], see [257].

	Point (600, 10)L			Point (600, 10)R		
	SUSY	XQ-SDM	XQ-VDM	SUSY	XQ-SDM	XQ-VDM
eff. SR1	0.015	0.015	0.016	0.014	0.015	0.014
eff. SR2	0.012	0.012	0.012	0.011	0.012	0.011
eff. SR3*	0.0097	0.0096	0.010	0.0092	0.0095	0.0094
excl. σ [pb]	0.0196	0.0199	0.0189	0.0209	0.0201	0.0205
mass limit/σ_{SUSY}	619	618	622	613	617	615
mass limit/σ_{XQ}	805	803	808	798	802	800
$1-$CLs	0.98	1	1	0.97	1	1

	Point (600, 300)L			Point (600, 300)R		
	SUSY	XQ-SDM	XQ-VDM	SUSY	XQ-SDM	XQ-VDM
eff. SR1*	0.0074	0.0064	0.0062	0.0066	0.0060	0.0053
eff. SR2	0.0039	0.0032	0.0031	0.0035	0.0032	0.0026
eff. SR3	0.0022	0.0016	0.0017	0.0018	0.0016	0.0013
excl. σ [pb]	0.0647	0.0759	0.0772	0.0726	0.0805	0.0910
mass limit/σ_{SUSY}	522	510	509	514	506	497
mass limit/σ_{XQ}	687	671	670	676	666	655
$1-$CLs	0.59	1	1	0.54	1	1

Table 4.4.: Efficiencies in the three SRs, cross-section (σ) excluded at 95% CL, corresponding extrapolated top-partner mass limits in GeV, and CLs exclusion value from the hadronic stop analysis of ATLAS derived with CHECKMATE. "mass limit/σ_{SUSY}" means that the excluded σ is translated to a mass limit using the SUSY production cross-section from Figure 4.3, while "mass limit/σ_{XQ}" means the limit is estimated using the XQ cross-section. The exclusion CL is obtained considering the corresponding cross-sections at 600 GeV, $\sigma(\tilde{t}_1\tilde{t}_1^*) = 0.024$ pb for stop production and $\sigma(T\bar{T}) = 0.167$ pb for XQ production. The most sensitive SR used for the limit setting is marked with a star.

and the topological variable $\Delta\phi(E_T^{\text{miss}}, \text{jet})$. Various signal regions are defined targeting $\tilde{t}_1 \to t\tilde{\chi}_1^0$ or $\tilde{t}_1 \to b\tilde{\chi}_1^+$ decays with small or large mass differences between the stop and the neutralino or chargino. The two signal regions most sensitive to our benchmark scenarios are $\tilde{t}_1 \to t\tilde{\chi}_1^0$, high ΔM, $E_T^{\text{miss}} > 300$ GeV (denoted SR-A in the following) and $\tilde{t}_1 \to b\tilde{\chi}_1^+$, high ΔM, $E_T^{\text{miss}} > 250$ GeV (denoted SR-B in the following).

As an illustrative example, we show in Table 4.5 the cut-flow for SR-A for Point (600, 10)R, which is the most sensitive SR for this benchmark. The only noticeable difference, though hardly of the level of 5% in the cut efficiency, arises from the requirement of at least four jets. All other cuts have again almost the same effects on the SUSY and XQ models. Altogether, starting from the same number of events, we end up with slightly more SUSY than XQ events in this SR, but this difference is only 6–7%.

Table 4.6 summarises the total efficiencies in the two most important SRs of this analysis, the cross-sections excluded at 95% CL and the corresponding top-partner mass limits in GeV for all four benchmark scenarios. Note that, for large mass splitting, the SRs SR-B which is optimized for $\tilde{t}_1 \to b\tilde{\chi}_1^+$ decays and SR-A optimized for $\tilde{t}_1 \to t\tilde{\chi}_1^0$ have very similar sensitivities. In fact we observe that the most sensitive SR depends on the top polarisation. Events with left polarised tops are more likely to pass the additional requirement of SR-B on the leading b-jet, $p_T > 100$ GeV. Concretely, in the SUSY scenario the expected upper limits are 0.0290 pb in SR-A versus 0.0251 pb in SR-B for (600,10)L and 0.0291 pb vs. 0.0295 pb for (600,10)R. CMS has observed a small underfluctuation in both these SRs: 2 observed events vs. 4.7 ± 1.4 expected in SR-A and 5 observed events vs. 9.9 ± 2.7 expected in SR-B. Overall the observed cross-section limit is somewhat lower in the left-polarised scenario. An analogous observation holds for the XQ scenarios; the differences between SUSY and XQ scenarios are negligible.

	SUSY	XQ-SDM	XQ-VDM
Initial no. of events	200000	200000	200000
≥ 1 candidate lepton	51097 (-74.45 %)	50700 (-74.65 %)	50417 (-74.79 %)
≥ 4 central jets	23737 (-53.55 %)	21333 (-57.92 %)	20997 (-58.35 %)
$E_T^{\rm miss} > 50$ GeV	23203 (-2.25 %)	20848 (-2.27 %)	20548 (-2.14 %)
$E_T^{\rm miss} > 100$ GeV	21640 (-6.74 %)	19393 (-6.98 %)	19206 (-6.53 %)
≥ 1 b-tagged jet	18339 (-15.25 %)	16643 (-14.18 %)	16512 (-14.03 %)
isol lepton and track veto	17370 (-5.28 %)	15892 (-4.51 %)	15750 (-4.61 %)
hadronic tau veto	17061 (-1.78 %)	15646 (-1.55 %)	15487 (-1.67 %)
$M_T > 120$ GeV	13811 (-19.05 %)	12788 (-18.27 %)	12691 (-18.05 %)
$\Delta\phi(E_T^{\rm miss}$, j1 or j2) > 0.8	12006 (-13.07 %)	11251 (-12.02 %)	11164 (-12.03 %)
$\chi^2 < 5$	7079 (-41.04 %)	6771 (-39.82 %)	6750 (-39.54 %)
$E_T^{\rm miss} > 300$ GeV	4138 (-41.55 %)	3820 (-43.58 %)	3929 (-41.79 %)
$M_{\rm T2}^W > 200$ GeV	3030 (-26.78 %)	2830 (-25.92 %)	2851 (-27.44 %)

Table 4.5.: Cut-flow for SR-A of the CMS stop search in the 1-lepton channel for Point (600, 10)R, derived with the MADANALYSIS 5 recast code [252]. Note that the event weighting to account for trigger and lepton identification efficiencies and for initial-state radiation effects is not included in this cut-flow. More details about these aspects and their implementation of the recast code can be found in the original references [160] and [252].

	Point (600, 10)L			**Point (600, 10)R**		
	SUSY	XQ-SDM	XQ-VDM	SUSY	XQ-SDM	XQ-VDM
eff. SR-A	0.0108	0.0109	0.0111	0.0108*	0.0106*	0.0107*
eff. SR-B	0.0181*	0.0176*	0.0184*	0.0154	0.0152	0.0153
excl. σ [pb]	0.0169	0.0173	0.0166	0.0210	0.0213	0.0211
mass limit/σ_{SUSY}	631	629	633	613	611	612
mass limit/σ_{XQ}	820	818	822	798	796	797
$1-$CLs	0.99	1	1	0.97	1	1

	Point (600, 300)L			**Point (600, 300)R**		
	SUSY	XQ-SDM	XQ-VDM	SUSY	XQ-SDM	XQ-VDM
eff. SR-A	0.00360	0.00366	0.00346	0.00340	0.00321	0.00315
eff. SR-B	0.00748*	0.00685*	0.00632*	0.00597*	0.00570*	0.00536*
excl. σ [pb]	0.0399	0.0448	0.0480	0.0507	0.0530	0.0563
mass limit/σ_{SUSY}	560	551	546	541	538	533
mass limit/σ_{XQ}	733	722	715	710	706	700
$1-$CLs	0.81	1	1	0.72	1	1

Table 4.6.: Efficiencies for SR-A and SR-B cross-sections excluded at 95% CL, corresponding extrapolated top-partner mass limits in GeV, and CLs exclusion value from the 1-lepton stop analysis of CMS, derived with the MADANALYSIS 5 recast code [252]. The most sensitive SR used for the limit setting is indicated by a star.

Finally, for smaller mass gaps, SR-B is more sensitive in all considered scenarios and we observe differences at the level of 10–15% in the total signal selection efficiencies, which translate into up to about 20% differences in the excluded cross-sections, or $\lesssim 5\%$ in the estimated mass limits. The uncertainty from considering scenarios that lead to left or right polarised tops is of similar magnitude. The latter is consistent with the observation in [160] that the limits on the $\tilde{t}_1$ and $\tilde{\chi}_1^0$ masses vary by $\pm$10–20 GeV depending on the top-quark polarisation; the polarisation dependence in the $\tilde{t}_1 \to b\tilde{\chi}_1^+$ channel can be somewhat larger.

The corresponding ATLAS search [227] for this channel is implemented in CHECKMATE. Here, the signal selection requires a least one "baseline" lepton with $p_T > 10$ GeV, which is tightened to exactly one isolated lepton with $p_T > 25$ GeV when defining the signal

	SUSY	XQ-SDM	XQ-VDM
Initial no. of events	200000	200000	200000
Trigger	158881 (-20.56 %)	158929 (-20.54 %)	160073 (-19.96 %)
DQ	154759 (-2.59 %)	155073 (-2.43 %)	156148 (-2.45 %)
1 baseline electron	30142 (-80.52 %)	29980 (-80.67 %)	30019 (-80.78 %)
1 signal electron	22342 (-25.88 %)	22177 (-26.03 %)	22169 (-26.15 %)
≥ 3 jets $p_T \geq 25$ GeV	19865 (-11.09 %)	19241 (-13.24 %)	19262 (-13.11 %)
≥ 4 jets $p_T \geq 25$ GeV	14458 (-27.22 %)	13275 (-31.01 %)	13355 (-30.67 %)
...			
tN_med e	1892 (-86.91 %)	1951 (-85.30 %)	1987 (-85.12 %)
bCd_high1 e	1792 (-87.61 %)	1651 (-87.56 %)	1748 (-86.91 %)
bCd_bulk e	4359 (-69.85 %)	4180 (-68.51 %)	4262 (-68.09 %)
1 baseline μ	27993 (-81.91 %)	28381 (-81.70 %)	28119 (-81.99 %)
1 signal μ	23123 (-17.40 %)	23383 (-17.61 %)	23088 (-17.89 %)
≥ 3 jets $p_T \geq 25$ GeV	20695 (-10.50 %)	20624 (-11.80 %)	20302 (-12.07 %)
≥ 4 jets $p_T \geq 25$ GeV	15197 (-26.57 %)	14448 (-29.95 %)	14163 (-30.24 %)
...			
tN_med μ	2108 (-86.13 %)	1970 (-86.36 %)	1977 (-86.04 %)
bCd_high1 μ	1790 (-88.22 %)	1821 (-87.40 %)	1747 (-87.67 %)
bCd_bulk μ	4582 (-69.85 %)	4415 (-69.44 %)	4340 (-69.36 %)

Table 4.7.: Partial cut-flows for the ATLAS stop search in the 1-lepton channel for Point (600, 10)R, derived with CHECKMATE. Shown are the effects of the pre-selection cuts and the final numbers of events in specific signal regions. The cut-flows are given separately for electrons and muons.

regions.[9] Events containing additional baseline leptons are rejected. The analysis comprises 15 non-exclusive SRs, 4 of which target $\tilde{t}_1 \to t\tilde{\chi}_1^0$ (labelled 'tN_'), 9 target $\tilde{t}_1 \to b\tilde{\chi}_1^+$ (labelled 'bC_'), and the last 2 target 3-body and mixed decays. A minimum number of jets ranging between 2 and 4 is required depending on the SR, together with b-tagging requirements and an E_T^{miss} cut of at least 100 GeV. As for the CMS analysis, a number of kinematic variables (m_T, am_{T2}, $\Delta\phi(E_T^{\text{miss}}, \vec{p}_T(\text{jet}))$, etc.) are exploited for reducing the background. The relevant SRs for our benchmark points are tN_med, bCd_high and bCd_bulk.[10] tN_med targets medium stop masses, bCd_high targets high stop masses and bCd_bulk targets scenarios with large mass difference between stop and chargino and between chargino and neutralino. Of course, for the limit setting only the most sensitive one is used. A partial cut-flow example is given in Table 4.7 for Point (600, 10)R. The results for all four benchmark points are summarised in Table 4.8.

As in the CMS analysis, we observe very similar sensitivities in several signal regions, and it depends on details of the scenario which SR turns out as the best one. It should be noted here that small differences in selection efficiencies can have a considerable impact on the observed limit if they yield different SRs as the most sensitive one. In particular, ATLAS has observed more events than expected in SR bCd_high1 (16 observed events vs. 11 ± 1.5 expected). Consequently, limits obtained from this SR are weaker than those using tN_med (12 observed vs. 13 ± 2.2 expected) or bCd_bulk_d (29 observed vs. 26.5 ± 2.6 expected). This is relevant, for example, for Point (600, 10)L. Nonetheless, the differences when comparing SUSY, XQ-SDM and XQ-VDM cases remain small, in particular always well below the 20–30% estimated systematic uncertainty inherent to recasting with fast simulation tools. It is also worth pointing out that, in contrast to its CMS counterpart, this ATLAS analysis tends to give stronger limits for $\tilde{t}_R$ than for $\tilde{t}_L$ scenarios. The effect is more pronounced for smaller mass differences, in agreement with Figure 24 in [227]. Overall, the sensitivity to

[9] Except for the SR with soft-lepton selections which employ a $p_T > 6(7)$ GeV requirement for muons (electrons).

[10] Note that the ATLAS search has a dedicated SR to target boosted final states, tN_boost. This SR is not considered here, as the relevant "topness" variable is not implemented in CHECKMATE.

	Point (600, 10)L			Point (600, 10)R		
	SUSY	XQ-SDM	XQ-VDM	SUSY	XQ-SDM	XQ-VDM
eff. bCd_bulk_d	0.0298*	0.0287	0.0297	0.0278*	0.0264*	0.0270*
eff. bCd_high1	0.0208	0.0204*	0.0210*	0.0179	0.0174	0.0175
excl. σ [pb]	0.0250	0.0335	0.0324	0.0267	0.0281	0.0274
mass limit/σ_{SUSY}	598	574	577	593	588	590
mass limit/σ_{XQ}	780	750	754	773	768	770
$1-$CLs	0.94	1	1	0.93	1	1

	Point (600, 300)L			Point (600, 300)R		
	SUSY	XQ-SDM	XQ-VDM	SUSY	XQ-SDM	XQ-VDM
eff. bCd_high1	0.00919*	0.00810*	0.00761*	0.00777	0.00691	0.00638
eff. tN_med	0.00927	0.00869	0.00836	0.00877*	0.00862*	0.00775*
excl. σ [pb]	0.0742	0.0845	0.0898	0.0509	0.0517	0.0579
mass limit/σ_{SUSY}	512	502	498	541	540	531
mass limit/σ_{XQ}	673	661	656	709	708	697
$1-$CLs	0.35	1	1	0.69	1	1

Table 4.8.: Efficiencies for selected SRs, cross-sections excluded at 95% CL , corresponding extrapolated top-partner mass limits in GeV, and CLs exclusion values for the ATLAS stop search in the 1-lepton channel, derived with CHECKMATE. The most sensitive SR used for the limit setting is indicated by a star.

polarisation effects, while larger than for the CMS analysis, remains small.

Stop search in the 2-leptons final state

Let us next discuss the 2-lepton final state considered in the ATLAS analysis [228]. This analysis searches for direct stop-pair production with $\tilde{t}_1 \to b\tilde{\chi}_1^+ \to bW^{(*)}\tilde{\chi}_1^0$ or $\tilde{t}_1 \to t\tilde{\chi}_1^0 \to bW\tilde{\chi}_1^0$, targeting leptonic W decays. Events are required to have exactly two oppositely charged signal leptons (electrons, muons or one of each, defining same flavour (SF) and different-flavour (DF) selections). At least one of these electrons or muons must have $p_T > 25$ GeV and $m_{ll} > 20$ GeV. Events with a third preselected electron or muon are rejected. The analysis is subdivided into a "leptonic mT2" and "hadronic mT2" analysis, as well a multivariate analysis (MVA), which cannot be reproduced with our simulation frameworks. The "leptonic mT2" (4 SRs) and "hadronic mT2" (1 SR) analyses respectively use m_{T2} and $m_{T2}^{b-\text{jet}}$ as the key discriminating variable. Other kinematic variables used include $\Delta\phi_j$ ($\Delta\phi_l$), the azimuthal angular distance between the p_T^{miss} vector and the direction of the closest jet (highest p_T lepton).

The "leptonic mT2" analysis has 4 overlapping SRs defined by $m_{T2} > 90$, 100, 110 and 120 GeV. From these, seven statistically independent SRs denoted S1–S7 are defined in the (jet selections, m_{T2}) plane, where 'jet selections' refers to the number of jets with a certain minimum p_T, see Figure 13 in [228]. The most sensitive one for our benchmark points is S5, which has $m_{T2} > 120$ GeV and at least two jets with $p_T(\text{jet1}) > 100$ GeV and $p_T(\text{jet2}) > 50$ GeV.

Table 4.9 shows a cut-flow example for the SF selection for Point (600, 10)R, as well as an abbreviated version for the DF selection. Note that the leptonic W decay was enforced in PYTHIA to increase statistics. The SF selection gives less events than the DF one because the Z veto removes about 20% of events in the former but none in the latter. The combined count for SR S5 is given as the last line in the table. As was already the case for the other analyses, no significant differences occur at any particular step of the cut-flow. At the end we are left with the marginal difference of 4% more XQ than SUSY events in a total selection efficiency of barely 3 permil (when considering events where the W is allowed to decay to anything).

	SUSY	XQ-SDM	XQ-VDM
Initial no. of events	200000	200000	200000
2 leptons, $p_T > 10$ GeV	63129 (-68.44 %)	63877 (-68.06 %)	63604 (-68.20 %)
same flavour	31464 (-50.16 %)	32040 (-49.84 %)	31643 (-50.25 %)
isolation	28096 (-10.70 %)	28538 (-10.93 %)	28234 (-10.77 %)
opposite sign	27961 (-0.48 %)	28402 (-0.48 %)	28078 (-0.55 %)
$m_{ll} > 20$ GeV	27457 (-1.80 %)	27874 (-1.86 %)	27586 (-1.75 %)
$p_T(l) > 25$ GeV	26505 (-3.47 %)	26948 (-3.32 %)	26625 (-3.48 %)
Z veto	21448 (-19.08 %)	21682 (-19.54 %)	21374 (-19.72 %)
$\Delta\phi_j > 1$	12664 (-40.95 %)	13463 (-37.91 %)	13375 (-37.42 %)
$\Delta\phi_b < 1.5$	11779 (-6.99 %)	12638 (-6.13 %)	12460 (-6.84 %)
$m_{T2} > 120$ GeV	4824 (-59.05 %)	5441 (-56.95 %)	5368 (-56.92 %)
S5 – SF (2 jets, $p_T > 100, 50$ GeV)	2378 (-50.70 %)	2621 (-51.83 %)	2446 (-54.43 %)
different flavour	31665 (-49.84 %)	31837 (-50.16 %)	31961 (-49.75 %)
...			
$m_{T2} > 120$ GeV	5955 (-59.74 %)	6515 (-58.31 %)	6697 (-57.45 %)
S5 – DF (2 jets, $p_T > 100, 50$ GeV)	3032 (-49.08 %)	3013 (-53.75 %)	3030 (-54.76 %)
S5 – SF+DF	5410	5634	5476

Table 4.9.: Cut-flow example for the ATLAS stop search in the 2-lepton channel for Point (600, 10)R, derived with CHECKMATE. Here, the leptonic W decay was enforced to enhance statistics.

	SUSY	XQ-SDM	XQ-VDM
Initial no. of events	200000	200000	200000
2 leptons, $p_T > 10$ GeV	60379 (-69.81 %)	61193 (-69.40 %)	60812 (-69.59 %)
same flavour	30109 (-50.13 %)	30508 (-50.14 %)	30419 (-49.98 %)
isolation	26759 (-11.13 %)	27108 (-11.14 %)	27066 (-11.02 %)
opposite sign	26660 (-0.37 %)	26994 (-0.42 %)	26987 (-0.29 %)
$m_{ll} > 20$ GeV	26043 (-2.31 %)	26364 (-2.33 %)	26381 (-2.25 %)
$p_T(l) > 25$ GeV	25062 (-3.77 %)	25251 (-4.22 %)	25345 (-3.93 %)
Z veto	19570 (-21.91 %)	19765 (-21.73 %)	19642 (-22.50 %)
$\Delta\phi_j > 1$	11797 (-39.72 %)	12485 (-36.83 %)	12522 (-36.25 %)
$\Delta\phi_b < 1.5$	11270 (-4.47 %)	11943 (-4.34 %)	12035 (-3.89 %)
$m_{T2} > 120$ GeV	4390 (-61.05 %)	4785 (-59.93 %)	4815 (-59.99 %)
S5 – SF (2 jets, $p_T > 100, 50$ GeV)	2711 (-38.25 %)	2803 (-41.42 %)	2841 (-41.00 %)
different flavour	30270 (-49.87 %)	30685 (-49.86 %)	30393 (-50.02 %)
...			
$\Delta\phi_j > 1$	15273 (-38.59 %)	16117 (-36.31 %)	15896 (-36.21 %)
$\Delta\phi_b < 1.5$	14683 (-3.86 %)	15505 (-3.80 %)	15260 (-4.00 %)
$m_{T2} > 120$ GeV	5581 (-61.99 %)	6149 (-60.34 %)	5985 (-60.78 %)
S5 – DF (2 jets, $p_T > 100, 50$ GeV)	3524 (-36.86 %)	3562 (-42.07 %)	3503 (-41.47 %)
S5 – SF+DF	6235	6365	6344

Table 4.10.: Cut-flow example for the ATLAS stop search in the 2-lepton channel for Point (600, 10)L, derived with CHECKMATE. To be compared with Table 4.9. Ws were again forced to decay leptonically to enhance statistics.

The picture is similar for Point (600, 10)L, for which the cut-flow is given in Table 4.10. Noteworthy is the fact that the initial difference in Points (600, 10)R and (600, 10)L from the 2 lepton selection (the first cut) is inverted by the last cut, so that in the final SR there remain more events for (600, 10)L than for (600, 10)R. This is a consequence of the dependence on the top polarisation already noted in the parton-level plots in Figures 4.4 and 4.5.

In both cases, as can be seen from Table 4.11, there is again no significant difference in the total efficiencies and excluded cross-sections between SUSY, XQ-SDM and XQ-VDM scenarios.

Gluino/squark search in the 2–6 jets final state

For completeness, we also include a generic SUSY search (nominally for squarks and gluinos) in final states containing high-p_T jets, missing transverse momentum and no elec-

	Point (600, 10)L			Point (600, 10)R		
	SUSY	XQ-SDM	XQ-VDM	SUSY	XQ-SDM	XQ-VDM
efficiency	0.00314	0.00334	0.00323	0.00276	0.00285	0.00286
excl. σ [pb]	0.0470	0.0443	0.0455	0.0535	0.0520	0.0518
mass limit/σ_{SUSY}	547	552	550	537	539	540
mass limit/σ_{XQ}	717	723	720	705	707	708
$1-$CLs	0.79	1	1	0.74	1	1

	Point (600, 300)L			Point (600, 300)R		
	SUSY	XQ-SDM	XQ-VDM	SUSY	XQ-SDM	XQ-VDM
efficiency	0.00134	0.001425	0.00138	0.00111	0.00118	0.00100
excl. σ [pb]	0.109	0.104	0.108	0.133	0.125	0.148
mass limit/σ_{SUSY}	484	487	484	469	473	462
mass limit/σ_{XQ}	638	642	639	620	626	611
$1-$CLs	0.49	1	1	0.43	1	1

Table 4.11.: Efficiencies, cross-sections excluded at 95% CL, corresponding extrapolated top-partner mass limits in GeV, and CLs exclusion value for the ATLAS stop search in the 2-lepton channel, derived with CHECKMATE. All numbers correspond to the most sensitive signal region, SR5.

trons or muons in our analysis. Concretely, we here consider the ATLAS analysis [213] via the MADANALYSIS 5 recast code [253]. (A CHECKMATE implementation of the same analysis was done in [214]). Our original purpose was to compare the performance of the hadronic stop analysis to that of a multi-jet analysis which was not optimized for the $t\bar{t} + E_T^{\rm miss}$ signature. But, as we will see, the effective mass $M_{\rm eff}$ variable employed in the generic gluino/squark search offers a useful complementary probe.

Regarding the signal selection, the ATLAS analysis [213] comprises 15 inclusive SRs characterized by increasing minimum jet multiplicity, N_j, from two to six jets. Hard cuts are placed on missing energy and the p_T of the two leading jets: $E_T^{\rm miss} > 160$ GeV, $p_T(j_1) > 130$ GeV and $p_T(j_2) > 60$ GeV. For the other jets, $p_T > 60$ or 40 GeV is required depending on the SR. In all cases, events are discarded if they contain electrons or muons with $p_T > 10$ GeV. Depending on N_j, additional requirements are placed on the minimum azimuthal separation between any of the jets and the $E_T^{\rm miss}$, $\Delta\phi({\rm jet}, E_T^{\rm miss})$, as well as on $E_T^{\rm miss}/\sqrt{H_T}$ or $E_T^{\rm miss}/M_{\rm eff}(N_j)$. Finally, a cut is placed on $M_{\rm eff}({\rm incl.})$, which sums over all jets with $p_T > 40$ GeV and $E_T^{\rm miss}$. A cut-flow example is shown in Table 4.12 for Point (600,10)R for a SR with 4 jets (SR `4jl`). Note that, starting from 200K events, we end up with about 15% (11%) more SUSY than XQ-SDM (XQ-VDM) events in this SR. The reason for this is that the cuts on $p_T(j)$ and $M_{\rm eff}$ remove somewhat more XQ than SUSY events, as expected from the distributions in Figure 4.4.

Table 4.13 summarises the total efficiencies in the most important SRs of this analysis together with the cross-sections excluded at 95% CL and the corresponding estimated top-partner mass limits for all four benchmark scenarios. We observe about 20% difference in the excluded cross-sections between SUSY and XQ interpretations. However, the mass limits derived from the excluded cross-sections are not reliable because for this search the total efficiencies strongly depend on the top-partner mass. As we will see in the next section, while this analysis does provide a limit on $T\bar{T}$ production because of the larger cross-section, it is not sensitive to $\tilde{t}_1\tilde{t}_1^*$ production.

4.2.4. Results in the Top-partner versus DM Mass Plane

Having analysed the differences, or lack thereof, in the cut efficiencies of the experimental analyses for our four benchmark points, we next perform a scan in the plane of top-partner

	SUSY	XQ-SDM	XQ-VDM
Initial no. of events	200000	200000	200000
$E_T^{\text{miss}} > 160$ GeV	158489 (-20.76%)	158497 (-20.75%)	159683 (-20.16%)
$N_j > 1$	150908 (-4.78%)	150121 (-5.28%)	151311 (-5.24%)
lepton veto	100139 (-33.64%)	100462 (-33.08%)	101404 (-32.98%)
$p_T(j_1) > 130$ GeV	62585 (-37.50%)	58754 (-41.52%)	59482 (-41.34%)
$p_T(j_2) > 60$ GeV	62045 (-0.86%)	58188 (-0.96%)	58886 (-1.00%)
$p_T(j_3) > 60$ GeV	56729 (-8.57%)	52649 (-9.52%)	53312 (-9.47%)
$p_T(j_4) > 60$ GeV	39150 (-30.99%)	34856 (-33.80%)	35258 (-33.86%)
$\Delta\phi(j_1, E_T^{\text{miss}}) > 0.4$	38811 (-0.87%)	34616 (-0.69%)	35000 (-0.73%)
$\Delta\phi(j_2, E_T^{\text{miss}}) > 0.4$	37199 (-4.15%)	33304 (-3.79%)	33635 (-3.90%)
$\Delta\phi(j_3, E_T^{\text{miss}}) > 0.4$	35447 (-4.71%)	31870 (-4.31%)	32211 (-4.23%)
$\Delta\phi(j_4, E_T^{\text{miss}}) > 0.2$	34535 (-2.57%)	31064 (-2.53%)	31435 (-2.41%)
$E_T^{\text{miss}}/\sqrt{H_T} > 10$	25451 (-26.30%)	23522 (-24.28%)	24004 (-23.64%)
$M_{\text{eff}}(\text{incl.}) > 1$ TeV	17695 (-30.47%)	15062 (-35.97%)	15714 (-34.54%)

Table 4.12.: Cut-flow for the `4jl` SR of the ATLAS gluino and squark search in the 2–6 jets channel for Point (600, 10)R, derived with the MADANALYSIS 5 recast code [253].

	Point (600, 10)L			**Point (600, 10)R**		
	SUSY	XQ-SDM	XQ-VDM	SUSY	XQ-SDM	XQ-VDM
efficiency	0.08898	0.07454	0.07752	0.08847	0.07531	0.07857
excl. σ [pb]	0.0535	0.0639	0.0612	0.0538	0.0631	0.0605
mass limit/σ_{SUSY}	537	523	527	537	524	528
mass limit/σ_{XQ}	705	688	692	704	689	693
$1 - \text{CLs}$	0.65	1	1	0.66	1	1

	Point (600, 300)L			**Point (600, 300)R**		
	SUSY	XQ-SDM	XQ-VDM	SUSY	XQ-SDM	XQ-VDM
efficiency	0.05183	0.04242	0.04159	0.05231	0.04281	0.04020
excl. σ [pb]	0.257	0.313	0.320	0.254	0.311	0.330
mass limit/σ_{SUSY}	424	410	409	424	411	407
mass limit/σ_{XQ}	563	547	545	564	547	542
$1 - \text{CLs}$	0.13	0.67	0.66	0.13	0.68	0.65

Table 4.13.: Efficiencies, cross-sections excluded at 95% CL and corresponding extrapolated top-partner mass limits in GeV for the ATLAS gluino and squark search in the 2–6 jets channel, derived with the MADANALYSIS 5 recast code [253]. The last entry is the CLs exclusion value. The most sensitive SR is 4jl for the (600, 10) mass combination and 4jlm for the (600, 300) mass combination. Note that for this search the efficiencies strongly depend on the top-partner mass, so the extrapolation of the mass limit is unreliable; this is to large extent due to the cut on M_{eff}.

versus DM mass to derive the 95% CL exclusion lines. For definiteness, we keep the couplings fixed to the same values as for the (600, 10)L and (600, 10)R benchmark points.

Figure 4.6 presents the results for the ATLAS fully hadronic stop search implemented in CHECKMATE (top row), the CMS 1-lepton stop search recast with MADANALYSIS 5 (middle row) and the ATLAS stop search in the 2-lepton final state recast with CHECKMATE (bottom row). The left panels are for the couplings of Point (600, 10)L, the right panels for the couplings of Point (600, 10)R, see Table 4.2. Shown are the 95% CL exclusion lines obtained from SUSY, XQ-SDM and XQ-VDM event simulation (dashed black, full black and full grey lines, respectively), as well as the exclusion lines obtained from rescaling SUSY efficiencies with XQ cross-sections (dotted black line). For each bin, the most sensitive SR used for the limit setting in the SUSY, XQ-SDM and XQ-VDM case is indicated by a coloured symbol as shown in the plot legends. Note that the SR naming follows that of the corresponding experimental publication, and that the most relevant signal regions for each

search are described in Section 4.2.3. For reference, the official ATLAS/CMS exclusion lines are also shown as full red lines.

For the CMS 1-lepton search, our exclusion line for left stops agrees remarkably well with the official CMS line (from the cut-based analysis). This is somewhat accidental, as *i)* the official CMS limit is for unpolarised stops, and *ii)* in our simulation the limit is mostly obtained from a SR optimised for decays to bottom and chargino, not from one optimised for decays to top and neutralino. On the other hand, the fairly large discrepancy for the ATLAS 2-lepton search is explained by the fact that the official exclusion curve was obtained using an MVA not available in CHECKMATE.

We see that over most of the mass plane, the best SR is the same for SUSY, XQ-SDM and XQ-VDM. (For the points where they are different, the sensitivities of the best and 2nd best SRs are actually quite similar.) The main conclusions which can be inferred from the plots are the following:

1. There are no significant differences between the XQ scenarios where the top partner decays to scalar or vector DM. This is expected because in the narrow-width approximation the process is largely dominated by the resonant contribution, the cross-section of which can be factorised into production cross-section times branching ratios. Since in our framework the branching ratios are 100% in the $t + \mathrm{DM}$ channel, there are no relevant differences between different DM hypotheses.

2. The contours obtained by rescaling the SUSY efficiencies with the XQ cross-sections coincide quite well with the "true" XQ exclusion lines obtained by simulating XQ events. This means that efficiency maps or cross-section upper limit maps for the stop–neutralino simplified model can safely be applied to the XQ case under consideration in this study. It would thus be of advantage if the official maps by ATLAS and CMS extended to high enough masses to cover the 95% CL reach for fermionic top partners, which is currently not the case.[11]

The situation is different for the generic gluino/squark search in the multi-jet + E_T^{miss} channel shown in Figure 4.7.[12] Contrary to the estimated stop mass limit of about 400–500 GeV in Table 4.13, in the scan we do not obtain any limit on stops from this analysis. As already mentioned in Section 4.2.3, the reason is that the efficiency of the M_{eff} cut strongly depends on the overall mass scale, rendering the extrapolation of the limit unreliable. This can also be seen from the fact that the most sensitive SR changes more rapidly with the top-partner mass, see the colour code in Figure 4.7. (The CHECKMATE implementation of the same analysis gives slightly stronger constraints on the SUSY case, excluding the region $m_{\tilde{t}} \approx 300 - 400$ GeV and $m_{\tilde{\chi}_1^0} \lesssim 50$ GeV, see results below.) Likewise, also the limit for the XQ case derived from the scan differs from the estimated one in Table 4.13, although here the effect goes in the opposite direction: the actual limit is stronger than the extrapolated one. In fact, due to the increased efficiencies at high mass scales, this search can give stronger constraints on the XQ case than the stop searches, extending the limit up to $m_T \approx 900$–950 GeV for $m_{\mathrm{DM}} \lesssim 300$ GeV. The naive rescaling of SUSY efficiencies with XQ cross-sections (dashed lines) however somewhat overestimates the reach for the XQ scenario. For

[11] For example the 1-lepton search from CMS [160] provides cross section upper limits for masses below 800 GeV only.

[12] To produce this figure, we have extended the MADANALYSIS 5 recast code with the SRs `2jl`, `4jm` and `6jm`, which are not present in the PAD version [253]. We note, however, that these SRs could not be validated, as no cut-flows or kinematic distributions are available for them from ATLAS.

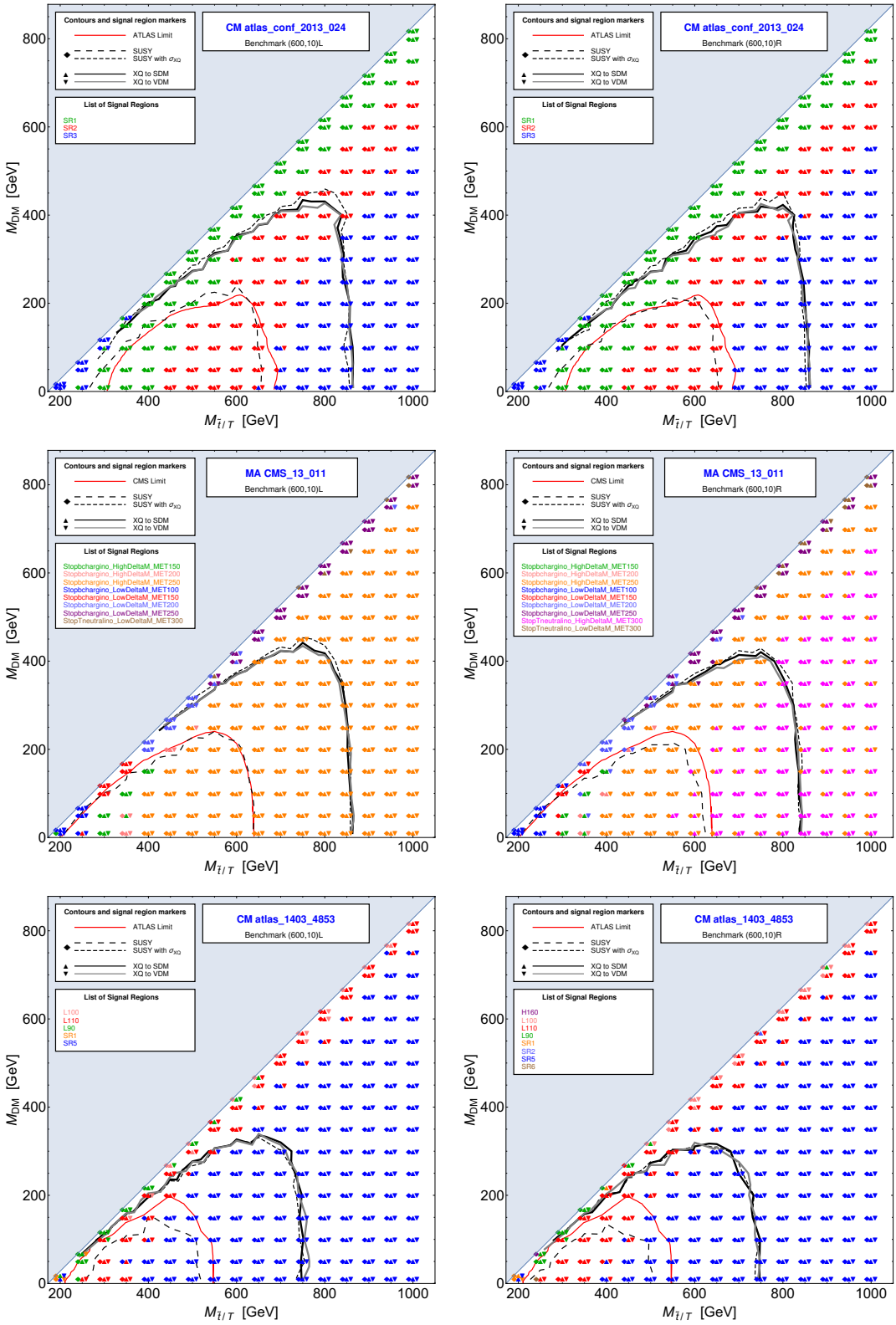

Figure 4.6.: Comparisons of constraints in the top-partner versus DM mass plane for the fully hadronic stop search from ATLAS recast with CHECKMATE (top), the 1-lepton stop search from CMS recast with MADANALYSIS 5 (middle), and the 2-lepton stop search from ATLAS recast with CHECKMATE (bottom). See text for details.

this kind of analysis it will thus be interesting to produce efficiency maps specifically for the XQ model.

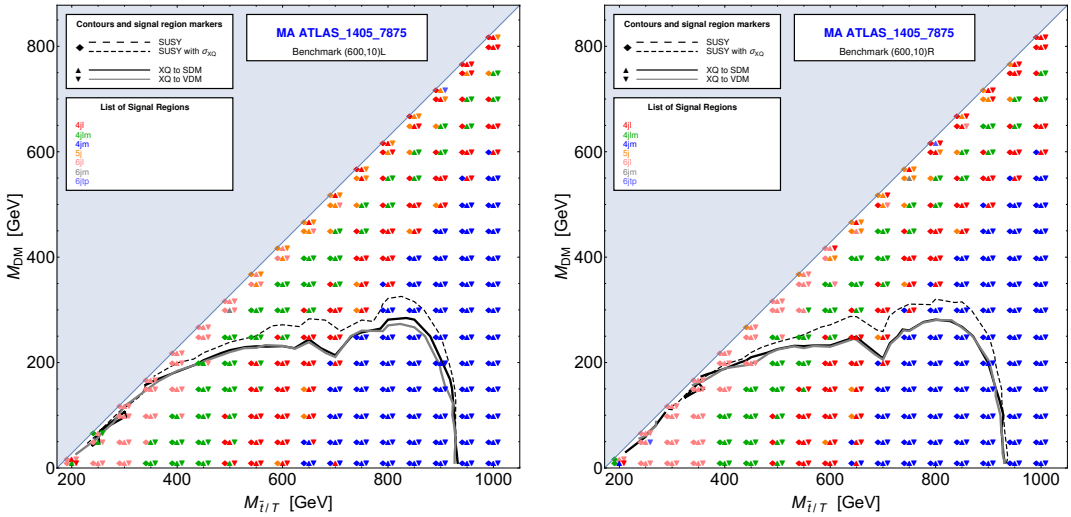

Figure 4.7.: Comparison of constraints in the top-partner versus DM mass plane based on the MADANALYSIS 5 recast code for the ATLAS gluino/squark search with 2–6 jets. As in Figure 4.6, the various lines indicate the regions excluded at 8 TeV for the SUSY and XQ cases, and for the case where the SUSY efficiencies are applied to the XQ cross-sections. The plots also contain the information which SRs are the most sensitive ones for each point of the scan. Note that no stop–neutralino mass limit is obtained from this analysis.

Additional CheckMATE Results

As mentioned in Section 4.2.3, the ATLAS analyses [227] (1-lepton stop) and [213] (2–6 jets gluino/squark) are also implemented in CHECKMATE. For completeness, we show in Figure 4.8 the CHECKMATE results for these two analyses together with the constraints obtained when considering all CHECKMATE ATLAS analyses simultaneously.

For the 1-lepton stop search from ATLAS, top row in Figure 4.8, we note that the official SUSY limit is less well reproduced than for the corresponding CMS search recast with MADANALYSIS 5, cf. the middle row of plots in Figure 4.6. This is expected, as the signal region `tN_boost` of the ATLAS search, which is optimised for high mass scales and boosted tops and is indeed the most sensitive SR for stop masses around 600 GeV, is not implemented in CHECKMATE. Moreover, there is a larger dependence on the top polarisation, as can be seen from the limit curves but also from the colour codes identifying the most sensitive SRs. Nonetheless, the resulting limit on XQs is very similar to that obtained from recasting the CMS search with MADANALYSIS 5. The fact that a stronger limit is obtained for $\tilde{t}_R$ then for $\tilde{t}_L$ was also mentioned in the experimental paper, see Figure 24 in [227].

For the gluino/squark search in the 2–6 jets channel, middle row in Figure 4.8, we observe some differences with respect to the corresponding MADANALYSIS 5 results in Figure 4.7 in what concerns the best SRs. This can occur when several SRs have comparable sensitivity. The final 95% CL limit curves for XQs are however very similar in CHECKMATE and MADANALYSIS 5. The main difference is that the CHECKMATE implementation gives a small exclusion for the SUSY case in the range $m_{\tilde{t}_1} \approx 300$–$400$ GeV and $m_{\tilde{\chi}_1^0} \lesssim 50$ GeV, while with MADANALYSIS 5 one obtains only about 80–90% CL exclusion in this region.

Running all CHECKMATE ATLAS analyses simultaneously, one finds that up to top partner masses of about 700 GeV, the 1-lepton stop search [227] is always more sensitive than the hadronic stop search from the conference note [226]. Although from the top row of plots in Figure 4.6 the hadronic analysis seems to give the stronger limit, this comes from the fact that less events were observed in the three SRs of [226] than expected; comparing the expected limits, the search in the 1-lepton channel gives the stronger constraint. It is thus [227] which is used for the limit setting in this mass range. Above $m_T \approx 700$ GeV, the gluino/squark search in the 2–6 jets channel [213] is the most sensitive analysis and used for the limit setting.

4.2.5. Conclusions

We have studied how various analyses targeting $t\bar{t} + E_T^{\text{miss}}$ signatures, carried out by ATLAS and CMS in the context of SUSY searches, perform for models with fermionic top partners. Taking a simplified XQ model with one extra T quark and one DM state and comparing it to a simplified stop–neutralino model, we found that given the same kinematical configuration, SUSY and XQ efficiencies are very similar. The situation is different for generic multi-jet + E_T^{miss} searches targeting light-flavour squark and gluino production: here we found larger efficiencies for the SUSY than for the XQ case.

Putting everything together, we conclude that cross-section upper limit maps and efficiency maps obtained for stop simplified models in stop searches can also be applied to analogous models with fermionic top partners and a DM candidate, provided the narrow-width approximation applies. An exception may be the region of very small mass differences, where uncertainties in the total cut efficiencies become sizeable, though this does not influence much the actual limit.[13] To fully exploit the applicability to different top partner models, we encourage the experimental collaborations to present their cross-section upper limit and efficiency maps for a wide enough mass range, covering not only the reach for stops but also the reach for fermionic top partners. For the generic multi-jet + E_T^{miss} searches, on the other hand, it would be worthwhile to have efficiency maps specifically for the XQ model. As a service to the reader and potential user of our work, we provide the efficiency maps which we derived with CHECKMATE and MADANALYSIS 5 as auxiliary material [258].

The similarity of SUSY and XQ efficiencies also means that, should a signal be observed in $t\bar{t} + E_T^{\text{miss}}$ events, it is not immediately obvious whether it comes from scalar or fermionic top partners. Since the production cross-section (assumed here to be pure QCD) is significantly larger for fermionic than for scalar top partners, one way of discrimination may be to correlate the effective mass scale, M_{eff}, or the effective transverse mass [259], with the observed number of events, see Figure 4.9 for an illustrative example. (This was also observed in [260]. However, as pointed out in [225], for small XQ–DM mass splittings the decay products become softer and the discrimination from the SUSY case by cross-section and M_{eff} is lost.) Moreover, in the case of fermionic top partners, a corroborating signal may show up in generic gluino/squark searches, which have much less sensitivity to scalar top partners (compare Figure 4.7). Finally, the distinction between the two scenarios may be refined by considering special kinematic distributions as discussed in [261–263].

[13] However, this region could become important for scenarios in which multiple degenerate or nearly-degenerate top-partners occur, as in this case the cross-section might be enhanced by interference effects. Separate efficiency maps for the scalar or fermionic top partners would therefore be useful in this regime.

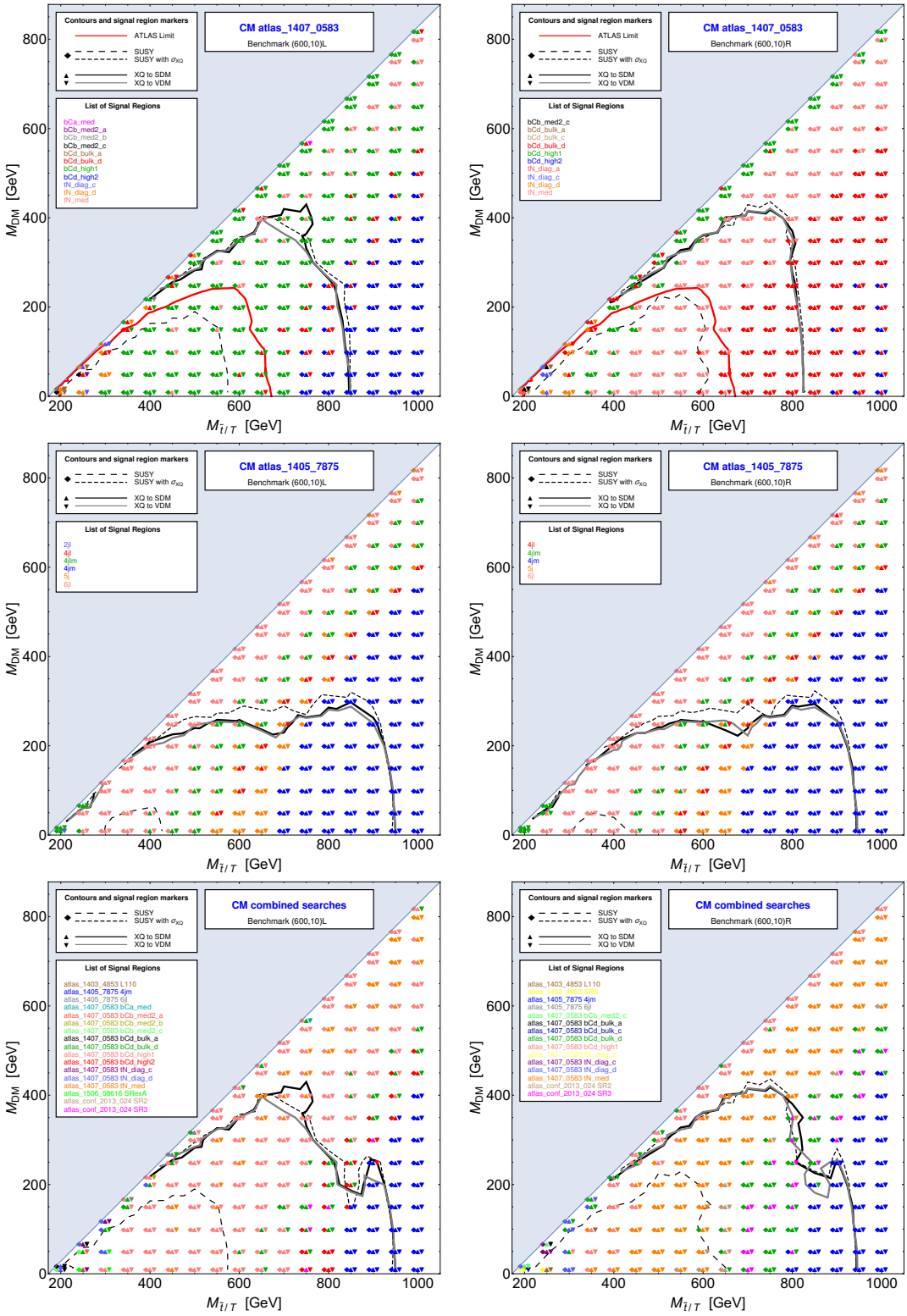

Figure 4.8.: Additional comparison of constraints in the top-partner versus DM mass plane based on ATLAS analyses implemented in CHECKMATE: 1-lepton stop search [227] (top row), generic gluino/squark search [253] (middle row) and combination of all CHECKMATE ATLAS analyses (bottom row). As before, the left panels are for the couplings of Point (600, 10)L, the right panels for the couplings of Point (600, 10)R.

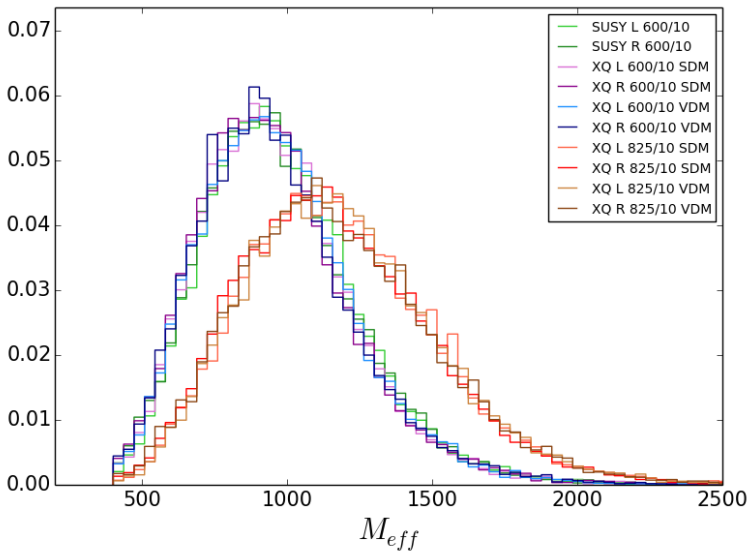

Figure 4.9.: Comparison of the M_{eff} distributions for SUSY and XQ scenarios, after preselection cuts of the CMS 1-lepton stop search [160]. Here, M_{eff} is computed as $\sum p_T(\text{jets}) + p_T(l) + E_T^{\text{miss}}$. The green, violet and blue histograms are for the default (600, 10) benchmark points, while the orange and brown histograms show XQ scenarios that would give roughly the same visible cross-sections as the (600, 10) SUSY cases.

4.3. Simplified Model Interpretations for Dilepton + E_T^{miss} Searches

In the next Chapter we will study SMS constraints on the parameter space of the MSSM and some of its extensions, considering for example scenarios where a mixed, mostly RH sneutrino is the LSP and a DM candidate (the MSSM+RN defined in Section 1.3.3). In such scenarios the $l^+l^- + E_T^{\text{miss}}$ signature is often important. Under the SMS assumption this signature, arising from chargino-pair production $pp \to \tilde{\chi}_1^+\tilde{\chi}_1^-$ followed by $\tilde{\chi}_1^\pm \to l^\pm\tilde{\nu}_{l1}$, can be constrained using existing cross section limits on the slepton-neutralino SMS derived in the context of pair production of charged sleptons, $pp \to \tilde{l}^+\tilde{l}^-$ followed by $\tilde{l}^\pm \to l^\pm\tilde{\chi}_1^0$.

This can only be valid if the signal selection efficiencies in both scenarios are comparable. To test this assumption, we use the recast code [264] for the ATLAS search in final states with two leptons and missing transverse momentum, ATLAS-SUSY-2013-11 [265], which is available in the framework of the MADANALYSIS 5 PAD [189].

We consider two benchmark simplified model scenarios, an MSSM one with $(m_{\tilde{l}^\pm},\ m_{\tilde{\chi}_1^0}) = (270,\ 100)$ GeV and an MSSM+RN one with $(m_{\tilde{\chi}_1^\pm},\ m_{\tilde{\nu}_1}) = (270,\ 100)$ GeV. Events are generated with MADGRAPH 5 [175, 247] and PYTHIA 6.4 [202] and then passed through DELPHES 3 [184] for the simulation of the detector effects.[14] For simplicity, in the following we restrict our study to pair-production of selectrons for the MSSM case, and pair-production of charginos decaying exclusively via electrons in the MSSM+RN case.

The event selection requires two opposite sign (OS), same flavor (SF) leptons with high

[14] Note that for the reconstruction of events with a sneutrino LSP it is necessary to define the sneutrino as E_T^{miss}, by adding a corresponding `EnergyFraction` entry in the DELPHES card.

transverse momentum, concretely $p_T > 35$ GeV and $p_T > 20$ GeV.[15] Figure 4.10 compares the p_T distributions in the two benchmark scenarios, in the left panel for the harder electron, e_1, in the right panel for the second electron, e_2. The bin sizes are chosen such that the first bin corresponds to the events that do not pass the $p_T > 35$ GeV (left panel) or $p_T > 20$ GeV (right panel) requirement. We see that the electrons originating from selectron-pair production tend to be harder than those originating from chargino-pair production.

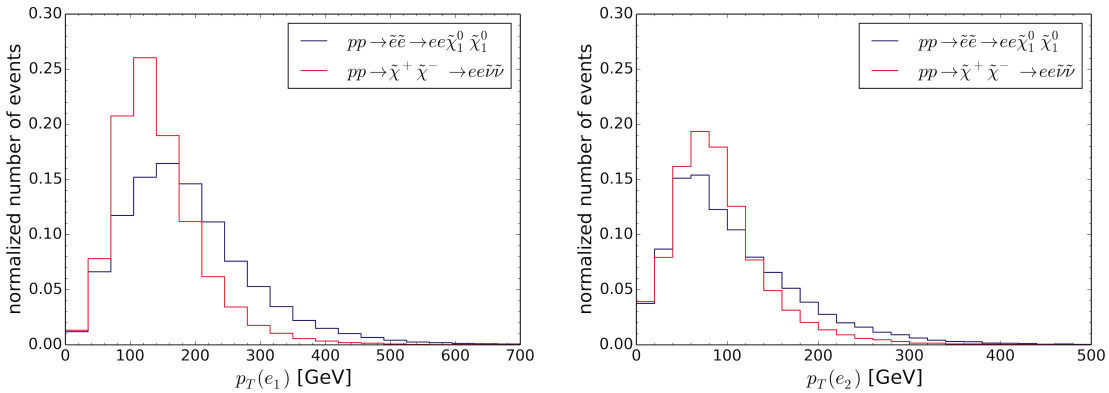

Figure 4.10.: Comparison of the p_T distributions of electrons originating from selectron decays in the MSSM and from chargino decays in MSSM+RN, at the level of reconstructed events. The benchmark scenarios used are $(m_{\tilde{l}^\pm},\ m_{\tilde{\chi}_1^0}) = (270,\ 100)$ GeV for the MSSM case and $(m_{\tilde{\chi}_1^\pm},\ m_{\tilde{\nu}_1}) = (270,\ 100)$ GeV for the MSSM+RN case. See text for details.

The analysis further requires the invariant mass of the lepton pair to be outside the Z window, and τ's and jets are vetoed. Finally, three signal regions are defined by thresholds on the stransverse mass m_{T2} that is used for reducing the $t\bar{t}$ and Wt backgrounds: $m_{T2} > 90$, > 120 and > 150 GeV. The m_{T2} distributions after the preselection cuts are shown in Figure 4.11. It can be seen that the distributions intersect around the minimum required value of $m_{T2} = 90$ GeV; events with electrons originating from chargino decays are more likely to pass this cut.

To see the net effect on the signal efficiencies, Table 4.14 shows the complete cut-flow comparison for the two benchmark scenarios. As expected, differences arise in the first cut, selecting high p_T OS lepton pairs, and when applying the lower bounds for m_{T2}. Because of the softer p_T distribution in case of chargino production+decay, there are fewer events passing the first cut for this scenario. However, the opposite is true for the m_{T2} cut. Ultimately, the efficiencies are comparable in all signal regions, and even somewhat higher for the MSSM+RN scenario.

To check that this is still true closer to the kinematic edge, we reproduce the cut-flows for a second set of benchmark scenarios with an LSP mass of 200 GeV. As can be seen in Table 4.15, we find a similar behaviour in this case. We conclude that we can safely apply the SMS upper limits given by the experimental collaborations in the context of slepton-pair production in the MSSM to constrain chargino-pair production followed by decays into $l\tilde{\nu}_l$ in the MSSM+RN.

[15] We consider here only the part of the analysis that is relevant for the SMS result used to constrain the sneutrino LSP scenario.

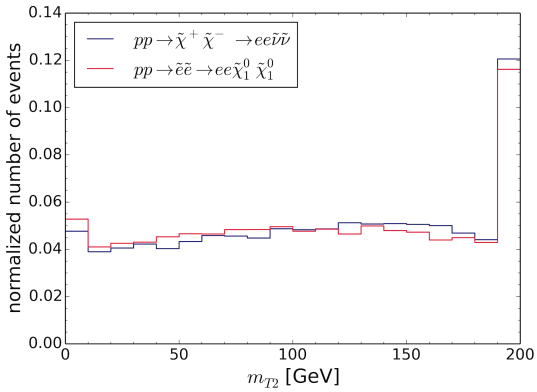

Figure 4.11.: Comparison of the m_{T2} distributions for the two benchmark scenarios after all preselection cuts.

Table 4.14.: Comparison of the cut-flows for $pp \to \tilde{e}\tilde{e} \to e^+e^-\widetilde{\chi}_1^0\widetilde{\chi}_1^0$ and $pp \to \widetilde{\chi}_1^+\widetilde{\chi}_1^- \to e^+e^-\tilde{\nu}_1\tilde{\nu}_1$ with $(m_{\tilde{l}^\pm},\ m_{\widetilde{\chi}_1^0}) = (270,\ 100)$ GeV and $(m_{\widetilde{\chi}_1^\pm},\ m_{\tilde{\nu}_1}) = (270,\ 100)$ GeV, respectively.

Cut	Slepton production	Chargino production
Common preselection		
Initial number of events	50000	50000
2 OS leptons	35133	33464
$m_{ll} > 20$ GeV	35038	33337
τ veto	35007	33318
ee leptons	35007	33318
jet veto	20176	19942
Z veto	19380	18984
Different m_{T2} regions		
$m_{T2} > 90$ GeV	11346	11594
$m_{T2} > 120$ GeV	8520	8828
$m_{T2} > 150$ GeV	5723	5926

Table 4.15.: As Table 4.14 but for $(m_{\tilde{l}^{\pm}},\ m_{\tilde{\chi}_1^0}) = (270,\ 200)$ GeV and $(m_{\tilde{\chi}_1^{\pm}},\ m_{\tilde{\nu}_1}) = (270,\ 200)$ GeV.

Cut	Slepton production	Chargino production
Common preselection		
Initial number of events	50000	50000
2 OS leptons	29291	27244
$m_{ll} > 20$ GeV	29082	26964
τ veto	29050	26956
ee leptons	29050	26956
jet veto	16834	16114
Z veto	15281	14025
Different m_{T2} regions		
$m_{T2} > 90$ GeV	3028	3198
$m_{T2} > 120$ GeV	85	140
$m_{T2} > 150$ GeV	0	0

CHAPTER

FIVE

CONSTRAINING SUPERSYMMETRIC MODELS

In Chapter 1 we introduced supersymmetry as a potential solution to several open questions in particle physics. We argued that in supersymmetric solutions to the hierarchy problem we expect superpartners with masses around the weak scale, in particular the top squarks, gluinos and higgsinos should be light. Moreover, to describe thermal DM as a neutralino LSP, the valid parameter space region limits neutralino masses to be around the TeV scale or lighter, see e.g. [59].

In Chapter 2 we then discussed how such TeV scale SUSY partners can be tested in direct LHC searches, but also noted that there are a number of additional constraints that can be relevant. Higgs physics and electroweak precision observables provide powerful tests of SUSY models. Moreover, indirect constraints from the flavor sector can also be important [266]. Finally, the prediction of the observed relic density and limits from direct and indirect DM searches are also crucial.

A comprehensive study of the parameter space of supersymmetric models therefore includes a number of tests. Typically it is much faster to check DM, Higgs and flavor constraints, as compared to constraints from SUSY searches. On the one hand this means that we should only consider the LHC phenomenology of parameter points that pass a preselection based on these constraints. On the other hand, when studying large parameter spaces it is important to test the LHC constraints in an efficient manner, as this will essentially determine how many points can be tested given the available CPU time. Using SMS constraints can be practical to obtain the global picture. In fact there are many studies that have used SModelS or FastLim [193] to constrain the MSSM parameter space, see for example [267–270]. Moreover, SModelS can be used out of the box to constrain non-MSSM scenarios, as explained in Chapter 3. Note however that the underlying SMS assumption should be tested for alternative scenarios, see Chapter 4.

In this Chapter we review constraints obtained with SModelS on the parameter space of the MSSM and some extensions. First, in Section 5.1, we compare the coverage of pMSSM points that can be obtained when considering only SMS results, to the exclusion power of a full simulation performed by ATLAS [196]. This study shows how the coverage can be improved when including efficiency map results in the SModelS database. In particular scenarios with light gluinos are discussed to point out the importance of asymmetric branch topologies.

Next, in Section 5.2 we consider constraints on the MSSM+RN model introduced in Section 1.3.3. The work presented is based on [72], published in JHEP in May 2015. We have used SModelS v1.0.1 to study the LHC Run 1 constraints on MSSM+RN scenarios where

a mixed, mostly RH sneutrino is a viable DM candidate.

We then consider in Section 5.3 constraints on the UMSSM model introduced in Section 1.3.5. This is based on [92], published in JHEP in September 2015. SModelS v1.0.1 is used to evaluate the constraints from LHC Run 1 SUSY searches. This work also includes detailed discussions of a number of contraints from Higgs physics, Z' searches, collider searches for long-lived particles, flavor physics and DM searches.

Note that both [72] and [92] were using SModelS v1.0.1, and therefore include only upper limit map constraints but no efficiency map constraints. Potential improvements from including also efficiency map constraints are highlighted in Section 5.1.

5.1. On the Coverage of the pMSSM by Simplified Model Results

The virtue of SMS based reinterpretation, namely that any full model decomposes into many different SMS, defines also its main challenge: depending on the complexity of the mass and decay patterns, a full model may not be fully reconstructed by SMS. The question that arises is to what extent full models can really be constrained by SMS results. Here we address this question for the 19-parameter pMSSM introduced in Section 1.3.2. Our work is based on the ATLAS pMSSM study [196], in which the points from an extensive pMSSM scan were tested against the constraints from 22 ATLAS searches from LHC Run 1. ATLAS made the SLHA spectra of the whole scan public on HepData [271] together with information about which point is excluded by which analyses. This is extremely useful information, which we here use to test the constraining power of SMS results by means of SModelS.

We first describe the setup of the analysis in Section 5.1.1. Our results are discussed in Section 5.1.2, where we compare the exlusion obtained with SModelS to the one of ATLAS and illustrate how the coverage is improved when including efficiency maps in addition to upper limit maps. Moreover, we analyse the importance of asymmetric decay branches and long cascade decays, to understand the potential for increasing the coverage. Conclusions are presented in Section 5.1.3.

Note that this study is work in progress and here we present only part of the results. In particular we do not analyse in detail how points with light, non-compressed scenarios can escape SMS constraints, and we specify only one main topology required to improve the coverage by SMS results. A full paper with a more detailed discussion is in preparation [272].

5.1.1. Setup of the Analysis

ATLAS has studied in total more than 310k parameter points, with a neutralino LSP and SUSY masses below 4 TeV. These points satisfied constraints from previous collider searches, flavor and electroweak precision measurements, cold dark matter relic density and direct dark matter searches. In addition the mass of the light Higgs was required to be between 124 and 128 GeV. The point are classified into three sets according to the nature of the LSP: bino-like (103,410 points), wino-like (80,233 points) and higgsino-like (126,684 points). About 40% of all these points were excluded by at least one of the 22 ATLAS Run 1 searches.

These points excluded by ATLAS are the centre of interest of our study. The reason is that we want to compare the exclusion coverage obtained using SMS results only to what is

obtained in a full simulation study. We restrict our analysis to the sets with bino-like (42,039 points) or higgsino-like (48,703 points) LSP, neglecting points with a wino-like LSP, as most of them lead to a displaced vertex signature which cannot be studied with the current version of SModelS. We further remove points from the bino- and higgsino-like LSP data sets if they contain any long lived sparticles—this concerns however only a small number of points. Likewise, points which ATLAS found to be excluded only by heavy Higgs searches are also not considered here, because no corresponding searches are included in the SModelS database. This selection leaves us with 38,575 parameter points with a bino-like LSP and 45,594 parameter points with a higgsino-like LSP to be tested with SModelS.

We use version 1.1.1 of SModelS, which works with upper limit and efficiency map type results, see Chapter 3. The official ATLAS and CMS Run 1 results available in SModelS were augmented with several 'home-grown' efficiency maps in the v1.1.1 database,[1] and we further extend this database with FastLim [193] efficiency maps as explained in [204]. Note that for a fair comparison with [196], we employ only the 8 TeV results in the SModelS database. The cross sections for all points are first calculated via a SModelS interface to Pythia 8.2 [179, 202] and NLLfast [127–134]. All points are then decomposed in SModelS and tested against the full available 8 TeV database. We consider as excluded all points where $r = \sigma_{theory}/\sigma_{UL} > 1$. Points that are not excluded are further studied using the coverage module.

5.1.2. Results

The results are summarized in Table 5.1, where we list the total number of points studied (i.e. the points excluded by ATLAS SUSY searches in [196]), the number of points that can be excluded by SModelS ($r > 1$) when using only the upper limit results in the database, and the number of points that can be excluded when using the full 8 TeV database, that is including efficiency map results. We see that in particular the coverage of bino-like LSP scenarios can be improved by using efficiency maps. Concretely the coverage improves from 44% (UL results only) to 55% (full database). Similarly the coverage for the higgsino-like LSP scenarios is increased from 55% to 63%. In both cases, this is largely because of the improved constraints of light gluino scenarios when including efficiency map results, as illustrated in Figure 5.1. The main reason is that efficiency maps allow us to combine the signal for all topologies contributing to the same signal region before comparing against an overall cross section limit. Moreover, some asymmetric decay branches are included in the EM-type results but not in the UL-type results in the database. Therefore, while UL results often constrain only a small fraction of the total gluino production (determined by the gluino decay branching ratios), this can be considerably improved when using EM results.

Note, however, that there are still many points with light gluinos which cannot be excluded by the SMS results in the SModelS database. To understand this better we show in Figure 5.2 the coverage in the gluino vs. neutralino mass plane. For comparison the exclusion line obtained in [213] for a simplified model where pair-produced gluinos decay exclusively as $\tilde{g} \to qq\tilde{\chi}_1^0$ is also drawn in Figure 5.2. We see that light gluinos escape SMS limits especially in the compressed region where monojet type searches become important. This is in agreement with the example exclusion line. Moreover, while the coverage is good for very light gluinos up to about 600 GeV, it drops for intermediate gluino masses around 1 TeV and

[1] In particular the efficiency maps we produced for gluino topologies, T5, T5WW(off), T5ZZ(off), T5tttt, T5bbbb and T6bbWW will be relevant in the discussion below. See [199] for explanation of the naming scheme. The generation of the home-grown efficiency maps is described in [204].

	Bino-like LSP	Higgsino-like LSP
Total number of points	38575	45594
Number of points excluded – UL results only	16957	25005
Number of points excuded – full database	21171	28659

Table 5.1.: Summary of results, listing the number of ATLAS-excluded pMSSM points tested in this study, the number of points excluded by SMODELS when using UL-type results only, and the number of points excluded when using the full 8 TeV database including EM-type results.

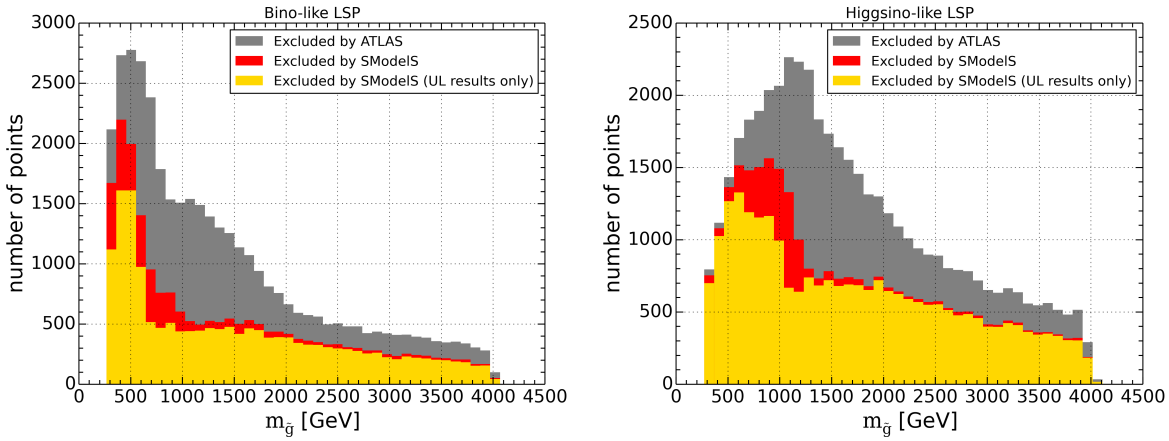

Figure 5.1.: Number of points excluded by SMODELS when using the full 8 TeV database (in red) and when using only UL results (in yellow), as a function of the gluino mass. For reference the total number of ATLAS-excluded points is also shown (in grey). On the left for bino-like LSP and on the right for higgsino-like LSP.

higher, as can be observed in Figure 5.1 as well. This is in particular pronounced for the bino-like LSP scenario. Concretely the coverage of bino-like LSP scenarios is 80% when considering only points with light gluinos ($m_{\tilde{g}} < 600$ GeV), but drops to 60% when considering all points with $m_{\tilde{g}} < 1400$ GeV. Similarly the coverage of higgsino-like LSP scenarios drops from 97% ($m_{\tilde{g}} < 600$ GeV) to 74% ($m_{\tilde{g}} < 1400$ GeV). Note that for bino-like LSP scenarios light gluinos are mainly found in the compressed region where $m_{\tilde{g}} - m_{\tilde{\chi}_1^0} < 100$ GeV, which is not the case for higgsino-like LSP scenarios.

The somewhat better coverage of non-compressed sub-TeV gluinos in the higgsino-like LSP set can be understood as follows. In the case of a bino-like LSP, unless the gluino-LSP mass difference is small, direct decays into the LSP often have only 30% or less branching ratio. Decays into wino- or higgsino-like states are often more important, leading to cascade decays into the LSP and to asymmetric branches with different final states and different mass vectors. This reduces the fraction of gluino signatures covered by SMS results, and as the total cross section reduces with increasing gluino mass, the fraction that can be constrained is no longer large enough to exclude the point. For higgsino-like LSP scenarios on the other hand the second neutralino $\tilde{\chi}_2^0$ as well as the lighter chargino $\tilde{\chi}_1^\pm$ are nearly degenerate with the LSP, and their decay can often be mass compressed in SMODELS. Consequently contributions from decays into higgsinos can be summed up. Moreover, gluino decays into third generation final states are expected to be dominant.

Another important consideration is how far the points which escape the SMODELS exclusion are from exclusion. To this end, we show in Figure 5.3 the maximum r values found

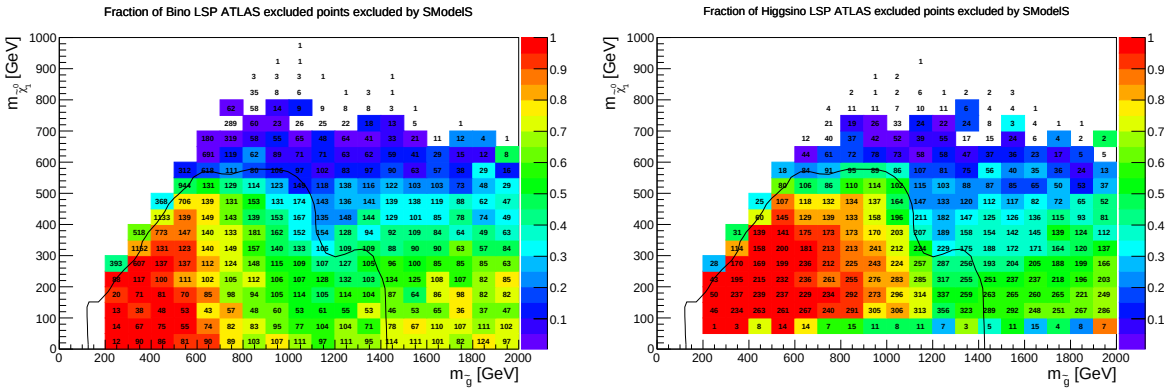

Figure 5.2.: Coverage in the gluino vs neutralino mass plane, for gluino masses up to 2 TeV, for bino-like LSP scenarios (left) and higgsino-like LSP scenarios (right). The color code indicates the fraction of points excluded by SModelS, the text gives the total number of points tested in each bin. For comparison the exclusion line obtained in [213] for a simplified model where gluino pair production is followed by the direct decay $\tilde{g} \to qq\tilde{\chi}_1^0$ is drawn in black.

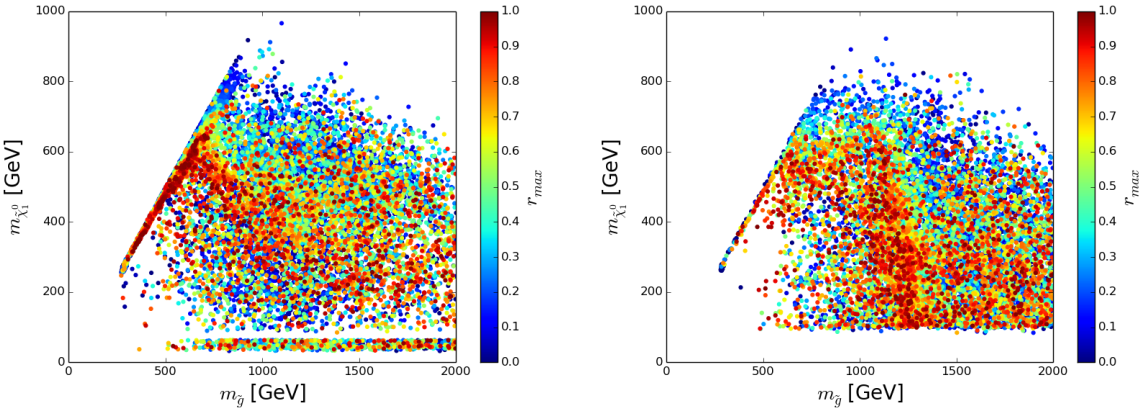

Figure 5.3.: Maximum r value reported by SModelS for allowed points, for gluino masses up to 2 TeV, for bino-like LSP scenarios (left) and higgsino-like LSP scenarios (right). Note that the highest values of r are shown on top.

for all non-exlcuded points. Note that many points, especially in the region of intermediate gluino masses and in the more compressed region, are in fact close to the exclusion limit. We therefore expect that the coverage can be further improved when adding additional efficiency maps, thus allowing to test a larger fraction of the total cross section. Note also that we find that 10% of bino-like LSP scenarios and 12% of higgsino-like LSP scenarios have $0.8 < r < 1.2$, which allows a rough estimate of the uncertainties involved in the limit setting. In turn, we find $r > 1.2$ for 50% of bino-like LSP and 58% of higgsino-like LSP scenarios.

To understand the possibilities of improving the coverage, without going into details about the specific missing topologies, we show in Figures 5.4 and 5.5 the relative cross section that goes into missing topologies with asymmetric branches (left) or long cascade decays (right), for bino-like LSP scenarios and higgsino-like LSP scenarios respectively. Note that, follwing the definition given in Section 3.2.5, asymmetric branch topologies have at most one intermediate particle in each branch, and the number of free parameters is therefore

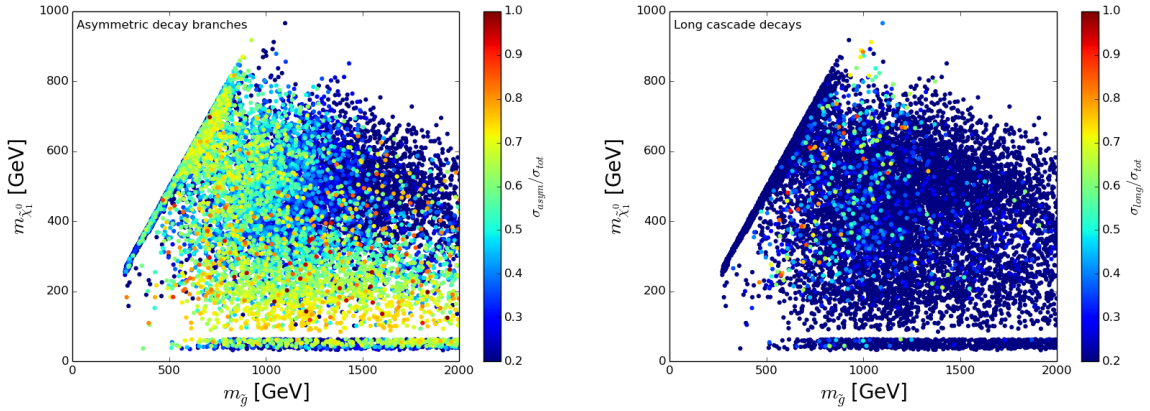

Figure 5.4.: Relative cross section in unconstrained decays with asymmetric branches (left) and long cascade decays (right), for scenarios with a bino-like LSP. Here the total cross section σ_{tot} refers to the full 8 TeV SUSY cross section. Only allowed points with total cross section larger than 10 fb have been considered.

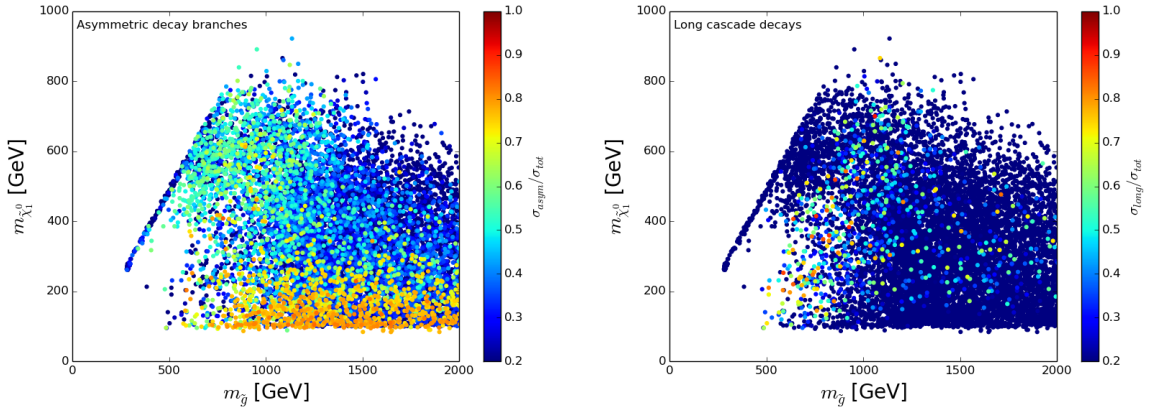

Figure 5.5.: Same as Figure 5.4 but for points with a higgsino-like LSP.

viable for an SMS interpretation. On the other hand long cascade decays typically have too many free parameters, and we no longer consider a simplified model description viable. We see that in fact topologies with asymmetric decay branches are important for a large number of both bino- and higgsino-like LSP scenarios, whereas long cascade decay topologies are dominant only in a few points.

Finally we specify that a particularly important missing topology with asymmetric branches arises from gluino-squark associate production, giving a 3 jet + E_T^{miss} final state. This is important in particular when the light-flavor squarks are highly split and the gluino can decay to a single on-shell squark. The relevant process is $pp \to \tilde{g}\tilde{q}$ followed by $\tilde{q} \to q\tilde{\chi}_1^0$ on one branch and $\tilde{g} \to q\tilde{q} \to q\bar{q}\tilde{\chi}_1^0$ on the other branch, which reads as "[[[jet]],[[jet],[jet]]]" in SModelS language. The same topology is also possible when gluinos are lighter than all squarks and decay dominantly via a loop decay to a gluon and the neutralino LSP. In this case we have $pp \to \tilde{g}\tilde{q}$ followed by $\tilde{g} \to g\tilde{\chi}_1^0$ on one branch and $\tilde{q} \to q\tilde{g} \to qg\tilde{\chi}_1^0$ on the other branch. Figure 5.6 shows the cross section of the "[[[jet]],[[jet],[jet]]]" missing topology in the plane of gluinos mass vs. mass of lightest squark. Note that searches for gluino-squark production are typically interpreted either in a simplified model where gluinos and squarks are completely mass-degenerate, or in a minimal gluino-squark model where all

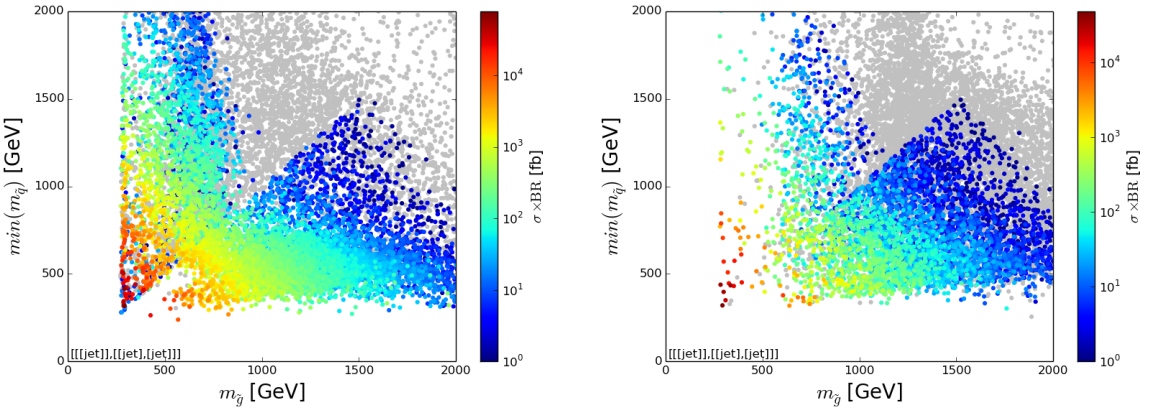

Figure 5.6.: Cross section for the "[[[jet]],[[jet],[jet]]]" missing topology, in the gluino vs. squark mass plane, for bino-like LSP (left) and higgsino-like LSP (right).

production processes (gluino pairs, squark pairs, and gluino-squark associate production) are combined [213]. Consequently, such results cannot be used for reinterpretation in generic models where typically the gluino mass differs from the squark masses, and where the relative importance of the various production and decay channels will be different from the minimal gluino-squark model description.

5.1.3. Conclusions

In summary we found that in the context of the pMSSM about 55% (63%) of bino-like LSP (higgsino-like LSP) scenarios excluded by ATLAS in a comprehensive event simulation study can also be excluded using SMS results. This includes a significant improvement from using EM-type results as well as UL-type results in the SModelS database. The coverage is about 10% lower when using UL-type results only.

Analysing the missing topologies for points escaping all SMS limits we found that asymmetric decay branches are by far dominant, while long cascade decays are rarely important. The SModelS EM database should therefore be extended with asymmetric decay branch topologies to further improve the coverage by SMS results. A particularly important missing topology is the gluino-squark simplified model, see Figure 5.6. Note that there are in fact various production and decay channels that are important when both gluinos and squarks are light, and the relative importance depends on a number of parameters. To constrain generic models the efficiencies of each topology should therefore be evaluated separately, such that the set of efficiency maps can be used to test the total cross section.

Finally it is interesting to note that when both gluino and squarks are light, the associated gluino-neutralino production can also have sizable cross sections, leading to e.g. 2 jets + E_T^{miss} signatures, where the two jets stem from a three-body gluino decay. This topology is not constrained by the currently available SMS limits.

5.2. Constraints on Sneutrino Dark Matter

The searches at Run 1 of the LHC at centre-of-mass energies of 7–8 TeV have already pushed the mass limits of SUSY particles quite high, well above 1 TeV for 1st/2nd gener-

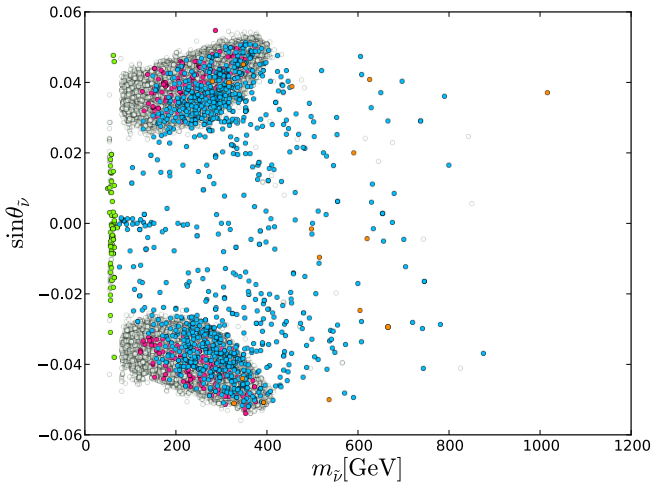

Figure 5.7.: Parameter points where the sneutrino LSP is a good DM candidate, as a function of the sneutrino mass and mixing angle, taken from [280]. Parameter points with characteristic mass spectrum are highlighted in color. Green points denote the Higgs resonance region, orange points have a long-lived stau NLSP, magenta points have a bino NLSP (with $(m_{\tilde{\chi}_1^0} - m_{\tilde{\nu}})/m_{\tilde{\nu}} < 0.1$), and for blue points $(m_{\tilde{\chi}_1^\pm} - m_{\tilde{\nu}})/m_{\tilde{\nu}} < 0.1$

ation squarks and gluinos [161, 162].[2] It should be kept in mind, however, that the LHC limits sensitively depend on the presence of particular decay modes, and are considerably weakened in case of compressed [147] or stealth [273] spectra. Besides, the squark/gluino mass limits from Run 1 searches vanish completely in case the neutralino LSP is heavier than about 600 GeV (current Run 2 results push this limit to neutralino LSP masses above 1 TeV, see e.g. [274, 275]).

Moreover, the SUSY mass limits depend sensitively on the nature of the LSP. Most experimental analyses indeed assume that the LSP is the lightest neutralino of the MSSM. A particularly interesting alternative, described in Section 1.3.3, is a mainly RH mixed sneutrino in the MSSM augmented by a RH neutrino superfield.

The phenomenology of the MSSM+RN model was previously investigated in [64, 75, 276]. Indirect detection and cosmology were discussed in [70, 71, 277], and LHC signatures in [278–280] (see also [281–283] for related LHC studies). Reference [280] gave an update of the status of the sneutrino as DM after the Higgs mass measurements, by exploring the SUSY parameter space with the soft breaking terms fixed at the GUT scale, and assessing also the impact of the exclusion bound for DM direct searches from LUX [284]. The allowed parameter space is summarised in Figure 5.7. In particular the sneutrino can be a good DM candidate even for small mixing angles, if annihilation via Higgs is resonant (green points) or in case of wino or higgsino NLSP co-annihilation (blue points). For larger mixing angles the sneutrino can be a good DM candidate, independent of the concrete mass spectrum.

Here we extend the work of [280] by investigating to what extent the results from SUSY searches at Run 1 of the LHC, published in terms of SMS limits, constrain the sneutrino-LSP scenario. Moreover, we discuss the most promising topologies for which no SMS results exist but would enhance the LHC sensitivity to sneutrino DM. To this aim, we make use of the SModelS v1.0.1 package [191, 192, 285] to compare the predictions of the MSSM+RN

[2] These limits were further extended by early Run 2 searches, see Section 2.4.

	Observable	Value/Constraint	Ref.
Measurements	m_h	125.85 ± 0.4 GeV (exp) ± 4 GeV (theo)	[28, 286]
	$\text{BR}(B \to X_s\gamma) \times 10^4$	$3.55 \pm 0.24 \pm 0.09$ (exp)	[287]
	$\text{BR}(B_s \to \mu^+\mu^-) \times 10^9$	$3.2^{+1.4}_{-1.2}$ (stat) $^{+0.5}_{-0.3}$ (sys)	[288]
	$\Omega_{\text{DM}}h^2$	0.1186 ± 0.0031 (exp) $\pm 20\%$ (theo)	[289]
Limits	$\Delta\Gamma_Z^{\text{invisible}}$	< 2 MeV (95% CL)	[290]
	$\text{BR}(h \to \text{invisible})$	$< 20\%$ (95% CL)	[291]
	$m_{\tilde{\tau}}$	> 85 GeV (95% CL)	[292]
	$m_{\tilde{\chi}_1^+}, m_{\tilde{e},\tilde{\mu}}$	> 101 GeV (95% CL)	[290]
	$m_{\tilde{g}}$	> 308 GeV (95% CL)	[293]
	σ_n^{SI}	$< \sigma_{\text{LUX}}^{\text{SI}}$ (90% CL)	[284]

Table 5.2.: Summary of the observables and constraints used in this analysis.

model against the SMS limits published by ATLAS and CMS. This allows us to test the limits from a large variety of searches and at the same time draw conclusions about which additional topologies should be considered. This study was published in [72].

We describe the numerical procedure in Section 5.2.1, i.e. the sampling method and the application of SModelS to the MSSM+RN. Our numerical results are presented in Section 5.2.2. Note that the validity of applying SMS results from slepton searches (dilepton plus E_T^{miss} signature) to chargino-pair production followed by decays into leptons and sneutrinos was discussed in Section 4.3. Section 5.2.3 gives some details on scenarios with long-lived heavy charged particles, in particular gluinos or stops, which so far cannot be constrained by SMS results. Our conclusions are presented in Section 5.2.4.

5.2.1. Numerical Procedure

Sampling method over the model parameters

For definiteness, we study the MSSM+RN with soft terms defined at a high scale $M \sim M_{\text{GUT}}$ as in [280]. Allowing for non-universalities in the gaugino and scalar sectors, our set of free parameters is

$$M_1, M_2, M_3, m_L, m_R, m_N, m_Q, m_H, A_l, A_{\tilde{\nu}}, A_q, \tan\beta, \text{sgn}\mu\,. \tag{5.1}$$

Here the M_i are the gaugino masses, m_L, m_R, m_N are the charged slepton and sneutrino masses (equal for all flavors), m_Q is a common squark mass parameter, $m_H \equiv m_{H_u} = m_{H_d}$ denotes the common entry for the two Higgs doublet masses, and A_l, A_q and $A_{\tilde{\nu}}$ are the scalar trilinear couplings for the sleptons, squarks and sneutrinos respectively, same for all flavors. The absolute value of μ is obtained from the minimization of the Higgs potential, leaving only the sign of μ as a free parameter. The computation of the mass spectrum follows that explained in [280], where all details are provided.

The list of constraints implemented in the model likelihood function is given in Table 5.2. In particular, besides consistency with B-physics constraints, we require the Higgs mass m_h to be compatible with the ATLAS and CMS measurements [294, 295], which we combine by a statistical mean, as obtained in [296]. Its uncertainty is dominated by the theoretical error,

estimated to be around 4 GeV [297]. We also require that chargino and charged slepton masses fulfill the LEP bounds at 95% CL —notice that the tau slepton has a slightly less stringent lower bound of 85 GeV [292] as compared to selectrons and smuons— and we include the gluino mass bound from the D0 collaboration [293]. If $\tilde{\nu}_{\tau_1}$ is light enough to be produced in Z decay, we require its contribution to the Z invisible decay width to be smaller than 2 MeV [298]. Similarly, when the sneutrino mass is lighter than $m_h/2$, the Higgs can decay invisibly into sneutrino pairs. We require that such decays do not contribute more than 20% to the Higgs invisible branching ratio [291].

Regarding DM constraints, we require consistency with the measured relic abundance and with the bounds from direct detection experiments (constraints from indirect DM detection are also fulfilled). The experimental error on $\Omega_{\rm DM}h^2$ has become incredibly small due to the Planck measurement [289], while the theoretical one is still large. We use a conservative estimate of the order 20% [299] for the latter. Furthermore, we enforce the sneutrino SI scattering cross section off nuclei, $\sigma_n^{\rm SI}$, to be compatible with the 90% CL bound from LUX [284]. Note that recently presented first results from the XENON1T experiment have substantially improved the limits on $\sigma_n^{\rm SI}$, see Figure 1.3.

To evaluate the experimental observables we first computed the supersymmetric particle spectrum with a modified version of SOFTSUSY [173]. For the computation of the sneutrino relic density and elastic scattering cross-section the model has been implemented in FEYNRULES [171,300], by adding the appropriate term in the superpotential and in the soft SUSY breaking potential. We generate output files compatible with CALCHEP in order to use the public code `micrOMEGAs` [44]. The B-physics observables are computed by interfacing the program with SUPERISO [301].

The likelihood is constructed in a simple way. For measured quantities, we assume a Gaussian likelihood function with a variance given by combining in quadrature the theoretical and experimental variances. For observables for which only lower or upper limits are available, we use a likelihood modelled as a step function on the $x\%$ CL of the exclusion limit. The total likelihood function is then the product of the individual likelihoods associated to each experimental result. In order to save time in the sampling procedure, the slepton, chargino and gluino mass limits are, however, absorbed into the prior probability density functions: each parameter point generating a mass spectrum that violates one of these bounds is immediately discarded.

Given the likelihood function, we sample the posterior probability density function with the MULTINEST algorithm [302–304]. In order to cover all phenomenological interesting classes, we run separate chains that look either for light(ish) electroweakinos ($m_{\tilde{\chi}_1^\pm} < 900$ GeV), light sleptons ($m_{\tilde{l}} < 600$ GeV), or for light squark or gluinos ($m_{\tilde{q}} < 1.5$ TeV or $m_{\tilde{g}} < 1.5$ TeV). As for the choice of priors, we always take logarithmic priors on M_3, m_Q, A_Q, m_H, while we use both logarithmic and flat priors for $M_1, M_2, m_L, m_R, m_N, A_L, A_{\tilde{\nu}}, \tan\beta$, the sign of μ is fixed to +1 (details on the prior ranges are provided in [280]). In particular we perform two chains, one with log and one with flat priors, for each relevant data set: two chains for light electroweakinos (these two data sets coincide with the ones used in [280]), two chains for light sleptons and two chains for light squarks or gluinos. In each case, the other masses are left to vary freely from high to low values. The motivation for this is, as mentioned, to cover all potentially interesting cases; the results we will present in Section 5.2.2 are for all chains combined together.

The sampled points correspond to a 95% CL in volume of the posterior. (Since in this study we are not interested in statistical statements on the parameter space, we will however not exploit this feature.) The limits imposed by a step function are of course strictly obeyed

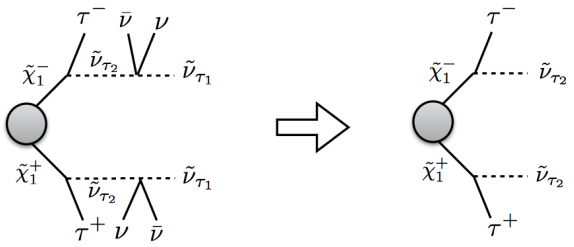

Figure 5.8.: Illustration of "invisible compression" in sneutrino LSP scenarios. The decays of the heavier sneutrino to the lighter one plus neutrinos are discarded in the final topology, leaving the $\tilde{\nu}_{\tau_2}$ as an effective LSP.

by all scan points. Moreover, we have checked that none of the individual constraints implemented by a Gaussian gets a large pull in the final sample. In particular, BR$(B \to X_s\gamma)$ and BR$(B_s \to \mu^+\mu^-)$ are in full agreement with the 95% CL experimental results [287, 288] for all points in the samples.

Once the sampling of the parameter space according to the constraints in Table 5.2 is completed, all the points in the chains are confronted against the LHC Run 1 results using the first version SModelS v1.0.1 [191, 192, 285] as explained in the next subsection.

Deriving LHC constraints with SModelS

The decomposition procedure works "out of the box" for the MSSM+RN model with a sneutrino LSP. Nonetheless some subtleties must be taken care of when processing the MSSM+RN scan points with SModelS.

We use the MSSM+RN model implemented in micrOMEGAs 3.2 [44] to compute the decay branching ratios, $\mathcal{B}$. The production cross sections for sleptons and sneutrinos (*i.e.* the sector modified with respect to the MSSM) are also computed with micrOMEGAs 3.2. For all other production processes, we use the default SModelS cross section calculator based on Pythia 6.4 [202] and NLLfast [128–134]. Electroweak cross sections are thus computed at leading order while strong productions are computed at NLO+NLL order.

Given the information on σ and $\mathcal{B}$ in the SLHA files, SModelS computes $\sigma \times \mathcal{B}$ for each topology that occurs, where we use $\sigma_{\text{cut}} = 0.05$ fb.

When dealing with an arbitrary spectrum of SUSY particles, it is possible that a part of the decay chain leads to completely invisible decays, *e.g.* a decay of a heavy sneutrino to a lighter one plus neutrinos in the current scenario. In such cases, SModelS compresses the invisible part of the decay chain (see Section 3.2.2). In the MSSM+RN this happens e.g. for the decay illustrated in Figure 5.8. All decays to neutrinos appearing after the last visible decay are disregarded, yielding an "effective LSP" for the particular event, which can be different from the true LSP. This procedure is called "invisible compression". Likewise, a neutralino may decay invisibly to a sneutrino and a neutrino; in this case the compressed topology resembles an MSSM topology.

In addition, if the mass gap between mother and daughter particles is small, the decay products will be too soft to be detected at the LHC. This is taken care of by the so-called "mass compression" in SModelS, discarding any SM particle that come from a vertex for which the mass splitting of the R-odd particles is less than a certain threshold. We use 5 GeV as the minimum required mass difference for the decay products to be visible.

Another comment is in order. The experimental constraints implemented in the database of SModelS v1.0.1 require final states containing E_T^{miss}. This means that scenarios with long-

lived particles ($c\tau > 10$ mm) leading to signatures with displaced vertices or heavy charged particle tracks cannot be tested with SModelS v1.0.1. In the MSSM, this occurs, *e.g.*, in wino-LSP scenarios where the $\widetilde{\chi}_1^\pm$ is highly mass-degenerate with the $\widetilde{\chi}_1^0$ and thus becomes long-lived. In the sneutrino LSP case, not only charginos can be long lived if the mass splitting with the sneutrino is small enough; other possibilities are, *e.g.*, long-lived gluinos or stops, if they are the next-to-lightest SUSY particle (NLSP). We perform a detailed check of all input points to avoid the erroneous application of SMS limits to such cases. Points that have visible decays from long-lived particles or heavy charged particle tracks with cross sections larger than $\sigma_{\rm cut}$ are discarded. A brief discussion of such scenarios can be found in Section 5.2.3.

Once the decomposition into SMS topologies, including mass and invisible compression, is completed and the checks that the SMS results actually apply are passed, a given point is confronted against the SMS results in the SModelS v1.0.1 database. Finally, for each matching result, the ratio r of the signal cross-section and the upper limit, $r = \sigma(\text{predicted})/\sigma(\text{excluded})$, is given, where σ effectively means $\sigma \times \mathcal{B}$ or the weight of the topology. A value of $r \geq 1$ means that the input model is likely excluded by the corresponding analysis.

5.2.2. Results

We now turn to analysing the impact of the LHC searches on the MSSM+RN parameter space. As explained in the previous Section, we here consider only points for which the SMS results apply, i.e. we discard points with non-prompt visible decays as well as points with long-lived charged particles. Scanning over the parameter space, we can then distinguish several cases:

- the SMS results in principle apply but no SMS constraints actually exist for the specific topologies of the point — these points will be labelled as *not tested*;[3]
- there exist (one or more) SMS results that test the specific topologies of the point but for each topology the total $\sigma \times \mathcal{B}$ is below the corresponding 95% CL upper limit — these points will be considered as *allowed*; and
- at least one topology has a $\sigma \times \mathcal{B}$ equal or above its 95% CL upper limit ($r \geq 1$) — these points will be considered as *excluded*.

Note that *not tested* points are of course also allowed, however we cannot compare the cross section prediction to an upper limit.

Let us start with the question which analyses are the most important ones for constraining the model. To this end, Figures 5.9 and 5.10 show a breakdown of most constraining analyses in the $\tilde{\nu}_{\tau_1}$ versus $\tilde{g}$ and $\tilde{\nu}_{\tau_1}$ versus $\widetilde{\chi}_1^\pm$ mass planes, respectively. Looking first at Figure 5.9, we see that the SMS interpretations of the hadronic SUSY searches [212, 213, 305–309] are constraining gluino masses up to about $m_{\tilde{g}} \approx 1200$ GeV and LSP masses of at most about $m_{\tilde{\nu}_{\tau_1}} \approx 500$ GeV. These searches mostly exclude points where either $\tilde{g} \to b\bar{b}\widetilde{\chi}_i^0$, $\tilde{g} \to t\bar{t}\widetilde{\chi}_i^0$ or $\tilde{g} \to q\bar{q}\widetilde{\chi}_i^0$ decays are dominant, followed by an invisible decay of the neutralino, $\widetilde{\chi}_i^0 \to \nu\tilde{\nu}$. Moreover, dilepton + $E_T^{\rm miss}$ searches [265, 310] exclude sneutrino LSP masses up to about $m_{\tilde{\nu}_{\tau_1}} \approx 210$ GeV, independent of the gluino mass. The process that is constrained here is

[3] This occurs if no simplified model result exists for the signal topologies of the point considered, but also if the mass vector of a topology lies outside that of the experimental constraint. Moreover, we include here also the points for which all signal topologies are discarded because of $\sigma \times \mathcal{B} < \sigma_{\rm cut}$.

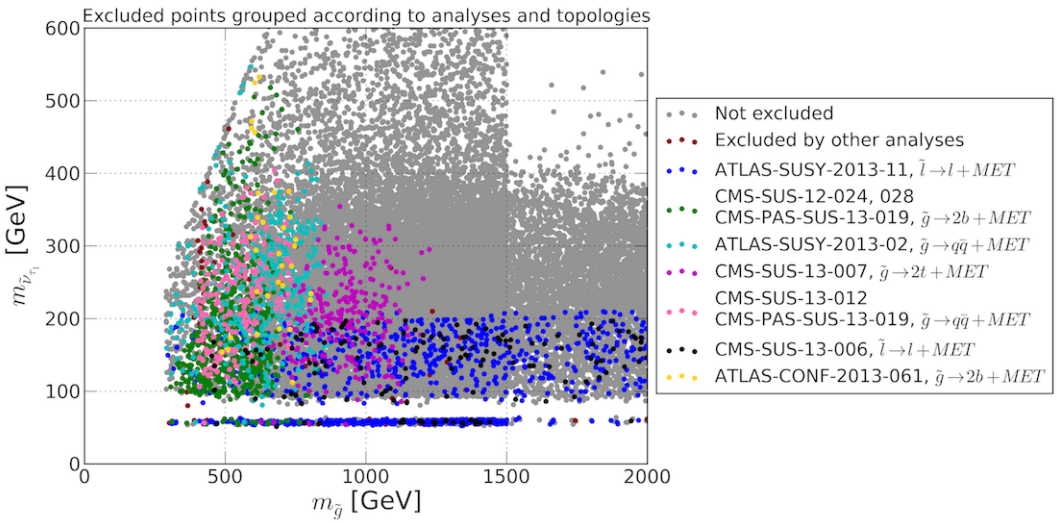

Figure 5.9.: For scan points that are excluded by the SMS limits, we show (in color) the breakdown of most constraining analyses in the $\tilde{\nu}_{\tau_1}$ vs. $\tilde{g}$ mass plane. To illustrate the coverage of the parameter space, we also show (in grey) the not excluded or not tested points.

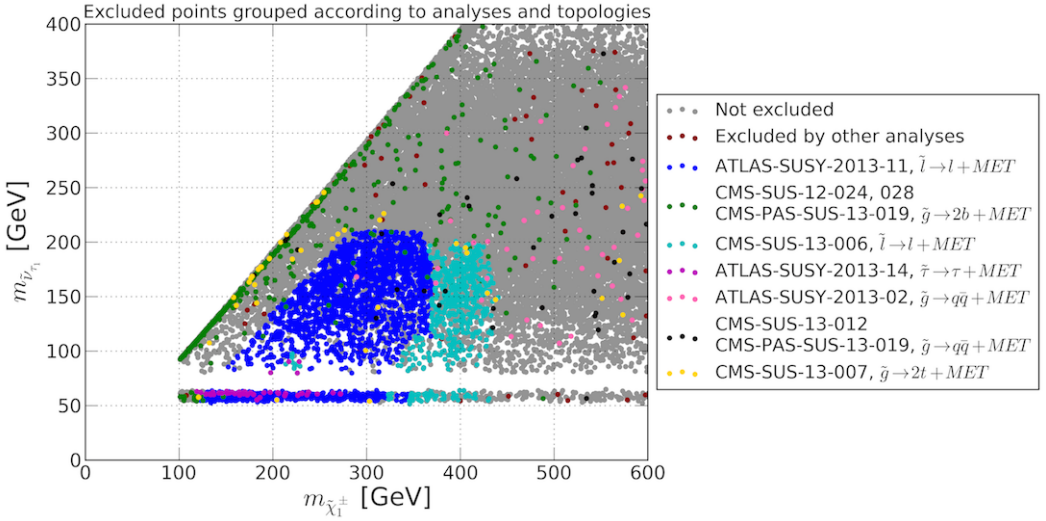

Figure 5.10.: As Figure 5.9 but in the $\tilde{\nu}_{\tau_1}$ vs. $\widetilde{\chi}_1^\pm$ mass plane.

Drell-Yan production of $\widetilde{\chi}_1^+\widetilde{\chi}_1^-$ followed by $\widetilde{\chi}_1^\pm \to l^\pm \tilde{\nu}_{l1}$ ($l = e$ or μ), with the $\tilde{\nu}_{l1} \to \tilde{\nu}_{\tau_1} + X$ decay being invisible (because of X being genuinely invisible or very soft). Consequently, in Figure 5.10 we see that chargino masses can be excluded up to about $m_{\widetilde{\chi}_1^\pm} \approx 440$ GeV by the dilepton + E_T^{miss} limits. (There is also a small region of parameter space at low masses where $\tau^+\tau^- + E_T^{\text{miss}}$ [311] gives the strongest limit.)

It is important to note here that the constraints on $\widetilde{\chi}_1^+\widetilde{\chi}_1^- \to l^+l^- + E_T^{\text{miss}}$ actually stem from the $\tilde{l}^+\tilde{l}^- \to l^+l^-\widetilde{\chi}_1^0\widetilde{\chi}_1^0$ simplified model and analogously for $\tau^+\tau^- + E_T^{\text{miss}}$, which has the opposite spin configuration than chargino-pair production followed by chargino decays into sneutrinos. The validity of applying the limits from the slepton searches to the case of chargino-pair production is discussed in Section 4.3.

Also noteworthy is the fact that most of the excluded points in Figures 5.9 and 5.10 have some grey points lying below them, which are not excluded or not tested at all. This is cor-

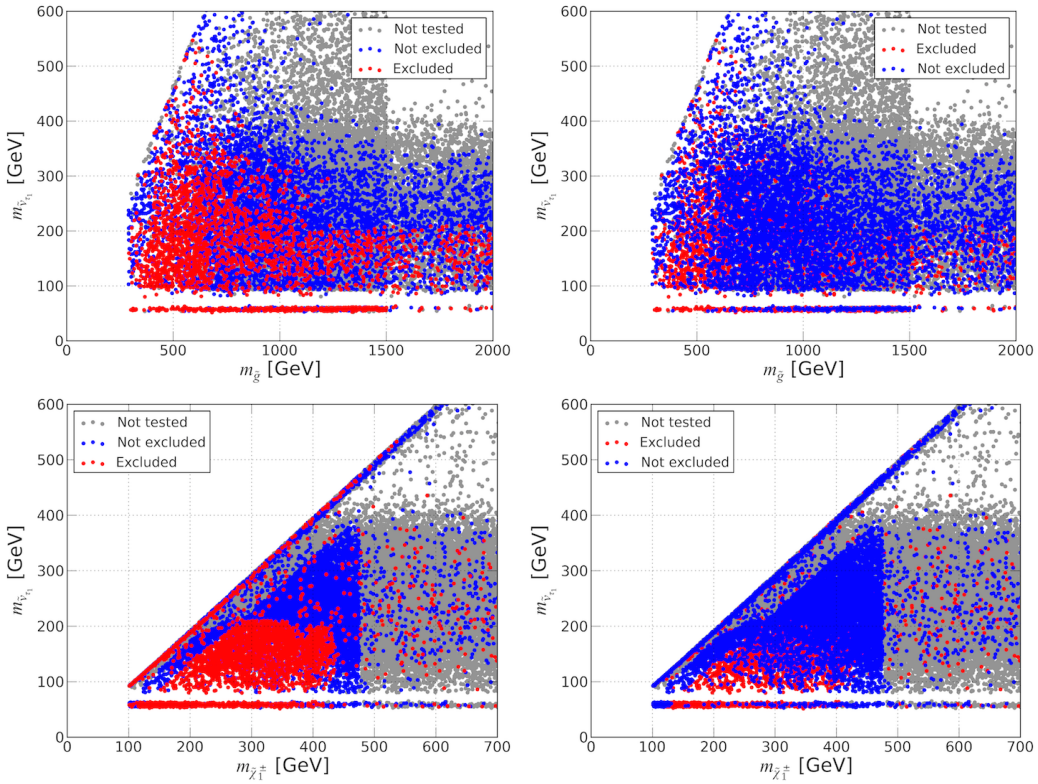

Figure 5.11.: Scatter plots of points for which SMS results apply. The top row shows the $\tilde{\nu}_{\tau_1}$ vs. $\tilde{g}$, the bottom row the $\tilde{\nu}_{\tau_1}$ vs. $\widetilde{\chi}_1^\pm$ mass plane. In the panels on the left, the points excluded by the SMS constraints (red) are plotted on top of those which are not excluded (blue); in panels on the right this plotting order is inverted. Also shown (in grey) are the "not tested" points, for which no SMS constraints exist.

roborated in Figure 5.11, where we present the summary of not tested, allowed and excluded points in the $\tilde{\nu}_{\tau_1}$ versus $\tilde{g}$ and $\tilde{\nu}_{\tau_1}$ versus $\widetilde{\chi}_1^\pm$ mass planes. In the plots on the left, the excluded points (red) are plotted on on top of the allowed points (blue), while in the plots on the right this plotting order is inverted. Points which are not tested (grey) are always plotted below. As can be seen, only a small part of the parameter space can genuinely be excluded by the SMS results—over most of the regions where the SMS results are valid, there are almost always parameter combinations such that the limits can be avoided.

For the dilepton signature originating from chargino-pair production, the chargino mixing plays an important rôle: wino-like charginos have a higher production cross section, and a higher branching fraction into $l\tilde{\nu}_{l1}$. The limits from $l^+l^- + E_T^{\text{miss}}$ searches therefore mostly affect scenarios with wino-like $\widetilde{\chi}_1^\pm$, while higgsino scenarios are much less constrained. For illustration see Figure 5.12, which shows the SMS-allowed points in the $\tilde{\nu}_{\tau_1}$ versus $\widetilde{\chi}_1^\pm$ mass plane—here the color map gives the size of the U_{11} entry of the chargino mixing matrix, indicating to the wino/higgsino content of the $\widetilde{\chi}_1^\pm$. As can be seen, in the region that is in principle constrained by the SMS results the surviving points feature $\widetilde{\chi}_1^\pm$s that have a large higgsino admixture ($|U_{11}| \lesssim 0.5$). These points have a lower $\widetilde{\chi}_1^+\widetilde{\chi}_1^-$ production cross section and the $\widetilde{\chi}_1^\pm$ decays preferably into $\tau\tilde{\nu}_{\tau_1}$ since the higgsino decay to e, μ is Yukawa suppressed; $\tau^+\tau^- + E_T^{\text{miss}}$ is however a more difficult signature experimentally and thus only constrains a small strip at low $\tilde{\nu}$ mass, cf. the purple points in Figure 5.10.

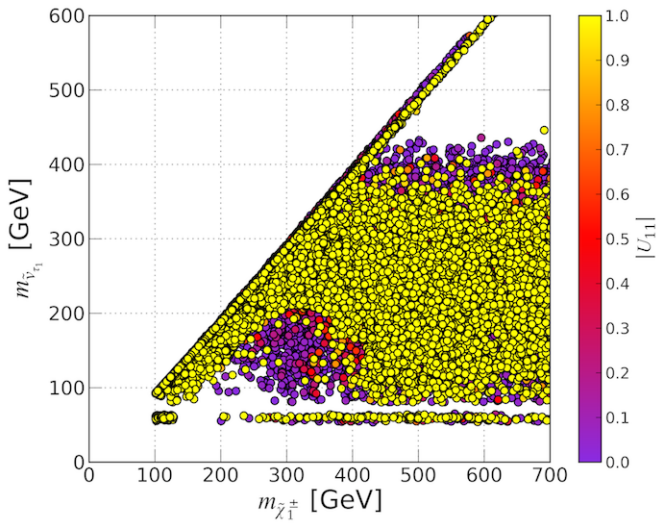

Figure 5.12.: Allowed points in the $\tilde{\nu}_{\tau_1}$ vs. $\widetilde{\chi}_1^\pm$ mass plane, with the color code indicating the wino/higgsino content of the $\widetilde{\chi}_1^\pm$ ($|U_{11}| = 1$ means a pure wino while $|U_{11}| = 0$ means a pure higgsino).

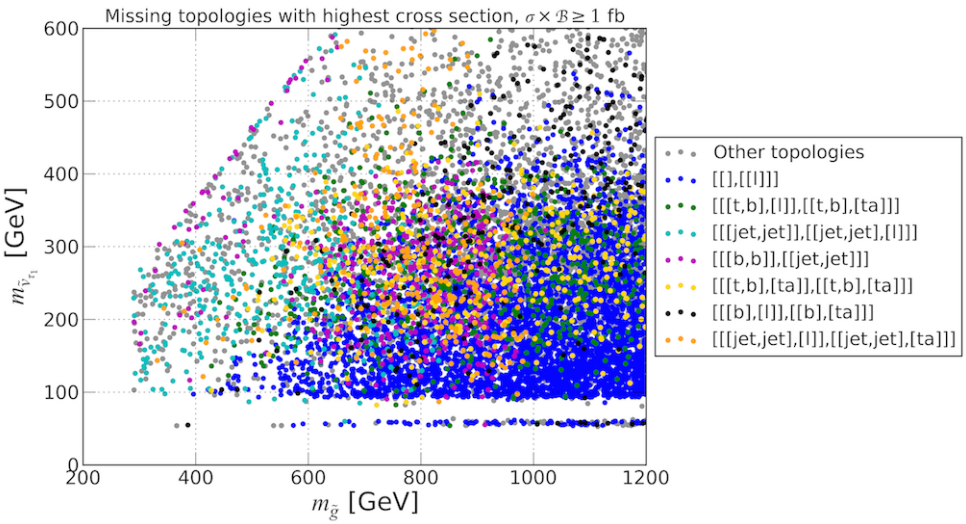

Figure 5.13.: Missing topologies with highest $\sigma \times \mathcal{B}$ in the $\tilde{\nu}_{\tau_1}$ vs. $\tilde{g}$ mass plane.

Missing topologies

The next question to ask is which are the most important signatures not covered by SMS results. Such information can be used to improve on the interpretation of the LHC searches for new physics. We call these uncovered signatures "missing topologies", see Section 3.2.5. The total weight is computed by summing over all diagrams giving the same topology, *i.e.* ignoring the mass vector of the SUSY states involved. Moreover, $l = e, \mu$ lepton flavors appearing in the final state are summed over (light quark flavors are always summed over). In the following, we only consider MSSM+RN scan points which are not excluded, and we demand that missing topologies have $\sigma \times \mathcal{B} \geq 1$ fb. The results can be presented in two ways, either by showing the most frequent missing topologies in a certain parameter space, or by selecting for each parameter point the missing topology with the highest cross section.

We choose the latter approach to show in Figure 5.13 the missing topologies in the sneutrino- vs. gluino-mass plane. The various processes are denoted in the bracket notation of SModelS,

explained in Section 3.1.1.

It is apparent that many points with gluino masses below about 1.2 TeV, for which the LHC searches should have good sensitivity, are not excluded by the SMS results because they feature "mixed topologies", where the two pair-produced gluinos undergo different decays (*e.g.* one gluino decaying into $b\bar{b}$ and the other one into light jets). Since the SMS results for pair-produced sparticles always assume two identical branches, these cases cannot be constrained by SModelS v1.0.1. Moreover, hadronic final states with additional leptons, as they arise from gluino decays into charginos and the chargino decaying further into a charged lepton (e, μ or τ) plus a sneutrino, do not have any SMS equivalent. Finally, there are no SMS results available for $\tilde{g} \to tb\widetilde{\chi}_j^{\pm}$, no matter of whether the chargino has any visible decays.[4]

It is also worth noting that over a large part of the parameter space single lepton + $E_T^{\rm miss}$ (`[[],[[l]]]` in bracket notation) is the most important missing topology. This signature arises from $\widetilde{\chi}_i^0\widetilde{\chi}_j^{\pm}$ production; its importance is corroborated in Figure 5.14, where one can see that it is indeed dominating the whole sneutrino- vs. chargino-mass plane. There are also cases where single W + $E_T^{\rm miss}$ is dominant. The cross section for single lepton + $E_T^{\rm miss}$ production, shown in Figure 5.15, can be very large and should give important additional constraints on the model. While searches for single lepton + $E_T^{\rm miss}$ were performed by both ATLAS [312] and CMS [313], unfortunately no suitable SMS interpretation exists for these analyses. Moreover, the $E_T^{\rm miss}$ cuts in these searches, targeting heavy resonances decaying to a lepton and a neutrino, are typically very hard to suppress the large SM background. As a consequence they are not efficient in constraining the chargino-neutralino production in the MSSM+RN.

Having both light electroweakinos and light staus can generate decay chains with more 'exotic' signatures, in particular $\widetilde{\chi}_i^{\pm}\widetilde{\chi}_j^0$ followed by $\widetilde{\chi}_i^{\pm} \to \nu\tilde{\tau}^{\pm} \to \nu W^{\pm}\tilde{\nu}_{\tau_1}$ and $\widetilde{\chi}_j^0 \to \tau^{\pm}\tilde{\tau}^{\mp} \to \tau^{\pm}W^{\mp}\tilde{\nu}_{\tau_1}$. This appears as `[[[nu],[W]],[[ta],[W]]]`[5] (yellow points) in Figure 5.14 and is interesting because the $\widetilde{\chi}_j^0$ decay produces with the same rate τ^+W^- and τ^-W^+: together with the chargino decay this gives rise to a same-sign W signature, $W^{\pm}W^{\pm}\tau^{\mp}$ + $E_T^{\rm miss}$.

Before proceeding it is instructive to take another look at the missing topologies arising from electroweakino and slepton production, but this time ordered by their frequency of occurrence. This is done in Figure 5.16. Not surprisingly we see that besides single lepton (e or μ), single τ is an important signature. Although it is less clean experimentally, the relative weight of single e, μ or τ + $E_T^{\rm miss}$ might potentially give information on the mass pattern of the mostly RH sneutrinos. Another important class of "missing topologies" are different-flavor dileptons (`[[[l]],[[ta]]]` and `[[[l]],[[l']]]`). Different-flavor dileptons + $E_T^{\rm miss}$ have in principle been considered by ATLAS and CMS in the context of chargino-pair production in the MSSM with the charginos decaying either into $W^{(*)}\widetilde{\chi}_1^0$ [265] or into $l\nu\widetilde{\chi}_1^0$ via on-shell sleptons/sneutrinos [265, 310]. However, the associated SMS limits do not apply to the sneutrino LSP case for various reasons. For example, the leptons from $\widetilde{\chi}_1^{\pm} \to W^{(*)}\widetilde{\chi}_1^0$ are generally softer than those from $\widetilde{\chi}_1^{\pm} \to l^{\pm}\tilde{\nu}_l$ decays (for the same $\widetilde{\chi}_1^{\pm}$ and LSP masses) because of the additional neutrinos in the W decay. The limits for the $\widetilde{\chi}_1^+\widetilde{\chi}_1^- \to 2 \times \tilde{l}\nu(\text{or } \tilde{\nu}l) \to 2 \times l\nu\widetilde{\chi}_1^0$ simplified model are also not applicable because they involve an additional intermediate mass scale.

[4] A constraint on this topology, for scenarios where the chargino decay is compressed and thus invisible, has since become available and gives important constraints on UMSSM scenarios, see Section 5.3.

[5] In this case the invisible decay via a neutrino cannot be compressed because it is followed by a visible decay into W and a sneutrino.

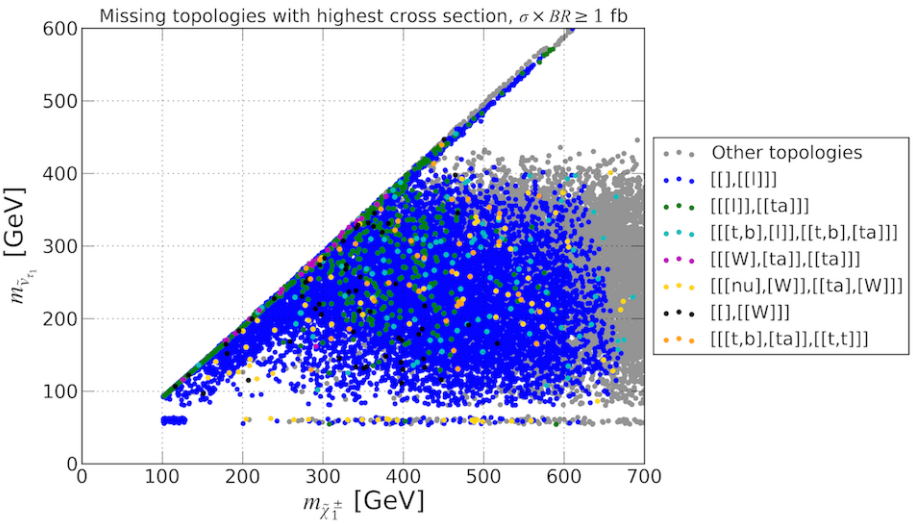

Figure 5.14.: Missing topologies with highest $\sigma \times \mathcal{B}$ in the $\tilde{\nu}_{\tau_1}$ vs. $\widetilde{\chi}_1^\pm$ mass plane.

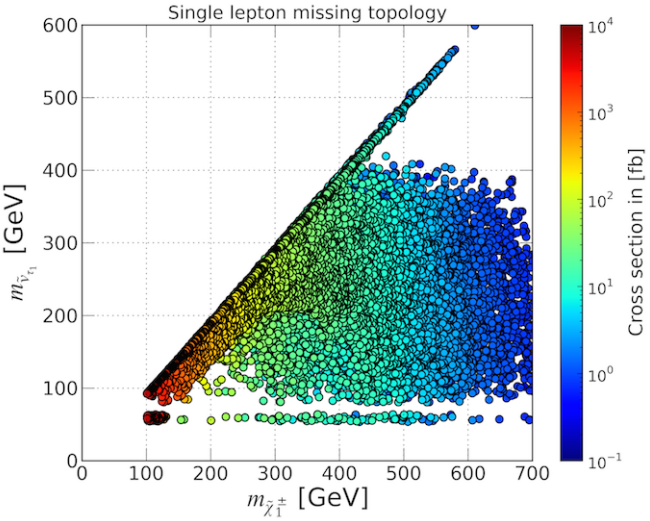

Figure 5.15.: Cross sections $\sigma \times \mathcal{B}$ for the single lepton + E_T^{miss} missing topology for not excluded or not tested points.

Finally, the `[[[W]],[[W],[ta]]]` topology again gives rise to same-sign W's, see the red triangles in Figure 5.16. Similarly it is possible to have same sign τ's arising from `[[[W],[ta]],[[ta]]]` (black stars). In this case, after $\widetilde{\chi}_i^0 \widetilde{\chi}_j^\pm$ production, the decay chain is $\widetilde{\chi}_i^0 \to W^\mp \widetilde{\chi}_k^\pm \to W^\mp \tau^\pm \tilde{\nu}_{\tau_1}$ and $\widetilde{\chi}_j^\pm \to \tau^\pm \tilde{\nu}_{\tau_1}$.

Complementarity with direct DM searches

Let us finally turn to the complementarity of LHC and direct DM searches—recall that all points in our scans are consistent with DM constraints, as described in Table 5.2. In Figure 5.17, left panel, we plot the allowed (gray), excluded (red) and not tested points (cyan) as a function of the sneutrino mass and the SI scattering cross section. In the same plot we also show the forecasted sensitivity of XENON1T after two years of scientific run [314] and the predicted value for neutrino coherent scattering on nuclei [315], which can be an irreducible background for direct detection experiments. From this plot, the complementarity

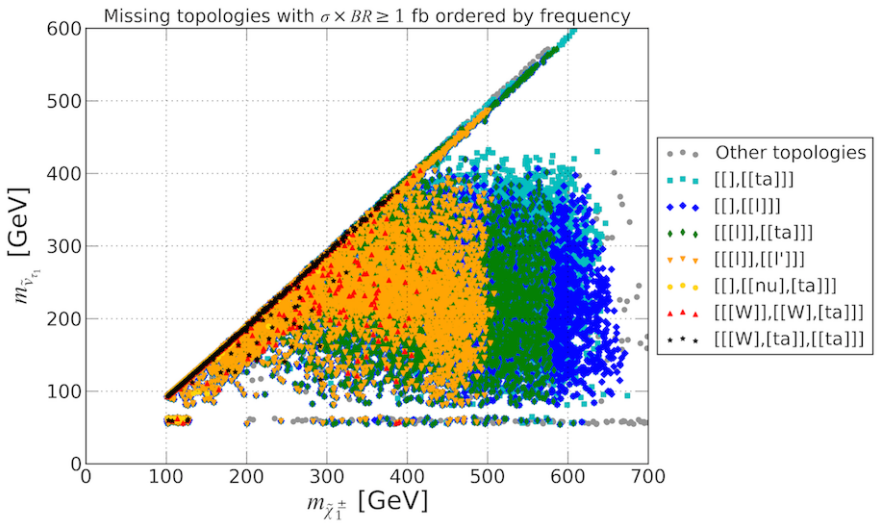

Figure 5.16.: Missing topologies with $\sigma \times \mathcal{B} \geq 1$ fb in the sneutrino- vs. chargino-mass plane ordered by frequency of occurrence. The ordering is from top to bottom in the legend, with single tau being the most frequent missing topology, followed by single lepton ($l = e, \mu$), lepton–tau, and so on. "Other topologies" are shown on top of the legend without considering their total count (however, each single one of them is less frequent than any of the topologies denoted explicitly).

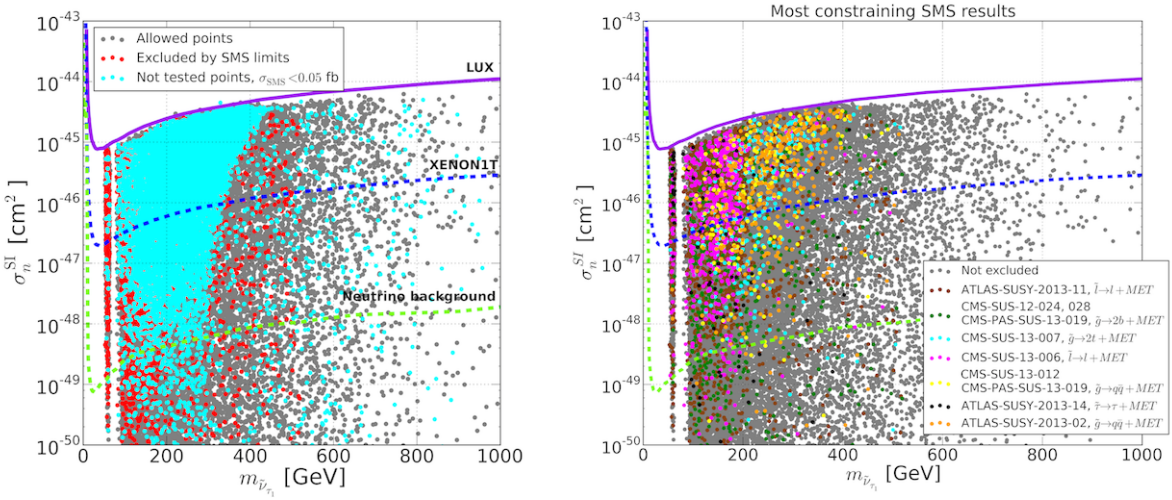

Figure 5.17.: Complementarity of LHC and direct DM detection experiments. The panel on the left shows SMS allowed, excluded and not tested points in the plane of σ_n^{SI} vs. $m_{\tilde{\nu}_{\tau_1}}$. The panel on the right shows the breakdown of most constraining analyses for the points that are excluded by the SMS limits (for the sake of comparison, the allowed points are shown in grey). In both panels, the solid magenta lines and the dashed blue lines are the exclusion limit by LUX [284] and the forecasted sensitivity of XENON1T experiment respectively, while the dashed light green line corresponds to the predicted neutrino coherent scattering on nuclei. Note that the limit has since been extended, in particular by early XENON1T results, see Figure 1.3.

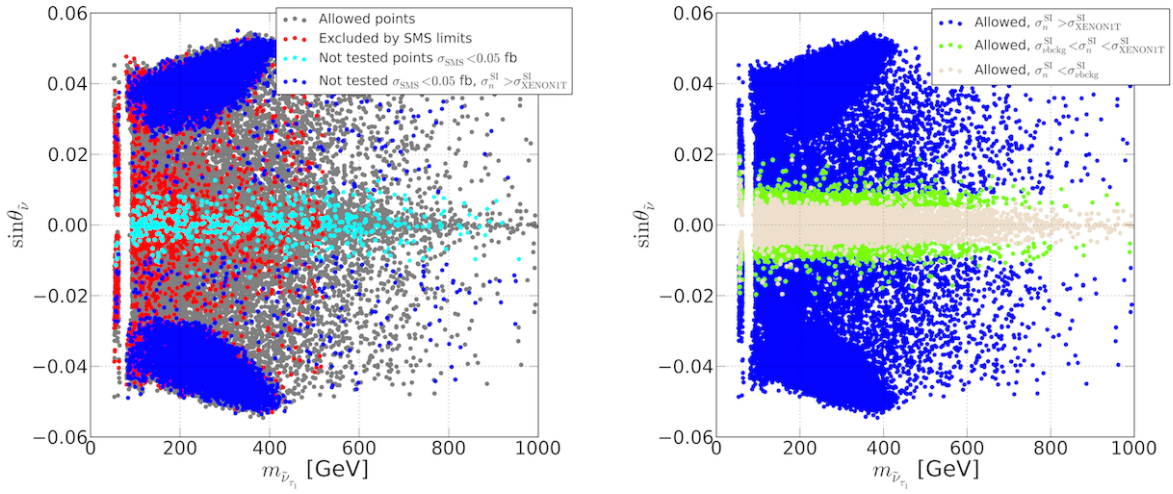

Figure 5.18.: On the left allowed (grey), excluded (red) and not tested (blue and cyan) points are shown in the plane of sneutrino mass versus mixing angle. The subset of points with exceedingly small $\sigma \times \mathcal{B}$ at the LHC but in the reach of XENON1T is visualised in blue. On the right, we show the SMS allowed points in the sneutrino mass versus mixing angle plane, subdivided in blue points, which are in the reach of XENON1T and in light green (light grey) points, which are above (below) the neutrino background.

between the two type of searches is striking. Points with a SI elastic cross section well below the neutrino background, and hence not detectable by direct detection experiments, are already excluded by SMS results. On the other hand, a bulk of points allowed (or even more interestingly, not tested) by SMS results is well in the reach of XENON1T. In fact early results from XENON1T [49] already exclude a large number of points, compare Figure 1.3. Notice however that there still exist combinations of parameters that allow sneutrino DM to escape both direct detection and LHC searches, represented by the cyan points below the neutrino background curve in Figure 5.17. In the MSSM+RN, DM direct searches are basically sensitive to the mass of the LSP and its couplings with the Higgs and Z bosons. The rest of the SUSY mass spectrum is not relevant. This is different with respect to the MSSM with the neutralino LSP, where the interaction with the quarks is mediated as well by squarks on t-channel. This is clearly visible in the right panel of Figure 5.17, which shows the most constraining SMS analyses. In Figures 5.9 and 5.10 these SMS analyses are typically correlated with the gluino or chargino mass, while now they are scattered all over the $\sigma_n^{\rm SI}$ versus $m_{\tilde{\nu}_{\tau_1}}$ plane.

The same set of allowed, excluded and not tested points are plotted as a function of the sneutrino mixing angle in the left panel of Figure 5.18. The bulk of not tested points in the reach of XENON1T (dark blue points) has, as expected, relatively large mixing angles, corresponding to sizeable contributions from Z boson exchange to the SI scattering cross section. Excluded red points are scattered everywhere in the $\sin\theta_{\tilde{\nu}}$ vs. $m_{\tilde{\nu}_{\tau_1}}$ plane and probe also very RH sneutrinos. In the right panel of Figure 5.18 we see that among the allowed points, XENON1T can constrain a large portion of the sneutrino parameter space, while the very RH sneutrinos will remain inaccessible to future direct detection detectors. In general the points with negligible mixing angles have $\tilde{\nu}_{\tau_1}$ as LSP and the neutralino as NLSP, which tends to be almost degenerate with chargino. The relic density is then actually achieved

by co-annihilation of neutralino-chargino and then communicated to the mostly sterile LSP (see [280] for details). Such scenarios are very difficult to test.

5.2.3. Lifetimes of long-lived Particles

As mentioned in Section 5.2.1, a considerable number of the scan points comprise long-lived sparticles. These occur mostly when enforcing light gluinos or squarks; in this case about 30 % of the points feature long-lived particles, while the fraction is below 1 % without this constraint. The long-lived particles are predominantly gluinos (85 %), mostly in the case where it is the NLSP, and in a few points where $\tilde{\chi}_1^0$ is slightly (up to about 50 GeV) lighter than the gluino. Apart from that we find points with long-lived stops or staus in case they are the NLSP, as well as few points with long-lived charginos. Here we will focus on the long-lived gluinos and stops, long-lived staus have been discussed before in [280].

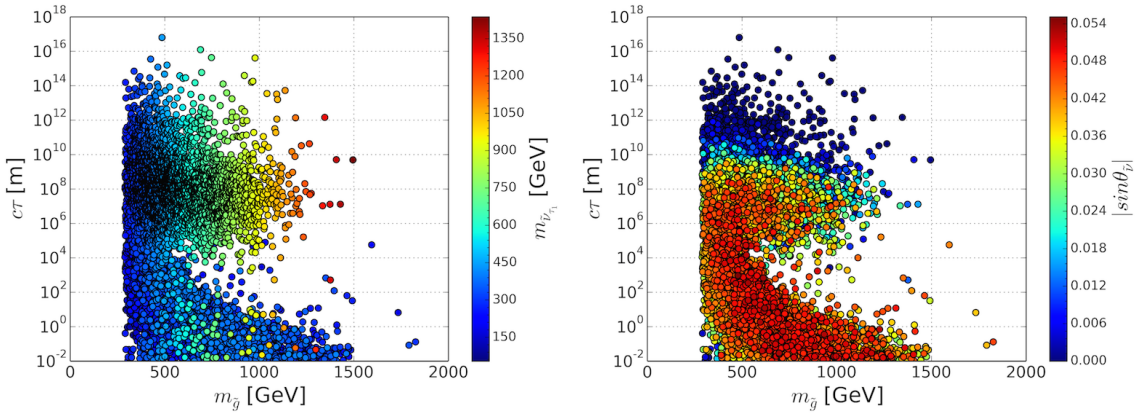

Figure 5.19.: Lifetimes $c\tau$ in [m] for long-lived gluinos, the color code indicates the LSP mass (left) and the sneutrino mixing angle (right).

In the MSSM long-lived gluinos appear when all squarks are extremely heavy, e.g. in split-SUSY scenarios. In case of the MSSM+RN with a sneutrino LSP additional causes come into play. If the gluino is the NLSP, its decay will proceed only via virtual squarks and gauginos, yielding an effective four body decay, $\tilde{g} \to qq\nu\tilde{\nu}$ (virtual $\tilde{q}$ and $\tilde{\chi}^0$) or $\tilde{g} \to qq'l\tilde{\nu}$ (virtual $\tilde{q}$ and $\tilde{\chi}^\pm$). The gluino lifetime will therefore depend not only on the squark mass, but also on the gaugino masses and mixings, as well as the sneutrino mixing angle. Meta-stable gluinos can thus appear even if the squarks are not completely decoupled. The gluino lifetime as a function of its mass is shown in Figure 5.19. The left plot illustrates the depencence on the sneutrino mass, the right plot the dependence on the sneutrino mixing. We can distinguish two general regions. First, we observe an exponential dependence of the lifetime on the gluino mass for decay lengths of 10 mm up to 10^4 m. Here the lifetime is largely independent of the sneutrino mass. Moreover lifetimes at constant gluino masses are longer for heavier squarks and gauginos. In this region we generally find large mixing angles $\sin\theta_{\tilde{\nu}}$, but heavy gauginos and squarks. Points with very small mixing angles may also appear in this region, in the case that the mass of the lightest neutralino is below the gluino mass. The second region, with lifetimes longer than 10^4 m, and up to 10^{17} m, shows a very different behaviour. We can see a clear correlation between gluino and sneutrino masses in this region, with longer lifetimes found for smaller mass splittings. The lifetimes moreover increase when

going to very small sneutrino mixing angles, with the maximum lifetimes achieved for $\sin\theta_{\tilde{\nu}}$ going to zero.

Likewise, if the stop is the NLSP[6] and has a small mass difference with the sneutrino, it can be long-lived, see Figure 5.20. As seen for the gluinos, the lifetime depends strongly on the sneutrino mixing.

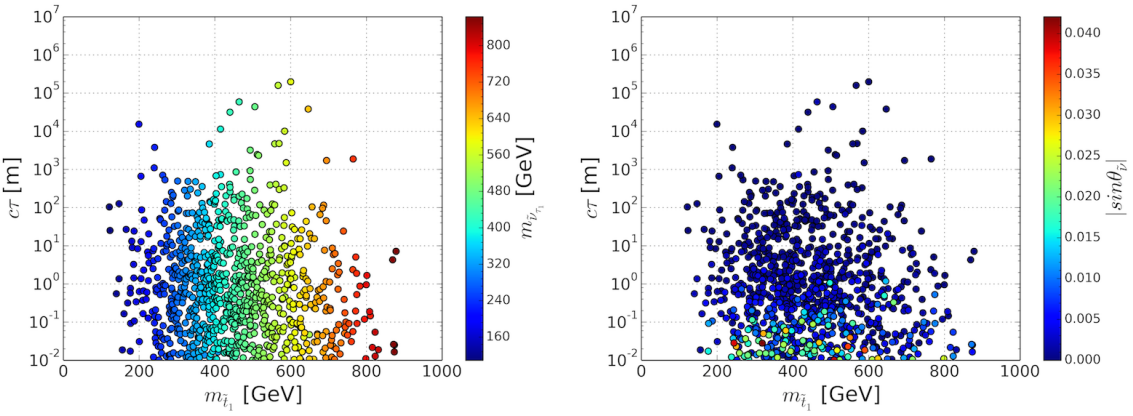

Figure 5.20.: Lifetimes $c\tau$ in [m] for long-lived stops, the color code indicates the LSP mass (left) and the sneutrino mixing angle (right).

Both long lived gluinos and long lived stops can be constrained by searches for R-hadrons, see [316,317] for R-hadrons escaping the detector, [318] for stopped R-hadrons, or [319] for metastable gluinos decaying in flight inside the detector. However, large uncertainties arise from modeling both the hadronisation and the strong interaction of the R-hadron with the detector, see example in Figure 2.7 (right). Note that almost all points are expected to be excluded by the recent results [164].

Additionally, cosmological constraints become important for gluino lifetimes of about 100 s (10^{10} m) [320]. Lifetimes of that order would affect the fraction of heavy nuclei produced during the Big Bang nucleosynthesis. Longer lifetimes can further be constrained by searches for diffuse gamma ray background, distortions in the CMBR and heavy isotopes [320].

5.2.4. Conclusions

Scenarios with a sneutrino as the LSP are an interesting alternative to MSSM models with neutralino LSPs. Indeed in the MSSM+RN the fermionic field contributes to neutrino masses while the scalar field contributes to the DM candidate, which is a mixed, however mostly RH, sneutrino.

The collider phenomenology of the MSSM+RN can be quite different from the typical MSSM case. It is therefore interesting and relevant to ask how the SUSY search results from Run 1 of the LHC, which were mostly designed with the MSSM in mind, constrain sneutrino LSP scenarios. To address this question, we used SModelS v1.0.1 for testing the MSSM+RN against more than 60 results from CMS and ATLAS searches in the context of SMS. More precisely, by considering the model parameter space where the sneutrino is a good DM candidate compatible with all current constraints, we assessed 1.) the constraining

[6] If the stop mass is close to the gluino mass, both stop and gluino may be long-lived.

power of the current SMS results on such scenarios and 2.) the most relevant signatures not covered by the SMS approach.

Concerning point 1.), we found that the dilepton + E_T^{miss} searches are among the most relevant ones, constraining sneutrino masses up to about 210 GeV and mostly wino-like charginos up to $m_{\widetilde{\chi}_1^\pm} \approx 440$ GeV. It is important to note here that this amounts to re-interpreting the ATLAS and CMS searches for $pp \to \tilde{l}^+\tilde{l}^- \to l^+l^-\widetilde{\chi}_1^0\widetilde{\chi}_1^0$ in terms of $pp \to \widetilde{\chi}_1^+\widetilde{\chi}_1^- \to l^+l^-\tilde{\nu}_l\tilde{\nu}_l$ (the validity of this is discussed in Section 4.3). Hadronic SUSY searches exclude gluinos masses up to $m_{\tilde{g}} \approx 1200$ GeV and LSP masses up to $m_{\tilde{\nu}_1} \approx 500$ GeV. Nonetheless in general we find that only a very limited portion of the parameter space can be properly excluded by SMS results. For most points in the $(m_{\tilde{g}}, m_{\tilde{\nu}_1})$ or $(m_{\widetilde{\chi}_1^\pm}, m_{\tilde{\nu}_1})$ planes there exist parameter combinations that allow to avoid all limits. Indeed, most of the parameter space is either allowed (SMS constraints exist for the specific topologies of the point but all $\sigma \times \mathcal{B}$ of these topologies are below their 95% CL upper limits) or not tested at all (there are no existing SMS constraints for the specific topologies of the point or each topology has a $\sigma \times \mathcal{B}$ which is smaller than 1 event at LHC Run 1). Direct DM searches are complementary to the SMS constraints: many points that are not tested by SMS results can potentially be excluded by XENON1T. Vice versa, points well below the neutrino background, hence not reachable by future DM detectors, are already excluded by SMS results.

The second main result concerns point 2.), i.e. the study of the allowed points in terms of missing topologies. In the hadronic sector, pair-produced gluinos with masses well in the reach of LHC Run 1 are not constrained because they feature one or more of the following:

- additional leptons: since the gluino cannot directly decay into the sneutrino LSP, the hadronic final state is often accompanied by leptons;
- mixed topologies: each of the pair-produced gluinos undergoes a different decay;
- the gluinos decay into tb final states.

None of these possibilities are covered by the SMS results available at the time of publication. Note here that the last two items are also common in the MSSM, as described in [191], see also Section 5.1 for a discussion of mixed topologies in the pMSSM. For electroweak production, missing topologies include:

- single leptons;
- single Ws;
- different-flavour opposite-sign leptons;
- same-sign W's or same-sign taus (accompanied respectively by additional leptons/taus, or Ws).

While such signatures have been searched for by the SUSY and/or exotics groups in ATLAS and CMS, the results do not exist in terms of appropriate SMS interpretations. Such an SMS interpretation would be very interesting in particular for the mono-lepton + E_T^{miss} case, which promises to have a considerable impact for constraining the MSSM+RN model.[7]

[7] This could be done analogous to the existing $\widetilde{\chi}_1^\pm\widetilde{\chi}_2^0$ ($\widetilde{\chi}_1^\pm \to W^\pm\widetilde{\chi}_1^0$, $\widetilde{\chi}_2^0 \to Z^0\widetilde{\chi}_1^0$) simplified models that are already assessed by the ATLAS and CMS SUSY groups, but with the chargino decaying to 100% into $l^\pm\tilde{\nu}_l$ and the neutralino decaying 100% into $\nu\tilde{\nu}_l$. However, since the chargino and neutralino masses need not be degenerate, we propose to consider as a first step $\widetilde{\chi}_1^\pm\widetilde{\chi}_1^0$ production followed by $\widetilde{\chi}_1^\pm \to l^\pm\tilde{\nu}_l$ and $\widetilde{\chi}_1^0 \to \nu\tilde{\nu}_l$. The cross section upper limits should be provided in the chargino- versus sneutrino mass plane for different neutralino masses, for the cases $l = e, \mu$ and $l = \tau$, and if computationally feasible also for $l = e, \mu, \tau$ assuming equal rates.

Note however that this type of signature has large SM background, rendering experimental searches challenging. Indeed the typical W' searches require very hard $E_T^{\rm miss}$ cuts, and are not efficient to constrain the MSSM+RN model. Other search strategies employing e.g. the M_T variable may give relevant constraints, see [321].

5.3. Probing U(1) Extentions of the MSSM

In Section 1.3.5 the U(1) extended MSSM (UMSSM) was introduced as another compelling extension of the MSSM. It can adress the μ problem in the MSSM and is well motivated in the context of GUT models.

In the UMSSM model considered here purely RH sneutrinos are charged under the additional U(1) symmetry, hence this model gives a new viable dark matter candidate in addition to the lightest neutralino as observed in [91]. Note that this differs from the mixed sneutrino scenario discussed in the previous section, as the hypercharge coupling is now considered to be identically zero. The properties of a RH sneutrino DM were also examined in the $U(1)_{B-L}$ [99] and $U(1)_{B-L} \times U(1)_R$ extensions of the MSSM [322]. Note that in such models the sneutrino vev's were found to play an important role in the vacuum stability [323]. Furthermore the Z' can contribute to the stabilization of the Higgs potential [324].

Here we explore the parameter space of the UMSSM (derived from E_6) that is compatible with both collider and dark matter observables. We include in particular the Higgs mass and signal strengths in all channels, LHC constraints on Z' and on supersymmetric particles, new results from B-physics, as well as the relic density and direct detection of dark matter. Specifically we take into account the Run 1 LHC results for supersymmetric particle searches based on simplified models using SModelS v1.0.1 [191]. This allows us to also highlight the signatures not well constrained by current searches despite a spectrum well below the TeV scale. One salient feature of the model is that large D-term contributions can significantly reduce the mass of RH squarks thus splitting the u-type and d-type squarks and weakening the constraints on first generation squarks. Another feature, which is also found in the MSSM, is that the relic density upper limit favors a neutralino with a large higgsino or wino component as the LSP. Scenarios with a higgsino LSP can easily escape current search limits. For example simplified model limits from top squark searches rely on the assumption that one decay channel is dominant, while for higgsino LSP branching ratios into $t\tilde{\chi}_i^0$ and $b\tilde{\chi}_i^+$ can both be large, thus the mixed channels where each stop decay into a different final state are important. Since a higgsino or wino LSP may be associated with a chargino which is stable at the collider scale, we also impose the D0 and ATLAS limits originating from searches for long-lived particles. On the remaining parameter space, we then discuss the expected spectra of SUSY particles, the expectations for the signal strengths for the Higgses as well as dark matter observables in direct and indirect detection.

In general we do not attempt to explain the observed discrepancy with the standard model expectations in the muon anomalous magnetic moment. However, we highlight the region where the model can explain this discrepancy and investigate how it may escape simplified model limits from the LHC. The interplay between the muon anomalous magnetic moment constraint, LHC and DM limits was recently studied in the MSSM [325].

In contrast to previous studies [91,97] we explore the impact of LHC8TeV results on Higgs and new particle searches from the 8 TeV run on scenarios with arbitrary U(1) originating from E_6. Moreover we consider both the cases of a neutralino and a RH sneutrino dark matter. We further examine the implications of dark matter searches in these scenarios. An attractive feature of the model is the possibility to obtain $m_h = 125$ GeV despite small values

of $\tan\beta$. The phenomenology of Higgs and SUSY searches could thus differ from that of the much-studied MSSM. This work was published in [92].

The constraints used in our study are presented in Section 5.3.1. Section 5.3.2 contains the results for several sectors of the model after applying a basic set of constraints mostly related to Higgs and B-physics observables and after applying the DM relic abundance limits. Section 5.3.3 is dedicated to the application of the LHC simplified models searches on the remaining allowed parameter space of the UMSSM and a summary and suggestions for future probes is given in Section 5.3.4. Section 5.3.5 shows prospects for probing the Higgs sector and Section 5.3.6 prospects from astroparticle searches. Our conclusions are presented in Section 5.3.7.

5.3.1. Constraints on the Model

Higgs physics

For the Higgs sector we require that the light[8] Higgs mass lies in the range $m_{h_1} = 125.1 \pm 3\,\mathrm{GeV}$ allowing for a theoretical uncertainty around 2 GeV. We impose constraints on the Higgs sector keeping only points allowed by `HiggsBounds-4.1.3` [326] and by `HiggsSignals-1.2.0` [327] at 95% CL (p-value above 0.05). We also use constraints contained in `NMSSMTools` [328], in particular the one on the heavy Higgs search in the $\tau^+\tau^-$ decay mode that rules out some of the large $\tan\beta$ region.

Note that the Yukawa couplings evaluated at the SUSY scale which enter the computation of the Higgs boson masses must remain perturbative. We require that all Yukawa couplings stay below $\sqrt{4\pi}$ at the SUSY scale. This condition will impose restrictions on both the small and the very large $\tan\beta$ values (recall that $\tan\beta$ is not a free parameter of the model). Yukawa couplings within the perturbative limit can nevertheless induce a very large width for some of the Higgs states, since we work in the context of elementary Higgs particles we impose the condition $\Gamma(h_i)/m_{h_i} < 1$.

Collider searches for Z'

One of the main constraint on this model comes from the direct collider searches for a Z' boson in the two-lepton decay channel. Limits have been obtained at the LHC by the ATLAS [79] and CMS [80] collaborations for pp collisions, here we consider Run 1 searches at a center-of-mass energy of 8 TeV. In [80] limits were obtained with an integrated luminosity of 19.7 fb^{-1} (20.6 fb^{-1}) in the dielectron (dimuon) channel and lead to $M_{Z_2} > 2.57$ TeV for $\theta_{E_6} = \theta_\psi$, assuming only SM decay modes.[9] Such limits however depend on the couplings of the Z_2, hence on θ_{E_6}. To reinterpret this limit for any value of θ_{E_6}, we first simulate Monte Carlo signals for Z' production using the same Monte Carlo generator and PDF set as in [79], respectively PYTHIA 8.165 [203] and MSTW2008LO [141], for a large set of θ_{E_6} values. We get results compatible with with the ones derived in [330] as well as the one obtained by the CMS collaboration [80]. Then we interpolate our limits for any possible choice of θ_{E_6}. Note that the coupling of Z_2 to the standard model fermions also weakly depends on α_Z. We have checked that this dependence does not modify significantly the Z_2 limits and are well below PDF uncertainties [79]. Furthermore in the UMSSM the Z_2

[8] Strictly speaking it is also possible that the Higgs at 125 GeV corresponds to h_2, however we did not find such points in the scan.

[9] Recent LHC Run 2 results from ATLAS extend the exclusion limit to masses between 3.36 and 4.05 TeV depending on the model [329]. These limits are not included in this study.

can decay into supersymmetric particles, RH neutrinos and Higgs bosons, thus reducing the branching ratio into leptons. The limits on the Z_2 mass are therefore weakened [331–334]. To take this effect into account we determine in a second step the modified leptonic branching ratio for each point in our scan, and re-derive the corresponding limit.

For any value of θ_{E_6} we restrict the scan to $|\alpha_Z| < 10^{-3}$ [103]. In addition, the mixing between Z^0 and Z' can be constrained by the $\Delta\rho$ parameter [335]. This observable, which measures the deviation of the ρ-parameter of the standard model from unity, receives a specific UMSSM tree-level contribution because Z_1 is no longer purely the Z^0 boson. In the limit where $M^2_{Z'} \gg M^2_{Z^0}, \Delta^2_Z$, which is the case for the TeV scale Z', this new contribution reads [335]

$$\Delta\rho_Z = \alpha_Z^2 \frac{M^2_{Z_2}}{M^2_{Z_1}}. \tag{5.2}$$

We compute $\Delta\rho$ for each point in the parameter space using a `micrOMEGAs` routine which also contains leading one-loop third generation sfermions and leading two-loop QCD contributions. We impose the upper bound $\Delta\rho < 8.8 \times 10^{-4}$ [336].

Collider searches for SUSY particles

First we impose generic constraints from LEP on neutralinos, charginos, sleptons and squarks. For the latter we ignore the possibility of very compressed spectra and use the generic limit at 103 GeV. Lighter compressed squarks can in any case be constrained from LHC monophoton searches [337, 338] and monojet analyses [147].

Powerful and comprehensive constraints on supersymmetric partners have been obtained by ATLAS and CMS using the data collected at 7 and 8 TeV. Searches were performed for a wide variety of channels and results were presented both in the framework of specific models, such as the MSSM, and in the context of SMS. Here we use the SMS results to find the main constraints on the UMSSM. We base our analysis on SModelS v1.0.1 [191,192],the version used includes more than 60 SMS results from both ATLAS and CMS.

The input SLHA files, including tree-level production cross sections, are generated using `micrOMEGAs_4.1.5` [339], for strongly produced particles, SModelS then calls NLL-fast [128–134] to compute the k-factor at NLO+NLL order. As a minimum weight in the decomposition we have used a cutoff σ_{cut} of 0.03 fb. Both mass and invisible compression (as explained in Section 3.2.2) are enabled, using 5 GeV as the minimum mass splitting for mass compression.

Note that topologies that contain long-lived charged particles corresponding to $c\tau > 10$ mm are not tested against SMS results within SModelS v1.0.1. However searches for long-lived particles leaving charged tracks in the detector have been performed at the Tevatron [340] and the LHC [316,317] and were interpreted in the context of long-lived charginos or in the context of the pMSSM [341]. When the neutralino LSP is dominantly wino, typically, the NLSP chargino will be stable at the collider scale. We have therefore considered the D0 and ATLAS upper limits for points with charginos in the mass range $100 - 300$ GeV and $450 - 800$ GeV, and decay lengths $c\tau > 10$ m and 21 m respectively. We have not included the limits from CMS as these cannot be simply reinterpreted for direct production of chargino pairs [316]. Long-lived gluinos or squarks are also possible, we have not considered these cases since the interpretation of a given experimental analysis relies on the modeling of R-hadrons, thus introducing large uncertainties.[10] Moreover we have not implemented current limits on long-lived staus as these rarely occur in the parameter space considered.

[10] See also discussion in Section 5.2.3 about long-lived gluino and squark scenarios in the MSSM+RN.

Flavour physics

Indirect constraints coming from the flavour sector, especially those involving B-Mesons, play an important role in defining the allowed parameter space of supersymmetric models, e.g. [266, 342–344]. The constraints imposed on the model are listed in Table 5.3, though we do not in general require agreement with the measured value of Δa_μ. We do however highlight the specific regions consistent with the measured value of the muon anomalous magnetic moment. These mostly correspond to regions with a light LH smuon/sneutrino as mentioned in Section 1.3.5. To compute these observables, we have adapted the `NMSSMTools` routine to the UMSSM, for more details see [95]. The most powerful constraints are ΔM_s and ΔM_d for small values of $\tan\beta$ while $\mathcal{B}(\bar{B}^0 \to X_s\gamma)$ and $\mathcal{B}(B_s^0 \to \mu^+\mu^-)$ are also important to constrain some large values of $\tan\beta$. We also compute $\mathcal{B}(\bar{B}^0 \to X_s\mu^+\mu^-)$ but this channel does not give additional constraints. Uncertainties coming from CKM matrix elements, rare decays, hadronic parameters and theory are taken into account when computing the observables listed in Table 5.3, see [95]. The most important uncertainties in our computation of flavour observables are theoretical (10%) and from the CKM element $|V_{ts}| = (42.9 \pm 2.6) \times 10^{-3}$ [345].

Constraint	Range
$\mathcal{B}(B^\pm \to \tau^\pm\nu_\tau)$	[0.70, 1.58]$\times 10^{-4}$ [346]
$\mathcal{B}(\bar{B}^0 \to X_s\gamma)$	[2.99, 3.87]$\times 10^{-4}$ [347]
$\mathcal{B}(B_s^0 \to \mu^+\mu^-)$	[1.6, 4.2]$\times 10^{-9}$ [348]
ΔM_s	[17.805, 17.717] ps^{-1} [349]
ΔM_d	[0.504, 0.516] ps^{-1} [350]
Δa_μ	[7.73, 42.14]$\times 10^{-10}$ [105, 106, 351]

Table 5.3.: Flavour constraints used and their allowed ranges which correspond to the experimental results (or to the difference between the experimental value and the standard model expectation for Δa_μ) $\pm\, 2\sigma$.

Dark matter

The value of the dark matter relic density has recently been measured precisely by the Planck collaboration and a combination of Planck power spectra, Planck lensing and other external data leads to [38]

$$\Omega h^2 = 0.1188 \pm 0.0010. \tag{5.3}$$

We will impose only the 2σ upper bound from Eq. (5.3) on the value of the relic density. That is we assume that either there is another component of dark matter or that there exists some regeneration mechanism that can bring the dark matter within the range favoured by Planck [352, 353].

This measurement puts a strong constraint on the parameter space of the UMSSM whether the dark matter candidate is the lightest neutralino or the supersymmetric partner of the right-handed neutrino. Since the three RH sneutrinos have the same coupling to all other particles in the model we assume for simplicity that the third generation sneutrino is the lightest. In previous studies it was shown that the favoured mass for the RH sneutrino LSP was near $M_{Z_2}/2$, although much lighter sneutrinos could also be found, especially near $m_{h_1}/2$ or when coannihilation was present [91]. As in the MSSM the lightest neutralino covers a large

range of mass, the main new features being the possibility of a singlino LSP [354–356] and the possibility for this singlino to have a non-negligeable bino' component. Typical MSSM features can also be observed as the example of wino LSP annihilating efficiently into W's and strongly degenerate in mass with chargino NLSP. However sometimes the mass degeneracy between the NLSP and the LSP can be sufficiently small to give an absolutely stable charged NLSP. When focusing on relic density constraints we will systematically discard these configurations.

One of the strongest constraint on DM arises from direct detection. We implement the upper limit from the LUX collaboration [284] taking `micrOMEGAs` default values for the quark coefficients in the nucleons. This upper limit strongly constrains the scenarios where the LSP is $\mathcal{O}(100\,\text{GeV})$. Note that recently presented first results from the XENON1T experiment have substantially improved the limits on σ_n^{SI}, see Figure 1.3. Another relevant constraint is the one from FermiLAT searches for DM annihilation from the dwarf spheroidal satellite galaxies of the Milky Way where limits obtained for DM annihilation into $b\bar{b}$ and $\tau^+\tau^-$ can constrain scenarios with DM masses below 100 GeV [50].

5.3.2. Results

Parameter	Range	Parameter	Range
$m_{\tilde{\nu}_{\tau R}}$	[0, 2] TeV	μ, M_1	$[-2, 2]$ TeV
M_{Z_2}	[2.2, 7] TeV	$M_2, A_\lambda, A_t, A_b, A_l$	$[-4, 4]$ TeV
M_1'	$[-20, 20]$ TeV	M_3	[0.4, 12] TeV
θ_{E_6}	$[-\pi/2, \pi/2]$ rad	$m_{\tilde{F}_i}, m_{\tilde{\nu}_j}$	[0, 4] TeV
α_Z	$[-10^{-3}, 10^{-3}]$ rad	m_t	173.34 ± 1 GeV [357]

Table 5.4.: Range of the free parameters where concerning the soft mass terms we define $F \in \{Q, u, d, L, e\}$, $i \in \{1, 2, 3\}$ and $j \in \{1, 2\}$ and where $m_{\tilde{F}_2} = m_{\tilde{F}_1}, m_{\tilde{\nu}_2} = m_{\tilde{\nu}_1}$.

After imposing universality for the sfermion masses of the first and second generation and fixing the trilinear coupling of the first two generation sfermions to 0 GeV, the UMSSM features 24 free parameters. The range used for these parameters in the scans are listed in Table 5.4. In addition we have allowed the top mass to vary. We perform a random scan over the free parameters and impose first the set of basic constraints: the Higgs mass and couplings allowed by `HiggsBounds`, `HiggsSignals` and our modified `NMSSMTools` routines, perturbative Yukawas for top and bottom quarks, agreement with LEP limits on sparticles and LHC limits on the Z' and finally a neutral LSP. We then include the constraints from B-physics. Another scan is done to highlight the regions of parameter space which give sufficient New Physics contribution to Δa_μ. For this we restrict the soft masses of the second generation of sleptons to [0, 2] TeV and we impose all flavor constraints listed in the previous section.

For all points that satisfy these sets of constraints in both scans, around 4×10^5, we found that the maximum tree-level mass for the Higgs reached only $m_{h_1} \approx 107$ GeV and was above the Z_1 mass only for mixing angles $\alpha_Z > 2 \times 10^{-5}$, see Figure 5.21a. Thus a contribution from the radiative corrections in the stop/top sector is still required to reach a Higgs mass of 125 GeV. Nevertheless the full range of values of $\tan\beta$ is allowed. Small values of $\tan\beta > 1$

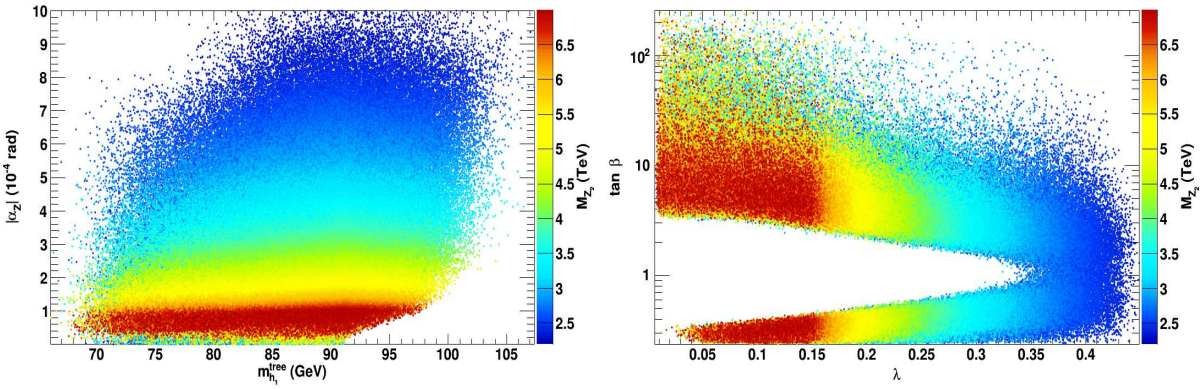

(a) (b)

Figure 5.21.: (a) α_Z as a function of the tree-level component of m_{h_1} and (b) $\tan\beta$ as a function of λ. For both plots M_{Z_2} is taken as colour code.

require a large value of λ to compensate the small MSSM-like tree-level contribution to the light Higgs mass, see Figure 5.21b. This also means that v_s (as defined in Section 1.3.5), hence M_{Z_2}, cannot be too large given the range assumed for the μ parameter, see Eq. (1.51). Radiative corrections from the top/stop sector are expected to be large for $\tan\beta < 1$ since the top Yukawa coupling increases as $1/\sin\beta$, which explains why a larger range for λ is allowed when $\tan\beta < 1$.

It is well known that large one-loop corrections from the stop sector require heavy stops and/or large mixing [358]. The mixing parameter $X_t = A_t - \mu/\tan\beta$ is indeed found to be large when $M_S = \sqrt{m_{\tilde{t}_1} m_{\tilde{t}_2}} < 1$ TeV while heavy stops (associated with large M_S) allow no mixing, see Figure 5.22a. The heavier the Z_2 the larger the minimal value for the scale M_S where zero mixing is allowed.

The spectrum for supersymmetric particles differs significantly from the case of the MSSM and NMSSM, depending on the choice of $U(1)'$ charges. The lightest stop mass can be as light as 300 GeV for $\theta_{E_6} \sim 0.66$ (Figure 5.22b), this value corresponds to the largest negative contribution to the stop mass from the D-term, see Section 1.3.5. When $\theta_{E_6} < 0$ the lightest stop is at least 670 GeV. Similar values are found for both LH and RH up-type squarks, modulo mixing effects. Such light squark masses are well within the range of exclusion of LHC searches within the MSSM, hence the need to reinvestigate the impact of these searches within the UMSSM discussed in the next section. The $\tilde{d}_R$ mass receives a large negative D-term contribution for $\theta_{E_6} = -\tan^{-1}(3\sqrt{3/5}) \approx -1.16$. For this value it can be as light as allowed by LEP (103 GeV), see Figure 5.22d. For $\theta_{E_6} > 0$, the RH d-squark is above the TeV scale while the LH one can be light since $m_{\tilde{d}_L} = m_{\tilde{u}_L}$. This implies also that a light sbottom, say below 500 GeV, can be found for either value of θ_{E_6}, see Figure 5.22c. In one case it is mostly LH and in the other RH. Note that an increase in the lower limit on the Z' mass will lead to larger squark masses except for the specific values of θ_{E_6} where one gets a very large D-term contribution. Finally, the gluino mass is determined by M_3, hence can also be well below the TeV scale.

The impact of the flavour constraints is best displayed in the $\tan\beta - \theta_{E_6}$ plane, see Figure 5.23. As expected ΔM_s and ΔM_d are the most important constraints in our scans and exclude a large part of the parameter space when $\tan\beta < 1$, through the charged Higgs contribution [95]. The contribution from Double Penguin diagrams to these observables en-

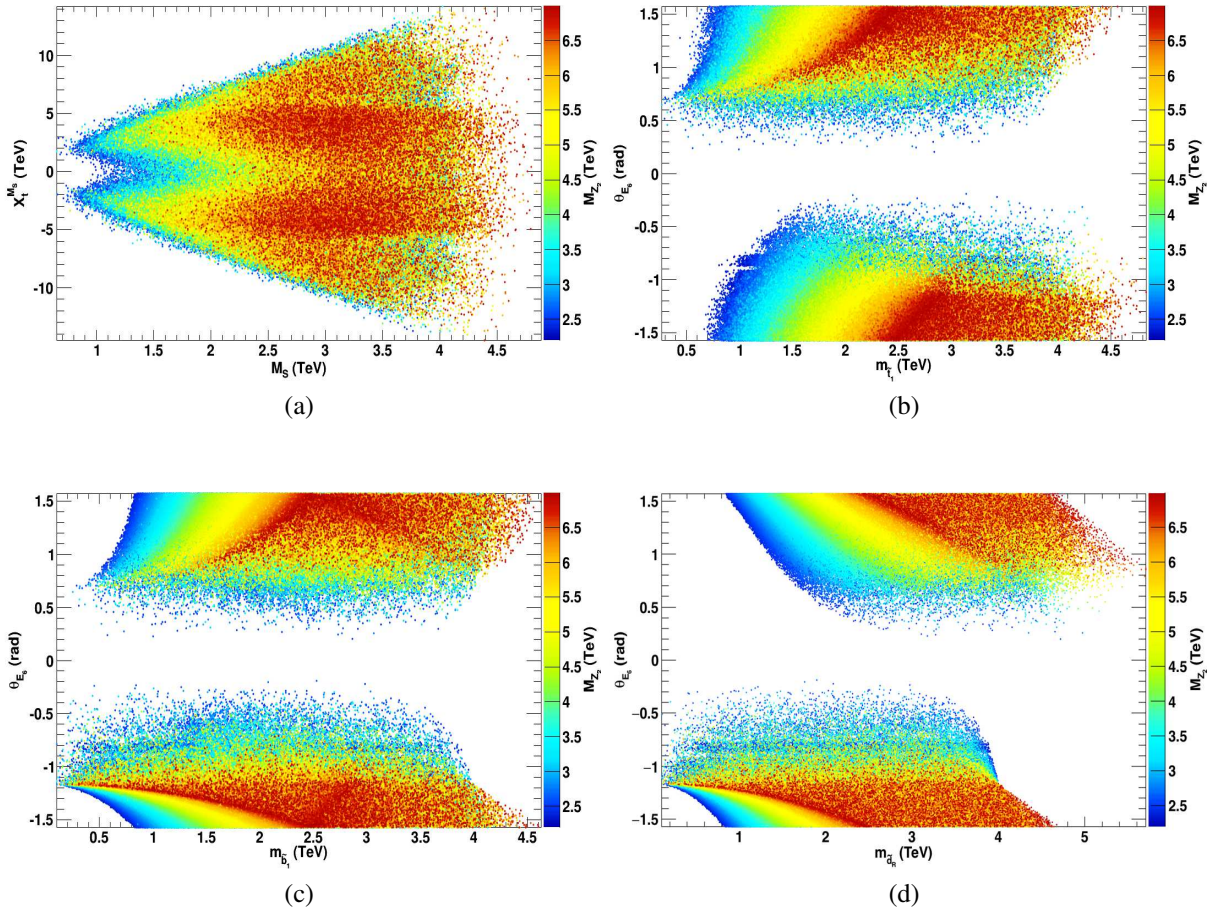

Figure 5.22.: (a) X_t as a function of M_S and θ_{E_6} as a function of (b) $m_{\tilde{t}_1}$, (c) $m_{\tilde{b}_1}$ and (d) $m_{\tilde{d}_R}$. For all plots M_{Z_2} is taken as colour code.

able exclusion of a few scenarios at large $\tan\beta$. $\mathcal{B}(B_s^0 \to \mu^+\mu^-)$ and $\mathcal{B}(\bar{B}^0 \to X_s\gamma)$ are important for scenarios at very large $\tan\beta$ but they mostly fail to exclude points, especially for cases where the mass of heavy neutral and charged MSSM-like Higgs bosons is above several TeVs. Finally the New Physics contribution to the deviation of the ρ-parameter from unity exclude only few points, mostly from the sfermion contributions. Actually the pure UMSSM contribution shown in Eq. (5.2) can barely reach 10^{-4} for the allowed values for α_Z and M_{Z_2} and is then negligible. Note that, as we will see in the next section, specific regions of the parameter space give large enough contributions to the anomalous magnetic moment of the muon.

Δa_μ

Special conditions are required to get agreement with the value of Δa_μ. Indeed the discrepancy between the theoretical and experimental value requires a large contribution from New Physics. In the UMSSM this comes in particular from diagrams involving smuon (LH sneutrino) and neutralino (chargino) exchange. A large UMSSM contribution requires either a light smuon/LH sneutrino or an enhanced Yukawa for the muon. The latter is found at very large values of $\tan\beta$, see Figure 5.24a. A light LH smuon mass arises for

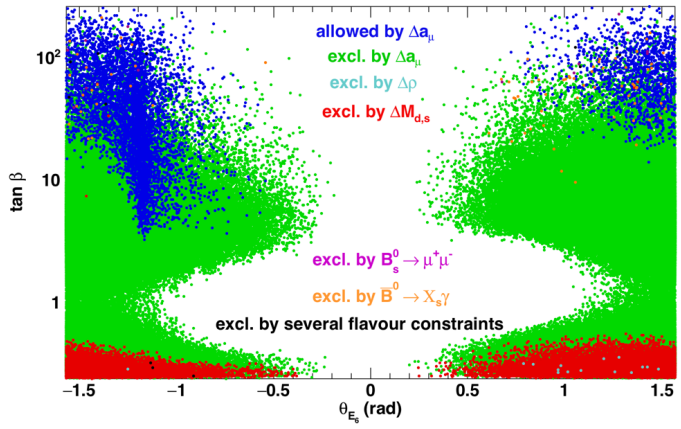

Figure 5.23.: Points of the scan in the $\tan\beta$ - θ_{E_6} plane where the colour code shows the flavour process that provides the main exclusion. The region that is compatible with Δa_μ is also displayed. The flavour observables are computed with the `NMSSMTools` routine adapted to the UMSSM.

$\theta_{E_6} = -\tan^{-1}(3\sqrt{3/5}) \approx -1.16$ corresponding to a large negative D-term contribution as explained in Section 1.3.5. Future collider limits on the Z' mass, say above 5 TeV, will severely constrain scenarios for positive values of θ_{E_6} that are in agreement with the latest value of Δa_μ, see Figure 5.24b. Note that the distribution of points in the $\theta_{E_6} - m_{\tilde{\mu}_L}$ plane is similar to the one found in the general scan where consistency with the muon anomalous magnetic moment is not required, except that heavier sleptons are allowed in that case.

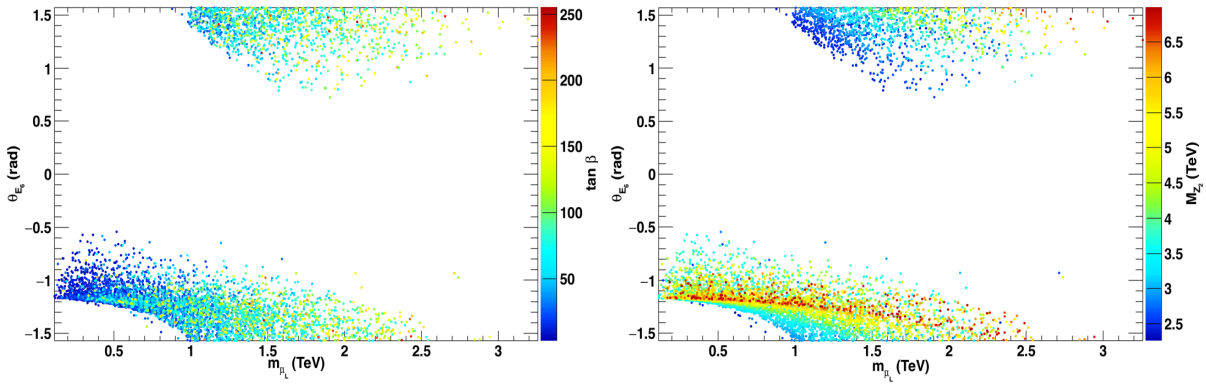

(a) (b)

Figure 5.24.: Points allowed by Δa_μ in the $\theta_{E_6} - m_{\tilde{\mu}_L}$ plane, the colour code corresponds to (a) different values of $\tan\beta$ and (b) M_{Z_2}.

Dark matter relic abundance

In this model the LSP can either be a neutralino or a RH sneutrino. The annihilation properties of the neutralino LSP are determined by its composition (Figure 5.25). As in the NMSSM, the pure bino or singlino LSP is typically overabundant unless it can benefit

from a resonance enhancement. Note that in this model the Higgs singlet is very heavy so that resonant annihilation of a singlino through the Higgs singlet works only for heavy singlinos[11]. The dominantly singlino LSP is found only for masses above 250 GeV. Some admixture of a higgsino/wino component or coannihilation processes can however reduce the relic density to $\Omega h^2 \approx 0.1$ for any mass. Coannihilation can occur with gluinos or other gauginos as well as with sfermions. As in the MSSM the dominantly higgsino or wino LSP annihilates very efficienty into gauge boson pairs and therefore leads to an under-abundance of dark matter unless the higgsino (wino) LSP mass is roughly above 1 (1.5) TeV. Note that the $\tilde{B}'$ component of the LSP is never dominant, because the vev of the singlet, which mostly drives the mass of the $\tilde{S}$ and the $\tilde{B}'$, Eq. (1.63), is always above 6 TeV. For $|M_1'| \ll |v_s|$, $\tilde{S}$ and $\tilde{B}'$ are both shifted towards large masses whereas for $|M_1'| \gg |v_s|$ the singlino benefit from a seesaw-type mechanism which allows a singlino LSP down to 250 GeV. This close relation between $\tilde{B}'$ and $\tilde{S}$ is illustrated in Figure 5.26.

We note that the fraction of points that satisfy the 2σ Planck upper bound is much higher in the scan where we impose the constraint on Δa_μ than in the general scan. The main reason is that it is easier to satisfy the relic density upper bound with a bino LSP when the sleptons are light.

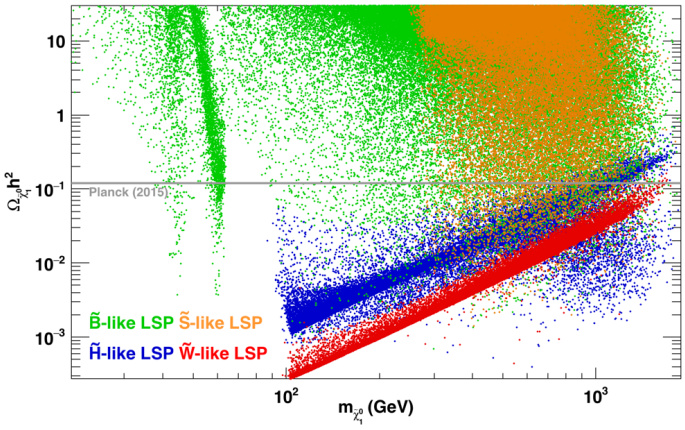

Figure 5.25.: Relic density of $\tilde{B}$ (green), $\tilde{W}$ (red), $\tilde{H}$ (blue) and $\tilde{S}$ (orange) LSP. The 2σ upper bound from Planck is shown in grey.

Sneutrino dark matter is typically overabundant as sneutrino annihilation channels are not very efficient. Agreement with the upper bound set by Planck requires either $m_{\tilde{\nu}_R} \approx m_{h_1}/2$ or $M_{Z_2}/2$ as found in [91]. The latter case requires $m_{\tilde{\nu}_R}$ above the TeV scale when considering current limits on the Z' mass, here we consider DM below 2 TeV. Annihilation into W or Z_1 pairs through Higgs boson exchange was also found to be efficient enough for $m_{\tilde{\nu}_R} \gtrsim 100$ GeV [91]. However this process, which depends mostly on the singlet nature of the Higgs boson exchanged, will not give a large enough contribution if the lower limit on M_{Z_2} increases as shown in Figure 5.27. Sneutrino LSP masses in the range $100 - 1000$ GeV are also allowed if some coannihilation mechanism, involving e.g. the lightest neutralino or other sfermions, helps reduce the relic abundance. The low density of points in this region (see Figure 5.27) reflects the fact that the importance of such coannihilation processes require the adjustment of uncorrelated parameters in the model.

[11] For an analysis of a scenario with a light singlino DM see [81].

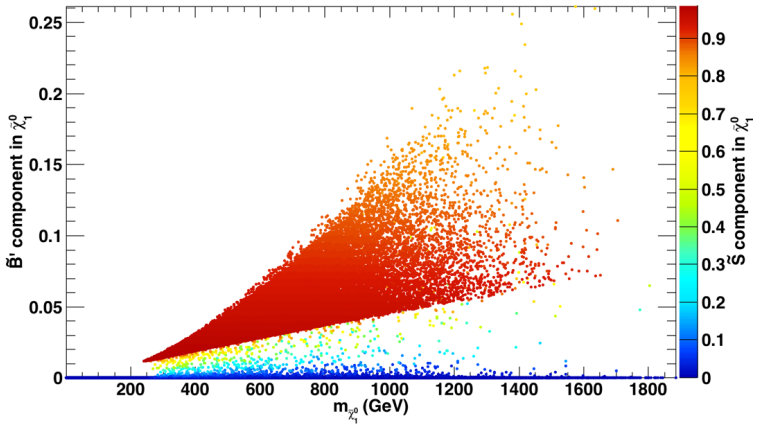

Figure 5.26.: $\tilde{B}'$ component in the neutralino LSP as a function of its mass with the $\tilde{S}$ component in the neutralino LSP as colour code.

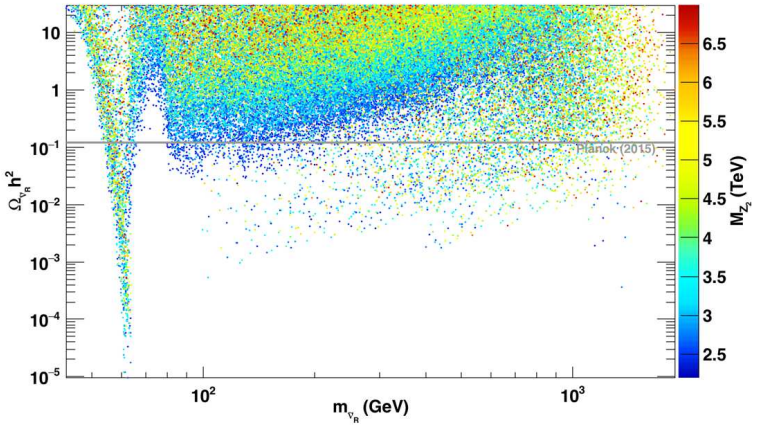

Figure 5.27.: Relic density for $\tilde{\nu}_{\tau R}$ LSP with M_{Z_2} as colour code. The 2σ upper bound from Planck is shown in grey.

5.3.3. Impact of LHC Searches for SUSY Particles

After having imposed the basic constraints, flavour constraints and an upper bound on the relic density $\Omega h^2 < 0.1208$ (corresponding to the 2σ upper limit of Eq. (5.3)), we next consider the impact of LHC searches for SUSY particles based on SMS results and using SModelS. To analyse the impact of the SMS results we group the points into four categories. As in Section 5.2 we classify the points as follows. Points excluded by SModelS are labeled as excluded, points where the SMS results apply but the cross section is below the experimental upper limit are labeled as not excluded. Points where no SMS result applies are labeled as not tested. Finally points with long-lived particles cannot yet be tested in SModelS. Points that are not excluded are then examined in more details to determine the signatures that could best be used to further probe them with upcoming data. We divide the study in three steps. First, we consider scenarios with a neutralino LSP and find that the most stringent constraints on supersymmetric particles are obtained for light gluino or light squarks [213, 359, 360]. Second, we concentrate on points compatible with the mea-

surements of the muon anomalous magnetic moment and that still have a neutralino LSP. This dedicated scan provides a significant number of points with light sfermions and allows us to ascertain the impact of slepton searches. Finally we investigate scenarios with a RH sneutrino LSP, among these we do not characterize the ones that are compatible with the muon $(g-2)$ because of the small number of points involved. The possibilities to probe all points with long-lived charginos are then considered separately regardless of the dark matter candidate. Our results for the constraints on the SUSY spectra are presented in Section 5.3.4 where we combine all sets.

Neutralino LSP

In most points with a neutralino LSP, the LSP is actually either dominantly wino or higgsino, see Figure 5.25. Points with a wino LSP are however mostly not considered in the SModelS v1.0.1 analysis because they lead to long-lived charginos. Therefore the most common configuration for the supersymmetric spectra relevant for SMS results is one with three dominantly higgsino particles with similar masses : the LSP, the second neutralino and the lightest chargino. Moreover since the jets/leptons produced in the decay of the chargino (second neutralino) to the LSP are too soft to be detected the chargino (second neutralino) will often lead to a E_T^{miss} signature. We will see that this has important consequences when using the SMS results. In particular hardly any points can be excluded from electroweakinos searches as only few can exploit the decay channel into real gauge/Higgs boson. Furthermore we do not find constraints from decays into leptons via sleptons since sleptons are rarely light.

Gluino constraints In Figure 5.28 we show points with a neutralino LSP in the LSP and gluino mass plane for gluino masses up to 1200 GeV. On the left we show excluded points in red and allowed points in blue, moreover we indicate points with long-lived sparticles that cannot be tested in SModelS v1.0.1 in green and points not tested for the other reasons mentioned before in grey. The right panel indicates the topology giving the strongest constraint for each excluded point.

We find that gluino topologies, basically from gluino decaying into a pair of quarks and the LSP through virtual squark exchange, can exclude gluino masses up to 1100 GeV [213, 360, 362]. The exclusions differ from those of a simplified model, since in general there are many possible decay channels. The decay branching ratios of the gluino depend strongly on the nature of the LSP. For a higgsino LSP, the decay of the gluino via virtual stop is dominant because of the stronger coupling which depends on the top mass, the final state is $t\bar{t}\tilde{\chi}^0$ (when there is enough phase space) and/or $t\bar{b}\tilde{\chi}^-$ where the chargino is treated as an effective LSP. The strongest constraints are found when phase space allows only the decay into the chargino final state, as there is one dominant decay channel. In other scenarios (non-higgsino LSP) there is no such strong preference for one decay channel, and the signal cross section will be split up on several simplified model topologies. Moreover mixed decays, where each gluino decays into different quark pairs and the LSP occur frequently and are not constrained by SMS. Hence the exclusion will be considerably weaker than for the pure simplified model exclusion. For many configurations gluinos can decay to heavier gauginos yielding topologies with long cascades which are not covered by the SMS results used in SModelS. Moreover each different topology resulting from such processes is typically suppressed because of multiple branching fractions. Similarly points with gluino decaying via an on-shell sbottom are not yet included in SModelS while those decaying

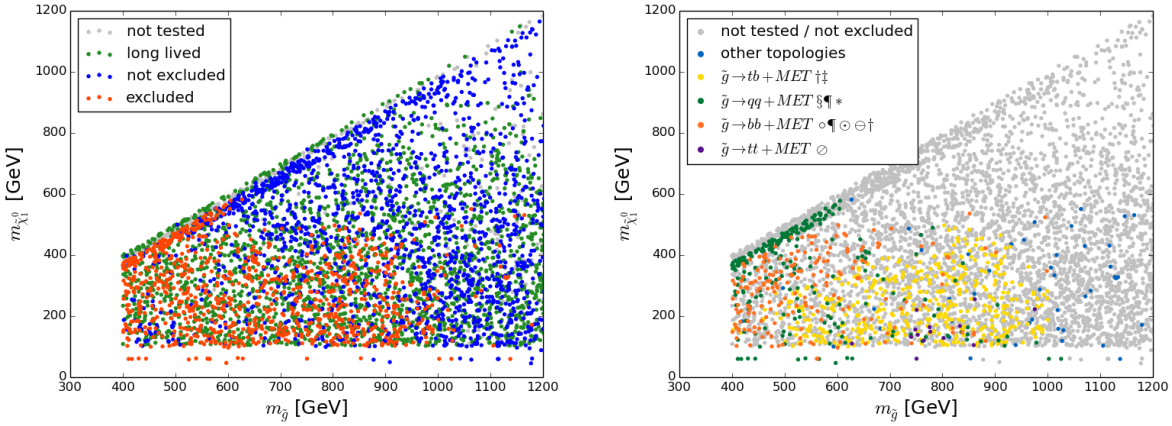

(a) (b)

Figure 5.28.: Exclusion with SModelS v1.0.1 in the LSP - gluino mass plane. (a) shows whether a point can be tested, and excluded, as well as points which cannot be tested because of long-lived sparticles or other reasons. (b) shows the most constraining topology for all excluded points. For the most frequently found topologies we specify the associated experimental searches : ‡ = [361], † = [362], ⊖ = [363], § = [213], ⊘ = [309], ∗ = [359], ∘ = [245], ¶ = [360] and ⊙ = [307].

via an on-shell stops can be tested by SMS. However we found that the cross sections are too small by two orders of magnitude for these points to be excluded.

Points with very light gluinos (below 500 GeV) may remain allowed even for light LSP (less than 200 GeV) if the branching ratio $\tilde{g} \to t\bar{b}\tilde{\chi}^-$ is dominant. This is because constraints in the region where $m_{\tilde{g}} \leq 500$ GeV available from ATLAS [364] (where the chargino is considered degenerate with the LSP) are very weak. This search was also considered in CMS [365] but the results are not incorporated in SModelS v1.0.1 as digitized data are not yet available. Furthermore results for this topology when the chargino is not degenerate with the LSP are only available for one specific mass ratio and therefore cannot be used.

We also found that most points with a light gluino and a dominantly singlino LSP feature a very compressed spectrum. This follows from the relic density constraint that favours coannihilation as mentioned in Section 5.3.2, thus these points will be hard to constrain from SUSY searches for gluinos.

Squark constraints The model can naturally give light squarks, as was shown in Section 5.3.2. However we observe that these are poorly constrained by the SMS limits. We show the excluded vs. allowed points as well as the most constraining topology for each point, here in the plane of the LSP and the lightest squark mass (including stop and sbottom), see Figure 5.29.

A first observation is that 1st and 2nd generation squark topologies can exclude points up to rather high squark masses (about 1200 GeV) in excess of the simplified models exclusions. This is expected since a light gluino will enhance the squark production cross sections. The applicability of the SMS results in this case is discussed in Section 4.1. Points along the kinematic edge can in general only be excluded by one heavier squark in the point, as such a

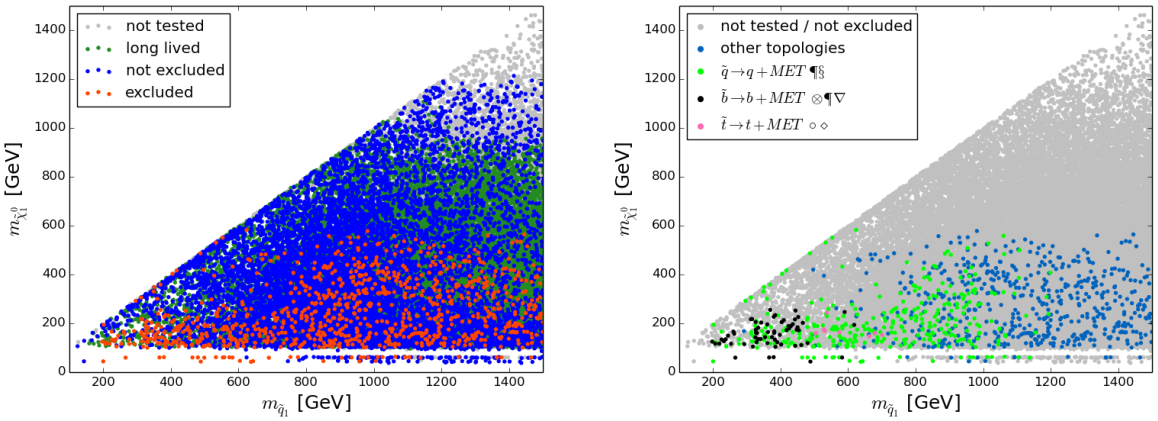

(a) (b)

Figure 5.29.: Exclusion with SModelS v1.0.1 in the LSP - squark mass plane below 1.5 TeV, where we select the mass of the lightest squark (including stop, sbottom). (a) has same colour code as in Figure 5.28a. (b) shows for all excluded points the most constraining topology. For the most frequently found topologies we show the associated experimental searches : § = [213], ○ = [245], ¶ = [360], ⊗ = [366], ⋄ = [160] and ∇ = [367].

compressed spectrum cannot be tested by the SMS results.

We find however that many points with light squarks remain unconstrained, even for large mass differences to the LSP. The first reason for this is that the simplified model exclusions depend critically on the assumption that the 8 squarks of the first and second generation are nearly degenerate. This is not the case in the UMSSM, where because of the new D-term contributions the mass of the RH d-type squarks can differ significantly from the other squark masses. Often their masses are not close enough to combine the production cross sections before comparing against an upper limit result [147][12]. We therefore find much weaker exclusions. The second reason is again tied to the nature of the LSP. Recall that most points, and in particular the unexcluded ones, feature a higgsino LSP, as shown in Figure 5.30, and that important signatures of light squarks with a higgsino LSP are not covered by existing SMS results.

To identify the main signatures for squarks that are not covered by SMS results, we discuss next the dominant missing topologies, separately for first/second generation and third generation squarks. A simplified model topology for which no matching experimental interpretation exists is labeled as "missing topology", see Section 3.2.5.

Here we use a simplified version of the SModelS bracket notation. The notation used for missing topologies keeps track of the branch and vertex structure. One branch is contained inside brackets, vertices are separated by a comma. Only outgoing R-even particles in a given vertex are specified, light quarks and gluons appear as jets (denoted by "j") while

[12] If several particles (such as squarks of different masses) contribute to the same topology, they will be combined if the corresponding masses are found to be compatible, as described in Section 3.2.3. This is evaluated for each experimental result and may hence differ for different experimental analyses considering the same topology. Note that despite differences in the upper limits, the contributions of different mass configurations may still contribute to the same signal region. Using the appropriate efficiencies for each contribution might therefore improve the limits.

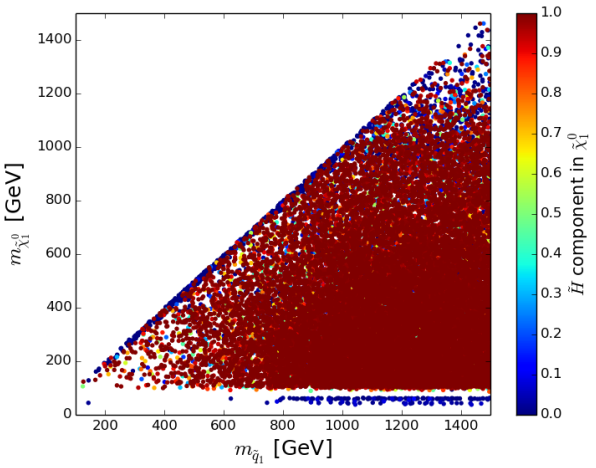

Figure 5.30.: Higgsino component of the LSP in the LSP - lightest squark mass plane below 1.5 TeV, for points that cannot be excluded by SModelS v1.0.1.

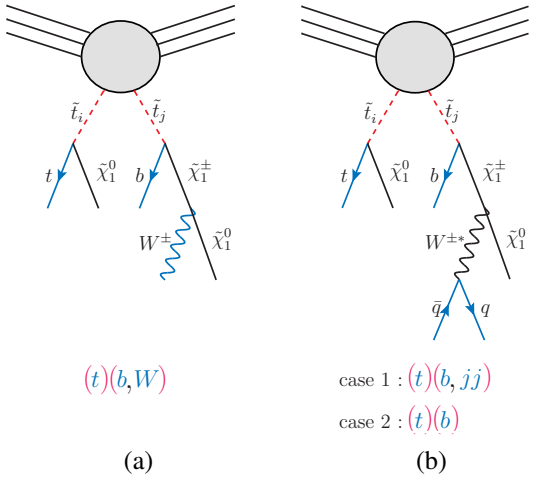

Figure 5.31.: Sample diagrams illustrating missing topologies and their notation in the case of stop pair production followed by an asymmetric decay to a neutralino LSP. Pair production, determining the branch structure is shown in red, R-even final state particles are indicated in blue.

third generation quarks are denoted by their name. E_T^{miss} from an outgoing DM candidate is always implied, and if no visible R-even particles appear in a branch it is denoted as "(inv)". An example is stop pair production, with $\tilde{t}_i \to t\tilde{\chi}_1^0$ in one branch and $\tilde{t}_j \to b\tilde{\chi}_1^\pm$, $\tilde{\chi}_1^\pm \to W^{\pm(*)}\tilde{\chi}_1^0$ in the other ($i, j \in \{1, 2\}$), illustrated in Figure 5.31. This topology is denoted as "$(t)(b, W)$" if the W is on-shell (Figure 5.31a). In scenarios with an off-shell W (as shown in Figure 5.31b) only the decay products will be listed, e.g. "$(t)(b, jj)$" for hadronic W decay (case 1). Finally if the mass gap between the chargino and the neutralino is smaller than the limit chosen for mass compression, the chargino decay is considered invisible, the topology is then listed as "$(t)(b)$" (case 2). [13]

[13] This notation directly translates to the SModelS nested bracket notation, where nested square brackets indicate the branches and vertices. The given example "$(t)(b, W)$" is then written as `[[[t]],[[b],[W]]]`.

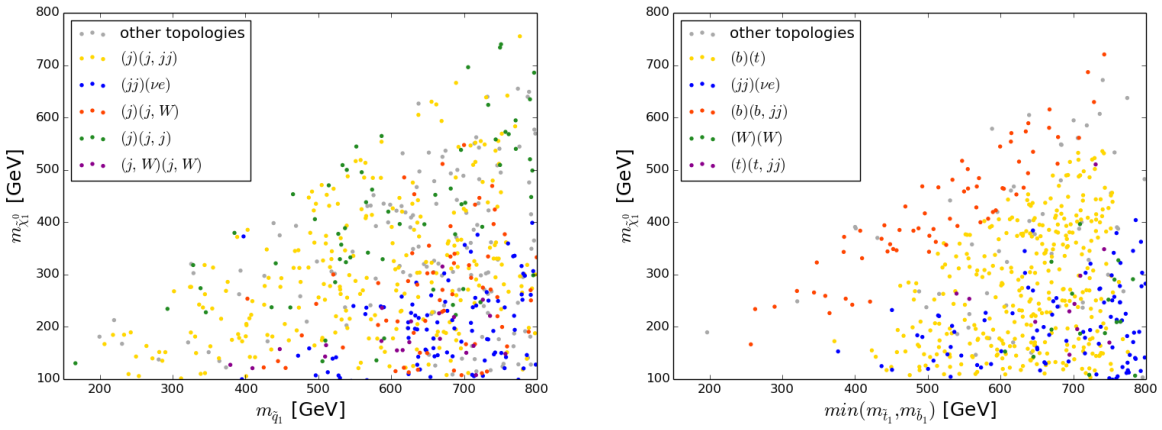

(a) (b)

Figure 5.32.: Missing topologies with highest cross section, for higgsino LSP, shown in (a) in the $m_{\tilde{\chi}_1^0} - m_{\tilde{q}_1}$ plane where q_1 is the lightest squark of the first and second generations. In (b) the mass of the lightest third generation squark is used. For both plots only masses below 800 GeV are displayed. Here we have not considered direct higgsino production which cannot be tested by 8 TeV LHC results.

In Figure 5.32a we show the missing topology with the highest cross section for points labeled as not tested or not excluded and with light first/second generation squarks. Here we select only points where the higgsino fraction in the LSP is greater than 80%. Moreover, to concentrate on topologies derived from squark production, we have removed any topology where one branch is fully invisible, thus getting rid of direct higgsino production. Indeed in chargino-neutralino production, the neutralino LSP leads to an invisible branch, moreover a chargino can also lead to an invisible branch when it is nearly degenerate with the neutralino since the soft jets that result from its decay cannot be detected. We further remove points in which the dominant missing topology has a weight smaller than 1 fb. We find that a main missing topology consists of 4 jets + E_T^{miss} deriving from one squark decaying to $q\tilde{\chi}_1^0$ and the other to $q\tilde{\chi}_2^0$ with the neutralino further decaying to the LSP via off-shell Z_1, giving the additional jets (mostly soft jets). A re-interpretation of the multijet analyses for this simplified model could be useful in constraining these points. Note that this topology is common in the compressed region where the squark - LSP mass difference is small. We also find 3 jets + E_T^{miss} topologies, stemming from squark-gluino production as described above. These are found mainly when both gluinos and squarks are light and the gluinos decay into a squark and a quark. Results for squark-gluino production within SMS exist only for almost mass degenerate gluinos and squarks. Note that for such points gluino pair production remains unconstrained as the gluino preferably decays to on-shell squarks, for which there are no SMS results. Similarly in scenarios where the gluino is lighter than the squark, squark pair production remains unconstrained as they decay dominantly via gluinos.

In case of larger squark - LSP mass splittings, we often find gauginos with a mass between those of the squark and the higgsinos. In this configuration, the squark can decay either to the LSP or to a heavier gaugino, that then decays into the LSP and a gauge boson or a Higgs (real or virtual). In particular we find that an important missing topology is the one where

each pair-produced squarks decays to a different channel, "$(j)(j,W)$", but "$(j,W)(j,W)$" is dominant in a few points.

The limits on the third generation squarks are also much weaker than in the simplified model. The reason is similar to the one invoked for gluino limits : with the higgsino LSP, a stop may decay either to $t\tilde{\chi}^0$ or to $b\tilde{\chi}^+$. Therefore, only a fraction of the total cross section can be constrained by the simplified model upper limit. Furthermore the "mixed" decays, where one of the pair produced stop decays via top and the other via bottom cannot be constrained as there are currently no SMS result for this channel. This shows up as an important missing topology, "$(b)(t)$", in Figure 5.32b. The situation is improved when efficiency maps are incorporated into SModelS, available in the latest version [204]. When the mass splitting between the stop and the LSP is below the top mass, the main missing topology is rather associated with sbottom pair production with one sbottom decaying to $b\tilde{\chi}_1^0$ and the other to $b\tilde{\chi}_2^0$, followed by $\tilde{\chi}_2^0 \to q\bar{q}\tilde{\chi}_1^0$ via an off shell Z_1 leading to "$(b)(b,jj)$". Similarly "$(t)(t,jj)$" appears at large mass splittings. An important missing topology is the one associated with chargino pair production with charginos decaying to the LSP and jets or leptons via a virtual W, "$(jj)(\nu e)$". We further find a few points where direct production of heavy charginos, decaying via W, gives the dominant missing topology "$(W)(W)$".

Note that listing missing topologies with the largest cross section can sometimes be misleading as the background was not taken into consideration. It is certainly possible that a signature with a smaller cross section gives a better signal to background ratio. Examples are leptonic vs. hadronic decays of the W, or decays into b-quark as compared to decay into light jets.

Neutralino LSP : Δa_μ and slepton constraints

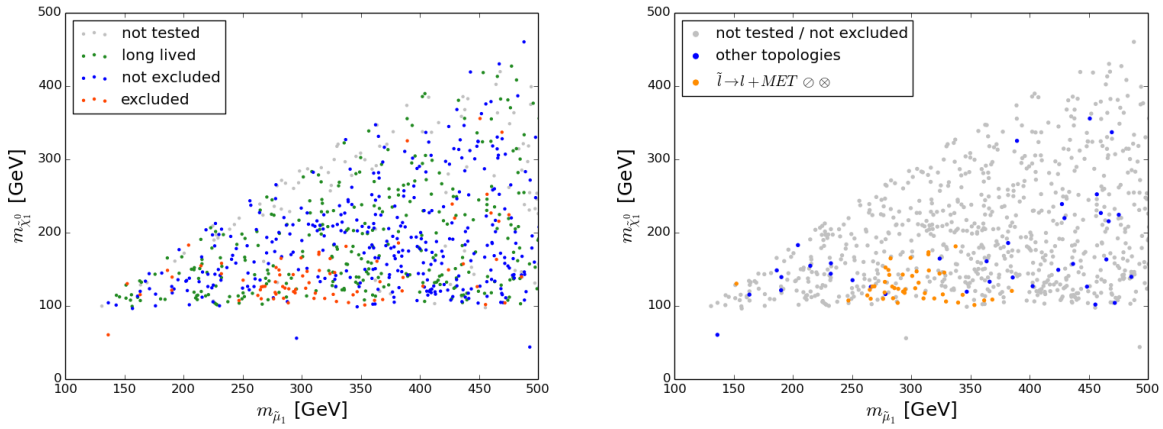

(a) (b)

Figure 5.33.: Exclusion with SModelS v1.0.1 in the $m_{\tilde{\chi}_1^0} - m_{\tilde{\mu}_1}$ plane below 500 GeV. (a) has same colour code as in Figure 5.28a. (b) is showing for all excluded points the most constraining topology. For the most frequently found topology we show the associated experimental searches : ⊘ = [265] and ⊗ = [310].

We have separately studied points where the muon anomalous magnetic moment constraint is fulfilled. Because of the light smuons (and selectrons) additional LHC constraints

from slepton SMS topologies become relevant. These constraints played a marginal role in the general scan considering the small fraction of points with light sleptons. We show the exclusions in Figure 5.33. Excluded points are found mainly in a small region in the mass plane, for light smuon masses $m_{\tilde{\mu}_1}$ between 250 and 380 GeV. These exclusions are slightly weaker than the ones obtained in ATLAS and CMS [265, 310] which assume all sleptons decay into $l\tilde{\chi}_1^0$ while here sleptons can also decay into $\nu_L^l \tilde{\chi}_1^+$. Moreover for weakly interacting particles we only compute the production cross section at leading-order while SMS include NLO cross sections. A single point is excluded by the slepton SMS result despite a very small mass difference between smuon and LSP. However, in this case it is not actually the slepton production that is being constrained, but pair produced charginos, each of them decaying to a left handed sneutrino which then decays invisibly to the neutralino. The signature is identical to that of slepton pair production, giving a 2 lepton and missing energy final state and was discussed in Section 5.2. Other exclusions come from gluino and squark topologies, as described in the previous section.

RH sneutrino LSP

In the case of a sneutrino LSP we have to bear in mind that since these sneutrinos are RH all decays of heavier sparticles must proceed via a neutralino. When the neutralino is the NLSP it decays invisibly into $\nu_R \tilde{\nu}_R^*$ or $\bar{\nu}_R \tilde{\nu}_R$, therefore signatures resemble those associated with a neutralino LSP. When decays through an on-shell neutralino are not allowed, we effectively find additional neutrinos in the decay vertex to sneutrino, for example in the squark decay $\tilde{q} \to q\nu_R\tilde{\nu}_R$. The signature is essentially the same as for a squark decaying into a neutralino LSP since the neutrino will contribute only to the E_T^{miss}, but the event kinematics can be changed due to the additional invisible particle in the vertex. This issue remains to be investigated and these signatures are not treated in SModelS v1.0.1.

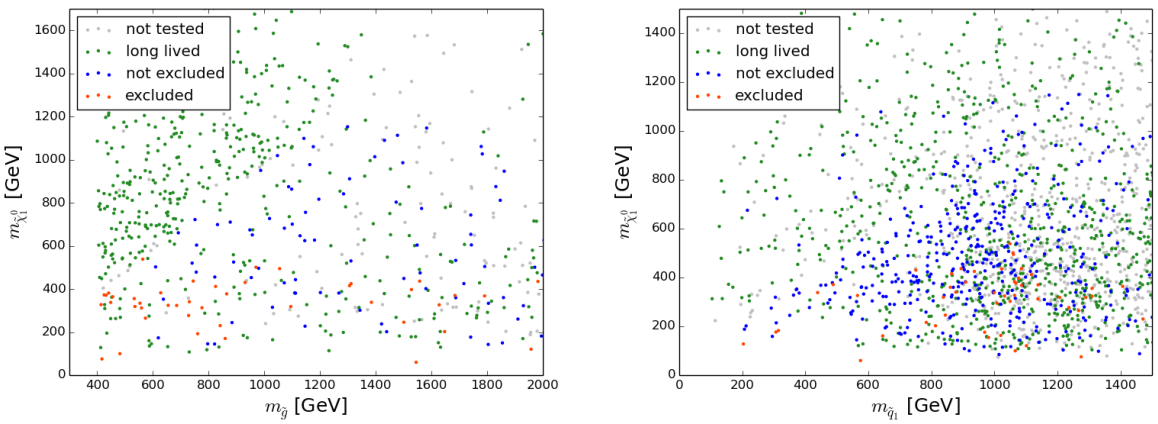

(a) (b)

Figure 5.34.: Exclusion with SModelS v1.0.1 for points with RH sneutrino LSP (a) in the neutralino - gluino mass plane and (b) in the neutralino - lightest squark mass plane. Points with very heavy neutralinos and squarks are not displayed.

Figure 5.34 is showing points with a RH sneutrino LSP in the $\tilde{\chi}_1^0 - \tilde{g}$ and $\tilde{\chi}_1^0 - \tilde{q}_1$ mass planes. One striking feature is that in this scenario there are many points with long-lived

gluinos or squarks. Those are mainly found when the lightest neutralino is heavier than the gluino or squark since decays into RH sneutrino LSP can only proceed via some virtual sparticle and are hence suppressed. Among the points that can be tested, only a small number can actually be excluded. The exclusion channels are similar to the ones for the neutralino LSP discussed above and involve a decay of a gluino or squark through a neutralino which further decays into the LSP. We find no exclusion from electroweak production. It is therefore instructive to consider the missing topologies. To clarify again the notation used for missing topologies, we show in Figure 5.35 the case of chargino-neutralino production for a sneutrino LSP. The neutralino decays to a neutrino and a sneutrino, making this branch entirely invisible, hence indicated by "(inv)". The signature of the chargino decay will depend on whether the intermediate neutralino is on-shell or not, indicated by cases 1 and 2. If the neutralino is on-shell its decay will be invisible and it can be considered as an effective LSP, yielding the topology "$(\mathrm{inv})(W)$". If on the other hand the decay to on-shell neutralino is not possible, the chargino will effectively decay directly as $\tilde{\chi}_1^{\pm} \to W^{\pm}\nu_R\tilde{\nu}_R$, the topology is then described as "$(\mathrm{inv})(W\nu)$". Recall that in the SMODELS nested bracket notation, this topology is denoted by `[[],[[W,nu]]]`.

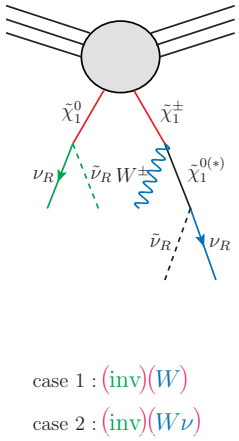

Figure 5.35.: Diagram illustrating missing topologies and their notation in the case of chargino-neutralino production where the sneutrino is the LSP. Pair production, determining the branch structure is shown in red, R-even final state particles are indicated in blue and the invisible branch is represented in green.

We show (for all not excluded or not tested points) the missing topology with the highest cross section, selecting only the five most frequent ones, see Figure 5.36. At low neutralino masses topologies from neutralino-chargino production are often dominant, with the charginos decaying either directly to $W\tilde{\nu}_R\nu_R$, "$(\mathrm{inv})(W\nu)$", or via $W^*\tilde{\chi}_1^0$, "$(\mathrm{inv})(jj)$". In both scenarios the neutralino decay is invisible. Note that for the missing topologies we do not distinguish between LH or RH neutrinos. The SMS limits on chargino-neutralino production with $W^{(*)}$ final state cannot be applied for either topology. The reason is that SMS results assume that the process involves one of the heavier neutralinos which then decays via a gauge boson and the LSP, whereas here only the chargino decays into visible particles. Moreover, in the first case, there is an additional neutrino in the decay. In the second case the decay products of the W^* are very soft because of the degeneracy between the lightest chargino and neutralino. Pair produced charginos decaying to $W\tilde{\chi}_1^0$ also provide an important topology, "$(W)(W)$". Both the lightest and heaviest chargino can contribute to this topology. A similar topology with off-shell W's also occurs although it is suppressed by the

hadronic branching ratio. Note that current SMS results for this topology only give weak constraints and are not included in this study.

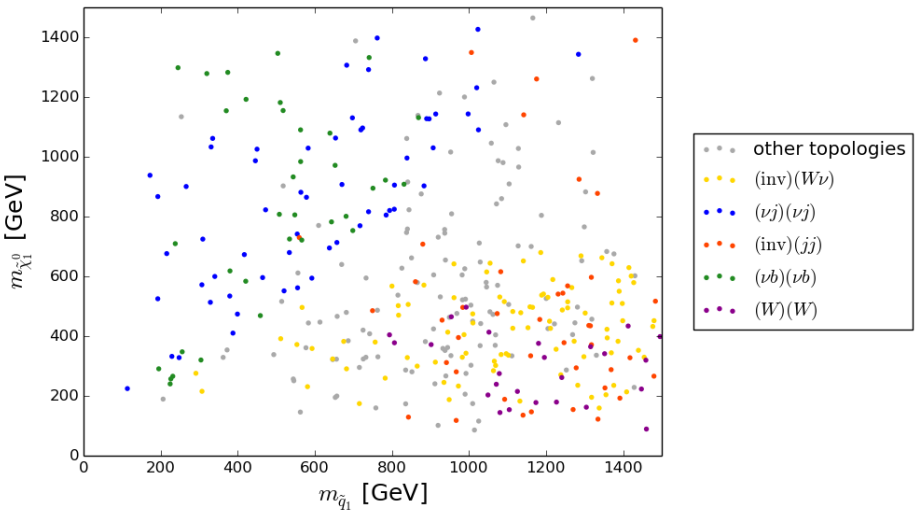

Figure 5.36.: Missing topologies with the highest cross section in the neutralino - lightest squark mass plane, for points with a RH sneutrino LSP that are not excluded by SModelS v1.0.1 and that do not involve long-lived sparticles.

Finally topologies associated with squark pair production are also frequently dominant, for light squarks and heavier neutralino we find squarks decaying directly to the right handed sneutrino, $\tilde{q} \to q\nu_R\tilde{\nu}_R$ with either a light quark or a b-quark, corresponding to the topologies "$(\nu j)(\nu j)$" and "$(\nu b)(\nu b)$" in Figure 5.36. Missing topologies involving gluinos are similar to the ones in the neutralino LSP case, note however that when lighter than $\tilde{\chi}_1^0$ the gluino is likely to be long-lived, or otherwise to decay via 4-body, $\tilde{g} \to jj\nu_R\tilde{\nu}_R$.

Long-lived charged NLSP

The D0 collaboration has searched for pair produced long-lived charginos [340], putting upper limits on the production cross section for chargino masses between 100 and 300 GeV. Since experimental limits are given separately for wino and higgsino-like chargino, we use the relevant result and in case of large mixing i.e. wino fraction in $\tilde{\chi}_1^\pm$ between 0.3 and 0.7) we apply the more conservative limit. Note that the limit is only marginally different in the two cases. Results are shown in Figure 5.37a. We find that long-lived charginos lighter than about 230 GeV are excluded.

In addition, the ATLAS collaboration has searched for long-lived charginos from either pair production of charginos or chargino-neutralino production [316], yielding upper limits on the combined cross section for chargino masses between 450 and 800 GeV. We have checked that the less constrained chargino-neutralino contribution is never larger than in the scenario considered by ATLAS, thus ensuring that the application of the upper limit is always conservative. Note that in addition to chargino pair production we generally consider only $\tilde{\chi}_1^\pm\tilde{\chi}_1^0$ production, except when this is essentially zero then we include also $\tilde{\chi}_1^\pm\tilde{\chi}_2^0$ production. This may occur if the LSP is bino or singlino and degenerate in mass with the chargino[14].

[14]This degeneracy can follow from imposing the relic density upper limit which in this case will be satisfied because of the contribution from efficient coannihilation channels involving the chargino and heavier neutralinos [368].

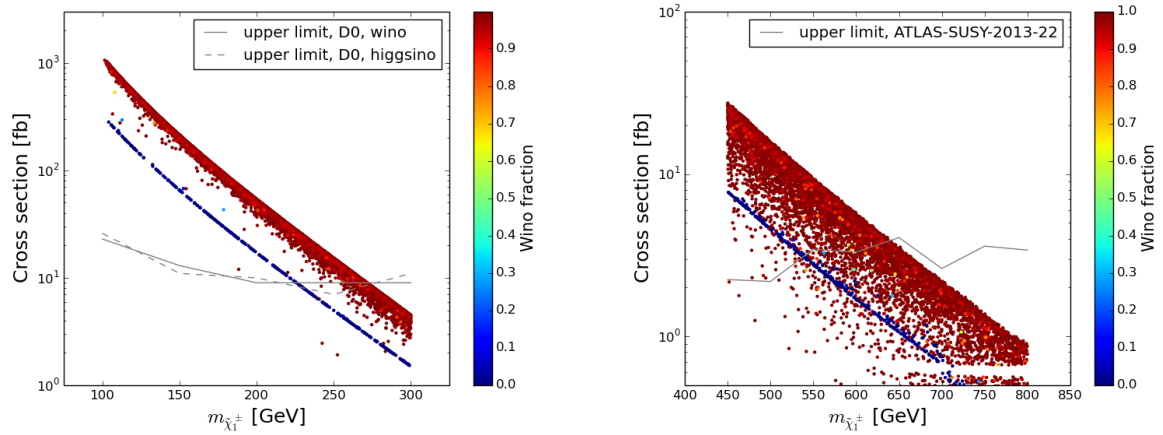

(a) (b)

Figure 5.37.: Points tested by searches for long-lived charginos: (a) the chargino pair production cross section and the corresponding upper limits from D0 (b) sum of chargino pair and chargino neutralino production cross sections and the corresponding upper limit from ATLAS. The colour code indicates the wino fraction in $\tilde{\chi}_1^\pm$.

Results are shown in Figure 5.37b. We find that even at low masses some points cannot be excluded, because interference between light squark exchange diagrams lead to small production cross sections. However, a large number of points, with chargino masses up to about 650 GeV, can be excluded. Note that in both cases we have used linear interpolation between the given data points. We expect that smaller masses (below 450 GeV) should be excluded as well, but at the time of publication existing searches in that mass range consider long-lived staus (ATLAS) or long-lived leptons (neutral under $SU(2)_L$, see [316]) and were not applicable here.

Finally we point out the potential of such a search at 13 TeV. In Figure 5.38, the cross section for pair production of charginos with decay lengths $c\tau > 10$ mm is displayed. Here all points that have not yet been excluded are shown. We find that about one order of magnitude improvement over the current limit would allow to probe a large fraction of the points with a long-lived chargino below the TeV scale. Note that in this Figure we have included long-lived charginos decaying either inside or outside the detectors. Each category includes a significant number of points. Therefore both types of searches could be used to test the model further. Constraints on charginos decaying inside the detector have recently been updated by the ATLAS search [369], and can likely exclude scenarios with light charginos and intermediate lifetimes, compare Figure 2.7 (left).

5.3.4. Summary after LHC Constraints

Exclusion potential of current LHC searches on the UMSSM

To summarize the impact of the LHC constraints on the sfermion spectrum we display in Figure 5.39 the excluded/non-excluded points in the plane $\theta_{E_6} - m_{\tilde{f}}$ for $\tilde{f} \in \{\tilde{t}_1, \tilde{b}_1, \tilde{d}_R\}$ as well as $\tilde{f} = \tilde{\mu}_L$ for the sample where the muon anomalous magnetic moment constraint is imposed. Among the non excluded points those that satisfy all constraints have a different

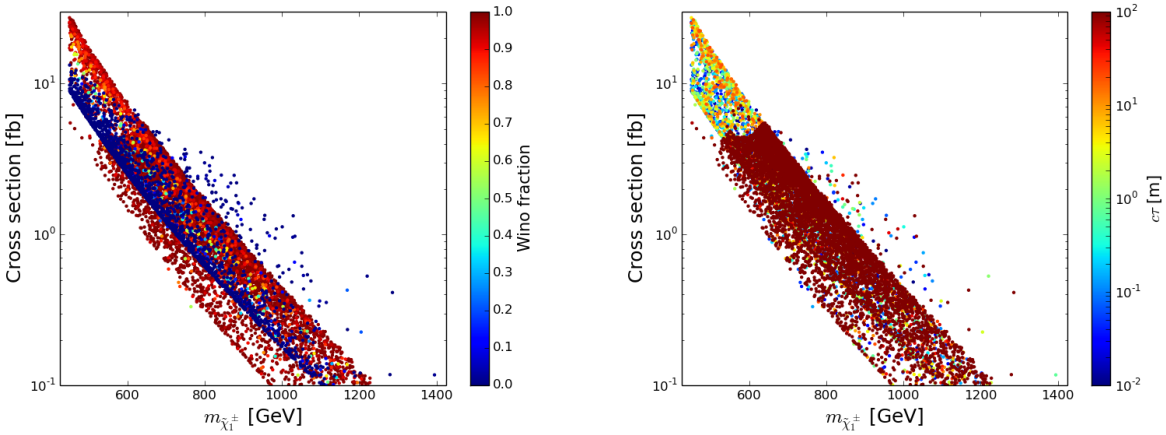

(a) (b)

Figure 5.38.: Chargino pair production cross section at 13 TeV, for unexcluded points with long-lived charginos where the colour code indicates either (a) the wino fraction in $\tilde{\chi}_1^\pm$ or (b) $c\tau < 100$ m.

colour code than those that are associated with a long-lived NLSP or that are not tested by SModelS v1.0.1. In all cases the excluded points are scattered and represent only a fraction of all points. It should be stressed again that many scenarios with squark masses well below 1 TeV are allowed. When the agreement with Δa_μ is not required we found that 45% (41%) of the points that were confronted with the LHC limits had a long-lived sparticle in the case of a neutralino (RH sneutrino) LSP, 16% (17%) were tested by SModelS of which 10% (11%) were excluded. The remainder of the points was not testable by SModelS either because of too low cross sections or lack of SMS result. We additionally found that 42% (24%) of the sample with long-lived NLSP were excluded by long-lived chargino searches. In the case where the muon anomalous magnetic moment constraint is required and for a neutralino LSP the amount of points tested by SModelS is larger (34%, out of which 11% are excluded), whereas the fraction of points with long-lived sparticles is smaller (30%, out of which 44% can be excluded). Extending these searches for long-lived charginos to the full mass range would therefore clearly provide a powerful probe of the model. Moreover, when the RH sneutrino is the LSP a large fraction of the points involves long-lived gluinos and squark. These scenarios could test the model further, but require reliable limits on R-hadrons. Note that to facilitate the interpretation of limits on long-lived charginos, it would be useful if limits on the direct chargino pair and neutralino-chargino production were separately provided by the experimentalists.

Many of the points that are in agreement with the measured value of the muon anomalous magnetic moment, even those associated with a very light smuon cannot be completely excluded, see Figure 5.39d. The LHC13TeV with higher luminosity will allow to extend the reach for smuons in the conventional lepton + E_T^{miss} channel. Unfortunately the light charginos that are present in this case cannot be probed easily as once again they are often dominantly higgsino and hence almost degenerate with the LSP.

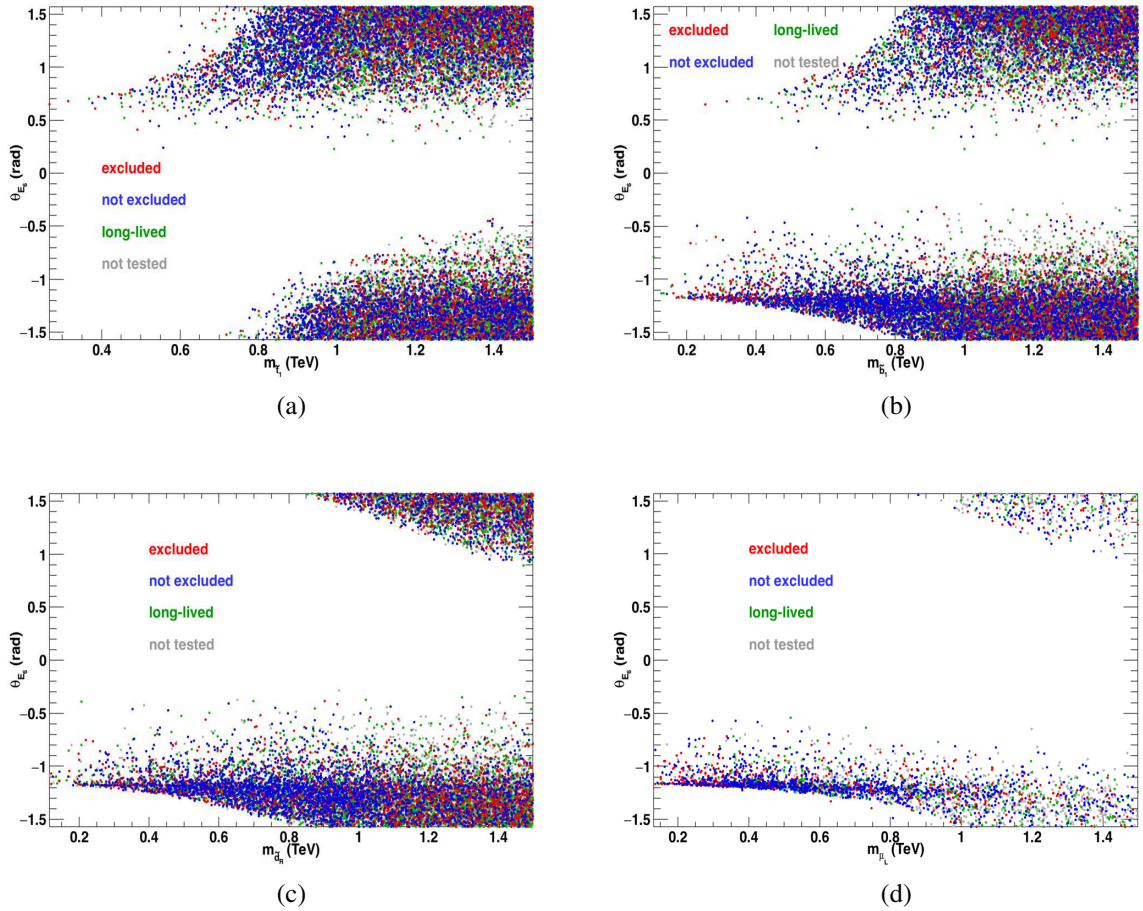

Figure 5.39.: Points in the $\theta_{E_6} - m_{\tilde{f}}$ plane for (a) $\tilde{f} = \tilde{t}_1$, (b) $\tilde{f} = \tilde{b}_1$, (c) $\tilde{f} = \tilde{d}_R$ and (d) $\tilde{f} = \tilde{\mu}_L$. For all plots $m_{\tilde{f}} < 1.5$ TeV and the colours correspond to not tested (grey), long-lived (green), not excluded (blue) and excluded (red) configurations using SModelS v1.0.1 and the searches for long-lived charginos. For (d) only points satisfying Δa_μ are represented.

Suggestions for future LHC searches

Conventional searches for a new Z' provide the most distinctive signature of the UMSSM. In addition we have pointed out in previous sections many additional signatures that are still unconstrained by current SMS results. Here we summarize the main missing topologies found for each scenario.

As expected, the most distinctive SUSY signatures in the UMSSM are found in the case of a RH sneutrino LSP. We have already stressed that long-lived gluinos or squarks are fairly common in such scenarios and could therefore provide further constraints on the model. We have also found that the following topologies could be used to probe the model either by reinterpreting current LHC data or by exploiting Run 2 data.

- mono-W, "(inv)$(W\nu)$", from chargino neutralino production with $\tilde{\chi}_1^0 \to \nu_R \tilde{\nu}_R$ and $\tilde{\chi}_1^\pm \to W^\pm \nu_R \tilde{\nu}_R$. The single W can be energetic enough to lead to visible decay products, leptons or jets as long as there is a large mass difference between the chargino and sneutrino LSP. Such a topology occurs also for a neutralino LSP (as in the MSSM)

but only when there is a large $\tilde{\chi}_1^\pm - \tilde{\chi}_1^0$ mass splitting to allow $\tilde{\chi}_1^\pm \to W^\pm \tilde{\chi}_1^0$, which is not the most common configuration after imposing DM constraints.

- dijets + $E_T^{\rm miss}$, "$(\nu j)(\nu j)$" or $b\bar{b}$ + $E_T^{\rm miss}$, "$(\nu b)(\nu b)$", from squark pair production with $\tilde{q} \to q\nu_R\tilde{\nu}_R$ where q here stands for either light jets or b-jets. This occurs when the squark is lighter than all neutralinos and therefore has to decay directly to the sneutrino LSP. Such a configuration is clearly only possible in a model with a sneutrino LSP. The dijet + $E_T^{\rm miss}$ signature is of course common to squark pair production in the MSSM, however it remains to be seen how the additional ν_R in the decay will affect the efficiencies, hence could lead to different exclusions than in the case of the neutralino LSP.

Other important missing topologies include dijets + $E_T^{\rm miss}$, "(inv)$(j\ j)$", from chargino neutralino production with the same decays as the mono-W above except that the W is off-shell leading to soft final states as well as W pairs + $E_T^{\rm miss}$, "$(W)(W)$", from chargino pair production with $\tilde{\chi}_1^\pm \to W^\pm \tilde{\chi}_1^0 \to W^\pm \nu_R \tilde{\nu}_R$. These topologies also arise in the MSSM with a neutralino LSP and are poorly constrained from searches at Run 1 partly due to the small production cross section. The situation should however improve after accumulating more data in Run 2.

When the neutralino is the LSP, most SUSY signatures are the same as found in the MSSM. However we stress that having imposed only the upper limit on the dark matter relic density, most of our scenario have a wino/higgsino-like LSP. Thus, the SUSY signatures can differ from the bino LSP assumed in several SMS results. In particular, the chargino decay can be invisible and this will have an impact on many SUSY searches. In addition this implies that a significant fraction of the scenarios have a long-lived chargino and/or neutralino, hence the importance of searches for stable charged particles at collider scale and for displaced vertices.

Many of the topologies that could not be constrained by current SMS results are associated with asymmetric decays, that is the pair produced particles have two different decay chains whereas most SMS results assume identical decays for both particles. We emphasize here the missing topologies for the case of the higgsino LSP since it is hard to probe.

- 3 jets + $E_T^{\rm miss}$, "$(j)(j,j)$", from gluino-squark production with $\tilde{g} \to \tilde{q}q$ and $\tilde{q} \to q\tilde{\chi}_1^0$. Current SMS interpretations exist only for scenarios where the gluino and squarks are almost mass degenerate, and both decay directly to jets and LSP. Similarly the topology 4 jets + $E_T^{\rm miss}$, "$(j,j)(j,j)$", from gluino pair production with $\tilde{g} \to \tilde{q}q$ and $\tilde{q} \to q\tilde{\chi}_1^0$ arises from a process with a large production cross section that is not constrained by SMS results since the gluino decays via on-shell first or second generation squarks. Note that both these topologies are of special interest in the UMSSM where the limits on light squarks from direct squark production are much weaker because the squarks are not necessarily all degenerate.

- bt + $E_T^{\rm miss}$, "$(b)(t)$" , from stop (sbottom) pair production with asymmetric decays, $\tilde{t} \to t\tilde{\chi}_1^0$ and $\tilde{t} \to b\tilde{\chi}_1^+$ ($\tilde{b} \to b\tilde{\chi}_1^0$ and $\tilde{b} \to t\tilde{\chi}_1^-$) when the chargino is nearly degenerate with the LSP. This signature is a generic feature of models with wino/higgsino LSP and light third generation squarks [245, 267].

- 4 jets + $E_T^{\rm miss}$, "$(j)(j,jj)$", from squark pair production with asymmetric decays. Here one squark decays directly to the LSP, $\tilde{q} \to q\tilde{\chi}_1^0$ while the other decays via heavier neutralino, $\tilde{q} \to q\tilde{\chi}_2^0$ and $\tilde{\chi}_2^0 \to Z_1^* \tilde{\chi}_1^0$. A re-interpretation of the multi-jet analysis to study the effect of the soft jets from the virtual Z_1 on the efficiency would be useful.

- $2b$ + 2 jets + E_T^{miss}, "$(b)(b,jj)$", from sbottom pair production with asymmetric decays, same as above. Note that this topology is found for small mass difference between the sbottom and the LSP. Similarly the $2t$ + 2 jets, "$(t)(t,jj)$", from stop pair production is also a missing topology.

- 2 jets + W + E_T^{miss}, "$(j)(j,W)$", from squark pair production with asymmetric decays. One squark decays to LSP $\tilde{q} \to q\tilde{\chi}_1^0$ while the other decays $\tilde{q}_u \to q_d\tilde{\chi}_1^+$ with $\tilde{\chi}_1^+ \to W^+\tilde{\chi}_1^0$ or $\tilde{q} \to q\tilde{\chi}_2^0$ with $\tilde{\chi}_2^0 \to W^-\tilde{\chi}_1^+$ when the chargino decays invisibly. We find this when the mass splitting between the squark and the LSP is large. Note that typically there would be similar channels with Z_1 or h_1 in the final state instead of a W reducing the cross section for each single channel.

- 2 jets + WW + E_T^{miss}, "$(j,W)(j,W)$", from squark pair production, here both squarks can decay to chargino, followed by $\tilde{\chi}_1^\pm \to W^\pm\tilde{\chi}_1^0$ as above. This channel has been considered at the LHC but is not yet included in the SModelS database, moreover results are available only for specific mass relations. It would be preferable to provide SMS results that allow for interpolation over wide range of masses in different mass planes.

Note that many of these signatures found for the higgsino LSP feature asymmetric decay branches. As pointed out in Section 5.1 they are mainly unconstrained by the SMS results and should be included in the database to improve coverage. In particular the cross section in the "$(j)(j,j)$" signature can be large, compare Figure 5.6. On the other hand the "$(b)(t)$" and "$(j,W)(j,W)$" signatures are now covered by the results in the latest version of SModelS [204] and should give important additional constraints..

In addition the signature WW + E_T^{miss} from chargino pair production will be useful in constraining the model, although it currently gives only weak limits [265]. Similarly the signature 2 jets + lepton + E_T^{miss} from charginos decaying via virtual W's is often found, current data do not put useful constraints but these searches should be improved in the next Run. In fact results from a recent CMS search for $\tilde{\chi}_1^\pm\tilde{\chi}_2^0$ production followed by a decay to a neutralino LSP can already exclude highly compressed spectra down to mass differences of about 8 GeV when considering pure wino production cross sections [370]. Future results are thus expected to give important constraints on higgsino LSP scenarios.

5.3.5. Couplings and Signal Strengths for the Higgses

In the UMSSM a lightest Higgs scalar with a mass of 125 GeV is easily found. Typically this lightest scalar is doublet-like and behaves roughly as the SM Higgs. Measurements of the Higgs couplings at the LHC Run 2 could therefore provide additional probes of the model. For all points of the UMSSM scan that successfully pass all collider constraints we have computed the reduced couplings of the 125 GeV Higgs. The reduced couplings are defined as scaling factors of the couplings in the UMSSM relative to their SM counterparts. We find that the $h_1W^+W^-(h_1Z_1Z_1)$ couplings deviate by at most 1% from the SM couplings while there is more room for deviations in the quark couplings. The $h_1b\bar{b}$ reduced coupling (C_b) can be as large as 1.2 for large values of $\tan\beta$ while the $h_1t\bar{t}$ coupling (C_t) can be suppressed by at most 5% for low values of $\tan\beta$, see Figure 5.40a. Note that the couplings are generation universal. Modifications of the quark couplings induce a correction to the loop-induced couplings of the Higgs to gluons (C_g) and photons (C_γ). In particular since the top quark gives the largest contribution to C_g in the SM, we expect a reduction in C_g. Furthermore, this

should be correlated with a mild increase in C_γ as observed in Figure 5.40b. Supersymmetric particles can also contribute to the loop-induced coupling, for example light squarks can lead to $C_g > 1$ although the effect is again below 5%. Light sleptons and charginos will only contribute to C_γ. Again the effect typically does not exceed 5%.

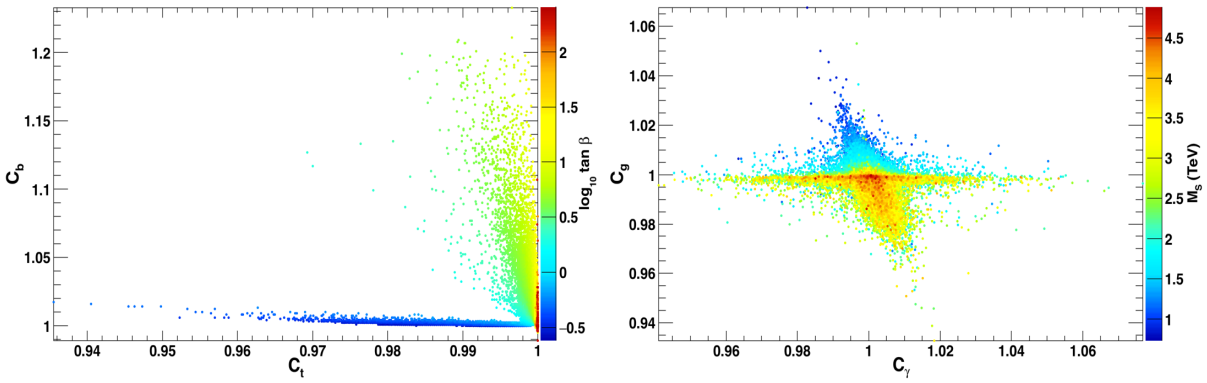

(a) (b)

Figure 5.40.: Reduced couplings of the light Higgs for all points satisfying collider and DM relic density constraints : (a) C_b vs. C_t with $\tan\beta$ as colour code, (b) C_g vs C_γ with M_S as colour code.

The effect on the Higgs signal strength can be much larger than on the reduced coupling. The signal strength in one channel is defined as the production cross section times branching ratio in the UMSSM relative to the SM expectation for a Higgs of the same mass. An increase in the total width, through an increase of the dominant $b\bar{b}$ partial width, will lead to a reduced branching ratio, hence to a reduced signal strength, in all other decay channels. Furthermore, when new decay modes are possible (here it means invisible decays into the LSP) the total width of the Higgs increases, thus reducing the signal strengths in all channels. For example the signal strength for the two-photon mode in gluon fusion $\mu^{\gamma\gamma}_{ggh_1}$ can be reduced by 25% as compared to the SM expectation, see Figure 5.41a. Because this large reduction comes from the total width we expect it to be completely correlated with the signal strength in the W fusion mode. A comparison with the signal strengths for the $b\bar{b}$ mode, Figure 5.41b, clearly shows that this reduction can be correlated with the one in the $b\bar{b}$ channel (when the invisible width is large) or with an increase in the signal strength in the $b\bar{b}$ channel when $C_b > 1$. Preliminary results from LHC Run 2, including signal strenght measurements, have been presented in LHCP in May 2017, analysing up to 35.9 fb$^-$1 of 13 TeV data, but do not change the global picture. The results found here are generally in agreement with the 2σ range of the results, see [371, 372].

The invisible width of h_1 is found to be below 25%. Recall that current limits from direct searches are 58% in CMS [373] while preliminary results from ATLAS in the vector boson fusion mode set the limit at 29% [374]. A stronger limit of 12% is obtained from global fits to the Higgs [375], however the latter applies only when all Higgs couplings are SM-like. In future runs, it is expected that the LHC could probe directly an invisible width of 17% [376].

Other probes of the Higgs sector can be performed by searching for the heavy Higgses at the LHC. After applying all constraints described in Section 5.3.1, which in particular include heavy Higgs searches at LHC8TeV, we find that the lowest allowed value for the

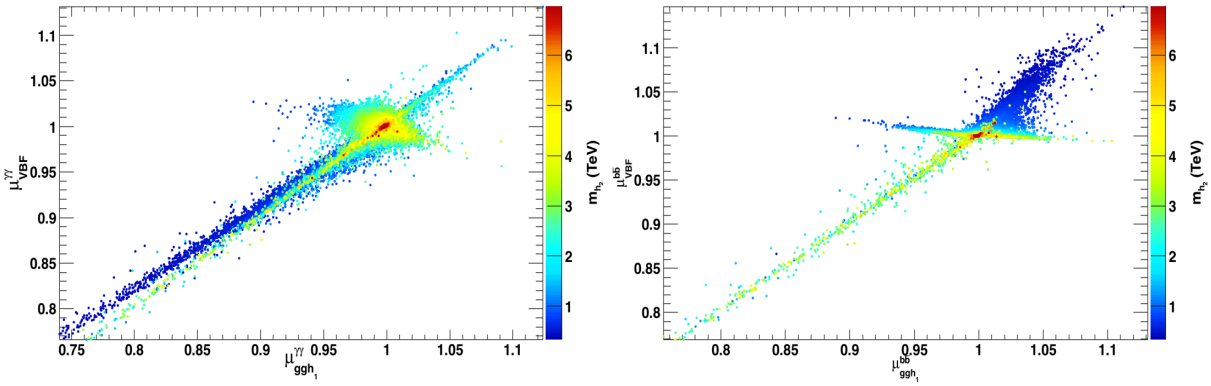

(a) (b)

Figure 5.41.: Signal strengths of the light Higgs into (a) $\gamma\gamma$ and (b) $b\bar{b}$ in the Vector boson fusion (VBF) vs. gluon fusion for all points satisfying collider and DM relic density constraints. For both plots m_{h_2} is taken as colour code.

mass of h_2 is around 340 GeV and can reach several TeV's. Below the TeV scale, the pseudoscalar is typically nearly degenerate with the doublet-like h_2 and the value of $\tan\beta$ ranges from 2-40 with a large fraction of the points with $\tan\beta < 10$ because of flavour and direct search limits.

To compare with the limits on searches (available at the time of publication) for heavy Higgs in the W^+W^- channel we have computed the signal strengths for $h_2 \to W^+W^-$ in both the VBF and gluon fusion mode. We expect this signal strength to be quite low (as we have argued above the coupling $h_1W^+W^-$ is SM-like). This means that in the decoupling limit the $h_2W^+W^-$ coupling is suppressed, $\cos(\alpha-\beta) \approx 0$ in the MSSM notation. Indeed we find that the signal strength is suppressed in the gluon fusion channel, $\mu^{\mathrm{WW}}_{\mathrm{gg}}(h_2) < 0.03$, due to the small branching into gauge boson final state and obviously even more so in the VBF production mode where the signal strength is well below 10^{-3}, see Figure 5.42a. Thus h_2 easily escapes current limits. Note furthermore that the largest signal strengths are found for low values of $\tan\beta$ and for h_2 much below the TeV scale, a region where potentially the $t\bar{t}$ channel offers a better probe, as discussed below.

In the sub-TeV region, preferred decay channels of h_2 are usually in the $b\bar{b}$ ($\tau^+\tau^-$) final states for moderate to large values of $\tan\beta$, as in the MSSM. However, for low values of $\tan\beta$, h_2 can decay exclusively into $t\bar{t}$, see Figure 5.42b. Moreover decays into the lightest Higgs can also be large (as much as 50% when $m_{h_2} < 360$ GeV) but drop rapidly reaching at most 10% when $m_{h_2} > 460$ GeV. In the MSSM it was shown that searches for heavy Higgs in the $t\bar{t}$ (hh) channel offer good discovery potential at LHC13TeV (with 300 fb^{-1}) for small values of $\tan\beta$, when $m_{h_2} < 1(0.5)$ TeV [377]. Hence, such searches should also probe of the UMSSM model further. However, decays of h_2 into supersymmetric particles can affect the main SM particle signatures. In particular decays into electroweakinos can reach 84% (86%) for the neutralino (RH sneutrino) LSP scenarios, while the invisible decay of h_2 into the neutralino LSP reaches at most 15%. Large branching fractions into electroweakinos are expected when the kinematically accessible states have a large higgsino/gaugino component, hence when μ, M_2 are small. These decay modes could therefore provide additional search channels for a second Higgs, see e.g. [378]. For a Higgs below the TeV scale, the decays into sfermions are generally kinematically forbidden. When they are allowed the branchings

never reach the percent level and are therefore negligible.

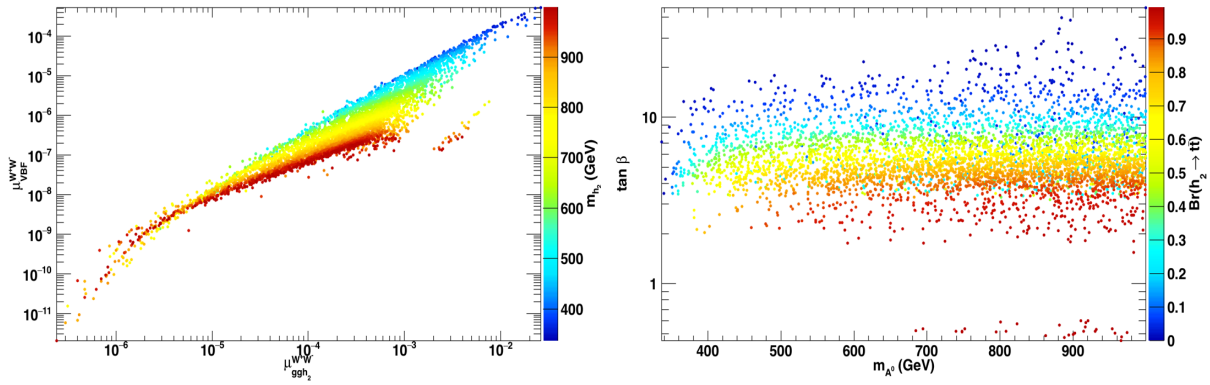

(a) (b)

Figure 5.42.: For all points satisfying collider and DM relic density constraints are displayed (a) the signal strengths for h_2 in gluon fusion and VBF modes in the W^+W^- final state, with $m_{h_2} < 1$ TeV as colour code. (b) $\mathcal{B}(h_2 \to t\bar{t})$ in the $\tan\beta - m_{A^0}$ plane with $m_{A^0} < 1$ TeV.

5.3.6. Dark Matter Probes

The correlation between LHC constraints and DM relic abundance on both the neutralino and RH sneutrino LSP scenarios is summarized in Figure 5.43. Clearly there is a strong preference for a RH sneutrino around 60 GeV, see Figure 5.43a. Moreover for the neutralino LSP case, the wino scenario (the lower branch in Figure 5.43b) is strongly constrained by searches for long-lived charginos. We now consider the predictions for DM observables.

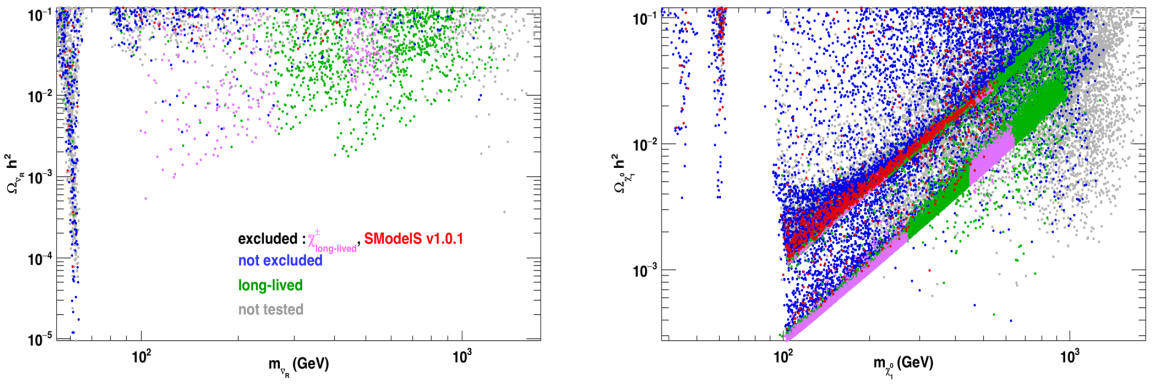

(a) (b)

Figure 5.43.: Relic density for (a) $\tilde{\nu}_{\tau R}$ or (b) χ_1^0 LSP with the same colour code as in Figure 5.39 except for the configurations excuded by searches for long-lived charginos which are highlighted in pink.

Direct searches for dark matter through their scattering on nuclei in a large detector provide a complementary method to probe supersymmetric dark matter. When examining the predictions for dark matter searches we use a rescaling factor to take into account cases where the LSP constitutes only a small fraction of the dark matter. The 2σ deviation from the central value measured by Planck is $\Omega h^2 = 0.1168$, hence we define the rescaling factor ξ as

$$\xi = \begin{cases} \frac{\Omega_{\text{LSP}} h^2}{0.1168} & \text{for } \Omega_{\text{LSP}} h^2 < 0.1168, \\ 1 & \text{for } \Omega_{\text{LSP}} h^2 \in [0.1168, 0.1208]. \end{cases} \tag{5.4}$$

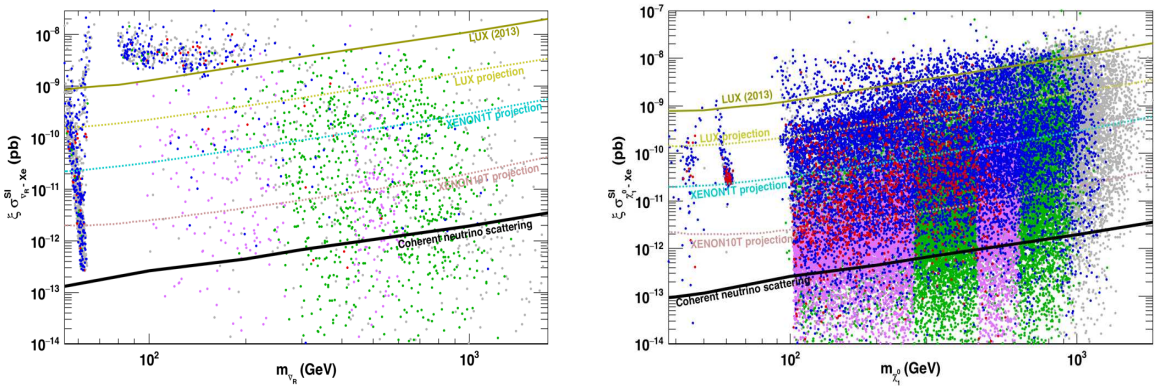

(a) (b)

Figure 5.44.: Rescaled direct detection cross section for (a) $\tilde{\nu}_{\tau R}$ or (b) $\tilde{\chi}^0_1$ LSP with the same colour code as in Figure 5.43. LUX exclusion (dark beige), projections from future large detectors as well as the neutrino background are also displayed.

Figure 5.44a shows that most of the RH sneutrino LSP points with a mass around 100 GeV are excluded by LUX. Those with a mass near 60 GeV escape the LUX upper limit but are generally within the reach of the future XENON1T detector. Other RH sneutrinos, which as we have argued before benefit from coannihilation and are therefore associated with a compressed spectrum, are safely below current exclusions. In some cases the predicted cross section is even below that of the coherent neutrino background and can therefore never be probed by direct detection. The scenarios with a neutralino LSP are hardly probed by LUX, see Figure 5.44b, only some of the mixed bino/higgsino points are excluded. The XENON1T will be able to probe many more points,[15] although a large fraction is beyond the reach of even a 10 ton detector, if not below the coherent neutrino background. These points are dominantly wino (hence labelled as long-lived) or singlino LSP. It is interesting to note that many of the points that are out of reach of direct detection detectors are associated with long-lived sparticles. To illustrate the complementarity with collider searches, we show in Figure 5.45a the points with a long-lived chargino which could be probed at LHC Run 2, that is the points in Figure 5.38 for which the cross section for chargino pair production is above 0.1 fb. Clearly, many of the points with charginos stable at the collider scale have

[15] First limits from the XENON1T experiment, recently presented in [49], already probe a large number of additional points, compare Figure 1.3.

a direct detection cross-section below the reach of XENON1T and even below the neutrino background. Note that the lowest value for the direct detection is about four orders of magnitude below the neutrino background (not shown in the Figure). It should also be emphasized that many points with a chargino lifetime that leads to displaced vertices (in blue and green in Figure 5.45a) are also beyond the reach of ton-scale detectors, hence we stress again the importance of probing these signatures at colliders. A quite different conclusion would be reached if we set the rescaling factor $\xi = 1$, that is assuming some regeneration mechanism for the neutralino LSP. As shown in Figure 5.45b, some of the mixed wino points are not allowed by LUX and a large fraction are within the reach of XENON1T. However even with these optimistic assumptions we find a few scenarios with a cross section below that of the coherent neutrino background that will never be tested.

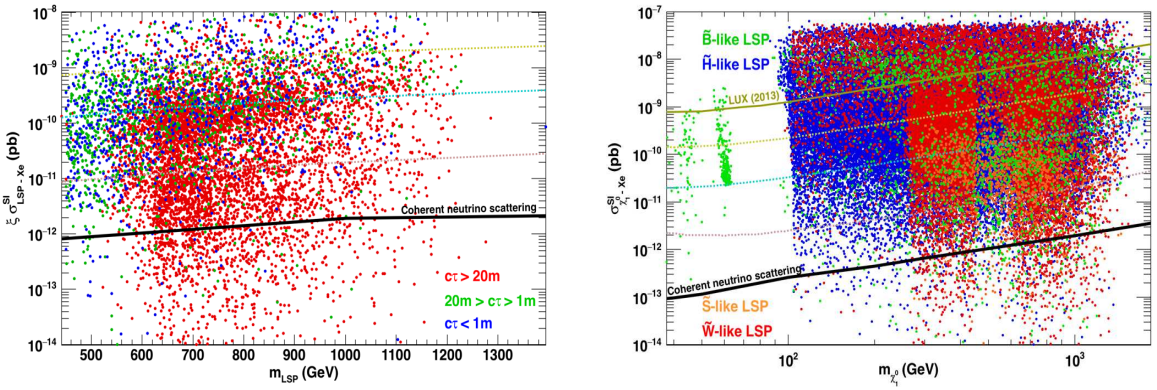

(a) (b)

Figure 5.45.: (a) Rescaled direct detection cross section with a $\tilde{\nu}_{\tau R}$ or a $\tilde{\chi}_1^0$ LSP for the same set of points as in Figure 5.38 and after applying the LUX bound. Chargino decay lengths $c\tau > 20$ m (red), between 20 m and 1 m (green) and below 1 m (blue) are represented. (b) Direct detection cross section without rescaling for $\tilde{B}$ (green), $\tilde{W}$ (red), $\tilde{H}$ (blue) and $\tilde{S}$ (orange) LSP, for all points satisfying collider and DM relic density constraints.

We also explore the possibility to probe DM with indirect detection, in particular using the limits obtained from observations of photons from dwarf spheroidal galaxies in the Milky Way by FermiLAT. For this we again rescale the cross section for points where the RH sneutrino or neutralino LSP cannot explain all the cosmologically measured dark matter. This means introducing a suppression by a factor ξ^2. We find that only a few points with a RH sneutrino LSP with a mass near 60 GeV are excluded by the FermiLAT limit from the $b\bar{b}$ channel, see Figure 5.46a. Some of these points were also excluded by LUX, however the predicted cross sections for most of the points are suppressed by at least two orders of magnitude as compared to current limits. For heavier LSP's the preferred annihilation channel is into W pairs. After applying the rescaling factor no exclusion can be obtained. Again, the predicted cross section is generally two orders of magnitude below the current limit, see Figure 5.46b. A quite different conclusion is reached if one does not apply the rescaling factor, then all winos with a mass below 500 GeV are excluded by FermiLAT as well as most of the higgsino LSP's with a mass below 200 GeV, see Figure 5.47. This is not a specific feature of the UMSSM and was already observed in the MSSM both for

photons [379, 380] and also antiprotons [381]. Note that the singlino LSP scenarios cannot be probed in this channel even without the rescaling.

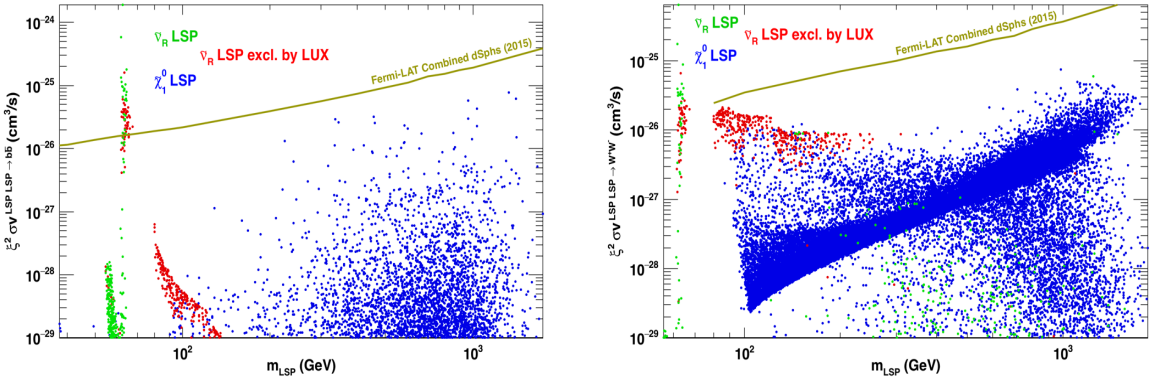

(a) (b)

Figure 5.46.: Rescaled annihilation cross section into (a) $b\bar{b}$ (b) W^+W^-, for $\tilde{\nu}_{\tau R}$ (green, red when excluded by LUX) or χ_1^0 (blue) LSP, for all points satisfying collider and DM relic density constraints. In both cases the FermiLAT limits are displayed.

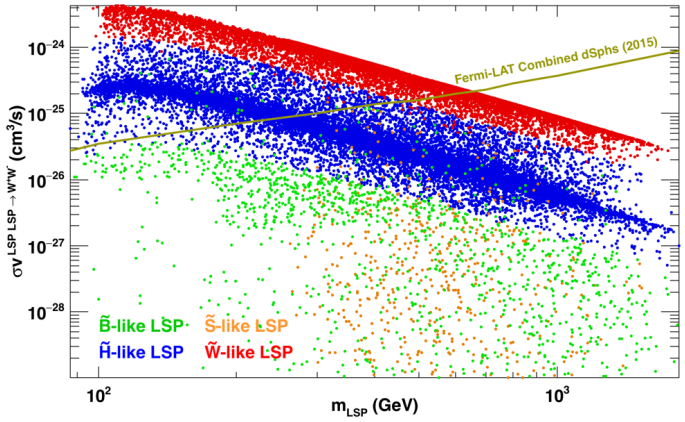

Figure 5.47.: Annihilation cross section into W^+W^- without rescaling for $\tilde{B}$ (green), $\tilde{W}$ (red), $\tilde{H}$ (blue) and $\tilde{S}$ (orange) LSP, for all points satisfying collider and DM relic density constraints.

5.3.7. Conclusions

We have reexamined the viability of the UMSSM model to describe physics beyond the standard model and dark matter after the results of the LHC Run 1 on the Higgs, on flavour observables and on new particle searches. We found compatibility with all latest experimental results for large regions of the parameter space for both a neutralino or RH sneutrino DM and explored potential future probes of the model at Run 2 of the LHC and in direct detection. Imposing only the upper bound on the relic density favors either sneutrino DM near

60 GeV or neutralino DM with a large wino and/or higgsino component - hence associated with either a long-lived chargino or a chargino which decays primarily into virtual W and the LSP. The latter feature is common also to the MSSM and has important consequences both for squark and gluino searches as well as for electroweakino searches at the LHC, since the chargino will either have a missing energy signature or yield soft decay products.

The most crucial test of the model in Run 2 of the LHC is the search for a Z' gauge boson, the most prominent characteristic of the model and the limits have already been extended by early results [329]. Another landmark of the model is the possibility of a RH sneutrino LSP. The collider signatures often resemble those of the MSSM but it remains to be seen whether the additional neutrino that appears in the decays affects the kinematics of the process, for example this is the case for the dijet + $E_T^{\rm miss}$ signature from squark production when the squark can only decay to the sneutrino LSP. We have also found a W+ $E_T^{\rm miss}$ channel that could lead to a single energetic lepton from chargino/neutralino production. Due to the presence of the sneutrino LSP, the W can be energetic enough to lead to visible decays even when the chargino and lightest neutralino are nearly degenerate, thus this is quite a distinct signature from the MSSM. Another striking feature of the sneutrino LSP scenario is the possibility to find long lived squarks and gluinos.

The main characteristic of the neutralino LSP scenarios is associated with the nature of the LSP, we found usually a dominantly wino or higgsino LSP. This implies that the chargino is often nearly degenerate with the LSP hence leads to invisible decay products or that the chargino is stable at the collider scale, hence the importance of the searches for long-lived/stable particles. This is not a unique feature of the model as long-lived charginos can also be found in the MSSM. We also found a number of topologies that could not be constrained by current SMS results, including 2, 3 or 4 jets + $E_T^{\rm miss}$ topologies with either light jets or third generation quarks. The main reason is that these topologies are associated with asymmetric decays, that is each of the pair produced particles has a different decay chain whereas most SMS results assume symmetric decays. The most striking example is a bt + $E_T^{\rm miss}$ topology that comes from stop pair production where one of the stop decays into a quark and the LSP and the other to a quark and an invisible chargino [382]. Note however that a recent result by CMS [245] gives limits on stop pair production for this topology independently of the relative branching fractions of each stop. It can be expected that this result will exclude most points with the bt + $E_T^{\rm miss}$ missing topology in scenarios where the neutralino is lighter than $\approx$ 200 GeV and the stop mass is below $\approx$ 700 GeV. Other examples include decays of squarks through a heavier neutralino. Furthermore we have stressed that there is a nice complementarity between the searches for stable charginos at colliders and the direct searches for DM. A significant number of the points which are below the reach of ton-scale detectors have a chargino which is either collider stable or lead to displaced vertices. Similarly the singlino LSP, which occurs for a small fraction of the points, can hardly be probed by DM direct detection.

Another feature of the UMSM is the split u-type/d-type RH squark masses which are found for specific choices of the $U(1)'$ charge. Despite conventional decays, these squarks are harder to detect. They do not benefit from contributions of all flavours of squarks and therefore the production cross section is lower.

As concerns the Higgs sector, the model predicts mostly a SM-like Higgs, although deviations up to 25% can be observed in the signal-strengths for either $\gamma\gamma$ or fermionic final states. Moreover an invisible branching fraction of the Higgs up to 25% can be found. Over some of the parameter space the second Higgs lies below the TeV scale and can be probed at LHC13TeV in the standard $\tau^+\tau^-$ mode relevant at large $\tan\beta$ but also in the $t\bar{t}$ or hh mode

at small values of $\tan\beta$.[16] It remains to be seen to which extent the SUSY decay modes can be exploited. Finally we should stress that the lowest values of $\tan\beta$ lead to quite enhanced rates for ΔM_s. Refining the constraints on the CKM elements which is one of the important source of uncertainties implies that this observable would strongly constrain the low $\tan\beta$ scenarios.

[16] In fact first LHC13TeV searches have already been presented, see for example [383–385].

CHAPTER

SIX

SIMPLIFIED MODELS FOR DARK MATTER SEARCHES AT THE LHC

Up to now we have considered SUSY models, and simplified models that were based on an MSSM description. LHC searches for SUSY partners are well motivated both by the naturalness problem and in the context of the WIMP paradigm. However, naturalness considerations are under increasing tension given the null observations at the LHC. Therefore collider searches testing more minimal WIMP scenarios, aiming only at describing the DM content of the universe, have recently gained attention. As discussed in Section 2.2, WIMP signals may be observed in collider experiments when the DM particles are produced in association with additional SM particles, for example an ISR jet or photon (mono-X searches). Note that there are fundamental differences between the interpretation of such mono-X searches and SUSY-like searches. While in SUSY searches it is often a good approximation to neglect the detailed model description and to describe the production only by an overall rate (SMS assumption, see Section 3.1), the same does not hold for the interpretation of mono-X searches. Due to the dependence on ISR as the main visible object allowing signal event selection, the interpretation depends crucially on the detailed production processes.

As a consequence the interpretation of DM searches at the LHC typically relies on a Lagrangian description of the DM interactions with SM particles. The minimal description, similar to the Fermi-interaction introduced in Section 1.1, describes the interaction in terms of effective operators, suppressed by a cut-off scale Λ. While this is a highly predictive framework (there are only two free parameters), its validity in the interpretation of LHC searches is limited, as will be discussed in Section 6.1.

Given the limited validity of the minimal effective field theory (EFT) description, a DM simplified model approach has been developed, with an explicit light mediator particle facilitating the interactions between DM and SM particles. A renormalizable Lagrangian, consistent with the SM symmetries, then describes the mediator interactions with SM and DM particles. Standard s-channel mediator simplified models for DM searches are classified by the spin and coupling of the mediator, into (pseudo)scalar and (axial)vector mediator models. The nature of the DM candidate is less important for the interpretation of collider searches, in particular when studying scenarios where the narrow width approximation holds. We will give a short review of these scenarios in Section 6.2.

Spin-2 s-channel mediators are an interesting alternative to the standard spin-0 and spin-1 mediator scenarios, especially because gravity mediators are naturally expected to couple to DM as well as SM particles. We have recently studied such scenarios in [386], considering a spin-2 mediator coupling to scalar, fermionic or vector DM. The results of this work, showing

how these scenarios are constrained by LHC DM and resonance searches, are presented in Section 6.3. Note that in contrast to the standard scalar and vector mediator models, where typically only couplings to quarks and DM particles are taken into account, we consider a universal coupling of the spin-2 mediator to all SM particles.

Finally we note that t-channel mediator models generally give SUSY like scenarios (e.g. mediator pair production that resembles squark pair production [387]). We will however not persue this in this thesis.

6.1. Interpretation of Dark Matter Searches

The most minimal interpretation of mono-X searches adds only the DM candidate to the SM description. Similar to the Fermi four-fermion contact interaction we can describe the interaction in terms of an EFT. Each operator of mass dimension d is then suppressed by a scale Λ^{d-4}, in the same way as the Fermi-interaction had an m_W^2 suppression, see Eq. (1.1), and typically only the lowest dimension operators are considered. Assuming that the coefficient of each operator ("Wilson coefficient") is of order 1, this approach allows an interpretation of the searches in a 2-dimensional parameter space (Λ, m_{DM}). However, given that the LHC is operating at high energies as compared to the typically tested suppression scales, the EFT approximation might not be valid, and it may be necessary to resolve the contact interactions.

Indeed the EFT validity condition $Q < \Lambda$, i.e. the momentum transfer Q should be smaller than the cut-off scale Λ, holds only for a fraction of events (depending on the operator under consideration) in the parameter space regions probed by the LHC [388]. Moreover, these low Λ regions are also the ones that predict the observed relic abundance, while higher Λ regions, where an EFT description for the interpretation of LHC searches becomes valid, generally result in DM overabundance [389]. The application of EFT limits to scenarios with light mediators might either under-estimate the true limit (when the process is resonantly enhanced) or over-estimate it. The latter occurs because the missing energy distribution in light mediator scenarios is generally softer than predicted by the EFT description [390].

We conclude that mono-X searches should not only be tuned to and interpreted in the context of the EFT description, but a more complete picture should also be considered, i.e. the DM simplified model description with a light mediator particle coupling DM and SM particles, as described in the next Section.

6.2. Overview of Dark Matter Simplified Models

A systematic approach to simplified model interpretations of LHC DM searches was first presented in [391], detailed recommandations were then specified in [392]. Here we introduce briefly the standard s-channel mediator simplified models considered by the ATLAS and CMS experiments, i.e. scalar and vector mediators coupling to a fermionic DM candidate. Recent results for these scenarios are presented in Section 6.2.1.

Scalar mediator

A scalar gauge singlet can couple to to fermionic or scalar DM particles. We can consider either a real or complex scalar. Typically either a real scalar ϕ or a light pseudoscalar a (assuming a decoupled associated scalar) is considered in the simplified model approach. In

a complete model the mediator can mix with the SM Higgs and have interactions with Higgs and electroweak gauge bosons. The details of these interactions are model-dependent, and generally only effective couplings to fermions are studied. For the example of a fermionic DM candidate χ we can describe the relevant interactions by the following Lagrangians:

$$\mathcal{L}_\phi \supset -\phi \sum_{f,i} g_f \frac{y_i^f}{\sqrt{2}} \bar{f}_i f_i - g_{DM} \phi \bar{\chi} \chi \tag{6.1}$$

$$\mathcal{L}_a \supset -ia \sum_{f,i} g_f \frac{y_i^f}{\sqrt{2}} \bar{f}_i \gamma_5 f_i - i g_{DM} a \bar{\chi} \gamma_5 \chi \tag{6.2}$$

where $f = u, d, l$ refers to fermion species, i runs over the 3 SM families and the couplings are parametrized by $g_x, x = f, \chi$.

Note that the couplings to SM quarks are weighted by the Yukawa couplings y_i^f to comply with MFV. An interesting consequence is that these scenarios are top-philic, as discussed in [393], where the phenomenology of the scalar mediator scenario was studied in detail. The pseudoscalar mediator scenario was recently studies in [394].

Note further that the description is only invariant under $SU(3) \times U(1)_{em}$ and not the full SM gauge group. Compelling gauge invariant completions of the scalar mediator scenarios can be obtained when considering models with two Higgs doublets (2HDM) [395, 396].

Vector mediator

A vector mediator arises naturally when extending the SM gauge group with an additional $U(1)'$ that is spontaneously broken, thus allowing mass terms for the vector mediator. The new vector boson V couples to the SM fermions and a fermionic DM χ as:

$$\mathcal{L}_V \supset \sum_f V_\mu \bar{f} \gamma^\mu (g_f^V - g_f^A \gamma_5) f + V_\mu \bar{\chi} \gamma^\mu (g_\chi^V - g_\chi^A \gamma_5) \chi \tag{6.3}$$

where now $f = q, l, \nu$ and MFV is ensured when the couplings g_f are flavor independent. In practice the purely vector scenario ($g^A = 0$) or the purely axialvector scenario ($g^V = 0$) are studied for the interpretation of collider searches. Note that the coupling structure is in general dictated by the assumed mass generation mechanism, see [397]. Recently theoretical constraints such as anomally cancellation implications, were studied in [398] and found to have important consequences, determining e.g. the minimum number of dark sector fermions, and relations between the $U(1)'$ charges of the SM fields.

6.2.1. LHC Search Results

The scalar and vector s-channel mediator simplified models have been adopted by the ATLAS and CMS experiments, and are the standard interpretation of mono-jet and mono-photon searches. Typically a minimal scenario is considered with a universal coupling g_q to all quarks, and no coupling to leptons. Note however that many consistent models with vector mediators predict a non-vanishing coupling to leptons as well [398, 399]. The LHC DM Working Group has therefore included the leptonic coupling g_l in their latest recommandation [400]. An important consequence is that the coupling to neutrinos provides an additional invisible decay channel (see also results for the spin-2 mediator with universal coupling discussed in the next Section).

The minimal setup (neglecting leptonic couplings) has four free parameters, the mediator and DM mass, and the mediator coupling to DM and SM particles. Results are typically presented in the mediator vs. DM mass plane, for fixed values of the couplings, and constraints from dijet resonance searches can be presented together with missing energy search results. Figure 6.1 shows such a summary of ATLAS search limits for the example of an axial-vector mediator coupling to a fermionic DM candidate, taken from [401]. Dijet resonance searches give strong constraints, with only small dependence on the DM mass, while DM searches can constrain only the on-shell region and are important mainly in the low mass region.

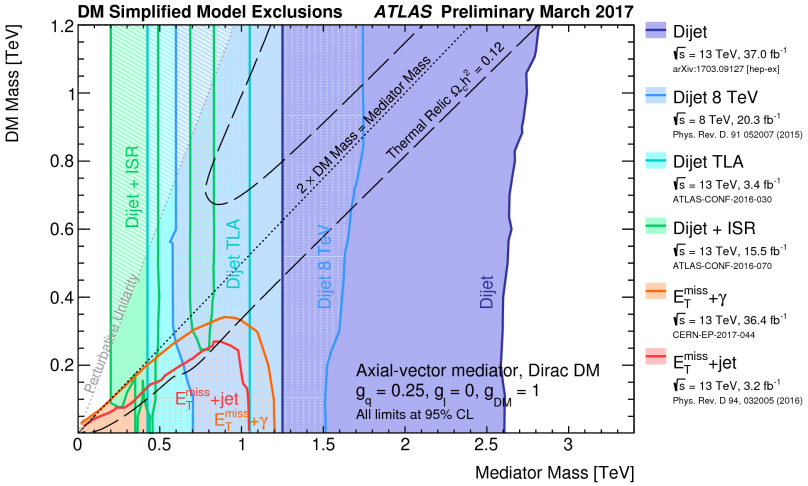

Figure 6.1.: Summary of ATLAS mass limits in the context of an axial-vector mediator coupling to Dirac DM.

Moreover, the cross section upper limits from the missing energy searches (in the mediator vs. DM mass plane) can be rescaled to obtain constraints on the same signature, but varying the coupling values (i.e. when changing the rate but not the event kinematics). Figure 6.2 shows the results for all four DM simplified models introduced above, obtained in the CMS mono-jet and mono-V search [402]. The color code gives the 95% CL limit in terms of σ_{UL}/σ_{th} for the indicated values of the couplings, and can be used to rescale the limits.

6.3. Simplified Dark Matter Models with a Spin-2 Mediator at the LHC

We now consider simplified DM models where a DM candidate couples to the SM particles via an s-channel spin-2 mediator, and study constraints on the model parameter space from searches in final states with and without missing energy in the current LHC data. This work follows the DMSIMP framework [403–405], which provides the DM model files for event generators such as MADGRAPH5 [175] as well as for DM tools such as `micrOMEGAs` [52, 205, 406] and MADDM [45, 54]. The same framework was used previously to study the cases of s-channel spin-1 and spin-0 mediators.

We note that, to keep the analysis of the LHC constraints fully general, we do not impose any astrophysical constraints like relic density or (in)direct detection limits on the DM candidate, as these partly depend on astrophysical assumptions. Moreover, in a full model, the DM may couple to other new particles that are irrelevant for the collider phenomenology

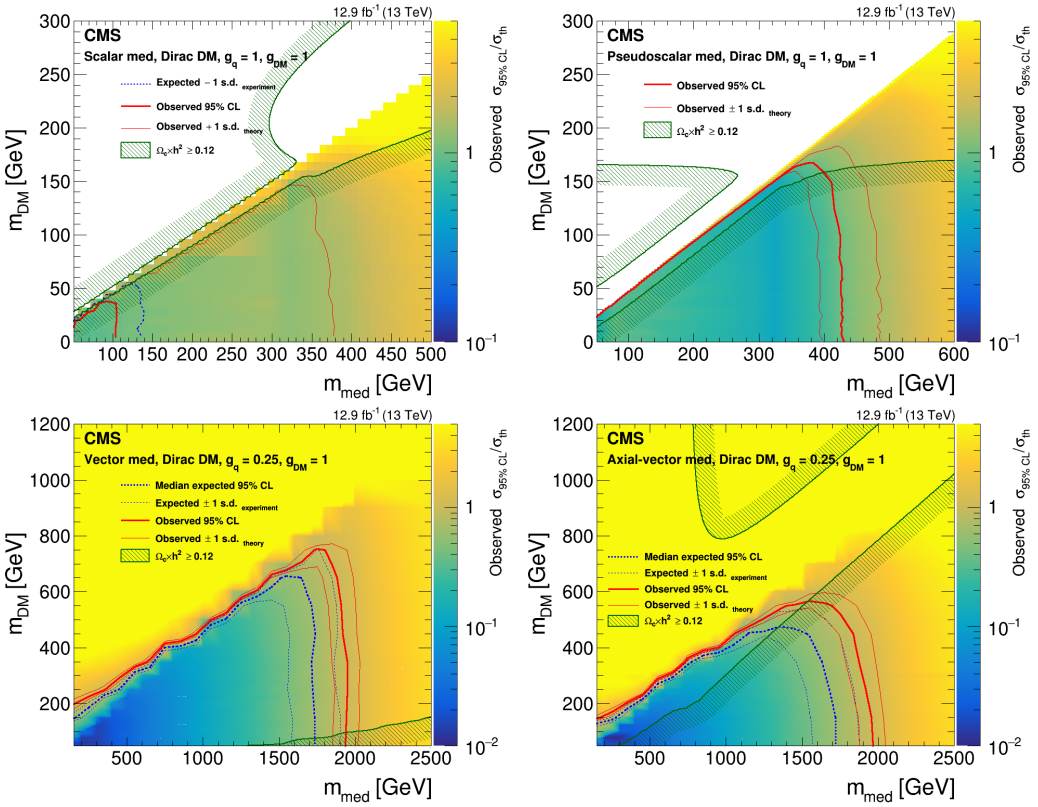

Figure 6.2.: Upper limits on DM simplified models with scalar (top left), pseudoscalar (top right), vector (bottom left) and pseudo-vector (bottom right) mediator coupling to Dirac DM, obtained in the CMS mono-jet and mono-V search [402].

discussed here. We refer readers to [115, 407] for the astrophysical constraints, and to [408] for a discussion of spectral features in indirect detection.

The simplified model is presented in Section 6.3.1, and the production and decays of the spin-2 mediator in Section 6.3.2. The re-interpretation of the LHC results is discussed in Section 6.3.3. Section 6.3.4 contains a summary and conclusions.

6.3.1. Model

Gravity-mediated DM was proposed in [115, 407], where the dark sector communicates with the SM sector through a new spin-0 particle (radion) and spin-2 particles (Kaluza–Klein (KK) gravitons) in warped extra-dimension models as well as in the dual composite picture (see also Section 1.4.2).

In this work, following the approach of simplified DM models, we consider DM particles which interact with the SM particles via an s-channel spin-2 mediator. The interaction Lagrangian of a spin-2 mediator (Y_2) with DM (X) is given by [115]

$$\mathcal{L}_X^{Y_2} = -\frac{1}{\Lambda} g_X^T \, T_{\mu\nu}^X Y_2^{\mu\nu} \,, \tag{6.4}$$

where Λ is the scale parameter of the theory, g_X^T is the coupling parameter, and $T_{\mu\nu}^X$ is the energy–momentum tensor of a DM field. Here, we consider three types of DM independently; a real scalar (X_R), a Dirac fermion (X_D), and a vector (X_V). The interaction with

SM particles is obtained by

$$\mathcal{L}_{\mathrm{SM}}^{Y_2} = -\frac{1}{\Lambda}\sum_i g_i^T\, T^i_{\mu\nu} Y_2^{\mu\nu}\,, \tag{6.5}$$

where i denotes each SM field, i.e. the Higgs doublet (H), quarks (q), leptons (l), and $SU(3)_C$, $SU(2)_L$ and $U(1)_Y$ gauge bosons (g, W, B). Following [409, 410] we introduce the phenomenological coupling parameters

$$g_i^T = \{g_H^T,\, g_q^T,\, g_l^T,\, g_g^T,\, g_W^T,\, g_B^T\} \tag{6.6}$$

without assuming any UV model.[1] The energy–momentum tensors of the DM are

$$\begin{aligned} T^{X_R}_{\mu\nu} &= -\frac{1}{2} g_{\mu\nu}(\partial_\rho X_R \partial^\rho X_R - m_X^2 X_R^2) \\ &\quad + \partial_\mu X_R \partial_\nu X_R\,, \end{aligned} \tag{6.7}$$

$$\begin{aligned} T^{X_D}_{\mu\nu} &= -g_{\mu\nu}(\overline{X}_D i\gamma_\rho \partial^\rho X_D - m_X \overline{X}_D X_D) \\ &\quad + \frac{1}{2} g_{\mu\nu}\partial_\rho(\overline{X}_D i\gamma^\rho X_D) \\ &\quad + \frac{1}{2}\overline{X}_D i(\gamma_\mu\partial_\nu + \gamma_\nu\partial_\mu) X_D \\ &\quad - \frac{1}{4}\partial_\mu(\overline{X}_D i\gamma_\nu X_D) - \frac{1}{4}\partial_\nu(\overline{X}_D i\gamma_\mu X_D)\,, \end{aligned} \tag{6.8}$$

$$\begin{aligned} T^{X_V}_{\mu\nu} &= -g_{\mu\nu}(-\frac{1}{4} F_{\rho\sigma}F^{\rho\sigma} + \frac{m_X^2}{2} X_{V\rho} X_V^\rho) \\ &\quad + F_{\mu\rho}F^\rho_\nu + m_X^2 X_{V\mu} X_{V\nu}\,, \end{aligned} \tag{6.9}$$

where $F_{\mu\nu}$ is the field strength tensor. Those of the SM fields are similar; see e.g. [411] for the explicit formulae.

Complying with the simplified model idea, it is instructive to consider universal couplings between the spin-2 mediator and the SM particles:

$$g_{\mathrm{SM}} \equiv g_H^T = g_q^T = g_l^T = g_g^T = g_W^T = g_B^T\,. \tag{6.10}$$

With this simplification, the model has only four independent parameters, two masses and two couplings:

$$\{m_X,\, m_Y,\, g_X/\Lambda,\, g_{\mathrm{SM}}/\Lambda\}\,, \tag{6.11}$$

where we dropped the superscript T for simplicity. Such a universal coupling to SM particles is realised, e.g., in the original Randall–Sundrum (RS) model of localised gravity [113]. The parameters are related as

$$m_Y/\Lambda = x_1\, k/\overline{M}_{\mathrm{Pl}}\,, \tag{6.12}$$

where $x_1 = 3.83$ is the first root of the Bessel function of the first kind, k is the curvature of the warped extra dimension, and $\overline{M}_{\mathrm{Pl}} = 2.4 \times 10^{18}$ GeV is the reduced four-dimensional Planck scale. On the other hand, in the so-called bulk RS model [412, 413], where the SM

[1] One may also assign independent coupling parameters for each flavour, especially for heavy flavours [411].

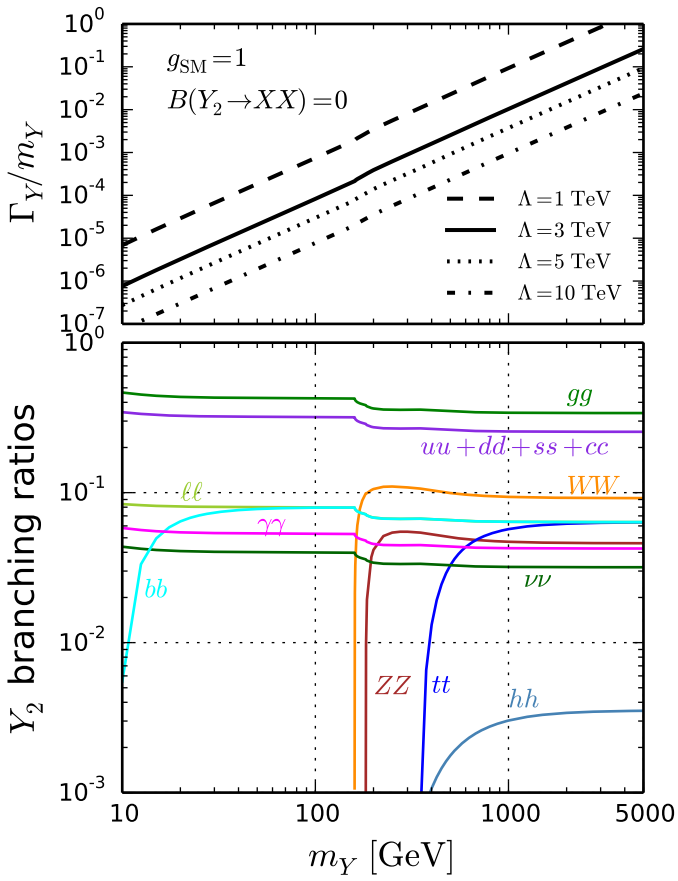

Figure 6.3.: Ratio of the mediator total width to its mass, Γ_Y/m_Y, (upper panel) and mediator branching ratios (lower panel) as a function of the mediator mass m_Y for $g_{\rm SM}=1$, where we assume a negligible branching ratio to the dark sector.

particles also propagate in the extra dimension, g_i^T can take different values depending on the setup.

In [411], the SM sector of the above model was implemented in FEYNRULES/NLOCT [169, 414] (based on [415–417]), and the Y_2 production and decay rates at NLO QCD accuracy were presented. In this work, we include the three DM species (X_R, X_D, X_V) with the corresponding interactions, and add the model into the DMSIMP framework [418] as the simplified DM model with a spin-2 mediator.

6.3.2. Phenomenology at the LHC

Decay of the Spin-2 Mediator

Regarding LHC phenomenology, let us begin by discussing the spin-2 mediator decays. The partial widths for the decays into a pair of spin-0 ($S=X_R,h$), spin-1/2 ($F=X_D,q,l$)

m_Y	branching ratios [%]							
[GeV]	jj	WW	tt	ZZ	$\gamma\gamma$	$\nu\nu$	ee	hh
100	86.5	0	0	0	5.3	4.0	2.7	0
500	79.1	9.9	3.3	5.0	4.4	3.3	2.2	0.2
1000	78.5	9.4	5.7	4.7	4.3	3.2	2.1	0.3

Table 6.1.: Branching ratios of the spin-2 mediator for $g_{\rm SM} = 1$ and $B(Y_2 \to XX) = 0$; jj includes gluons and five flavours of quarks, and $\nu\nu$ includes three flavours of neutrinos.

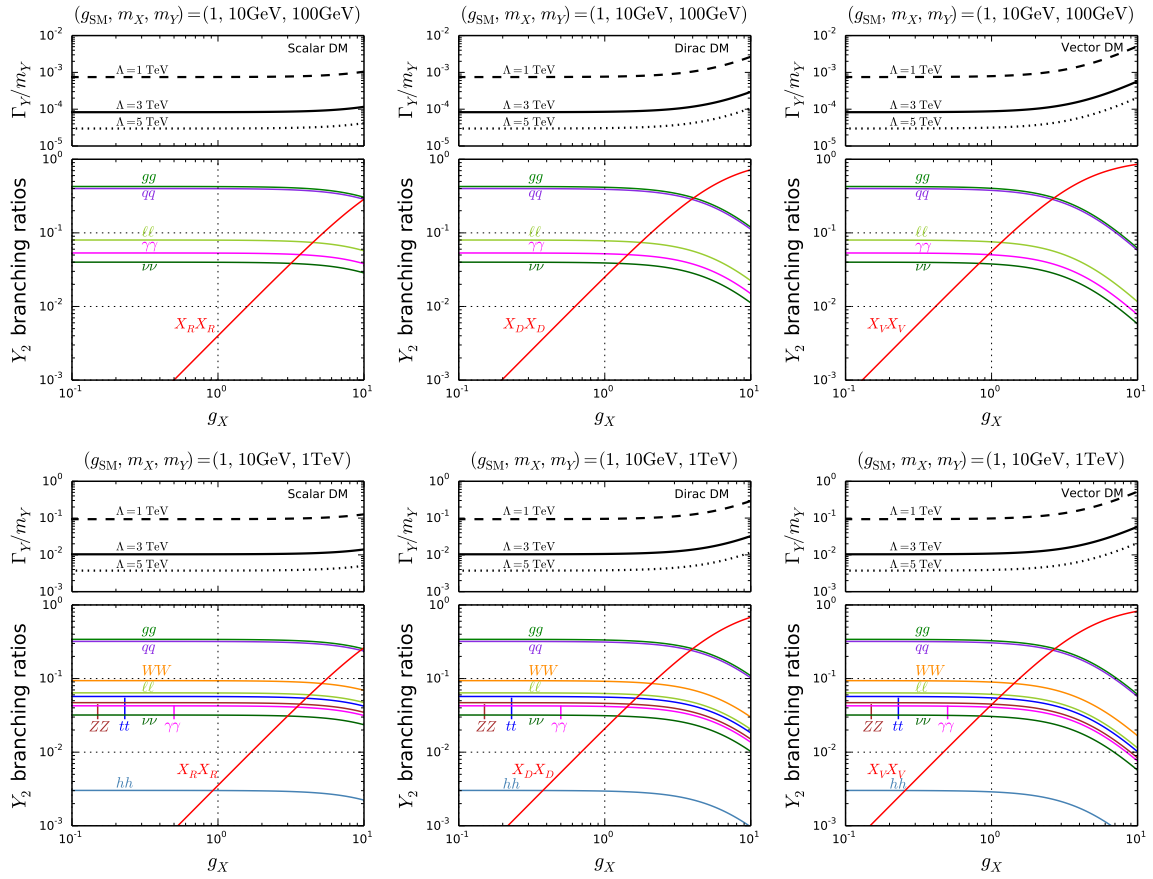

Figure 6.4.: Ratio of the mediator total width to its mass and mediator branching ratios as a function of the DM coupling g_X, for mediator masses of 100 GeV (top row) and 1 TeV (bottom row). The left, middle and right columns are for scalar, Dirac and vector DM, respectively. We take $g_{\rm SM} = 1$ and fix the DM mass to 10 GeV.

and spin-1 ($V = X_V, g, \gamma, Z, W$) DM or SM particles are given by

$$\Gamma_S = \frac{g_S^2 m_Y^3}{960\pi\Lambda^2}\,\beta_S^5\,, \tag{6.13}$$

$$\Gamma_F = \frac{g_F^2 N_\nu N_C^F m_Y^3}{160\pi\Lambda^2}\,\beta_F^3\,(1+\frac{8}{3}r_F)\,, \tag{6.14}$$

$$\Gamma_V = \frac{g_V^2 N_s N_C^V m_Y^3}{40\pi\Lambda^2}\,\beta_V\,f(r_V)\,, \tag{6.15}$$

where $\beta_i = \sqrt{1-4r_i}$ with $r_i = m_i^2/m_Y^2$, $g_\gamma = g_B\cos^2\theta_W + g_W\sin^2\theta_W$ and $g_Z = g_B\sin^2\theta_W + g_W\cos^2\theta_W$ with the weak-mixing angle θ_W, and $f(r_V) = 1 + \frac{1}{12}\kappa_H^2 - r_V(3 - \frac{20}{3}\kappa_H - \kappa_H^2) + r_V^2(6 - \frac{20}{3}\kappa_H + \frac{14}{3}\kappa_H^2)$ with $\kappa_H = g_H/g_V$. For gluons and photons, $\kappa_H = 0$ in $f(r_V)$, while $\kappa_H = 1$ for vector DM. The factors $N_\nu = 1/2$ for neutrinos and $N_s = 1/2$ for two identical particles, and are unity otherwise; $N_C^{F,V}$ is the number of colours. We note that $B(Y_2 \to Z\gamma) = 0$ for $g_W = g_B$ as the decay rate is proportional to $g_{Z\gamma}^2 = [(g_W - g_B)\cos\theta_W\sin\theta_W]^2$. We see that, due to the different overall prefactors, the partial widths become larger in order of scalar, fermion, vector DM. Moreover, the different powers (5, 3, 1) of the velocity factor β_i indicate that the decay proceeds mainly via a D, P, and S wave for the scalar, fermion, and vector case, respectively.

Figure 6.3 shows the Y_2 total width scaled by the mass, Γ_Y/m_Y, and the decay branching ratios for the case that only decays into SM particles are allowed. MADWIDTH [419] provides the partial decay rates numerically for each parameter point. In Table 6.1 we provide the explicit values for a few representative mass points. We see that, for a universal coupling $g_{\rm SM}$, decays into gluons and light quarks, leading to a dijet signature, are completely dominant ($\gtrsim 80\%$ depending on m_Y). The diphoton channel has 4–5% branching ratio; other diboson channels (WW and ZZ) as well as $t\bar{t}$ are important as well when kinematically allowed. Finally, it is important to note that decays into neutrinos have 3–4% branching ratio, leading to missing energy signatures independent of decays to DM.[2] The width is proportional to m_Y^3, and from the upper panel in Figure 6.3 we see that for $g_{\rm SM}/\Lambda \lesssim (3\ {\rm TeV})^{-1}$, the resonance is always very narrow ($\Gamma_Y/m_Y < 1\%$) up to $m_Y \sim 1$ TeV. Note here, that Λ is simply a scale parameter, not a physical cut-off of the theory.

When decays into DM are allowed, their relative importance depends on g_X and the type of DM (scalar, Dirac or vector) as illustrated in Figure 6.4; see also Eqs. (6.13)–(6.15). Two mass scales are considered: $m_Y = 100$ GeV and 1 TeV, with $m_X = 10$ GeV and $g_{\rm SM} = 1$.[3] We see that decays into DM can be important and even dominant, but the resonance remains narrow for any choice of $\Lambda \gtrsim 3$ TeV for $m_Y \lesssim 1$ TeV. Another important observation is that for scalar DM (X_R), for $g_X \sim g_{\rm SM}$ the decay into $Y_2 \to X_R X_R$ is practically irrelevant; one needs $g_X/g_{\rm SM} \approx 3$ for the decay into DM to exceed the one into neutrinos, and $g_X/g_{\rm SM} \approx 5$–6 to reach the 10% level. For Dirac (X_D) and vector (X_V) DM, the decays into DM and into neutrinos are of comparable magnitude at $g_X \sim g_{\rm SM}$, both contributing to missing-energy signatures. For $g_X/g_{\rm SM} = 2$, the branching ratio of $Y_2 \to X_D X_D$ ($X_V X_V$) attains about 10% (20%). These differences depending on the type of DM will be important later for the collider limits.

[2] These decay branching ratios were already presented in [420] for the case of the RS graviton. We repeat them here for the sake of completeness. Our numbers agree with [420] apart from a factor 1/2 for decays into neutrinos.

[3] As can be deduced from Figure 6.3, above the WW threshold up to high masses the picture does not change much apart from the $t\bar{t}$ and/or hh channels being open or not.

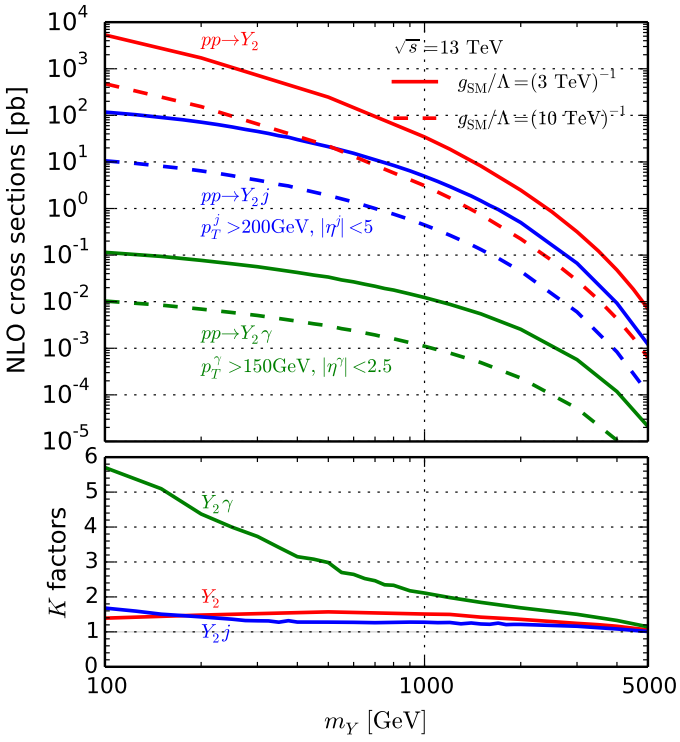

Figure 6.5.: Total cross sections at NLO accuracy for mediator productions at the 13 TeV LHC as a function of the mediator mass. Two choices of g_{SM}/Λ are considered: $(3\ \mathrm{TeV})^{-1}$ shown as solid lines and $(10\ \mathrm{TeV})^{-1}$ shown as dashed lines. For $Y_2 + \mathrm{jet}$ cuts of $p_T^j > 200$ GeV and $|\eta^j| < 5$ are imposed, and for $Y_2 + \mathrm{photon}$ cuts of $p_T^\gamma > 150$ GeV and $|\eta^\gamma| < 2.5$. K factors are also shown in the lower panel as a reference.

Production of the Spin-2 Mediator

Turning to the production modes, the potentially interesting channels are inclusive Y_2 production ($pp \to Y_2$), as well as the production with an extra hard tagging jet ($pp \to Y_2\, j$) or an electroweak boson (e.g. $pp \to Y_2\, \gamma$). With the Y_2 decaying into SM particles, the former gives resonant peak signatures (without missing energy). On the other hand, the latter two give the typical monojet or monophoton signatures when the mediator decays invisibly. Moreover, the latter two play a role in the low-mass resonance search in dijet events with ISR as seen later.

The Y_2 production cross sections at NLO QCD accuracy for pp collisions at 13 TeV are depicted in Figure 6.5 as a function of the mediator mass.We employ MadGraph5 [175] to calculate the cross sections and generate events with the LO/NLO NNPDF2.3 [421]. The factorisation and renormalisation scales are taken at the sum of the transverse masses of the final states as a dynamical scale choice. In our simplified model, the cross sections depend solely on g_{SM}/Λ and scale with $(g_{\mathrm{SM}}/\Lambda)^2$. The dashed lines showing $g_{\mathrm{SM}}/\Lambda = (10\ \mathrm{TeV})^{-1}$ are therefore an order of magnitude below the corresponding solid lines for $g_{\mathrm{SM}}/\Lambda = (3\ \mathrm{TeV})^{-1}$. Also noteworthy is the fact that $pp \to Y_2$ is mostly gluon-initiated for the low-mass case [420]; 97%, 83%, and 28% of the LO total rate for $m_Y = 100$ GeV, 1 TeV, and 5 TeV, respectively, stem from gg fusion. Since the radiation of an initial-state photon (Z/W) can only occur in the quark-initiated process, $Y_2 + \mathrm{photon}$ (Z/W) production is very much suppressed as compared to $Y_2 + \mathrm{jet}$ production. This is also the reason that the

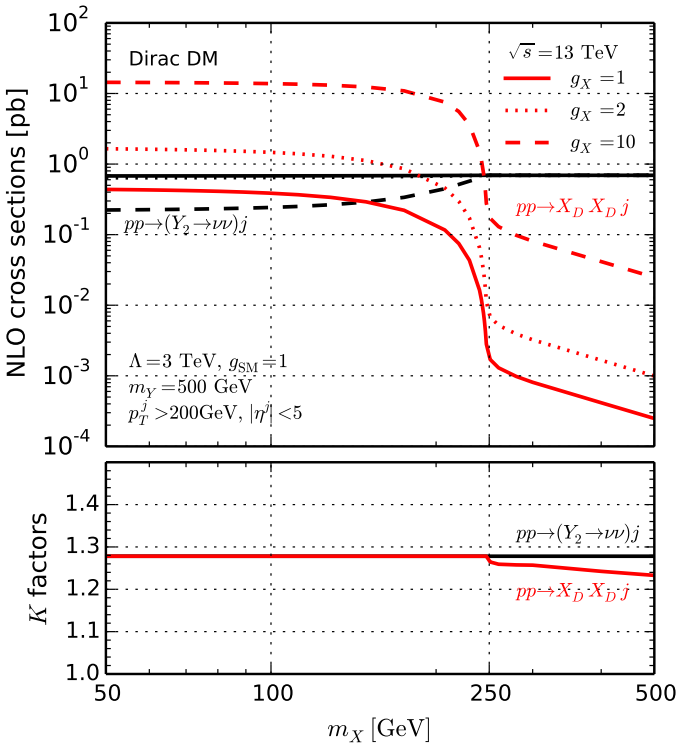

Figure 6.6.: Total cross sections at NLO accuracy for monojet final states with $g_X = 1$ (solid), 2 (dotted) and 10 (dashed) for $m_Y = 500$ GeV as a function of the DM mass, where we take $\Lambda = 3$ TeV and $g_{\rm SM} = 1$ and impose $p_T^j > 200$ GeV and $|\eta^j| < 5$. The red lines are for the (Dirac) DM channel, the black lines for the neutrino. K factors are also shown in the lower panel as a reference.

process has a huge K factor especially in the low-mass region [411].[4]

In the context of DM searches, the monojet signature is expected to give important constraints on the model. The fiducial cross sections for $pp \to Y_2 j$ with $p_T^j > 200$ GeV and $|\eta^j| < 5$ are shown in Figure 6.5, where one can estimate the monojet cross section by taking into account the Y_2 branching ratio into DM particles (and/or neutrinos) when $m_Y > 2m_X$. In Figure 6.6 we also plot the fiducial cross sections for $pp \to j + E_T^{\rm miss}$ as a function of the DM mass, separating the contributions from neutrinos (black lines) and DM (red lines) produced through the spin-2 mediator. For definiteness, we take $m_Y = 500$ GeV, $\Lambda = 3$ TeV, $g_{\rm SM} = 1$ and compare $g_X = 1$, 2 and 10 for Dirac DM. As already seen in Figure 6.4, their relative importance depends on g_X. For $m_Y < 2m_X$, a pair of DM is produced via the off-shell mediator and the cross section is strongly suppressed. Therefore, the neutrino contribution always dominates the monojet signature for the $m_Y < 2m_X$ region even if $g_X/g_{\rm SM} = 10$. For the other DM types, scalar and vector, the picture is similar, but the relative importance to the neutrino channel is different; see Figure 6.4. This is one of the characteristic features of the spin-2 mediator DM model with universal couplings, as compared to the s-channel spin-1 and spin-0 models, whose mediators do not couple to charged leptons and neutrinos in the minimal setup [422].

6.3.3. Constraints from current LHC Data

Searches with missing energy

The ATLAS and CMS experiments have been searching for new physics in a large variety of final states. As mentioned above, in the context of DM searches, the monojet signature is regarded as particularly interesting. In practice, at 13 TeV, the monojet analyses require one hard jet recoiling against $E_T^{\rm miss}$, but allow for additional jets from QCD radiation. Therefore one can expect that multijet+$E_T^{\rm miss}$ searches are also relevant [423, 424].

To work out the current constraints on the spin-2 mediator DM model from these searches, we consider the following early Run 2 analyses:

- ATLAS monojet with 3.2 fb^{-1} [425],
- ATLAS 2–6 jets + $E_T^{\rm miss}$ with 3.2 fb^{-1} [426].

In the monojet analysis [425], a simplified DM model with an s-channel spin-1 mediator is considered. Events are required to have at least one hard jet with $p_T > 250$ GeV and $|\eta| < 2.4$, and a maximum of four jets with $p_T > 30$ GeV and $|\eta| < 2.8$ are allowed. Several inclusive and exclusive signal regions (SRs) are considered with increasing $E_T^{\rm miss}$ requirements from 250 GeV to 700 GeV. The multijet+$E_T^{\rm miss}$ analysis [426] is designed to search for squarks and gluinos in supersymmetric models, where neutralinos lead to missing energy. Several SRs are characterised by minimum jet multiplicity from two to six; $E_T^{\rm miss} > 200$ GeV is required for all SRs, while different thresholds are applied on jet momenta and on the azimuthal separation between jets and $E_T^{\rm miss}$.

To reinterpret the above analyses in the context of our spin-2 mediator simplified DM model, we use CHECKMATE2 [187], which is a public recasting tool providing confidence limits from simulated signal events and includes a number of 13 TeV analyses. We generate hadron-level signal samples by using the tree-level matrix-element plus parton-shower

[4] The K factors in Figure 6.5 are slightly different from the ones reported in [411] due to different PDF choices and different kinematical cuts. See [411] for details on theoretical uncertainties.

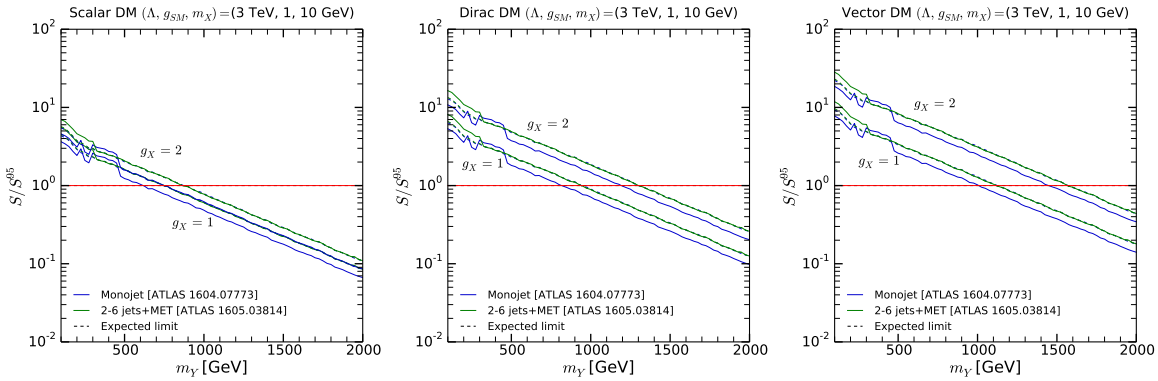

Figure 6.7.: Ratio of signal events over the number of events excluded at 95% CL as a function of the mediator mass, for $g_X = 1$ or 2 with $\Lambda = 3$ TeV, $g_{\rm SM} = 1$ and $m_X = 10$ GeV, where the ATLAS 13 TeV (3.2 fb^{-1}) monojet [425] and multijet+$E_T^{\rm miss}$ [426] analyses are considered. From left to right: scalar, Dirac and vector DM.

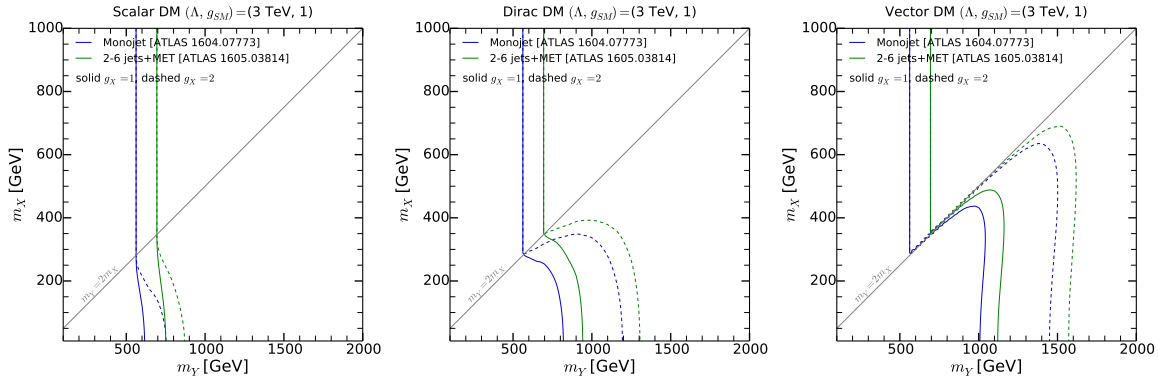

Figure 6.8.: 95% CL exclusion from the ATLAS 13 TeV (3.2 fb^{-1}) monojet [425] and multijet+$E_T^{\rm miss}$ [426] analyses in the plane of the DM vs. mediator masses, for $g_X = 1$ or 2 with $\Lambda = 3$ TeV and $g_{\rm SM} = 1$. From left to right: scalar, Dirac and vector DM.

(ME+PS) merging procedure. In practice, we make use of the shower-k_T scheme [215], implemented in MADGRAPH5 [175] with PYTHIA6 [202], and generate signal events with parton multiplicity from one to two partons. We impose $E_T^{\rm miss} > 200$ GeV and set $Q_{\rm cut} = 200$ GeV for the merging separation parameter at the parton level; these values are chosen for an efficient event generation without affecting the final results. The event rate is normalised to the $pp \to Y_2 j$ NLO cross sections shown in Figure 6.5. (Note, however, that NLO corrections may also affect the shapes of the kinematic distributions, as shown for the spin-1 and spin-0 cases in [404]; a detailed study of this aspect will be reported elsewhere.)

It turns out that, for an on-shell mediator of given mass, the selection efficiencies are independent of the mass and spin of the invisible decay products. Moreover, contributions from off-shell production are negligible for the scenarios considered here. The efficiencies can thus be evaluated as a function of the mediator mass only. In the following, we normalise the number of events with NLO cross sections, shown in Figure 6.5, and the total branching ratio into invisible final states (DM and neutrino). We note that for a given mediator mass the leading jet for the spin-2 mediator case is harder and more forward than that for the

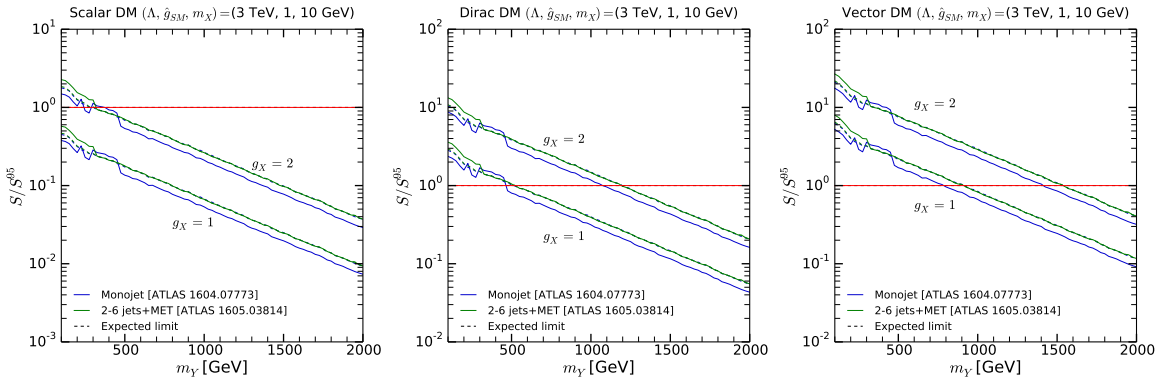

Figure 6.9.: Same as Figure 6.7, but for the leptophobic scenario.

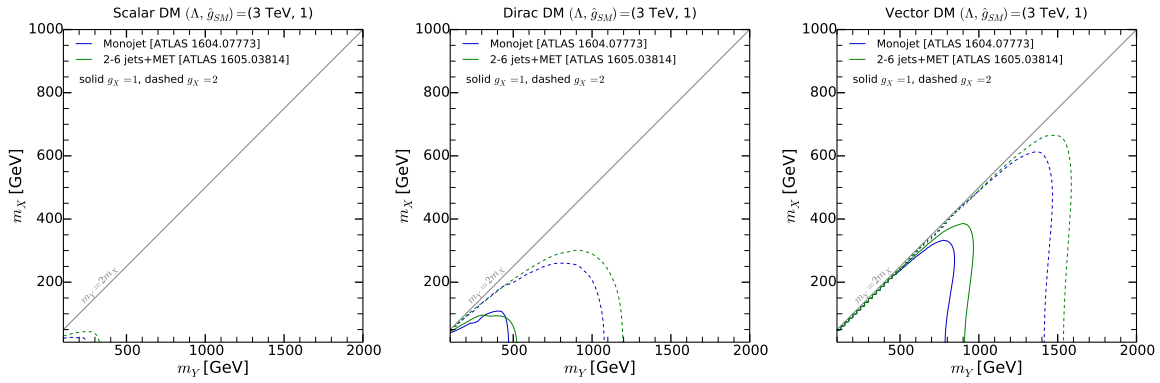

Figure 6.10.: Same as Figure 6.8, but for the leptophobic scenario.

spin-1 case. This is partly because the spin-2 mediator with a parton is produced not only through the $q\bar{q}$ and qg initial states but also dominantly through the gg initial state, and partly because the spin-2 mediator is also emitted from a gluon as well as from the $gggY_2$ and $q\bar{q}gY_2$ four-point vertices.

Figure 6.7 shows the ratio of signal events over the number of events excluded at 95% CL, S/S^{95}, as a function of the mediator mass, for the three types of DM (taking $g_X = 1$ or 2 with $\Lambda = 3\,\text{TeV}$, $g_{\text{SM}} = 1$ and $m_X = 10$ GeV as a benchmark case). As expected from the discussion in the previous section, the scalar DM case is the least constrained, with the E_T^{miss} coming dominantly from the neutrino channel; for $g_X = 1$ (2), we find the limit $m_Y \gtrsim 600$ (750) GeV from the monojet analysis and $m_Y \gtrsim 750$ (850) GeV from the multijet+E_T^{miss} analysis.[5] For Dirac DM the limit increases to $m_Y \gtrsim 950$ (1300) GeV owing to the contribution from $Y_2 \to X_D X_D$. Finally, for vector DM we have $m_Y \gtrsim 1100$ (1550) GeV. For the monojet analysis, the inclusive SR with the E_T^{miss} cut of 500, 600, and 700 GeV (denoted as IM5, IM6, and IM7 in [425]) gives the limit for the low ($100 \sim 300$ GeV), middle ($300 \sim 450$ GeV), and high ($\gtrsim 450$ GeV) mass region, respectively. For the multijet+E_T^{miss} analysis, the 2-jet loose (2jl) SR gives the limit for the mass range of $100 \sim 300$ GeV, while the 2-jet medium (2jm) SR does for $\gtrsim 300$ GeV. See [426] for the detailed selection criteria.

As the production rate scales as $1/\Lambda^2$, the upper limit of Λ can be estimated from the

[5] While both analyses have very similar sensitivity, i.e. their expected limits are basically the same, the monojet results have over- and under-fluctuations in some SRs. Therefore the expected and observed limits slightly differ from each other for the monojet analysis. Overall, the multijet+E_T^{miss} analysis tends to give the stronger limit.

decay mode	reference	limit Tab./Fig.	limit on	$\sqrt{s}$ (TeV)	L (fb^{-1})
jj	ATLAS-CONF-2016-069 [430]	Tab. 2 (Res)	$\sigma(\text{Gaussian}) \times B \times A$	13	15.7
$jj(+j/\gamma)$	ATLAS-CONF-2016-070 [150]	Tab. 4/3 (Res)	$\sigma(\text{Gaussian}) \times B \times A$	13	15.5
WW	ATLAS-CONF-2016-062 [431]	Fig. 6	$\sigma(G_{\text{RS}}) \times B$	13	13.2
bb	ATLAS-CONF-2016-060 [432]	Fig. 7(b) (Res)	$\sigma(\text{Gaussian}) \times B \times A \times \epsilon_{2b}$	13	13.3
tt	CMS-PAS-B2G-15-002 [433]	Tab. 4 (1%)	$\sigma(Z') \times B$	13	2.6
ZZ	ATLAS-CONF-2016-082 [434]	Fig. 10(d)	$\sigma(G_{\text{RS}}) \times B$	13	13.2
$\gamma\gamma$	CMS 1609.02507 [435]	Fig. 6(middle)	$\sigma(G_{\text{RS}}) \times B$	13+8	16.2+19.7
ll	ATLAS-CONF-2016-045 [329]	Fig. 3(c)	$\sigma(Z') \times B$	13	13.3
hh	ATLAS-CONF-2016-049 [436]	Fig. 11	$\sigma(G_{\text{RS}}) \times B$	13	13.3
$\gamma\gamma$	ATLAS 1407.6583 [437]	Fig. 4, HepData [438]	$\sigma(H) \times B \times A$	8	20.3
	CMS 1506.02301 [439]	Fig. 6	$\sigma(G_{\text{RS}}) \times B$	8	19.7
WW	ATLAS 1512.05099 [440]	Auxiliary Fig. 3	$\sigma(G_{\text{RS}}) \times B$	8	20.3
ZZ	ATLAS 1512.05099 [440]	Auxiliary Fig. 4	$\sigma(G_{\text{RS}}) \times B$	8	20.3

Table 6.2.: Constraints from resonance searches used in this study.

plots. For instance, for vector DM with $m_Y = 100$ GeV, Λ should be larger than around 10 TeV for $g_{\text{SM}} = g_X = 1$. It should be noted that, due to the K factors of $1.7 - 1.2$ for $m_Y = 100 - 2000$ GeV (see Figure 6.5), these limits are slightly stronger than what would be obtained with LO production rates.

The 95% CL exclusion in the m_X vs. m_Y plane is shown in Figure 6.8. Due to the different threshold behaviours, as seen in Eqs. (6.13)–(6.15), the excluded region near $m_Y = 2m_X$ strongly depends on the type of DM.

We note that we compared the CheckMATE results with those obtained by the equivalent analysis implementations in MadAnalysis 5 [188, 189] (recast codes [427, 428]) and Rivet 2.5 [167] for a couple of representative mass choices and found agreement at the level of 20% within all three tools.

The monophoton (as well as mono-Z/W) signature could also be interesting to explore the spin-2 model. However, as seen in Section 6.3.2, the production rate for a pair of DM with a photon is strongly suppressed. We checked that there is no constraint for the above benchmark points from the CMS 13 TeV monophoton analysis (12.9 fb^{-1}) [429].

An interesting alternative to the universal coupling g_{SM} is a leptophobic scenario with

$$g_l^T \ll \hat{g}_{\text{SM}} \equiv g_H^T = g_q^T = g_g^T = g_W^T = g_B^T \,. \tag{6.16}$$

In this case, the E_T^{miss} signatures come exclusively from decays into DM, because Y_2 decays into neutrinos are switched off. Moreover, constraints from dilepton resonance searches, which as we will see in the next subsection are quite severe, are evaded. The results for the leptophobic scenario are presented in Figures 6.9 and 6.10 in analogy to Figures 6.7 and 6.8. As expected, the $m_Y < 2m_X$ region is no longer constrained. Also, for $g_X = 1$, the exclusion becomes considerably weaker for all the DM types; in particular there is no more constraint for scalar DM. For $g_X = 2$, except scalar DM, the mediator decays into DM dominates the neutrino decay mode even for the universal coupling scenario (see Figure 6.4), and hence the m_Y limits are very similar.

Resonance searches

Direct resonance searches can also be used to explore s-channel mediator DM models, see e.g. [393, 441] for the spin-1 and spin-0 mediator models, respectively. Results from Run 2 data are already available for a large variety of final states (dijet, dilepton, diphoton, WW, ZZ, $b\bar{b}$, $t\bar{t}$, hh) from ATLAS [150, 329, 430–432, 434, 436] and CMS [433, 435, 442–445], and give powerful constraints for mediator masses of a few hundred GeV up to several TeV.

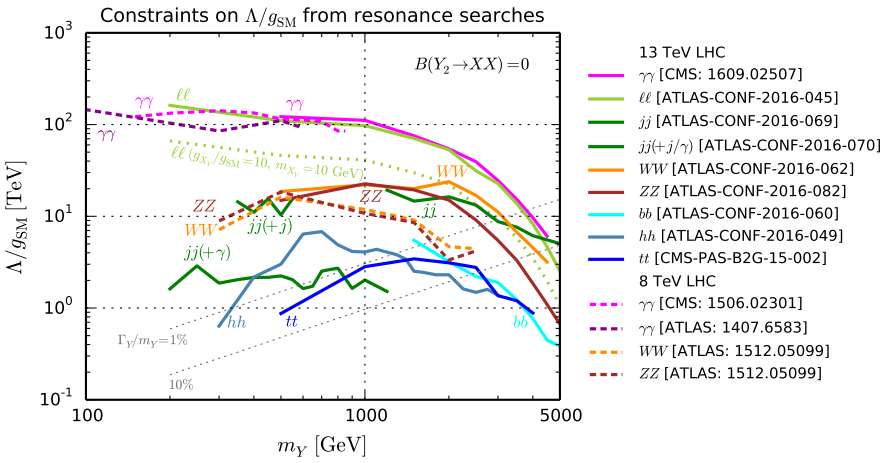

Figure 6.11.: Constraints on $\Lambda/g_{\rm SM}$ from observed 95% CL upper limits of resonance searches at the 13 TeV (solid) and 8 TeV (dashed) LHC as a function of the spin-2 mediator mass. We assume a negligible branching ratio to DM, except for a dotted line, where the vector DM coupling $g_X/g_{\rm SM} = 10$ with $m_X = 10$ GeV is taken into account as a reference. Regions below each line are excluded. Information on the mediator width-to-mass ratio is given by the grey dotted lines.

Lower masses are partly covered by Run 1 results.

Table 6.2 lists the current resonance search results which we use to constrain our spin-2 simplified model. The RS massive graviton is considered in the analyses for pairs of electroweak gauge or Higgs bosons [431, 434–436, 439, 440] as one of the new physics hypotheses. For the fermionic and jet final states in [150, 329, 430, 432, 433], on the other hand, Z' and a model-independent Gaussian-shaped resonance have been studied. Except the dijet and di-b-jet analyses at 13 TeV and the low-mass diphoton analysis at 8 TeV from ATLAS, the limits are provided directly on the cross section in the given channel, and hence we obtain the model constraints by simply using the Y_2 production cross section and the branching ratio discussed in Section 6.3.2. For the analyses with different hypotheses from the spin-2 resonance, we assume that the acceptance and efficiency are similar. When limits are given on the fiducial cross section, $\sigma \times B \times A$, we generate LO events normalised by the NLO cross section and apply the fiducial cuts at the parton level by using MADANALYSIS5 [446].

We recall that, for a given mediator mass, the Y_2 production cross section depends solely on $g_{\rm SM}/\Lambda$, while the branching ratio depends also on the parameters related to DM, i.e. g_X and m_X, as well as on the type of DM. In the decoupling limit of the dark sector, the constraints on $\Lambda/g_{\rm SM}$ are the most stringent. When decays to DM are relevant, the branching ratios to SM particles become smaller and hence the constraints are weakened.

Figure 6.11 shows the constraints on $\Lambda/g_{\rm SM}$ from the observed 95% CL upper limits of the resonance searches listed in Table 6.2 as a function of the mediator mass, where we assume a negligible branching ratio to DM particles, i.e. $g_X \ll 1$ and/or $m_Y < 2m_X$. Although the branching ratio is small, $B(Y_2 \to \gamma\gamma) \sim 4\%$ at high mass, the diphoton resonance searches give the most stringent limit for the whole mass range, resulting in $\Lambda/g_{\rm SM} \gtrsim 100$ TeV for $m_Y \lesssim 1$ TeV. The dilepton channel, also having a branching ratio of about 4%, provides a similarly strong constraint for mediator masses above 200 GeV. The dijet and WW/ZZ resonance searches lead to a constraint of a few tens of TeV on $\Lambda/g_{\rm SM}$ for around 1 TeV mediator mass. We note again that the limits are obtained based on the NLO production

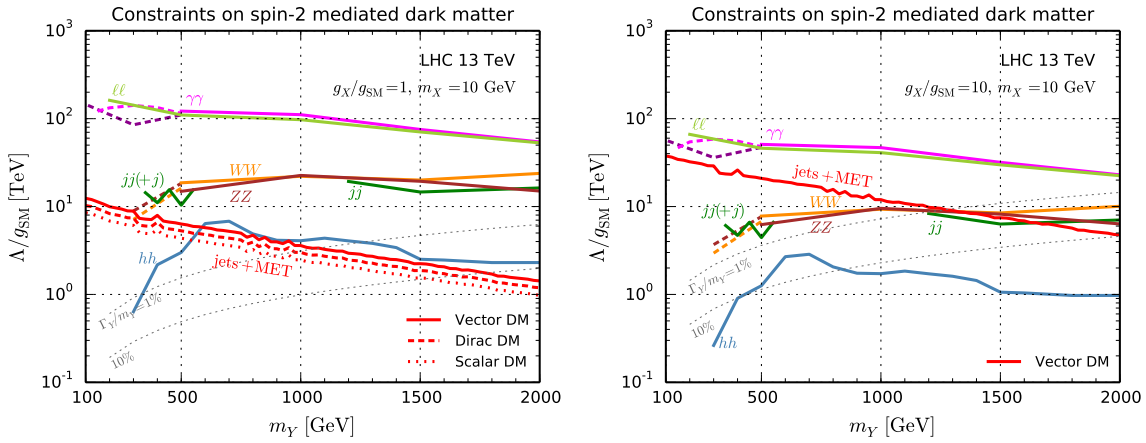

Figure 6.12.: Summary of the constraints on $\Lambda/g_{\rm SM}$ from searches with and without missing energy at the 13 TeV LHC as a function of the spin-2 mediator mass, for $m_X = 10$ GeV with $g_X/g_{\rm SM} = 1$ (left) and 10 (right). The labelling of the constraints from resonance searches is the same as in Figure 6.11. For $g_X/g_{\rm SM} = 1$ the differences among the different types of DM for the limits from the resonance searches are not visible. For $g_X/g_{\rm SM} = 10$, however, they are quite relevant so only the vector DM case is shown. The figure assumes a universal $g_{\rm SM}$ but is also valid for the leptophobic case when ignoring the ll lines.

rates which are larger than the LO ones, especially for $pp \to (Y_2 \to jj)\gamma$; see Figure 6.5. We also note that, as indicated by grey dotted lines in Figure 6.11, the mediator width can be very large at high mass and low $\Lambda/g_{\rm SM}$; as the experimental analyses often assume a narrow width, this region has to be regarded with caution.

The weakening of the constraints when Y_2 decays into DM are allowed is demonstrated for the dilepton channel in Figure 6.11, depicted by a dotted line, where we assume vector DM and take $g_X = 10$ and $m_X = 10$ GeV. For instance, at $m_Y = 1$ TeV, the dilepton (electron and muon) branching ratio becomes 0.8%, i.e. the dilepton production rate becomes smaller by a factor of five, reducing the limit on $\Lambda/g_{\rm SM}$ by $1/\sqrt{5}$. As seen in Figure 6.4, the above assumption gives the largest DM branching ratio within the scenarios we consider.[6] Therefore, the diphoton resonance searches, and for $m_Y > 200$ GeV also the dilepton resonance searches, provide stronger constraints on the universal coupling scenario than the searches with missing energy.

To avoid such severe constraints from resonance searches, it is interesting to consider scenarios beyond the universal coupling case. The dilepton constraints could be avoided, for example, in the leptophobic scenario, $g_l^T = 0$, as already discussed in the previous subsection. To avoid the diphoton constraints is somewhat more complicated. One possibility would be the gravity-mediated DM model [115, 407], where the KK graviton mainly couples to massive particles —DM, Higgs, massive gauge bosons and top quarks— while the couplings to photons, gluons and light quarks are highly suppressed. In such scenarios, the branching ratios and the production cross sections of the spin-2 resonance strongly depend on the setup and can be very different from those in the universal coupling case. In fact associated production of the mediator with a W or Z boson, or mediator production in vector boson fusion may be more relevant than s-channel production in $q\bar{q}$ or gg fusion. While such setups can in principle be studied easily in the simplified model framework by appropriately

[6] In Figure 6.11 there is hardly any difference between the $g_X \ll 1$ and $g_X = 1$ cases.

choosing the free parameters g_X^T and g_i^T in Eq. (6.6), such an analysis is beyond the scope of this work. A final caveat is that non-universal couplings to gluons and quarks, $g_g^T \neq g_q^T$, give rise to a unitarity violating behaviour at higher order in QCD [417]. We therefore only consider phenomenological scenarios with $g_g^T = g_q^T$.

6.3.4. Summary

We considered a simplified DM model where the DM candidate couples to the SM particles via an s-channel spin-2 mediator, Y_2, and studied the constraints from the current LHC data. In particular, we compared the constraints from searches with and without missing energy.

For universal couplings of the mediator to SM particles, we found that diphoton resonance searches provide the strongest constraints, $\Lambda/g_{\rm SM} \gtrsim 100$ TeV for Y_2 masses up to ~ 1 TeV. For $\Lambda/g_{\rm SM} = 10$ (3) TeV, the exclusion extends up to 4 (beyond 5) TeV in m_Y. The dilepton channel provides a similarly strong constraint for mediator masses above 200 GeV. Monojet and multijet+$E_T^{\rm miss}$ searches are competitive only if the mediator decays into photons and leptons are heavily suppressed; in this case they could provide complementary constraints to the other resonance searches in particular in the low-mass region below 0.5–1 TeV, depending on $g_X/g_{\rm SM}$.

For $m_Y < 2m_X$, $E_T^{\rm miss}$ signatures arise solely from Y_2 decays into neutrinos, leading to $m_Y \gtrsim 700$ GeV for $g_X/\Lambda = g_{\rm SM}/\Lambda = (3\ {\rm TeV})^{-1}$, based on 3.2 fb^{-1} of data at $\sqrt{s} = 13$ TeV. For $m_Y > 2m_X$, the limit crucially depends on g_X and the type of dark matter. The dependence on the DM mass is less pronounced unless one approches the threshold region. For $m_X = 10$ GeV and $g_X/\Lambda = g_{\rm SM}/\Lambda = (3\ {\rm TeV})^{-1}$, we found $m_Y \gtrsim 750$, 950, and 1100 GeV for scalar, Dirac, and vector DM, respectively. This increases to 850, 1300, and 1550 GeV when doubling g_X. We note that the obtained limits are based on the NLO-QCD predictions, which give a larger production rate than at the LO. The K factor depends on the mediator mass and the production channel.

The complementarity among the different searches is illustrated in Figure 6.12, where we have rescaled the reach of the jets + $E_T^{\rm miss}$ searches from 3.2 to 15 fb^{-1} in order to make a fair comparison. We see that, for the same amount of data, in case of $g_X \simeq g_{\rm SM}$ the missing energy searches are roughly competitive with the dijet and heavy diboson (WW, ZZ) searches, pushing $\Lambda/g_{\rm SM}$ beyond 20 TeV. (As mentioned, when the dilepton and diphoton constraints hold, they give even stronger limits.)

For $g_X/g_{\rm SM} = 10$ (or $g_X/\hat{g}_{\rm SM} = 10$), also the resonance constraints strongly depend on the type of DM. Therefore, in the right plot in Figure 6.12 only the vector DM case is shown. We see that the jets+$E_T^{\rm miss}$ searches give stronger constraints than the dijet and heavy diboson searches up to mediator masses of about 1.2 TeV. The dilepton and diphoton constraints are weakened by about a factor of two but still give the strongest constraints.

We note that our study on resonance searches in Section 6.3.3 can be applied not only for spin-2 mediated DM models but also for usual RS-type graviton searches; see also, e.g. [447]. As a final remark we like to point out that in a full model the presence of KK excitations might alter the LHC phenomenology as compared to the simplified model scenarios discussed here. Examples are limits on gauge KK modes providing additional constraints on light gravitons, or KK excitations of the DM fields contributing to $E_T^{\rm miss}$ signatures. While this goes well beyond the simplified model picture, it is certainly an interesting topic for future studies.

CHAPTER

SEVEN

CONCLUSIONS

The interpretation of LHC searches for new physics in a generic model depends on a potentially large number of free parameters, and the relation between the parameters and the LHC signature is typically highly complex. This thesis examined to what extent simplified models can be a useful tool in the interpretation of LHC searches for new physics, especially those with new sources of missing energy from a dark matter candidate. They facilitate the communication between theoretical description and experimental observation, and allow an intuitive interpretation of LHC searches in a signature based description. In addition to their conceptual appeal, they allow for a fast reinterpretation of LHC searches in generic models. SUSY searches at the LHC are typically interpreted in an SMS context, and since Run 2 also dark matter searches are generally interpreted in terms of dark matter simplified models.

To make the most of the existing SMS results, sophisticated software tools are required. For example the SModelS framework is mapping generic models onto SUSY-like simplified models, and providing a fast, automatised test agains a large number of LHC search results. Under the so-called SMS assumption, explained in Chapter 4, this procedure is not limited to the MSSM, and may even apply to non-SUSY models. SModelS works out of the box for alternative scenarios with a new $\mathbb{Z}_2$ symmetry, one only needs to define all BSM particles as even or odd.

For all scenarios considered here we found that the SMS assumption is approximately valid, as typically the differences in efficiencies in the most sensitive signal region and the resulting upper limits are around 20% or lower.

Somewhat larger differences can be found when additional radiation from the initial state is important for the signal region selection. This may be the case in compressed scenarios or in generic multi-jet + E_T^{miss} searches, as discussed e.g. in Sections 4.1 and 4.2. While the differences in mass limits in the SMS context remain marginal, recasting tools based on event simulation may be used to improve precision in those cases.

Concretely we found that (top) squark searches can be used to constrain fermionic (top) quark partners, arising for example in UED scenarios. Since the production cross sections of fermionic quark partners is much higher than that of a scalar quark, extending the efficiency and upper limit maps to higher masses would allow to constrain these scenarios further. Similarly, extending slepton search interpretations to higher masses would allow to further constrain chargino production giving rise to the same topology (when $\tilde{\chi}^{\pm} \to l^{\pm}\tilde{\nu}_l$), with higher cross sections. Note that in all results presented in this thesis, the narrow width approximation was considered a prerequesite. When considering generic SMS descriptions the couplings are generally free parameters, potentially leading to large widths. This is not

the case in SUSY models where the couplings are fixed by the Yukawa and gauge couplings. Width effects on the interpretation were recently studied in [448] for extra heavy quarks decaying to a scalar or vector dark matter candidate.

SModelS was used in three phenomenological studies presented here. In addition to reporting the exclusion limits, SModelS also determines the topology coverage, returning in particular information about missing topologies. For the example of the pMSSM we found that about $50 - 60\%$ of parameter points excluded by ATLAS in a comprehensive event simulation study can also be excluded using SMS results. Using the SModelS coverage information we further found that in particular asymmetric branch topologies are required to improve the coverage. Particularly important topologies not considered by any existing SMS interpretation arise when both gluino and squarks are light. We can use recasting tools based on event simulation to add efficiency maps for such missing simplified model topologies to the SModelS database, for any signature covered by the existing search strategies. On the other hand, long cascade decays, for which an SMS interpretation is no longer viable, are rarely important.

We also used SModelS v1.0.1 to constrain the MSSM+RN and the UMSSM and found that mixed sneutrino LSP scenarios are often well constrained by the existing SMS results. In particular slepton search results apply to the chargino-sneutrino simplified model, constraining points with light charginos. Evaluating the missing topologies of the allowed points we further found that chargino-neutralino production gives rise to a single lepton + $E_T^{\rm miss}$ topology with potentially large cross sections. Note however that this type of signature has large SM background, and may not be constrained by existing corresponding searches. The same type of search may constrain the UMSSM model, where we found the $W + E_T^{\rm miss}$ final state to be important. Sneutrino LSP scenarios in the UMSSM are currently only constrained by SMS results if the corresponding decay proceeds via an intermediate neutralino that acts as an effective LSP in the event. This is because visible decays to the purely RH sneutrino always include additional neutrinos in the final state. They are expected to alter the event kinematics, and therefore the efficiencies and upper limits. These effects have not yet been investigated.

For neutralino LSP scenarios in the UMSSM we found that the SMS limits are often not effective in excluding parameter points, even in case of light gluinos and/or the squarks. This is similar to the MSSM, and mainly because of asymmetric decay branches not constrained by SModelS v1.0.1. Note that limits are expected to be improved with the latest version of SModelS, allowing the use of efficiency map results, and therefore the combination of signal topologies contributing to one signal region. This improvement was in fact demonstrated for pMSSM scenarios in Section 5.1. The problem with asymmetric branches remains however.

For both neutralino and sneutrino LSP scenarios we found that long-lived particle searches are often important. A wino or higgsino like LSP scenario may lead to charginos decaying inside or outside the ATLAS or CMS detector, and searches for displaced vertices or charged tracks give important constraints. Constraints on electrically charged particles decaying outside the detector will be included in future versions of SModelS, as explained in Section 3.4. Moreover, in sneutrino LSP scenarios we often find that the gluinos are long-lived, even if the squarks are not fully decoupled. Because of their large production cross section, most points with a long-lived gluino studied here are already excluded. A caveat is however that the limits rely on the modelling of R-hadrons. In general searches for non-prompt decays and long-lived particles and their interpretation have gained a lot of interest recently, and are discussed in the framework of the LHC LLP working group.

Regarding simplified model interpretations of LHC dark matter searches we studied in particular scenarios with an s-channel spin-2 mediator. We found that the universal coupling scenario is strongly constrained by resonance searches. Alternatively one can study bulk-RS type scenarios, where the mediator couples mainly to massive particles, i.e. the massive gauge bosons, the Higgs and the top quark, as well as a dark matter candidate. Such scenarios are very different from the universal coupling scenario considered here. First because the production cross sections are much lower and the main production channels are expected to be via vector boson fusion or top loops. Moreover, in a complete study, Kaluza-Klein excitations of the gauge bosons should also be considered. This interesting alternative is currently under investigation.

The latest exclusion limits (see examples in Section 2.4) are already approaching the projected discovery reach at Run 2 and 3 of the LHC [449]. Nevertheless our aim is to maximize the use of the available LHC data. This implies a close theory-experiment interaction, and the requirement of sophisticated tools for reinterpretation. Maximally exploiting the reinterpretation options of a given experimental search allows us to fully understand the implications of its results. More globally the reinterpreation of all relevant available searches may allow us to identify blind spots and design additional search strategies. Given the lack of any convincing signal at the LHC the discussion was based on constraints and exclusion limits. We note however that the same set of tools can be used for the interpretation of a possible signal. Simplified model based tools may be used for a bottom-up interpretation of excesses, fitting first the reduced set of SMS parameters. On the other hand, recasting tools based on event simulation can be used to test a complete Lagrangian description and set of free parameters against the measured results. Note also that when aiming to describe a signal, it is also important to verify that the description is in agreement with previous negative results, and both negative and positive search results should be taken into account simultaneously.

In fact during the last years the development of new tools was siginificantly advanced, and many analyses have been implemented in reinterpretation tools (see discussion in Section 2.5). This has also improved the communication between phenomenologists and experimentalists as compared to just a few years ago [450]. Reinterpretation efforts have recently been streamlined via the LHC (re)interpretation workshops at CERN [451]. Moreover, a standard description of LHC analyses (similar to the standardised file formats introduced in Section 2.5.1) has been proposed. A description of this Les Houches Analysis Description Accord (LHADA) proposal was given in [452].

Apart from direct search results, Run 2 of the LHC will also provide new precise measurements of Higgs and SM processes which can be used to further constrain new physics scenarios. Moreover, regarding dark matter, direct detection experiments generally provide constraints complementary to those from LHC searches, and will cover a large part of the interesting parameter space for SUSY dark matter in the next years.

To obtain a comprehensive picture of the status of a given model, a global fit should take into account all available measurements and constraints to evaluate an overall likelihood function. This requires a number of different software tools to calculate all relevant observables, and a statistical procedure for the selection of parameter points and for the interpretation of the results. Many global fits in MSSM scenarios have been performed, see for example [453–457] for recent results. Moreover the new tool GAMBIT [458] provides a modular interface for performing global fits in generic BSM models. Note that in particular a fast evaluation of constraints from collider searches is important in global fits, which can therefore profit from new machine learning tools, but also from using SMS constraints.

The naturalness as well as the WIMP paradigm are currently on trial, in collider and dark

matter direct detection searches. To maximise the extent to which we can test and understand them, an interplay between experimental and theoretical physics is essential. In this thesis we put forward simplified model descriptions as an efficient tool to facilitate such an interplay, allowing to understand the LHC search results in a model-independent fashion, and also to study their impact on generic BSM models.

APPENDIX

A

HIGGS SECTOR OF THE UMSSM

The Higgs potential is a sum of F-, D- and soft supersymmetry breaking-terms belonging to the UMSSM Lagrangian : $V^{\rm U}_{\rm tree} = V_{\rm F} + V_{\rm D} + V_{\rm soft}$, where

$$\begin{aligned} V_F &= |\lambda H_u \cdot H_d|^2 + |\lambda S|^2 \left(|H_d|^2 + |H_u|^2\right), \\ V_D &= \frac{(g_1^2+g_2^2)^2}{8}\left(|H_d|^2 - |H_u|^2\right)^2 + \frac{g_2^2}{2}\left(|H_d|^2|H_u|^2 - |H_u \cdot H_d|^2\right) \\ &\quad + \frac{g_1'^2}{2}\left(\mathcal{Q}'_{H_d}|H_d|^2 + \mathcal{Q}'_{H_u}|H_u|^2 + \mathcal{Q}'_S|S|^2\right)^2, \\ V_{\rm soft} &= m_{H_d}^2|H_d|^2 + m_{H_u}^2|H_u|^2 + m_s^2|S|^2 + (A_\lambda \lambda S H_u \cdot H_d + h.c.). \end{aligned} \tag{A.1}$$

At the minimum of the potential $V^{\rm U}_{\rm tree}$, the neutral Higgs fields are expanded as

$$H_d^0 = \frac{1}{\sqrt{2}}(v_d + \phi_d + i\varphi_d), \quad H_u^0 = \frac{1}{\sqrt{2}}(v_u + \phi_u + i\varphi_u), \quad S = \frac{1}{\sqrt{2}}(v_s + \sigma + i\xi), \tag{A.2}$$

while the charged Higgs :

$$H_d^- = -\cos\beta G_{W^-} + \sin\beta H^-, \quad H_u^+ = \sin\beta G_{W^+} + \cos\beta H^+, \tag{A.3}$$

with G_W the Goldstone boson.
The minimization conditions of $V^{\rm U}_{\rm tree}$ are [78]

$$\begin{aligned} \left(m_{H_d}^{\rm tree}\right)^2 &= -\frac{1}{2}\left[\frac{g_1^2+g_2^2}{4} + \mathcal{Q}'^2_{H_d} g_1'^2\right] v_d^2 + \frac{1}{2}\left[\frac{g_1^2+g_2^2}{4} - \lambda^2 - \mathcal{Q}'_{H_d}\mathcal{Q}'_{H_u} g_1'^2\right] v_u^2 \\ &\quad - \frac{1}{2}\left[\lambda^2 + \mathcal{Q}'_{H_d}\mathcal{Q}'_S g_1'^2\right] v_s^2 + \frac{\lambda A_\lambda v_s v_u}{\sqrt{2} v_d} \\ \left(m_{H_u}^{\rm tree}\right)^2 &= \frac{1}{2}\left[\frac{g_1^2+g_2^2}{4} - {}^2 - \mathcal{Q}'_{H_d}\mathcal{Q}'_{H_u} g_1'^2\right] v_d^2 - \frac{1}{2}\left[\frac{g_1^2+g_2^2}{4} + \mathcal{Q}'^2_{H_u} g_1'^2\right] v_u^2 \\ &\quad - \frac{1}{2}\left[\lambda^2 + \mathcal{Q}'_{H_u}\mathcal{Q}'_S g_1'^2\right] v_s^2 + \frac{\lambda A_\lambda v_s v_d}{\sqrt{2} v_u} \\ \left(m_S^{\rm tree}\right)^2 &= -\frac{1}{2}\left[\lambda^2 + \mathcal{Q}'_{H_d}\mathcal{Q}'_S g_1'^2\right] v_d^2 - \frac{1}{2}\left[\lambda^2 + \mathcal{Q}'_{H_u}\mathcal{Q}'_S g_1'^2\right] v_u^2 - \frac{1}{2}\mathcal{Q}'^2_S g_1'^2 v_s^2 + \frac{\lambda A_\lambda v_u v_d}{v_s \sqrt{2}}. \end{aligned} \tag{A.4}$$

The tree-level mass-squared matrices for the CP-even ($\mathcal{M}^0_+$) and CP-odd ($\mathcal{M}^0_-$) Higgs bosons can be written in the basis $\{H^0_d, H^0_u, S\}$ using the relations

$$\left(\mathcal{M}^0_+\right)_{ij} = \left.\frac{\partial^2 V^{\rm U}_{\rm tree}}{\partial\phi_i\partial\phi_j}\right|_0, \qquad \left(\mathcal{M}^0_-\right)_{ij} = \left.\frac{\partial^2 V^{\rm U}_{\rm tree}}{\partial\varphi_i\partial\varphi_j}\right|_0, \tag{A.5}$$

where $(\phi_1,\phi_2,\phi_3) \equiv (\phi_d,\phi_u,\sigma)$ and $(\varphi_1,\varphi_2,\varphi_3) \equiv (\varphi_d,\varphi_u,\xi)$. For the neutral CP-even Higgs bosons the relations are

$$\begin{aligned}
\left(\mathcal{M}^0_+\right)_{11} &= \left[\frac{g_1^2+g_2^2}{4} + \mathcal{Q}'^2_{H_d} g_1'^2\right] v_d^2 + \frac{\lambda A_\lambda v_s v_u}{\sqrt{2} v_d} \\
\left(\mathcal{M}^0_+\right)_{12} &= -\left[\frac{g_1^2+g_2^2}{4} - \lambda^2 - \mathcal{Q}'_{H_d}\mathcal{Q}'_{H_u} g_1'^2\right] v_u v_d - \frac{\lambda A_\lambda v_s}{\sqrt{2}} \\
\left(\mathcal{M}^0_+\right)_{13} &= \left[\lambda^2 + \mathcal{Q}'_{H_d}\mathcal{Q}'_S g_1'^2\right] v_s v_d - \frac{\lambda A_\lambda v_u}{\sqrt{2}} \\
\left(\mathcal{M}^0_+\right)_{22} &= \left[\frac{g_1^2+g_2^2}{4} + \mathcal{Q}'^2_{H_u} g_1'^2\right] v_u^2 + \frac{\lambda A_\lambda v_s v_d}{\sqrt{2} v_u} \\
\left(\mathcal{M}^0_+\right)_{23} &= \left[\lambda^2 + \mathcal{Q}'_{H_u}\mathcal{Q}'_S g_1'^2\right] v_s v_u - \frac{\lambda A_\lambda v_d}{\sqrt{2}} \\
\left(\mathcal{M}^0_+\right)_{33} &= \mathcal{Q}'^2_S g_1'^2 v_s^2 + \frac{\lambda A_\lambda v_u v_d}{v_s\sqrt{2}}.
\end{aligned} \tag{A.6}$$

For the CP-odd sector the mass matrix

$$\mathcal{M}^0_- = \frac{\lambda A_\lambda}{\sqrt{2}} \begin{pmatrix} \frac{v_s v_u}{v_d} & v_s & v_u \\ v_s & \frac{v_s v_d}{v_u} & v_d \\ v_u & v_d & \frac{v_u v_d}{v_s} \end{pmatrix}, \tag{A.7}$$

leads to

$$\left(m^{\rm tree}_{A^0}\right)^2 = \frac{\lambda A_\lambda \sqrt{2}}{\sin 2\beta} v_s \left(1 + \frac{v^2}{4 v_s^2}\sin^2 2\beta\right). \tag{A.8}$$

The charged Higgs mass at tree-level reads

$$\left(m^{\rm tree}_{H^\pm}\right)^2 = M_W^2 + \frac{\lambda A_\lambda \sqrt{2}}{\sin 2\beta} v_s - \frac{\lambda^2}{2} v^2. \tag{A.9}$$

A.1. Radiative Corrections in the Higgs Sector

To introduce radiative corrections in a gauge invariant manner we use an effective Lagrangian,

$$\begin{aligned}
-\mathscr{L}_{eff} = {} & \lambda_1 |H_d|^4/2 + \lambda_2 |H_u|^4/2 + \lambda_3 |H_d|^2 |H_u|^2 \\
& + \lambda_4 |H_u \cdot H_d|^2 + \lambda_5 ((H_u\cdot H_d)^2 + (H_u\cdot H_d)^{*2})/2 \\
& + (\lambda_6 |H_d|^2 + \lambda_7 |H_u|^2)((H_u\cdot H_d) + (H_u\cdot H_d)^*) \\
& + \lambda_8 |H_d|^2 |S|^2 + \lambda_9 |H_u|^2 |S|^2 \\
& + \lambda_s (S H_u\cdot H_d + S^* (H_u\cdot H_d)^*),
\end{aligned} \tag{A.10}$$

where λ_s is the only dimensionful parameter. To compute the λ's we adapt the `NMSSMTools` [328] code to the UMSSM. Here we do not consider pure UMSSM corrections from gauge contributions since the $U(1)$' gauge coupling is small compared to the Yukawa coupling of the top quark [78].

The minimization conditions for the loop improved Higgs potential become

$$\begin{aligned}
\left(m^c_{H_d}\right)^2 &= \left(m^{\text{tree}}_{H_d}\right)^2 + \lambda_s \frac{v_s v_u}{\sqrt{2} v_d} - \lambda_1 \frac{v_d^2}{2} - (\lambda_3 + \lambda_4 + \lambda_5)\frac{v_u^2}{2} + 3\lambda_6 \frac{v_u v_d}{2} + \lambda_7 \frac{v_u^3}{2 v_d} - \lambda_8 \frac{v_s^2}{2} \\
\left(m^c_{H_u}\right)^2 &= \left(m^{\text{tree}}_{H_u}\right)^2 + {}_s \frac{v_s v_d}{\sqrt{2} v_u} - \lambda_2 \frac{v_u^2}{2} - (\lambda_3 + \lambda_4 + \lambda_5)\frac{v_d^2}{2} + \lambda_6 \frac{v_d^3}{2 v_u} + 3\lambda_7 \frac{v_u v_d}{2} - \lambda_9 \frac{v_s^2}{2} \\
\left(m^c_{S}\right)^2 &= \left(m^{\text{tree}}_{S}\right)^2 + \lambda_s \frac{v_u v_d}{\sqrt{2} v_s} - \lambda_8 \frac{v_d^2}{2} - \lambda_9 \frac{v_u^2}{2}.
\end{aligned} \tag{A.11}$$

The corrected CP-even mass-squared matrix elements $(\mathcal{M}^c_+)_{ij}$ are

$$\begin{aligned}
\left(\mathcal{M}^c_+\right)_{11} &= \left(\mathcal{M}^0_+\right)_{11} + \lambda_1 v_d^2 + \left(\lambda_s \frac{v_s}{\sqrt{2}} - 3\lambda_6 \frac{v_d^2}{2} + \lambda_7 \frac{v_u^2}{2}\right) \frac{v_u}{v_d} \\
\left(\mathcal{M}^c_+\right)_{12} &= \left(\mathcal{M}^0_+\right)_{12} + (_3 + \lambda_4 + \lambda_5) v_u v_d - \frac{3}{2}(\lambda_6 v_d^2 + \lambda_7 v_u^2) - \lambda_s \frac{v_s}{\sqrt{2}} \\
\left(\mathcal{M}^c_+\right)_{13} &= \left(\mathcal{M}^0_+\right)_{13} + \lambda_8 v_s v_d - \lambda_s \frac{v_u}{\sqrt{2}} \\
\left(\mathcal{M}^c_+\right)_{22} &= \left(\mathcal{M}^0_+\right)_{22} + \lambda_2 v_u^2 + \left(\lambda_s \frac{v_s}{\sqrt{2}} + \lambda_6 \frac{v_d^2}{2} - 3\lambda_7 \frac{v_u^2}{2}\right) \frac{v_d}{v_u} \\
\left(\mathcal{M}^c_+\right)_{23} &= \left(\mathcal{M}^0_+\right)_{23} + {}_9 v_s v_u - \lambda_s \frac{v_d}{\sqrt{2}} \\
\left(\mathcal{M}^c_+\right)_{33} &= \left(\mathcal{M}^0_+\right)_{33} + \lambda_s \frac{v_u v_d}{\sqrt{2} v_s}.
\end{aligned} \tag{A.12}$$

The corrected CP-odd mass-squared matrix elements read

$$\begin{aligned}
\left(\mathcal{M}^c_-\right)_{11} &= \left(\mathcal{M}^0_-\right)_{11} + \left({}_6 \frac{v_d^2}{2} + \lambda_7 \frac{v_u^2}{2} - \lambda_5 v_u v_d + \lambda_s \frac{v_s}{\sqrt{2}}\right) \frac{v_u}{v_d} \\
\left(\mathcal{M}^c_-\right)_{12} &= \left(\mathcal{M}^0_-\right)_{12} + \lambda_6 \frac{v_d^2}{2} + \lambda_7 \frac{v_u^2}{2} - \lambda_5 v_u v_d + \lambda_s \frac{v_s}{\sqrt{2}} \\
\left(\mathcal{M}^c_-\right)_{13} &= \left(\mathcal{M}^0_-\right)_{13} + \lambda_s \frac{v_u}{\sqrt{2}} \\
\left(\mathcal{M}^c_-\right)_{22} &= \left(\mathcal{M}^0_-\right)_{22} + \left(\lambda_6 \frac{v_d^2}{2} + \lambda_7 \frac{v_u^2}{2} - \lambda_5 v_u v_d + \lambda_s \frac{v_s}{\sqrt{2}}\right) \frac{v_d}{v_u} \\
\left(\mathcal{M}^c_-\right)_{23} &= \left(\mathcal{M}^0_-\right)_{23} + \lambda_s \frac{v_d}{\sqrt{2}} \\
\left(\mathcal{M}^c_-\right)_{33} &= \left(\mathcal{M}^0_-\right)_{33} + \lambda_s \frac{v_u v_d}{\sqrt{2} v_s},
\end{aligned} \tag{A.13}$$

which leads to the one-loop corrected pseudoscalar mass

$$(m^c_{A^0})^2 = \left(m^{\rm tree}_{A^0}\right)^2 + \frac{2}{\sin 2\beta}\left\{\sqrt{2}\lambda_s v_s\left(1+x^2\right) + \lambda_{567}v^2 \right. \\ \left. + \left(\left[\sqrt{2}\lambda_s v_s\left(1+x^2\right) + \lambda_{567}v^2\right]^2 - 4\sqrt{2}\lambda_s v_s x^2 \lambda_{567} v^2\right)^{1/2}\right\}, \tag{A.14}$$

where $\lambda_{567} = -\lambda_5 \sin 2\beta + \lambda_6 c_\beta^2 + \lambda_7 c_\beta^2$ and $x = v \sin 2\beta / 2 v_s$.

Note that in `NMSSMTools` the CP-odd matrix $\mathcal{M}_-$ is defined in the basis of the two CP-odd bosons $\{A^0, S_I\}$, we must therefore perform the transformation $T^T \mathcal{M}_- T$ where

$$T = \begin{pmatrix} c_\beta & -s_\beta & 0 \\ s_\beta & c_\beta & 0 \\ 0 & 0 & 1 \end{pmatrix} \tag{A.15}$$

as in [368].

Finally, the charged Higgs mass is corrected as

$$(m^c_{H^\pm})^2 = \left(m^{\rm tree}_{H^\pm}\right)^2 + \left(\lambda_s \frac{v_s}{\sqrt{2}} + \lambda_6 \frac{v_d^2}{2} + \lambda_7 \frac{v_u^2}{2}\right)\frac{2}{\sin 2\beta} - (\lambda_4 + \lambda_5)\frac{v^2}{2}. \tag{A.16}$$

APPENDIX

B

THE CLS METHOD

Given a measurement, we want to evaluate how well a particular model describes the data. To this end we define a "test statistic" Q, for example as the likelihood ratio

$$Q(s) = \frac{L(s+b)}{L(b)} \tag{B.1}$$

where $s + b$ denotes the signal plus background hypothesis, and b the background only hypothesis. We can compute a confidence level (CL) for the $s + b$ hypothesis by considering the probability that the test statistic for the hypothesis is equal or below the observed value,

$$CL_{s+b} = P_{s+b}(Q \leq Q_{obs}). \tag{B.2}$$

A signal would thus be excluded at the $(1 - CL_{s+b})$ confidence level. However, this is not robust in searches with low statistics. For these one should also consider the CL for the background only hypothesis, i.e.

$$CL_b = P_b(Q \leq Q_{obs}). \tag{B.3}$$

We can thus define

$$CL_s = CL_{s+b}/CL_b, \tag{B.4}$$

and we consider the signal hypothesis exluded at $CL = 1 - CL_s$. The probabilities are typically evaluated in Toy Monte Carlo simulations, assuming a Gaussian distribution of the errors on the background prediction (with cut-off to avoid negative values), and drawing the number of events from a Poisson distribution. For details on the method see [459, 460].

APPENDIX

C

RUNNING SMODELS

C.1. Command-line Tool

runSModelS The usage of `runSModelS` is:

runSModelS.py [-h] -f FILENAME [-p PARAMETERFILE] [-o OUTPUTDIR] [-d] [-t] [-V] [-c] [-v VERBOSE] [-T TIMEOUT]

***arguments*:**

-h, --help show this help message and exit.

-f FILENAME, --filename FILENAME name of SLHA or LHE input file or a directory path (required argument). If a directory is given, loop over all files in the directory.

-p PARAMETERFILE, --parameterFile PARAMETERFILE name of the parameters file, where most options are defined (optional argument). If not set, use all parameters from `etc/parameters_default.ini`.

-o OUTPUTDIR, --outputDir OUTPUTDIR name of output directory (optional argument). The default folder is `./results/`.

-d, --development if set, SModelS will run in development mode and exit if any errors are found

-t, --force_txt force loading the text database.

-V, --version show program's version number and exit

-c, --run-crashreport parse crash report file and use its contents for a SModelS run. Supply the crash file simply via '– filename myfile.crash'.

-v VERBOSE, --verbose VERBOSE sets the verbosity level (debug, info, warning, error). Default value is "info".

-T TIMEOUT, --timeout TIMEOUT define a limit on the running time (in secs). If not set, run without a time limit. If a directory is given as input, the timeout will be applied for each individual file.

Parameter File The basic options and parameters used by `runSModelS.py` are defined in the parameters file. An example parameter file, including all available parameters together with a short description, is stored in `parameters.ini`. If no parameter file is specified, the default parameters stored in `etc/parameters_default.ini` are used. Below we describe each entry in the parameters file.

***path*:** relevant folder paths

- **databasePath**: the absolute (or relative) path to the database.

***options*:** main options for turning SModelS features on or off

- **inputType** (SLHA/LHE): determines the type of input file. Must be SLHA for SLHA input files or LHE for LHE input files.
- **checkInput** (True/False): if True, `runSModelS.py` will run the file check tool on the input file and verify if the input contains all the necessary information.
- **doInvisible** (True/False): turns invisible compression on or off during the decomposition.
- **doCompress** (True/False): turns mass compression on or off during the decomposition.
- **computeStatistics** (True/False): turns the likelihood and χ^2 computation on or off. If True, the likelihood and χ^2 values are computed for the EM-type results.
- **testCoverage** (True/False): set to True to run the coverage tool.

***parameters*:** basic parameter values for running SModelS

- **sigmacut** (float): minimum value for an element weight (in fb). Elements with a weight below sigmacut are neglected during decomposition of SLHA input files. The default value is 0.03 fb. Note that, depending on the input model, the running time may increase considerably if sigmacut is too low, while too large values might eliminate relevant elements.
- **minmassgap** (float): maximum value of the mass difference (in GeV) for performing mass compression. The default value is 5 GeV. Only used if doCompress = True.
- **maxcond** (float): maximum allowed value (in the [0,1] interval) for the violation of upper limit conditions. A zero value means the conditions are strictly enforced, while 1 means the conditions are never enforced. Only relevant for printing the summary or SLHA output which list only results passing the consitions.
- **ncpus** (int): number of CPUs. When processing multiple SLHA/LHE files, SModelS can be run in a parallelized fashion, splitting up the input files in equal chunks. ncpus $= -1$ uses the total number of CPU cores of the machine.

***database*:** allows for selection of a subset of experimental results from the database

- **analyses** (list of results): set to "all" to use all available results. If a list of experimental analyses is given, only these will be used. For instance, setting analyses = CMS-PAS-SUS-13-008, ATLAS-CONF-2013-024 will only use the experimental results from these analysis notes.
- **txnames** (list of topologies): set to "all" to use all available simplified model topologies. The topologies are labeled according to the txname convention. If a list of txnames is given, only the corresponding topologies will be considered. For instance, setting txnames = T2 will only consider experimental results for $pp \to \tilde{q} + \tilde{q} \to (jet + \tilde{\chi}_1^0) + (jet + \tilde{\chi}_1^0)$ and the output will only contain constraints for this topology.
- **dataselector** (list of datasets): set to "all" to use all available data sets. If dataselector = upperLimit (efficiencyMap), only UL-type results (EM-type results) will be used. Furthermore, if a list of signal regions (data sets) is given, only the experimental results containing these datasets will be used. For instance, if dataselector = SRA mCT150, SRA mCT200, only these signal regions will be used. The signal regions are identified by the names assigned by the corresponding experimental analysis.

***printer*:** main options for the output format

- **outputType** (list of outputs): use to list all the output formats to be generated. Available output formats are: summary, stdout, log, python, xml, slha.

***stdout-printer*:** options for the stdout or log printer

- **printDatabase** (True/False): set to True to print the list of selected experimental results to stdout.
- **addAnaInfo** (True/False): set to True to include detailed information about the txnames tested by each experimental result. Only used if printDatabase=True.
- **printDecomp** (True/False): set to True to print basic information from the decomposition (topologies, total weights, ...).
- **addElementInfo** (True/False): set to True to include detailed information about the elements generated by the decomposition. Only used if printDecomp=True.
- **printExtendedResults** (True/False): set to True to print extended information about the theory predictions, including the PIDs of the particles contributing to the predicted cross section, their masses and the expected upper limit (if available).
- **addCoverageID** (True/False): set to True to print the list of element IDs contributing to each missing topology. Only used if testCoverage = True. This option should be used along with addElementInfo = True so the user can precisely identify which elements were classified as missing.

***summary-printer*:** options for the summary printer

- **expandedSummary** (True/False): set to True to include in the summary output all applicable experimental results, False for only the strongest one.

***python-printer*:** options for the Python printer

- **addElementList** (True/False): set to True to include in the Python output all information about all elements generated in the decomposition. If set to True the output file can be quite large.

***xml-printer*:** options for the xml printer

- **addElementList** (True/False): set to True to include in the xml output all information about all elements generated in the decomposition. If set to True the output file can be quite large.

Particle Definitions For non-MSSM (incl. non-SUSY) input models, the user needs to modify the input file `particles.py`, specifying which BSM particles are even or odd under the assumed $\mathbb{Z}_2$ symmetry. Finally, if the user wants to check the input files for possible issues using the included SLHA and LHE file checkers, it is also necessary to define the BSM particle quantum numbers in `particles.py`. Below we give only small examples of how the entries should be formatted. Odd particles are specified in the `rOdd` dictionary as shown below.

```
rOdd = {1000021 : "gluino",
        1000022 : "N1",
        1000023 : "N2"}
```

Note that only the PDG ids are used, the assigned names are irrelevant when running SModelS. Similarly even particles are defined in the `rEven` dictionary, a few entries are shown below.

```
rEven = {25 : "higgs",
        -25 : "higgs",
         24 : "W+",
        -24 : "W-"}
```

In contrast to the odd particle definitions, the `rEven` dictionary is used to map the elements to the experimental results in the database, and it is important that the naming follows SModelS conventions for all SM particles relevant to constrain the model. Finally the quantum nubers are defined in the `qNumbers` dictionary, an example entry is given below.

```
qNumbers={1000024:[1,3,1]}
```

Here for the example of the lighter chargino (PDG id 1000024) the quantum numbers are listed as [2 * spin, 3 * electric charge, color dimension].

C.2. Interface to micrOMEGAs

The relevant function for writing the input files is

```
smodels(Pcm, nf, csMinFb, fileName, wrt)
```

where `Pcm` is the proton beam energy in GeV and `nf` is the number of parton flavors used to compute the production cross sections of the $\mathbb{Z}_2$-odd particles. (Note that u, d, $\bar{u}$, $\bar{d}$ and gluons are always included while s, c, and b quarks are included for `nf` $= 3, 4, 5$ respectively.) `csMinFb` defines the minimum production cross section in pb for $\mathbb{Z}_2$-odd particles; processes with lower cross sections are not added to the SLHA file passed to SModelS, here denoted by `fileName`. Finally, `wrt` is a steering flag for the screen output; if `wrt` $\neq 0$ the computed cross sections will be also written on the screen. If the model contains a SM-like Higgs, it is automatically identified, and the `particles.py` is written accordingly. In that way, the relevant elements can be matched to experimental results considering Higgs final states. The SMS decomposition and confrontation against the LHC limits is executed via a system call,

```
./runSModelS.py -f fileName -o ./ -p parameters.ini -particles ./ -v error
```

where `-o` sets the directory for the output file, `-v` controls the level of SModelS output (only error messages will be printed in this example) and `parameters.ini` is the file that can be used to set the run parameters. Running SModelS with the default parameters will produce two output files in the selected directory, a text summary in `filename.smodels` and an SLHA-type output in `filename.smodelsslha`.

The SLHA-type output format was designed for the SModelS–`micrOMEGAs` interface, it consists of the blocks SModelS_Settings and SModelS_Exclusion specifying the settings and constraints, and the blocks SModelS_Missing_Topos, SModelS_Outside_Grid, SModelS_Long_Cascade and SModelS_Asymmetric_Branches detailing information about the coverage by simplified models. Below we give a description of each block together with a sample output corresponding to the file `mssm1.par` in the MSSM directory of `micrOMEGAs` .

- `SModelS_Settings` lists the SModelS code and database versions as well as input parameters for the decomposition. For example:

```
BLOCK SModelS_Settings
 0 v1.1.0patch1              #SModelS version
 1 1.1.0patch1               #database version
 2 0.2                       #maximum condition violation
 3 1                         #compression (0 off, 1 on)
 4 5.0                       #minimum mass gap for mass compression [GeV]
 5 0.03                      #sigmacut [fb]
```

- `SModelS_Exclusion` contains as the first line (the `0 0` entry) the status information if a point is excluded (1), not excluded (0), or not tested (-1). The latter can occur in scenarios with long-lived charged particles or in scenarios where no matching SMS results are found.

  If a point is excluded (status 1), this is followed by a list of all results with $r > 1$, sorted by their r values. For each of these results, the topology identifier in terms of TxNames (entry 0), the r value (entry 1), for EM type results the expected r value (entry 2), a measure of condition violation (entry 3), and the analysis identifier (entry 4) are listed. Entries 5, 6 and 7 are relevant only for EM type results, and specify the most sensitive signal region (used for limit setting), the χ^2 and the likelihood value respectively.

  If the point is not excluded (status 0), the result with the highest r value is given instead to show whether a point is close to the exclusion limit or not.

  In this example, the highest r value corresponds to a dijet+MET search constraining squark production, with $\tilde{q} \to q\tilde{\chi}_1^0$ obtained by ATLAS [213]. Note that only the first part of the file is reproduced.

```
BLOCK SModelS_Exclusion
 0 0 1          #output status (-1 not tested, 0 not excluded, 1 excluded)
 1 0 T2                   #txname
 1 1 6.155E+00            #r value
 1 2 7.077E+00            #expected r value
 1 3 0.00                 #condition violation
 1 4 ATLAS-SUSY-2013-02   #analysis
 1 5 SR4jl-               #signal region
 1 6 2.298E+01            #Chi2
 1 7 3.403E-08            #Likelihood

 2 0 T2                   #txname
 2 1 6.020E+00            #r value
 2 2 N/A                  #expected r value
 2 3 0.00                 #condition violation
 2 4 CMS-SUS-13-019       #analysis
 2 5 (UL)                 #signal region
 2 6 N/A                  #Chi2
 2 7 N/A                  #Likelihood
```

- `SModelS_Missing_Topos` lists up to ten missing topologies sorted by their weights ($\sigma \times \mathcal{B}$). Each entry consists of the line number, the $\sqrt{s}$ in TeV, the weight and a description of the topology in the SModelS bracket notation. Note that this information is useful mainly for points that are not excluded.

```
BLOCK SModelS_Missing_Topos #sqrts[TeV] weight[fb] description
 0 8  1.322E+03 [[[jet]],[[jet],[jet]]]
 1 8  3.294E+02 [[[b],[b]],[[jet]]]
 2 8  2.792E+02 [[],[[jet]]]
 3 8  2.532E+02 [[[b]],[[jet]]]
 4 8  2.445E+02 [[[jet]],[[t],[b],[W]]]
 5 8  2.274E+02 [[[b],[W]],[[b],[nu],[ta]]]
 6 8  1.087E+02 [[[jet]],[[jet],[jet],[jet]]]
 7 8  4.709E+01 [[[jet],[jet]],[[jet],[jet]]]
 8 8  4.241E+01 [[[jet]],[[jet],[W]]]
 9 8  3.205E+01 [[[jet]],[[jet],[W],[W]]]
```

The blocks `SModelS_Outside_Grid`, `SModelS_Long_Cascade` and `SModelS_Asymmetric_Branches` are similar to the `SModelS_Missing_Topos` block, see description of the summary output in Section 3.3.

APPENDIX

D

RÉSUMÉ FRANÇAIS

D.1. Introduction

Le Modèle Standard (MS) de la physique des particules, qui décrit la physique des particules élémentaires a été construit en tirant profit d'interactions entre physique expérimentale et théorique. À partir du postulat de l'existance des particules élémentaires composant l'ensemble de la matière, le MS, visant à décrire la nature par un modèle théorique consistant, a été construit petit à petit. De nombreux résultats expérimentaux ont souvent remis en cause les hypothese théoriques forcant le développement de nouveaux modèles en accord avec les observations. Chacun des ces modeles doit nécessairement être en mesure de faire des prédictions testables expérimentalement. Ainsi, alors que les observations expérimentales guident le développement de théories plus complètes, les prédictions théoriques participent également au développement et à l'interprétation de nouvelles expériences. C'est ce va-et-vient continuel qui apporte une compréhension plus intime de la nature. Parmi les nombreux exemples présents en physique des particules, le développement de la théorie des interactions électro-faible est à noter.

Dans le chapitre introductif, nous introduisons le MS dans ce contexte en décrivant les tests expérimentaux qui ont mené à établir le MS comme le standard de la physique des particule élémentaires. De nombreux éléments définissant le MS apportent une motivation au développement des extensions. Nous discutons des défauts du MS, puis de possibles extensions qui les résolvent. Nous nous concentrons en particulier sur des modèles supersymétriques (SUSY) qui font l'objet d'une grande partie de cette thèse. Le but de cette thèse est de tirer profit des liens forts entre physique des particules expérimentale et théorique. Ces liens deviennent en effet plus ténus à mesure que les techniques expérimentales deviennent de plus en plus sophistiquées, et que les théoriciens considèrent des modèles de plus en plus complexes avec un grand nombre de paramètres libres (afin de résoudre les problèmes du MS sans toutefois en altérer les succès établis avec grande précision). Compte tenu de ces développements, il est important de mettre en place des méthodes et outils spécialisés permettant de relier les paramètres d'un modèle aux données expérimentales.

Ce travail de thèse est dédié aux tests de modèles de physique des particules à l'aide des collisions haute énergie se déroulant au Grand Collisionneur de Hadrons (LHC), dans le cadre de modèles dit simplifiés (ou spectres de modèles simplifiés SMS). Les SMS ont été proposés dans le but de minimiser la dépendance du modèle, tout en capturant les caractéristiques principales nécessaires à la détection. Ainsi ils peuvent guider les stratégies de recherche en collisionneur sans introduire de grand biais théorique. D'autre part, les résultats

obtenus dans ce contexte peuvent être aisément interprétés dans un grand nombre de modèles génériques, ce qui permet une compréhension efficace des observations expérimentales. La thèse est organisée comme suit. Nous décrivons en premier lieu la stratégie et l'interprétation des recherches au LHC dans le chapitre 2, où les modèles simplifiés seront introduits en détail. De plus, diverses approches de la réinterprétation des recherches du LHC sont discutées, ainsi que les outils nécessaires. Dans le chapitre 3, nous nous concentrons sur SModelS, un outil de réinterprétation basé sur le concept de SMS. Dans le chapitre 4 nous discutons des hypothèses permettant de traduire les interprétations dans des modèles simplifiés dans le cadre de modèles génériques, et montrons qu'elles sont valides dans des cas d'intérêt particuliers. Dans le chapitre 5, nous illustrons comment contraindre un modèle générique à l'aide de SModelS. Alors que la plus grande partie de ces travaux sont concentrés sur les SMS inspirés de modèles supersymétriques, nous étudions une description minimale à l'aide de modèle simplifié de la recherche de matière noire dans le chapitre 6. Quelques remarques finales sont présentées dans le chapitre 7.

D.2. Sommaire des Chapitres

D.2.1. Chapitre 2 – Recherche au LHC et interprétation

Ce chapitre présente des tests expérimentaux des extensions du MS, en particulier dans les expériences à haute énergie et dans les collisions de hadrons. La première partie décrit les éventuels signaux de SUSY ainsi que les canaux de production et de désintégration les plus importants. En conséquence de la parité R les partenaires SUSY des particules MS sont toujours produites en paires, et la désintégration finit toujours par une désintégration en partenaire SUSY le plus léger (LSP). Grace à leurs interactions fortes, les partenaires SUSY avec charge de couleur sont produit abondamment s'ils sont légers. S'ils sont lourds ce les sont les canaux électrofaible qui deviennet les plus importants. Par conséquent, la désintégration des partenaires SUSY résulte typiquement en une signature avec plusieurs jets et/ou leptons très énergétiques, et le LSP qui échappe à la détection.

La deuxième partie examine les différentes stratégies pour chercher un signal de nouvelle physique, en particulier en faisant la différence entre la recherche de nouvelles résonances et la recherche des nouvelle particules invisibles, i.e un candidat de matière noire. L'interprétation des recherches SUSY est discutée en détail, en particulier dans le contexte des SMS, et un court résumé des résultats récents du LHC est donné. La dernière partie de ce chapitre contient une synthèse des méthodes pour la réinterprétation des résultats de ces recherches dans des modèles génériques.

D.2.2. Chapitre 3 – SModelS

Après l'introduction des différentes méthodes de réinterprétation au chapitre 2, ce chapitre discute la réinterprétation des résultats SMS. Cette méthode permet une evaluation rapide mais conservative des contraintes obtenues par les recherches du LHC. Elle est donc particulièrement intéressante pour l'identification de régions permises ou exclues de l'espace des paramètres, ou pour rejeter rapidement des combinaisons de paramètres exclus avant une étude plus détaillée. De plus, il est possible d'identifier les recherches et signatures les plus sensibles, ainsi que des signatures importantes qui n'ont pas encore été considérées. Un avantage supplémentaire est le grand nombre de résultats SMS disponibles, ils sont en effet utilisés abondamment par ATLAS et CMS. On peut utiliser les SMS pour tester une grande

classe de modèles au-delà du MS, non limités aux modèles SUSY. En particulier l'outil SModelS [204] permet, indépendamment des détails du modèle, une décomposition permettant d'attribuer à un modèle générique possedant une symétrie $\mathbb{Z}_2$, une liste de SMS généralisés. Après la décomposition, SModelS effectue une comparaison automatique avec tous les résultats SMS inclus dans la base de données. De plus, SModelS donne une information sur les topologies qui ne sont pas couvertes par les résultats actuellement disponibles. Dans ce chapitre, les concepts principaux de la description utilisé par SModelS sont introduits. Ensuite, la procédure de décomposition et la comparaison avec les résultats sont présentés. Une courte présentation de l'utilisation du code est donnée. Finalement, des remarques sur la généralité de l'approche et des perspectives sont données.

D.2.3. Chapitre 4 – Validité de l'approche modèles simplifiés

Sous l'hypothèse SMS inspirée par la description OSET et décrite aux chapitres 2 et 3, SModelS peut être utilisé pour tester des modèles qui prédisent les même topologies que les signatures SUSY. Par exemple on peut tester des scénarios génériques MSSM, des modèles SUSY élargis ou des scénarios UED qui prédisent en général des signatures de type SUSY avec des particules de spin différents.

Dans ce chapitre nous présentons des tests de l'hypothèse SMS pour quelques signatures et topologies simples. On discute en premier lieu la signature double-jet $+E_T^{\mathrm{miss}}$ et l'interprétation en modèle simplifié squark-neutralino, en référence à la dépendance du mode de production et à la dépendance du spin. L'échange d'un gluino peut être important si le gluino n'est pas découplé, ce qui n'est pas considéré dans l'interprétation SMS standard. Si la cinématique de ces événements est très différente par rapport à celle des événements standards, l'application des résultats n'est pas valide pour les scénarios avec un gluino léger. La dépendance du spin est testé par une comparaison entre le modèle simplifié squark-neutralino et un scénario UED correspondant.

Ensuite une étude de la dépendance du spin est présenté pour la signature $t\bar{t} + E_T^{\mathrm{miss}}$. On considère d'un côté un modèle simplifié stop-neutralino et de l'autre un partenaire fermionique du top, avec désintégration vers un candidat de matière noire scalaire ou vecteur. De plus, on tient compte de la polarisation du top à l'état final. Les recherches avec zéro, un ou deux leptons dans état final sont considérés. La discussion se base sur [208], publié dans JHEP en novembre 2016.

Finalement une étude de la dépendance du spin pour la signature double-lepton $+E_T^{\mathrm{miss}}$ est présentée. Une comparison entre un modèle simplifié chargino-sneutrino et un modèle simplifié slepton-neutralino est effectuée. Le modèle simplifié chargino-sneutrino est relevant pour des modèles avec un LSP sneutrino, par exemple le MSSM+RN.

D.2.4. Chapitre 5 – Restreindre les modèles supersymétriques

La supersymétrie propose une solution à plusieurs questions ouvertes en physique des particules. Pour une solution supersymétrique du problème de la hiérarchie, on s'attend à ce que les partenaires SUSY aient une masse autour de l'échelle faible, en particulier les stops, gluinos et higgsinos doivent être légers. De plus, la masse du neutralino doit être de l'ordre du TeV ou en-deçà pour décrire la matière noire.

Dans le chapitre 2 nous avons discuté les méthodes pour la recherche des partenaires SUSY à l'échelle du TeV, en particulier par les expériences au LHC, mais nous avons également noté que plusieurs contraintes additionnelles peuvent être importantes. La physique

des secteurs Higgs et électro-faible offrent des tests importants des modèles SUSY ainsi qu'indirectement le secteur de la saveur. Finalement, les observations dans le secteur de la matière noire, la prédiction de la densité relique et les limites des recherches directes et indirectes, sont cruciales.

Une étude complète de l'espace des paramètres d'un modèle SUSY comprend donc plusieurs tests. En général il est rapide de confronter le modele aux observables de matière noire, du Higgs ou de la saveur contrairement aux observables liées aux recherches directes de particules SUSY au LHC. D'une part il est donc opportun d'analyser la phénoménologie au LHC seulement pour les scénarios compatible avec cette première catégorie d'observables. D'autre part, afin de sonder de grands espaces de paramètres, il est important de tester les contraintes LHC de manière efficace, ce qui détermine le nombre de points testé avec les resources disponibles. La réinterprétation des résultats SMS est adaptée pour obtenir une vision globale. Plusieurs études ont utilisé SModelS ou Fastlim pour tester les paramètres du MSSM, de plus SModelS peut être utilisé au-delá de ces modèles.

Dans ce chapitre nous utilisons SModelS pour tester les paramètres du MSSM et de quelques unes de ces extensions. En premier lieu, nous effectuons une comparaison entre les résultats obtenus par l'approche SMS et par une simulation des événements dans le détecteur dans le cas du pMSSM. Nous montrons l'amélioration de la couverture de l'espace des paramètres par les résultats SMS lorsque les cartes d'efficacité sont prises en compte. Pour les scénarios avec un gluino léger, nous discutons l'importance des topologies avec des branches asymétriques. Ensuite, nous examinons les contraintes sur le modèle MSSM+RN. La discussion se base sur [72], publié dans JHEP en mai 2015. Finalement les contraintes sur le modèle UMSSM sont discutées. La discussion se base sur [92], publié dans JHEP en septembre 2015.

D.2.5. Chapitre 6 – Modèles simplifiés pour la recherche de la matière noire au LHC

Jusqu'à présent nous avons considéré les modèles SUSY et les SMS à partir d'une description du MSSM. La recherche de partenaires SUSY est motivée par le problème de la hiérarchie et la possibilité d'un candidat SUSY à la matière noire. Cependant, les résultats nuls du LHC nous motivent à considérer également des scénarios plus minimaux, décrivant seulement la matière noire, sans mention du problème de la hiérarchie. Un signal de matière noire peut être observé si les particules invisibles sont produites en association avec des particules visibles du MS. Par exemple un jet ou photon émis par l'état initial, on parle de recherches mono-X. Notons une différence fondamentale entre l'interprétation d'une recherche mono-X et des recherches SUSY puisque le signal est déterminé par l'émission d'une particule MS par l'état initial, l'interprétation est nécessairement fonction du processus de production, et l'hypothèse SMS n'est pas valide.

En conséquence, l'interprétation des recherches mono-X se fait grâce à une description effective des interactions entre les particules impliquées. La description minimale est en terme d'opérateurs effectifs, supprimé par une échelle de nouvelle physique. Il s'agit d'une méthode très efficace pour l'interprétation (avec seulement deux paramètres libres), mais sa validité est limitée.

Pour cette raison, une approche à base de modèles simplifiés pour la recherche de la matière noire au LHC a été développé, celle-ci décrit de façon explicite l'interaction par un médiateur. On peut classifier les modèles simplifiés par le spin et la forme du couplage du médiateur, comme les modèles (pseudo)scalaire et (axial)vecteur par exemple. Dans ce

chapitre nous discutons un modèle avec médiateur de spin-2 et une particule de matière noire scalaire, fermionique ou vecteur. La discussion se base sur [386].

D.3. Conclusion

L'interprétation des recherches au LHC pour la nouvelle physique dépend des paramètres libres du modèle considéré, potentiellement un grand nombre. De plus, la connexion entre ces paramètres et les observables LHC est typiquement très compliquée. Dans cette thèse nous avons examiné jusqu'à quel point les modèles simplifiés sont utiles dans l'interprétation des recherches LHC pour la nouvelle physique, en particulier celles avec un candidat de matière noire. Les SMS facilitent la communication entre la description théorique et l'observation expérimentale, et permettent une interprétation intuitive des résultats LHC dans une description basée sur les signatures. En plus de leur attrait conceptuel, ils permettent une réinterprétation rapide dans le cadre de modèles génériques. D'ailleurs, les recherches des partenaires SUSY sont d'ordinaire interprétés en contexte SMS, et depuis le Run 2 du LHC celles de matière noire sont également le plus souvent interprétées en termes de modèles simplifiés.

Pour tirer profit au maximum des résultats SMS disponibles, des outils sophistiqués sont nécessaires. Par exemple, l'outil SModelS transpose les modèles génériques en SMS et permet de les confronter rapidement et de façon automatisé à un grand nombre de résultats LHC. SModelS fonctionne pour tout modèle avec une nouvelle symétrie $\mathbb{Z}_2$, il suffit de déclarer les nouvelles particules comme paire ou impaire sous cette symétrie. Pour tous les scénarios considérés dans cette thèse nous avons trouvé que l'hypothèse SMS est approximativement valide, et les différences en efficacité et en limite d'exclusion sont typiquement au plus d'environ 20%. Les différences sont plus grandes si la radiation de l'état initial est importante, par exemple dans les scénarios comprimés ou dans une recherche générique en état final multi-jet $+E_T^{\text{miss}}$ même si les différence en terme de limites sur la masse sont négligeables. Les outils de réinterprétation basés sur une simulation des évènements peuvent être utilisés pour améliorer la précision dans ces cas.

Concrètement nous avons trouvé que les recherches pour les partenaires SUSY des quarks peuvent également être utilisé pour tester les partenaires fermioniques, par exemple ceux présents dans les scénarios UED. Comme la section efficace est plus grande pour les partenaires fermioniques, une extension des résultats aux masses plus élevées permettait des contraintes additionnelles. De la même façon, une extension des interprétations des recherches pour les sleptons permettait des contraintes additionnelles pour la production des charginos dans le MSSM+RN.

Nous avons présenté trois études phénoménologiques utilisant SModelS. En plus des limites d'exclusion, SModelS peut être également utilisé pour établir les topologies qui permettraient d'améliorer la couverture de l'espace des paramètres, on les appelle topologies manquantes. Par exemple pour le pMSSM nous avons trouvé que 50-60% des scénarios exclus par ATLAS dans une étude avec évènements simulés sont aussi exclus si nous utilisons seulement les résultats SMS. Nous avons déterminé qu'en particulier les topologies avec des branches asymétriques sont nécessaires pour améliorer la couverture de l'espace des paramètres. De plus de nombreuses topologies manquantes apparaissent si le gluino et les squarks sont légers. Nous pouvons utiliser les outils pour la réinterprétation basée sur la simulation des évènements pour ajouter de nouvelles topologies dans la base de données de SModelS et ce pour toutes les topologies couvertes par les recherches actuelles. Par ailleurs, les topologies représentant des désintégrations longues, pour lesquelles une interprétation SMS n'est plus utile, sont rarement importantes.

Nous avons utilisé SModelS pour imposer des limites sur les modèles MSSM+RN et UMSSM, et nous avons trouvé que les scénarios avec un sneutrino LSP sont souvent fortement contraints par les résultat SMS disponibles. En particulier les interprétations des recherches pour les sleptons peuvent être utilisées pour contraindre un modèle simplifié chargino-sneutrino, et excluent des scénarios avec un chargino léger. Une topologie manquante importante a été identifiée: la production associée de chargino et neutralino, produisant une signature avec mono-lepton. Cette signature a un important bruit de fond MS et elle n'est pas testée par les recherches existantes. Le même état final est possible dans le UMSSM, avec la signature mono-W. Les scénarios avec un sneutrino LSP dans le UMSSM sont testés avec les résultats SMS disponibles seulement si un neutralino intermédiaire est le LSP effectif. Dans les autres cas, les produits de désintégration vers un sneutrino droit incluent toujours des neutrinos additionels dans l'état final et par consequent menent à une limite d'exclusion différente puisuqe la cinématique de l'évènement est différente.

Pour le scénarios avec un neutralino LSP dans le UMSSM nous avons trouvé que les résultats SMS sont souvent inefficaces pour contraindre les paramètres du modèle, même si le gluino et/ou les squarks sont légers. Les raisons sont similaires à celles discutés pour le pMSSM, en particulier parce que les résultats pour les topologies asymétriques ne sont pas disponibles dans la première version de SModelS. Une amélioration similaire à celle illustrée dans le cadre du pMSSM est attendue si l'on utilise la dernière version de SModelS.

Pour les scénarios avec neutralino ou sneutrino LSP nous avons trouvé que les recherches de particules de longue durée de vie sont souvent importantes. En effet, lorsque la LSP est principalement un wino ou higgsino, un chargino de longue durée de vie est probable. Les recherches pour un vertex déplacé ou pour une trace chargée donnent des contraintes importantes. Si le LSP est un sneutrino, nous avons trouvé que le gluino est souvent de longue vie, même si les squarks ne sont pas complètement découplés. À cause de leur grande section efficace de production, la plupart des scénarios discutés dans cette thèse ont été depuis exclus surtout lorsqu'on ne tient pas compte des grandes incertitudes provenant de la modélisation des R-hadrons. En général les recherches de particules à longue durée de vie ont suscitées beaucoup d'intérêt récemment, elles sont discutées dans le groupe de travail LHC LLP.

Concernant l'interprétation des recherches LHC pour la matière noire en termes des modèles simplifiés nous avons étudié en particulier des scénarios avec un médiateur de spin-2. Nous avons trouvé que le scénario avec un couplage universel est fortement limité par les recherches de nouvelles résonances. Alternativement il est possible de considérer des scénarios de type bulk-RS, dans lesquels le médiateur interagit en priorité avec les particules lourdes. Ce genre des scénarios est très different du scénario couplage universel considéré dans cette thèse. Premièrement parce que la section efficace est beaucoup plus petite, et les canaux primordiaux sont la fusion de bosons vecteurs et la boucle de quarks top. De plus, pour une étude complète, il faut aussi prendre en compte les excitations Kaluza-Klein des bosons vecteurs. Ces scénarios sont actuellement étudiés.

Les dernières limites d'exclusion du LHC sont déjà proches des limites projetées des Run 2 et 3 du LHC. Néanmoins l'objectif est de maximiser l'utilité des résultats LHC disponibles, ce qui implique une interaction proche entre les théoriciens et les expérimentateurs ainsi que des outils sophistiqués pour la réinterprétation. La réinterprétation permet de comprendre au mieux les implications des résultats, et d'identifier des signatures intéressantes et de proposer de nouvelles recherches.

Comme aucun nouveau signal n'a été observé par le LHC jusqu'à maintenant, l'analyse dans cette thèse est en termes des contraintes et limites. On note cependant que les mêmes

outils peuvent être utilisés pour l'interprétation d'un signal. Les SMS offrent une approche bottom-up, permettant d'obtenir les paramètres de modèles simplifiés. Les outils basés sur la simulation d'évènements peuvent être utilisés en complement pour tester plus à fond des modèles plus complète. Il sera aussi important de vérifier que la description d'un nouveau signal est en cohérence avec les autres résultats disponibles et de prendre en compte simultanéments les résultats positifs et négatifs.

Le développements d'outils pour la réinterprétation des résultats du LHC et le grand nombre de recherches comptabilisées ont contribués à intensifier les interactions entre expérimentalistes et phénoménologistes. Les effort de réinterprétation des résultats du LHC ont été coordonnés récemment dans le cadre de workshops sur la réinterprétation des résultats au CERN. De plus une description standardisée des recherches LHC est discutée, et une proposition a été présentée sous le nom de "Les Houches Analysis Description Accord Proposal". En plus des recherches directes, le Run 2 du LHC fournira aussi de nouvelles mesures précises des processus Higgs et MS. Ces résultats peuvent être utilisés pour tester les modèles de nouvelle physique. En outre, les recherches directes pour la matière noire sont souvent complémentaires aux recherches LHC, et testeront une grande partie des paramètres intéressants pour la matière noire supersymétrique dans les prochaines années.

Pour obtenir une vue globale du statut d'un certain modèle, une fit globale doit prendre en compte toutes les mesures et contraintes disponibles pour obtenir une fonction de probabilité totale. Cet objectif requiert de nombreux outils pour calculer toutes les observables relevantes, conjointement avec une méthode statistique pour sélectionner les paramètres et pour l'interprétation des résultats. Notons que l'évaluation rapide des contraintes LHC est important, et les fits globales profitent de nouvelle méthodes d'apprentissage automatique, mais également de la réinterprétation des résultats SMS.

Les solutions les plus naturelles du problème de la hiérarchie et du paradigme WIMP seront testés plus avant dans les prochaines années tant au collisionneurs que par les recherches directes de matière noire. Pour maximiser l'exploitation des données, une interaction entre la physique théorique et expérimentale est primordiale. Dans cette thèse nous proposons une description en termes de modèles simplifiés pour faciliter cette interaction, permettant de comprendre les résultats du LHC de façon indépendante du modèle concret, et également pour étudier leur impact sur les modèles génériques.

BIBLIOGRAPHY

[1] T. W. B. Kibble, "History of electroweak symmetry breaking," *J. Phys. Conf. Ser.* **626** no. 1, (2015) 012001, arXiv:1502.06276 [physics.hist-ph].

[2] J. Chadwick, "The intensity distribution in the magnetic spectrum of beta particles from radium (B + C)," *Verh. Phys. Gesell.* **16** (1914) 383–391.

[3] E. Fermi, "An attempt of a theory of beta radiation. 1.," *Z. Phys.* **88** (1934) 161–177.

[4] R. P. Feynman and M. Gell-Mann, "Theory of the fermi interaction," *Phys. Rev.* **109** (Jan, 1958) 193–198. http://link.aps.org/doi/10.1103/PhysRev.109.193.

[5] E. C. G. Sudarshan and R. E. Marshak, "Chirality invariance and the universal fermi interaction," *Phys. Rev.* **109** (Mar, 1958) 1860–1862. http://link.aps.org/doi/10.1103/PhysRev.109.1860.2.

[6] S. L. Glashow, "Partial Symmetries of Weak Interactions," *Nucl. Phys.* **22** (1961) 579–588.

[7] J. Goldstone, A. Salam, and S. Weinberg, "Broken Symmetries," *Phys. Rev.* **127** (1962) 965–970.

[8] F. Englert and R. Brout, "Broken symmetry and the mass of gauge vector mesons," *Phys. Rev. Lett.* **13** (Aug, 1964) 321–323. http://link.aps.org/doi/10.1103/PhysRevLett.13.321.

[9] P. W. Higgs, "Broken symmetries, massless particles and gauge fields," *Phys. Lett.* **12** (1964) 132–133.

[10] P. W. Higgs, "Broken Symmetries and the Masses of Gauge Bosons," *Phys. Rev. Lett.* **13** (1964) 508–509.

[11] G. S. Guralnik, C. R. Hagen, and T. W. B. Kibble, "Global conservation laws and massless particles," *Phys. Rev. Lett.* **13** (Nov, 1964) 585–587. http://link.aps.org/doi/10.1103/PhysRevLett.13.585.

[12] S. Weinberg, "A Model of Leptons," *Phys. Rev. Lett.* **19** (1967) 1264–1266.

[13] G. 't Hooft, "Renormalizable Lagrangians for Massive Yang-Mills Fields," *Nucl. Phys.* **B35** (1971) 167–188.

[14] O. W. Greenberg, "Spin and Unitary Spin Independence in a Paraquark Model of Baryons and Mesons," *Phys. Rev. Lett.* **13** (1964) 598–602.

[15] M. Y. Han and Y. Nambu, "Three Triplet Model with Double SU(3) Symmetry," *Phys. Rev.* **139** (1965) B1006–B1010.

[16] H. Fritzsch, M. Gell-Mann, and H. Leutwyler, "Advantages of the Color Octet Gluon Picture," *Phys. Lett.* **B47** (1973) 365–368.

[17] J. C. Collins, D. E. Soper, and G. F. Sterman, "Factorization of Hard Processes in QCD," *Adv. Ser. Direct. High Energy Phys.* **5** (1989) 1–91, arXiv:hep-ph/0409313 [hep-ph].

[18] **Gargamelle Neutrino** Collaboration, F. J. Hasert *et al.*, "Observation of Neutrino Like Interactions Without Muon Or Electron in the Gargamelle Neutrino Experiment," *Phys. Lett.* **46B** (1973) 138–140.

[19] **UA1** Collaboration, G. Arnison *et al.*, "Experimental Observation of Isolated Large Transverse Energy Electrons with Associated Missing Energy at s**(1/2) = 540-GeV," *Phys. Lett.* **122B** (1983) 103–116. [,611(1983)].

[20] **UA2** Collaboration, M. Banner *et al.*, "Observation of Single Isolated Electrons of High Transverse Momentum in Events with Missing Transverse Energy at the CERN anti-p p Collider," *Phys. Lett.* **122B** (1983) 476–485.

[21] M. Kobayashi and T. Maskawa, "CP Violation in the Renormalizable Theory of Weak Interaction," *Prog. Theor. Phys.* **49** (1973) 652–657.

[22] M. L. Perl *et al.*, "Evidence for Anomalous Lepton Production in e+ - e- Annihilation," *Phys. Rev. Lett.* **35** (1975) 1489–1492.

[23] S. W. Herb *et al.*, "Observation of a Dimuon Resonance at 9.5-GeV in 400-GeV Proton-Nucleus Collisions," *Phys. Rev. Lett.* **39** (1977) 252–255.

[24] **CDF** Collaboration, F. Abe *et al.*, "Observation of top quark production in $\bar{p}p$ collisions," *Phys. Rev. Lett.* **74** (1995) 2626–2631, arXiv:hep-ex/9503002 [hep-ex].

[25] **D0** Collaboration, S. Abachi *et al.*, "Search for high mass top quark production in $p\bar{p}$ collisions at $\sqrt{s} = 1.8$ TeV," *Phys. Rev. Lett.* **74** (1995) 2422–2426, arXiv:hep-ex/9411001 [hep-ex].

[26] M. Baak, M. Goebel, J. Haller, A. Hoecker, D. Ludwig, K. Moenig, M. Schott, and J. Stelzer, "Updated Status of the Global Electroweak Fit and Constraints on New Physics," *Eur. Phys. J.* **C72** (2012) 2003, arXiv:1107.0975 [hep-ph].

[27] J. F. Gunion, H. E. Haber, G. L. Kane, and S. Dawson, "The Higgs Hunter's Guide," *Front. Phys.* **80** (2000) 1–404.

[28] **ATLAS** Collaboration, G. Aad *et al.*, "Observation of a new particle in the search for the Standard Model Higgs boson with the ATLAS detector at the LHC," *Phys.Lett.* **B716** (2012) 1–29, arXiv:1207.7214 [hep-ex].

[29] **CMS** Collaboration, S. Chatrchyan *et al.*, "Observation of a new boson at a mass of 125 GeV with the CMS experiment at the LHC," *Phys.Lett.* **B716** (2012) 30–61, arXiv:1207.7235 [hep-ex].

[30] G. Panico and A. Wulzer, "The Composite Nambu-Goldstone Higgs," *Lect. Notes Phys.* **913** (2016) pp.1–316, arXiv:1506.01961 [hep-ph].

[31] S. Weinberg, "Baryon- and lepton-nonconserving processes," *Phys. Rev. Lett.* **43** (Nov, 1979) 1566–1570. http://link.aps.org/doi/10.1103/PhysRevLett.43.1566.

[32] R. N. Mohapatra and A. Y. Smirnov, "Neutrino Mass and New Physics," *Ann. Rev. Nucl. Part. Sci.* **56** (2006) 569–628, arXiv:hep-ph/0603118 [hep-ph].

[33] H. Georgi and S. L. Glashow, "Unity of all elementary-particle forces," *Phys. Rev. Lett.* **32** (Feb, 1974) 438–441. http://link.aps.org/doi/10.1103/PhysRevLett.32.438.

[34] S. P. Martin, "A Supersymmetry primer," arXiv:hep-ph/9709356 [hep-ph]. [Adv. Ser. Direct. High Energy Phys.18,1(1998)].

[35] F. Zwicky, "Die Rotverschiebung von extragalaktischen Nebeln," *Helv. Phys. Acta* **6** (1933) 110–127. [Gen. Rel. Grav.41,207(2009)].

[36] V. C. Rubin and W. K. Ford, Jr., "Rotation of the Andromeda Nebula from a Spectroscopic Survey of Emission Regions," *Astrophys. J.* **159** (1970) 379–403.

[37] K. Freese, "Review of Observational Evidence for Dark Matter in the Universe and in upcoming searches for Dark Stars," *EAS Publ. Ser.* **36** (2009) 113–126, arXiv:0812.4005 [astro-ph].

[38] **Planck** Collaboration, P. A. R. Ade *et al.*, "Planck 2015 results. XIII. Cosmological parameters," *Astron. Astrophys.* **594** (2016) A13, arXiv:1502.01589 [astro-ph.CO].

[39] M. Markevitch, A. H. Gonzalez, D. Clowe, A. Vikhlinin, L. David, W. Forman, C. Jones, S. Murray, and W. Tucker, "Direct constraints on the dark matter self-interaction cross-section from the merging galaxy cluster 1E0657-56," *Astrophys. J.* **606** (2004) 819–824, arXiv:astro-ph/0309303 [astro-ph].

[40] M. Milgrom, "A Modification of the Newtonian dynamics as a possible alternative to the hidden mass hypothesis," *Astrophys. J.* **270** (1983) 365–370.

[41] E. P. Verlinde, "Emergent Gravity and the Dark Universe," arXiv:1611.02269 [hep-th].

[42] F. Lelli, S. S. McGaugh, and J. M. Schombert, "Testing Verlinde's Emergent Gravity with the Radial Acceleration Relation," *Mon. Not. Roy. Astron. Soc.* **468** (2017) L68, arXiv:1702.04355 [astro-ph.GA].

[43] A. Hees, B. Famaey, and G. Bertone, "Emergent gravity in galaxies and in the Solar System," *Phys. Rev.* **D95** no. 6, (2017) 064019, arXiv:1702.04358 [astro-ph.GA].

[44] G. Belanger, F. Boudjema, A. Pukhov, and A. Semenov, "micrOMEGAs 3: A program for calculating dark matter observables," *Comput.Phys.Commun.* **185** (2014) 960–985, arXiv:1305.0237 [hep-ph].

[45] M. Backovic, K. Kong, and M. McCaskey, "MadDM v.1.0: Computation of Dark Matter Relic Abundance Using MadGraph5," *Physics of the Dark Universe* **5-6** (2014) 18–28, arXiv:1308.4955 [hep-ph].

[46] P. Gondolo, J. Edsjo, P. Ullio, L. Bergstrom, M. Schelke, and E. A. Baltz, "DarkSUSY: Computing supersymmetric dark matter properties numerically," *JCAP* **0407** (2004) 008, arXiv:astro-ph/0406204 [astro-ph].

[47] A. Arbey and F. Mahmoudi, "SuperIso Relic: A Program for calculating relic density and flavor physics observables in Supersymmetry," *Comput. Phys. Commun.* **181** (2010) 1277–1292, arXiv:0906.0369 [hep-ph].

[48] T. Marrodán Undagoitia and L. Rauch, "Dark matter direct-detection experiments," *J. Phys.* **G43** no. 1, (2016) 013001, arXiv:1509.08767 [physics.ins-det].

[49] **XENON** Collaboration, E. Aprile *et al.*, "First Dark Matter Search Results from the XENON1T Experiment," arXiv:1705.06655 [astro-ph.CO].

[50] **Fermi-LAT** Collaboration, M. Ackermann *et al.*, "Searching for Dark Matter Annihilation from Milky Way Dwarf Spheroidal Galaxies with Six Years of Fermi Large Area Telescope Data," *Phys. Rev. Lett.* **115** no. 23, (2015) 231301, arXiv:1503.02641 [astro-ph.HE].

[51] J. M. Gaskins, "A review of indirect searches for particle dark matter," *Contemp. Phys.* **57** no. 4, (2016) 496–525, arXiv:1604.00014 [astro-ph.HE].

[52] G. Belanger, F. Boudjema, A. Pukhov, and A. Semenov, "Dark matter direct detection rate in a generic model with micrOMEGAs 2.2," *Comput. Phys. Commun.* **180** (2009) 747–767, arXiv:0803.2360 [hep-ph].

[53] G. Belanger, F. Boudjema, P. Brun, A. Pukhov, S. Rosier-Lees, P. Salati, and A. Semenov, "Indirect search for dark matter with micrOMEGAs2.4," *Comput. Phys. Commun.* **182** (2011) 842–856, arXiv:1004.1092 [hep-ph].

[54] M. Backovic, A. Martini, O. Mattelaer, K. Kong, and G. Mohlabeng, "Direct Detection of Dark Matter with MadDM v.2.0," *Phys. Dark Univ.* **9-10** (2015) 37–50, arXiv:1505.04190 [hep-ph].

[55] R. K. Kaul, "Gauge Hierarchy in a Supersymmetric Model," *Phys. Lett.* **B109** (1982) 19–24.

[56] H. Baer and X. Tata, *Weak scale supersymmetry: From superfields to scattering events*. Cambridge University Press, 2006. http://www.cambridge.org/9780521290319.

[57] P. Z. Skands, B. Allanach, H. Baer, C. Balazs, G. Belanger, *et al.*, "SUSY Les Houches accord: Interfacing SUSY spectrum calculators, decay packages, and event generators," *JHEP* **0407** (2004) 036, arXiv:hep-ph/0311123 [hep-ph].

[58] N. Arkani-Hamed, A. Delgado, and G. F. Giudice, "The Well-tempered neutralino," *Nucl. Phys.* **B741** (2006) 108–130, arXiv:hep-ph/0601041 [hep-ph].

[59] G. Jungman, M. Kamionkowski, and K. Griest, "Supersymmetric dark matter," *Phys. Rept.* **267** (1996) 195–373, arXiv:hep-ph/9506380 [hep-ph].

[60] H. Baer, V. Barger, and H. Serce, "SUSY under siege from direct and indirect WIMP detection experiments," *Phys. Rev.* **D94** no. 11, (2016) 115019, arXiv:1609.06735 [hep-ph].

[61] **MSSM Working Group** Collaboration, A. Djouadi *et al.*, "The Minimal supersymmetric standard model: Group summary report," in *GDR (Groupement De Recherche) - Supersymetrie Montpellier, France, April 15-17, 1998*. 1998. arXiv:hep-ph/9901246 [hep-ph]. http://inspirehep.net/record/481987/files/arXiv:hep-s$_\beta$ph_9901246.pdf.

[62] M. Papucci, J. T. Ruderman, and A. Weiler, "Natural SUSY Endures," *JHEP* **09** (2012) 035, arXiv:1110.6926 [hep-ph].

[63] J. A. Casas, J. M. Moreno, S. Robles, K. Rolbiecki, and B. Zaldivar, "What is a Natural SUSY scenario?," *JHEP* **06** (2015) 070, arXiv:1407.6966 [hep-ph].

[64] N. Arkani-Hamed, L. J. Hall, H. Murayama, D. R. Smith, and N. Weiner, "Small neutrino masses from supersymmetry breaking," *Phys. Rev.* **D64** (2001) 115011, hep-ph/0006312.

[65] F. Borzumati and Y. Nomura, "Low scale seesaw mechanisms for light neutrinos," *Phys.Rev.* **D64** (2001) 053005, arXiv:hep-ph/0007018 [hep-ph].

[66] T. Asaka, K. Ishiwata, and T. Moroi, "Right-handed sneutrino as cold dark matter," *Phys. Rev.* **D73** (2006) 051301, hep-ph/0512118.

[67] F. Deppisch and A. Pilaftsis, "Thermal Right-Handed Sneutrino Dark Matter in the F(D)-Term Model of Hybrid Inflation," *JHEP* **0810** (2008) 080, arXiv:0808.0490 [hep-ph].

[68] D. G. Cerdeno and O. Seto, "Right-handed sneutrino dark matter in the NMSSM," *JCAP* **0908** (2009) 032, arXiv:0903.4677 [hep-ph].

[69] S. Khalil, H. Okada, and T. Toma, "Right-handed Sneutrino Dark Matter in Supersymmetric B-L Model," *JHEP* **1107** (2011) 026, arXiv:1102.4249 [hep-ph].

[70] K.-Y. Choi and O. Seto, "A Dirac right-handed sneutrino dark matter and its signature in the gamma-ray lines," *Phys.Rev.* **D86** (2012) 043515, arXiv:1205.3276 [hep-ph].

[71] C. Arina and N. Fornengo, "Sneutrino cold dark matter, a new analysis: Relic abundance and detection rates," *JHEP* **0711** (2007) 029, arXiv:0709.4477 [hep-ph].

[72] C. Arina, M. E. C. Catalan, S. Kraml, S. Kulkarni, and U. Laa, "Constraints on sneutrino dark matter from LHC Run 1," *JHEP* **05** (2015) 142, arXiv:1503.02960 [hep-ph].

[73] D. R. Smith and N. Weiner, "Inelastic dark matter," *Phys. Rev.* **D64** (2001) 043502, hep-ph/0101138.

[74] Y. Grossman and H. E. Haber, "Sneutrino mixing phenomena," *Phys. Rev. Lett.* **78** (1997) 3438–3441, hep-ph/9702421.

[75] G. Belanger, M. Kakizaki, E. Park, S. Kraml, and A. Pukhov, "Light mixed sneutrinos as thermal dark matter," *JCAP* **1011** (2010) 017, arXiv:1008.0580 [hep-ph].

[76] U. Ellwanger, C. Hugonie, and A. M. Teixeira, "The Next-to-Minimal Supersymmetric Standard Model," *Phys. Rept.* **496** (2010) 1–77, arXiv:0910.1785 [hep-ph].

[77] M. Cvetič, D. A. Demir, J. Espinosa, L. Everett, and P. Langacker, "Electroweak breaking and the mu problem in supergravity models with an additional U(1)," *Phys. Rev.* **D56** (1997) 2861, arXiv:hep-ph/9703317 [hep-ph].

[78] V. Barger, P. Langacker, H.-S. Lee, and G. Shaughnessy, "Higgs Sector in Extensions of the MSSM," *Phys. Rev.* **D73** (2006) 115010, arXiv:hep-ph/0603247 [hep-ph].

[79] **ATLAS** Collaboration, G. Aad *et al.*, "Search for high-mass dilepton resonances in pp collisions at $\sqrt{s} = 8$ TeV with the ATLAS detector," *Phys. Rev.* **D90** no. 5, (2014) 052005, arXiv:1405.4123 [hep-ex].

[80] **CMS** Collaboration, V. Khachatryan *et al.*, "Search for physics beyond the standard model in dilepton mass spectra in proton-proton collisions at $\sqrt{s} = 8$ TeV," *JHEP* **1504** (2015) 025, arXiv:1412.6302 [hep-ex].

[81] M. Frank and S. Mondal, "Light neutralino dark matter in $U(1)'$ models," *Phys. Rev.* **D90** no. 7, (2014) 075013, arXiv:1408.2223 [hep-ph].

[82] **ATLAS** Collaboration, "Measurements of the Higgs boson production and decay rates and coupling strengths using pp collision data at $\sqrt{s}$ = 7 and 8 TeV in the ATLAS experiment,". http://cds.cern.ch/record/2002212. ATLAS-CONF-2015-007, ATLAS-COM-CONF-2015-011.

[83] **CMS** Collaboration, V. Khachatryan *et al.*, "Precise determination of the mass of the Higgs boson and tests of compatibility of its couplings with the standard model predictions using proton collisions at 7 and 8 TeV," *Eur. Phys. J.* **C75** no. 5, (2015) 212, arXiv:1412.8662 [hep-ex].

[84] M. Cvetič and P. Langacker, "Implications of Abelian extended gauge structures from string models," *Phys. Rev.* **D54** (1996) 3570–3579, arXiv:hep-ph/9511378 [hep-ph].

[85] M. Cvetič and P. Langacker, "New gauge bosons from string models," *Mod. Phys. Lett.* **A11** (1996) 1247–1262, arXiv:hep-ph/9602424 [hep-ph].

[86] G. Cleaver, M. Cvetič, J. R. Espinosa, L. L. Everett, and P. Langacker, "Classification of flat directions in perturbative heterotic superstring vacua with anomalous U(1)," *Nucl. Phys.* **B525** (1998) 3–26, arXiv:hep-th/9711178 [hep-th].

[87] G. Cleaver, M. Cvetič, J. Espinosa, L. Everett, P. Langacker, *et al.*, "Physics implications of flat directions in free fermionic superstring models 1. Mass spectrum and couplings," *Phys. Rev.* **D59** (1999) 055005, arXiv:hep-ph/9807479 [hep-ph].

[88] G. Cleaver, M. Cvetič, J. Espinosa, L. Everett, P. Langacker, *et al.*, "Physics implications of flat directions in free fermionic superstring models. 2. Renormalization group analysis," *Phys. Rev.* **D59** (1999) 115003, arXiv:hep-ph/9811355 [hep-ph].

[89] P. Langacker, "Grand Unified Theories and Proton Decay," *Phys. Rept.* **72** (1981) 185.

[90] D. London and J. L. Rosner, "Extra Gauge Bosons in E(6)," *Phys. Rev.* **D34** (1986) 1530.

[91] G. Bélanger, J. Da Silva, and A. Pukhov, "The Right-handed sneutrino as thermal dark matter in U(1) extensions of the MSSM," *JCAP* **1112** (2011) 014, arXiv:1110.2414 [hep-ph].

[92] G. Belanger, J. Da Silva, U. Laa, and A. Pukhov, "Probing U(1) extensions of the MSSM at the LHC Run I and in dark matter searches," *JHEP* **09** (2015) 151, arXiv:1505.06243 [hep-ph].

[93] P. Langacker and J. Wang, "$U(1)'$ symmetry breaking in supersymmetric E(6) models," *Phys. Rev.* **D58** (1998) 115010, arXiv:hep-ph/9804428 [hep-ph].

[94] V. Barger, P. Langacker, I. Lewis, M. McCaskey, G. Shaughnessy, *et al.*, "Recoil Detection of the Lightest Neutralino in MSSM Singlet Extensions," *Phys. Rev.* **D75** (2007) 115002, arXiv:hep-ph/0702036 [HEP-PH].

[95] J. Da Silva, "Supersymmetric Dark Matter candidates in light of constraints from collider and astroparticle observables," arXiv:1312.0257 [hep-ph].

[96] P. Langacker, "The Physics of Heavy Z' Gauge Bosons," *Rev. Mod. Phys.* **81** (2009) 1199–1228, arXiv:0801.1345 [hep-ph].

[97] J. Kalinowski, S. King, and J. Roberts, "Neutralino Dark Matter in the USSM," *JHEP* **0901** (2009) 066, arXiv:0811.2204 [hep-ph].

[98] B. O'Leary, W. Porod, and F. Staub, "Mass spectrum of the minimal SUSY B-L model," *JHEP* **05** (2012) 042, arXiv:1112.4600 [hep-ph].

[99] L. Basso, B. O'Leary, W. Porod, and F. Staub, "Dark matter scenarios in the minimal SUSY B-L model," *JHEP* **1209** (2012) 054, arXiv:1207.0507 [hep-ph].

[100] M. E. Krauss, B. O'Leary, W. Porod, and F. Staub, "Implications of gauge kinetic mixing on Z' and slepton production at the LHC," *Phys. Rev.* **D86** (2012) 055017, arXiv:1206.3513 [hep-ph].

[101] G. Bélanger, J. Da Silva, and H. M. Tran, "Dark matter in U(1) extensions of the MSSM with gauge kinetic mixing," arXiv:1703.03275 [hep-ph].

[102] A. Leike, S. Riemann, and T. Riemann, "Z Z' mixing in presence of standard weak loop corrections," arXiv:hep-ph/9808374 [hep-ph].

[103] J. Erler, P. Langacker, S. Munir, and E. Rojas, "Improved Constraints on Z' Bosons from Electroweak Precision Data," *JHEP* **0908** (2009) 017, arXiv:0906.2435 [hep-ph].

[104] D. Cerdeno, C. Hugonie, D. Lopez-Fogliani, C. Munoz, and A. Teixeira, "Theoretical predictions for the direct detection of neutralino dark matter in the NMSSM," *JHEP* **0412** (2004) 048, arXiv:hep-ph/0408102 [hep-ph].

[105] **Muon g-2** Collaboration, G. Bennett *et al.*, "Final Report of the Muon E821 Anomalous Magnetic Moment Measurement at BNL," *Phys. Rev.* **D73** (2006) 072003, arXiv:hep-ex/0602035 [hep-ex].

[106] B. L. Roberts, "Status of the Fermilab Muon $(g-2)$ Experiment," *Chin. Phys.* **C34** (2010) 741–744, arXiv:1001.2898 [hep-ex].

[107] S. King, S. Moretti, and R. Nevzorov, "Theory and phenomenology of an exceptional supersymmetric standard model," *Phys. Rev.* **D73** (2006) 035009, arXiv:hep-ph/0510419 [hep-ph].

[108] D. B. Kaplan, "Flavor at SSC energies: A New mechanism for dynamically generated fermion masses," *Nucl. Phys.* **B365** (1991) 259–278.

[109] A. Pomarol and F. Riva, "The Composite Higgs and Light Resonance Connection," *JHEP* **08** (2012) 135, arXiv:1205.6434 [hep-ph].

[110] V. Sanz and J. Setford, "Composite Higgs models after Run2," arXiv:1703.10190 [hep-ph].

[111] N. Arkani-Hamed, S. Dimopoulos, and G. R. Dvali, "The Hierarchy problem and new dimensions at a millimeter," *Phys. Lett.* **B429** (1998) 263–272, arXiv:hep-ph/9803315 [hep-ph].

[112] Y. Uehara, "A Mini review of constraints on extra dimensions," *Mod. Phys. Lett.* **A17** (2002) 1551–1558, arXiv:hep-ph/0203244 [hep-ph].

[113] L. Randall and R. Sundrum, "A Large mass hierarchy from a small extra dimension," *Phys. Rev. Lett.* **83** (1999) 3370–3373, arXiv:hep-ph/9905221 [hep-ph].

[114] T. Gherghetta and A. Pomarol, "Bulk fields and supersymmetry in a slice of AdS," *Nucl. Phys.* **B586** (2000) 141–162, arXiv:hep-ph/0003129 [hep-ph].

[115] H. M. Lee, M. Park, and V. Sanz, "Gravity-mediated (or Composite) Dark Matter," *Eur. Phys. J.* **C74** (2014) 2715, arXiv:1306.4107 [hep-ph].

[116] N. Arkani-Hamed, M. Porrati, and L. Randall, "Holography and phenomenology," *JHEP* **08** (2001) 017, arXiv:hep-th/0012148 [hep-th].

[117] K. Agashe, R. Contino, and A. Pomarol, "The Minimal composite Higgs model," *Nucl. Phys.* **B719** (2005) 165–187, arXiv:hep-ph/0412089 [hep-ph].

[118] T. Appelquist, H.-C. Cheng, and B. A. Dobrescu, "Bounds on universal extra dimensions," *Phys. Rev.* **D64** (2001) 035002, arXiv:hep-ph/0012100 [hep-ph].

[119] N. Deutschmann, T. Flacke, and J. S. Kim, "Current LHC Constraints on Minimal Universal Extra Dimensions," arXiv:1702.00410 [hep-ph].

[120] J. Beuria, A. Datta, D. Debnath, and K. T. Matchev, "LHC Collider Phenomenology of Minimal Universal Extra Dimensions," arXiv:1702.00413 [hep-ph].

[121] S. Heinemeyer, W. Hollik, and G. Weiglein, "Electroweak precision observables in the minimal supersymmetric standard model," *Phys. Rept.* **425** (2006) 265–368, arXiv:hep-ph/0412214 [hep-ph].

[122] W. Altmannshofer, A. J. Buras, S. Gori, P. Paradisi, and D. M. Straub, "Anatomy and Phenomenology of FCNC and CPV Effects in SUSY Theories," *Nucl. Phys.* **B830** (2010) 17–94, arXiv:0909.1333 [hep-ph].

[123] Y. L. Dokshitzer, "Calculation of the Structure Functions for Deep Inelastic Scattering and e+ e- Annihilation by Perturbation Theory in Quantum Chromodynamics.," *Sov. Phys. JETP* **46** (1977) 641–653. [Zh. Eksp. Teor. Fiz.73,1216(1977)].

[124] V. N. Gribov and L. N. Lipatov, "Deep inelastic e p scattering in perturbation theory," *Sov. J. Nucl. Phys.* **15** (1972) 438–450. [Yad. Fiz.15,781(1972)].

[125] G. Altarelli and G. Parisi, "Asymptotic Freedom in Parton Language," *Nucl. Phys.* **B126** (1977) 298–318.

[126] A. Buckley, J. Ferrando, S. Lloyd, K. Nordström, B. Page, M. Rüfenacht, M. Schönherr, and G. Watt, "LHAPDF6: parton density access in the LHC precision era," *Eur. Phys. J.* **C75** (2015) 132, arXiv:1412.7420 [hep-ph].

[127] http://pauli.uni-muenster.de/ãkule_01/nllwiki/index.php/NLL-fast.

[128] W. Beenakker, R. Hopker, M. Spira, and P. M. Zerwas, "Squark and gluino production at hadron colliders," *Nucl. Phys.* **B492** (1997) 51–103, arXiv:hep-ph/9610490 [hep-ph].

[129] A. Kulesza and L. Motyka, "Threshold resummation for squark-antisquark and gluino-pair production at the LHC," *Phys. Rev. Lett.* **102** (2009) 111802, arXiv:0807.2405 [hep-ph].

[130] A. Kulesza and L. Motyka, "Soft gluon resummation for the production of gluino-gluino and squark-antisquark pairs at the LHC," *Phys. Rev.* **D80** (2009) 095004, arXiv:0905.4749 [hep-ph].

[131] W. Beenakker, S. Brensing, M. Kramer, A. Kulesza, E. Laenen, and I. Niessen, "Soft-gluon resummation for squark and gluino hadroproduction," *JHEP* **12** (2009) 041, arXiv:0909.4418 [hep-ph].

[132] W. Beenakker, S. Brensing, M. Kramer, A. Kulesza, E. Laenen, L. Motyka, and I. Niessen, "Squark and Gluino Hadroproduction," *Int. J. Mod. Phys.* **A26** (2011) 2637–2664, arXiv:1105.1110 [hep-ph].

[133] W. Beenakker, M. Kramer, T. Plehn, M. Spira, and P. M. Zerwas, "Stop production at hadron colliders," *Nucl. Phys.* **B515** (1998) 3–14, arXiv:hep-ph/9710451 [hep-ph].

[134] W. Beenakker, S. Brensing, M. Kramer, A. Kulesza, E. Laenen, and I. Niessen, "Supersymmetric top and bottom squark production at hadron colliders," *JHEP* **08** (2010) 098, arXiv:1006.4771 [hep-ph].

[135] **NNPDF** Collaboration, R. D. Ball *et al.*, "Unbiased global determination of parton distributions and their uncertainties at NNLO and at LO," *Nucl.Phys.* **B855** (2012) 153–221, arXiv:1107.2652 [hep-ph].

[136] W. Beenakker, C. Borschensky, M. Krämer, A. Kulesza, and E. Laenen, "NNLL-fast: predictions for coloured supersymmetric particle production at the LHC with threshold and Coulomb resummation," *JHEP* **12** (2016) 133, arXiv:1607.07741 [hep-ph].

[137] https://twiki.cern.ch/twiki/bin/view/LHCPhysics/SUSYCrossSections.

[138] B. Fuks, M. Klasen, D. R. Lamprea, and M. Rothering, "Gaugino production in proton-proton collisions at a center-of-mass energy of 8 TeV," *JHEP* **1210** (2012) 081, arXiv:1207.2159 [hep-ph].

[139] B. Fuks, M. Klasen, D. R. Lamprea, and M. Rothering, "Precision predictions for electroweak superpartner production at hadron colliders with Resummino," *Eur.Phys.J.* **C73** (2013) 2480, arXiv:1304.0790 [hep-ph].

[140] P. M. Nadolsky, H.-L. Lai, Q.-H. Cao, J. Huston, J. Pumplin, D. Stump, W.-K. Tung, and C. P. Yuan, "Implications of CTEQ global analysis for collider observables," *Phys. Rev.* **D78** (2008) 013004, arXiv:0802.0007 [hep-ph].

[141] A. Martin, W. Stirling, R. Thorne, and G. Watt, "Parton distributions for the LHC," *Eur. Phys. J.* **C63** (2009) 189–285, arXiv:0901.0002 [hep-ph].

[142] B. Fuks, M. Klasen, D. R. Lamprea, and M. Rothering, "Revisiting slepton pair production at the Large Hadron Collider," *JHEP* **1401** (2014) 168, arXiv:1310.2621.

[143] H.-L. Lai, M. Guzzi, J. Huston, Z. Li, P. M. Nadolsky, J. Pumplin, and C. P. Yuan, "New parton distributions for collider physics," *Phys. Rev.* **D82** (2010) 074024, arXiv:1007.2241 [hep-ph].

[144] B. C. Allanach and T. Cridge, "The Calculation of Sparticle and Higgs Decays in the Minimal and Next-to-Minimal Supersymmetric Standard Models: SOFTSUSY4.0," arXiv:1703.09717 [hep-ph].

[145] W. Porod, "SPheno, a program for calculating supersymmetric spectra, SUSY particle decays and SUSY particle production at e+ e- colliders," *Comput. Phys. Commun.* **153** (2003) 275–315, arXiv:hep-ph/0301101 [hep-ph].

[146] J. L. Hewett, B. Lillie, M. Masip, and T. G. Rizzo, "Signatures of long-lived gluinos in split supersymmetry," *JHEP* **09** (2004) 070, arXiv:hep-ph/0408248 [hep-ph].

[147] H. K. Dreiner, M. Kramer, and J. Tattersall, "How low can SUSY go? Matching, monojets and compressed spectra," *Europhys.Lett.* **99** (2012) 61001, arXiv:1207.1613 [hep-ph].

[148] T. Golling, "LHC searches for exotic new particles," *Prog. Part. Nucl. Phys.* **90** (2016) 156–200.

[149] G. Choudalakis, "On hypothesis testing, trials factor, hypertests and the BumpHunter," in *Proceedings, PHYSTAT 2011 Workshop on Statistical Issues Related to Discovery Claims in Search Experiments and Unfolding, CERN,Geneva, Switzerland 17-20 January 2011*. 2011. arXiv:1101.0390 [physics.data-an]. http://inspirehep.net/record/883244/files/arXiv:1101.0390.pdf.

[150] **ATLAS** Collaboration, "Search for new light resonances decaying to jet pairs and produced in association with a photon or a jet in proton-proton collisions at $\sqrt{s} = 13$ TeV with the ATLAS detector," Tech. Rep. ATLAS-CONF-2016-070, CERN, Geneva, Aug, 2016. http://cds.cern.ch/record/2206221.

[151] **CMS** Collaboration, "Search for light vector resonances decaying to a quark pair produced in association with a jet in proton-proton collisions at $\sqrt{s} = 13$ TeV," Tech. Rep. CMS-PAS-EXO-17-001, CERN, Geneva, 2017. http://cds.cern.ch/record/2264843.

[152] N. Arkani-Hamed, P. Schuster, N. Toro, J. Thaler, L.-T. Wang, B. Knuteson, and S. Mrenna, "MARMOSET: The Path from LHC Data to the New Standard Model via On-Shell Effective Theories," arXiv:hep-ph/0703088 [HEP-PH].

[153] J. Alwall, M.-P. Le, M. Lisanti, and J. G. Wacker, "Searching for Directly Decaying Gluinos at the Tevatron," *Phys. Lett.* **B666** (2008) 34–37, arXiv:0803.0019 [hep-ph].

[154] J. Alwall, M.-P. Le, M. Lisanti, and J. G. Wacker, "Model-Independent Jets plus Missing Energy Searches," *Phys. Rev.* **D79** (2009) 015005, arXiv:0809.3264 [hep-ph].

[155] J. Alwall, P. Schuster, and N. Toro, "Simplified Models for a First Characterization of New Physics at the LHC," *Phys.Rev.* **D79** (2009) 075020, arXiv:0810.3921 [hep-ph].

[156] D. S. M. Alves, E. Izaguirre, and J. G. Wacker, "Where the Sidewalk Ends: Jets and Missing Energy Search Strategies for the 7 TeV LHC," *JHEP* **10** (2011) 012, arXiv:1102.5338 [hep-ph].

[157] **LHC New Physics Working Group** Collaboration, D. Alves *et al.*, "Simplified Models for LHC New Physics Searches," *J.Phys.* **G39** (2012) 105005, arXiv:1105.2838 [hep-ph].

[158] **ATLAS** Collaboration, H. Okawa, "Interpretations of SUSY Searches in ATLAS with Simplified Models," in *Particles and fields. Proceedings, Meeting of the Division of the American Physical Society, DPF 2011, Providence, USA, August 9-13, 2011*. 2011. arXiv:1110.0282 [hep-ex]. https://inspirehep.net/record/930327/files/arXiv:1110.0282.pdf.

[159] **CMS** Collaboration, S. Chatrchyan *et al.*, "Interpretation of Searches for Supersymmetry with simplified Models," *Phys.Rev.* **D88** no. 5, (2013) 052017, arXiv:1301.2175 [hep-ex].

[160] **CMS** Collaboration, S. Chatrchyan *et al.*, "Search for top-squark pair production in the single-lepton final state in pp collisions at $\sqrt{s}$ = 8 TeV," *Eur. Phys. J.* **C73** no. 12, (2013) 2677, arXiv:1308.1586 [hep-ex].

[161] https://twiki.cern.ch/twiki/bin/view/AtlasPublic/SupersymmetryPublicResults.

[162] https://twiki.cern.ch/twiki/bin/view/CMSPublic/PhysicsResultsSUS.

[163] G. Chalons and D. Sengupta, "Closing in on compressed gluino-neutralino spectra at the LHC," *JHEP* **12** (2015) 129, arXiv:1508.06735 [hep-ph].

[164] **CMS** Collaboration, V. Khachatryan *et al.*, "Search for long-lived charged particles in proton-proton collisions at $\sqrt{s}$ = 13 TeV," *Phys. Rev.* **D94** no. 11, (2016) 112004, arXiv:1609.08382 [hep-ex].

[165] P. C. Bhat, "Multivariate Analysis Methods in Particle Physics," *Ann. Rev. Nucl. Part. Sci.* **61** (2011) 281–309.

[166] J. M. Butterworth, D. Grellscheid, M. Krämer, B. Sarrazin, and D. Yallup, "Constraining new physics with collider measurements of Standard Model signatures," *JHEP* **03** (2017) 078, arXiv:1606.05296 [hep-ph].

[167] A. Buckley, J. Butterworth, L. Lonnblad, D. Grellscheid, H. Hoeth, *et al.*, "Rivet user manual," *Comput.Phys.Commun.* **184** (2013) 2803–2819, arXiv:1003.0694 [hep-ph]. http://rivet.hepforge.org.

[168] A. Semenov, "LanHEP - A package for automatic generation of Feynman rules from the Lagrangian. Version 3.2," *Comput. Phys. Commun.* **201** (2016) 167–170, arXiv:1412.5016 [physics.comp-ph].

[169] A. Alloul, N. D. Christensen, C. Degrande, C. Duhr, and B. Fuks, "FeynRules 2.0 - A complete toolbox for tree-level phenomenology," *Comput. Phys. Commun.* **185** (2014) 2250–2300, arXiv:1310.1921 [hep-ph].

[170] F. Staub, "SARAH 4 : A tool for (not only SUSY) model builders," *Comput. Phys. Commun.* **185** (2014) 1773–1790, arXiv:1309.7223 [hep-ph].

[171] C. Degrande, C. Duhr, B. Fuks, D. Grellscheid, O. Mattelaer, *et al.*, "UFO - The Universal FeynRules Output," *Comput.Phys.Commun.* **183** (2012) 1201–1214, arXiv:1108.2040 [hep-ph].

[172] http://feynrules.irmp.ucl.ac.be/wiki/ModelDatabaseMainPage.

[173] B. Allanach, "SOFTSUSY: a program for calculating supersymmetric spectra," *Comput.Phys.Commun.* **143** (2002) 305–331, arXiv:hep-ph/0104145 [hep-ph].

[174] A. Djouadi, J.-L. Kneur, and G. Moultaka, "SuSpect: A Fortran code for the supersymmetric and Higgs particle spectrum in the MSSM," *Comput. Phys. Commun.* **176** (2007) 426–455, arXiv:hep-ph/0211331 [hep-ph].

[175] J. Alwall, R. Frederix, S. Frixione, V. Hirschi, F. Maltoni, *et al.*, "The automated computation of tree-level and next-to-leading order differential cross sections, and their matching to parton shower simulations," arXiv:1405.0301 [hep-ph].

[176] A. Pukhov, E. Boos, M. Dubinin, V. Edneral, V. Ilyin, D. Kovalenko, A. Kryukov, V. Savrin, S. Shichanin, and A. Semenov, "CompHEP: A Package for evaluation of Feynman diagrams and integration over multiparticle phase space," arXiv:hep-ph/9908288 [hep-ph].

[177] J. Alwall, A. Ballestrero, P. Bartalini, S. Belov, E. Boos, *et al.*, "A Standard format for Les Houches event files," *Comput.Phys.Commun.* **176** (2007) 300–304, arXiv:hep-ph/0609017 [hep-ph].

[178] W. Hollik, J. M. Lindert, and D. Pagani, "NLO corrections to squark-squark production and decay at the LHC," *JHEP* **03** (2013) 139, arXiv:1207.1071 [hep-ph].

[179] T. Sjöstrand, S. Ask, J. R. Christiansen, R. Corke, N. Desai, P. Ilten, S. Mrenna, S. Prestel, C. O. Rasmussen, and P. Z. Skands, "An Introduction to PYTHIA 8.2," *Comput. Phys. Commun.* **191** (2015) 159–177, arXiv:1410.3012 [hep-ph].

[180] M. Bahr, S. Gieseke, M. Gigg, D. Grellscheid, K. Hamilton, *et al.*, "Herwig++ Physics and Manual," *Eur.Phys.J.* **C58** (2008) 639–707, arXiv:0803.0883 [hep-ph].

[181] J. Alwall, S. Hoche, F. Krauss, N. Lavesson, L. Lonnblad, *et al.*, "Comparative study of various algorithms for the merging of parton showers and matrix elements in hadronic collisions," *Eur.Phys.J.* **C53** (2008) 473–500, arXiv:0706.2569 [hep-ph].

[182] G. L and L. P., *StdHep User Manual*, 2006. http://cepa.fnal.gov/psm/stdhep/.

[183] M. Dobbs and J. B. Hansen, "The HepMC C++ Monte Carlo event record for High Energy Physics," *Comput. Phys. Commun.* **134** (2001) 41–46.

[184] **DELPHES 3** Collaboration, J. de Favereau, C. Delaere, P. Demin, A. Giammanco, V. Lemaître, A. Mertens, and M. Selvaggi, "DELPHES 3, A modular framework for fast simulation of a generic collider experiment," *JHEP* **02** (2014) 057, arXiv:1307.6346 [hep-ex].

[185] M. Cacciari, G. P. Salam, and G. Soyez, "FastJet User Manual," *Eur. Phys. J.* **C72** (2012) 1896, arXiv:1111.6097 [hep-ph].

[186] M. Drees, H. Dreiner, D. Schmeier, J. Tattersall, and J. S. Kim, "CheckMATE: Confronting your Favourite New Physics Model with LHC Data," *Comput. Phys. Commun.* **187** (2014) 227–265, arXiv:1312.2591 [hep-ph].

[187] D. Dercks, N. Desai, J. S. Kim, K. Rolbiecki, J. Tattersall, and T. Weber, "CheckMATE 2: From the model to the limit," arXiv:1611.09856 [hep-ph].

[188] E. Conte, B. Dumont, B. Fuks, and C. Wymant, "Designing and recasting LHC analyses with MadAnalysis 5," *Eur. Phys. J.* **C74** no. 10, (2014) 3103, arXiv:1405.3982 [hep-ph].

[189] B. Dumont, B. Fuks, S. Kraml, S. Bein, G. Chalons, E. Conte, S. Kulkarni, D. Sengupta, and C. Wymant, "Toward a public analysis database for LHC new physics searches using MADANALYSIS 5," *Eur. Phys. J.* **C75** no. 2, (2015) 56, arXiv:1407.3278 [hep-ph].

[190] J. S. Kim, D. Schmeier, J. Tattersall, and K. Rolbiecki, "A framework to create customised LHC analyses within CheckMATE," *Comput. Phys. Commun.* **196** (2015) 535–562, arXiv:1503.01123 [hep-ph].

[191] S. Kraml, S. Kulkarni, U. Laa, A. Lessa, W. Magerl, *et al.*, "SModelS: a tool for interpreting simplified-model results from the LHC and its application to supersymmetry," *Eur.Phys.J.* **C74** (2014) 2868, arXiv:1312.4175 [hep-ph].

[192] S. Kraml, S. Kulkarni, U. Laa, A. Lessa, V. Magerl, W. Magerl, D. Proschofsky-Spindler, M. Traub, and W. Waltenberger, "SModelS v1.0: a short user guide," arXiv:1412.1745 [hep-ph].

[193] M. Papucci, K. Sakurai, A. Weiler, and L. Zeune, "Fastlim: a fast LHC limit calculator," *Eur. Phys. J.* **C74** no. 11, (2014) 3163, arXiv:1402.0492 [hep-ph].

[194] D. Barducci, A. Belyaev, M. Buchkremer, J. Marrouche, S. Moretti, and L. Panizzi, "XQCAT: eXtra Quark Combined Analysis Tool," *Comput. Phys. Commun.* **197** (2015) 263–275, arXiv:1409.3116 [hep-ph].

[195] S. Caron, J. S. Kim, K. Rolbiecki, R. Ruiz de Austri, and B. Stienen, "The BSM-AI project: SUSY-AI-generalizing LHC limits on supersymmetry with machine learning," *Eur. Phys. J.* **C77** no. 4, (2017) 257, arXiv:1605.02797 [hep-ph].

[196] **ATLAS** Collaboration, G. Aad *et al.*, "Summary of the ATLAS experiment's sensitivity to supersymmetry after LHC Run 1 - interpreted in the phenomenological MSSM," *JHEP* **10** (2015) 134, arXiv:1508.06608 [hep-ex].

[197] G. Bertone, M. P. Deisenroth, J. S. Kim, S. Liem, R. Ruiz de Austri, and M. Welling, "Accelerating the BSM interpretation of LHC data with machine learning," arXiv:1611.02704 [hep-ph].

[198] P. Bechtle, S. Belkner, D. Dercks, M. Hamer, T. Keller, M. Krämer, B. Sarrazin, J. Schütte-Engel, and J. Tattersall, "SCYNet: Testing supersymmetric models at the LHC with neural networks," arXiv:1703.01309 [hep-ph].

[199] http://smodels.hephy.at/wiki/SmsDictionary.

[200] G. Belanger, N. D. Christensen, A. Pukhov, and A. Semenov, "SLHAplus: a library for implementing extensions of the standard model," *Comput. Phys. Commun.* **182** (2011) 763–774, arXiv:1008.0181 [hep-ph].

[201] "Extending the SLHA: cross section information.". http://phystev.in2p3.fr/wiki/2013:groups:tools:slha.

[202] T. Sjostrand, S. Mrenna, and P. Z. Skands, "PYTHIA 6.4 Physics and Manual," *JHEP* **0605** (2006) 026, arXiv:hep-ph/0603175 [hep-ph].

[203] T. Sjostrand, S. Mrenna, and P. Z. Skands, "A Brief Introduction to PYTHIA 8.1," *Comput. Phys. Commun.* **178** (2008) 852–867, arXiv:0710.3820 [hep-ph].

[204] F. Ambrogi, S. Kraml, S. Kulkarni, U. Laa, A. Lessa, V. Magerl, J. Sonneveld, M. Traub, and W. Waltenberger, "SModelS v1.1 user manual," arXiv:1701.06586 [hep-ph].

[205] D. Barducci, G. Belanger, J. Bernon, F. Boudjema, J. Da Silva, S. Kraml, U. Laa, and A. Pukhov, "Collider limits on new physics within micrOMEGAs," arXiv:1606.03834 [hep-ph]. To appear in CPC.

[206] http://smodels.hephy.at/wiki/ListOfAnalysesv11.

[207] J. Heisig, A. Lessa, and L. Quertenmont, "Simplified Models for Exotic BSM Searches," *JHEP* **12** (2015) 087, arXiv:1509.00473 [hep-ph].

[208] S. Kraml, U. Laa, L. Panizzi, and H. Prager, "Scalar versus fermionic top partner interpretations of $t\bar{t} + E_T^{\rm miss}$ searches at the LHC," *JHEP* **11** (2016) 107, arXiv:1607.02050 [hep-ph].

[209] L. Edelhäuser, J. Heisig, M. Krämer, L. Oymanns, and J. Sonneveld, "Constraining supersymmetry at the LHC with simplified models for squark production," *JHEP* **1412** (2014) 022, arXiv:1410.0965 [hep-ph].

[210] L. Edelhäuser, M. Krämer, and J. Sonneveld, "Simplified models for same-spin new physics scenarios," *JHEP* **04** (2015) 146, arXiv:1501.03942 [hep-ph].

[211] **CMS** Collaboration, S. Chatrchyan *et al.*, "Search for supersymmetry in hadronic final states with missing transverse energy using the variables α_T and b-quark multiplicity in pp collisions at $\sqrt{s} = 8$ TeV," *Eur. Phys. J.* **C73** no. 9, (2013) 2568, arXiv:1303.2985 [hep-ex].

[212] **CMS** Collaboration, S. Chatrchyan *et al.*, "Search for new physics in the multijet and missing transverse momentum final state in proton-proton collisions at $\sqrt{s}$= 8 TeV," *JHEP* **1406** (2014) 055, arXiv:1402.4770 [hep-ex].

[213] **ATLAS** Collaboration, G. Aad *et al.*, "Search for squarks and gluinos with the ATLAS detector in final states with jets and missing transverse momentum using $\sqrt{s} = 8$ TeV proton–proton collision data," *JHEP* **09** (2014) 176, arXiv:1405.7875 [hep-ex].

[214] J. Cao, L. Shang, J. M. Yang, and Y. Zhang, "Explanation of the ATLAS Z-Peaked Excess in the NMSSM," *JHEP* **06** (2015) 152, arXiv:1504.07869 [hep-ph].

[215] J. Alwall, S. de Visscher, and F. Maltoni, "QCD radiation in the production of heavy colored particles at the LHC," *JHEP* **0902** (2009) 017, arXiv:0810.5350 [hep-ph].

[216] I. Antoniadis, "A Possible new dimension at a few TeV," *Phys. Lett.* **B246** (1990) 377–384.

[217] G. Servant and T. M. P. Tait, "Is the lightest Kaluza-Klein particle a viable dark matter candidate?," *Nucl. Phys.* **B650** (2003) 391–419, arXiv:hep-ph/0206071 [hep-ph].

[218] C. Csaki, C. Grojean, J. Hubisz, Y. Shirman, and J. Terning, "Fermions on an interval: Quark and lepton masses without a Higgs," *Phys. Rev.* **D70** (2004) 015012, arXiv:hep-ph/0310355 [hep-ph].

[219] G. Cacciapaglia, A. Deandrea, and J. Llodra-Perez, "A Dark Matter candidate from Lorentz Invariance in 6D," *JHEP* **03** (2010) 083, arXiv:0907.4993 [hep-ph].

[220] H.-C. Cheng and I. Low, "TeV symmetry and the little hierarchy problem," *JHEP* **09** (2003) 051, arXiv:hep-ph/0308199 [hep-ph].

[221] H.-C. Cheng and I. Low, "Little hierarchy, little Higgses, and a little symmetry," *JHEP* **08** (2004) 061, arXiv:hep-ph/0405243 [hep-ph].

[222] I. Low, "T parity and the littlest Higgs," *JHEP* **10** (2004) 067, arXiv:hep-ph/0409025 [hep-ph].

[223] J. Hubisz and P. Meade, "Phenomenology of the littlest Higgs with T-parity," *Phys. Rev.* **D71** (2005) 035016, arXiv:hep-ph/0411264 [hep-ph].

[224] J. Hubisz, P. Meade, A. Noble, and M. Perelstein, "Electroweak precision constraints on the littlest Higgs model with T parity," *JHEP* **01** (2006) 135, arXiv:hep-ph/0506042 [hep-ph].

[225] H.-C. Cheng, I. Low, and L.-T. Wang, "Top partners in little Higgs theories with T-parity," *Phys. Rev.* **D74** (2006) 055001, arXiv:hep-ph/0510225 [hep-ph].

[226] **ATLAS** Collaboration, "Search for direct production of the top squark in the all-hadronic ttbar + etmiss final state in 21 fb-1 of p-pcollisions at sqrt(s)=8 TeV with the ATLAS detector," Tech. Rep. ATLAS-CONF-2013-024, CERN, Geneva, Mar, 2013.

[227] **ATLAS** Collaboration, G. Aad *et al.*, "Search for top squark pair production in final states with one isolated lepton, jets, and missing transverse momentum in $\sqrt{s}$ =8 TeV pp collisions with the ATLAS detector," *JHEP* **11** (2014) 118, arXiv:1407.0583 [hep-ex].

[228] **ATLAS** Collaboration, G. Aad *et al.*, "Search for direct top-squark pair production in final states with two leptons in pp collisions at $\sqrt{s} = 8$TeV with the ATLAS detector," *JHEP* **06** (2014) 124, arXiv:1403.4853 [hep-ex].

[229] G. Cacciapaglia, A. Deandrea, J. Ellis, J. Marrouche, and L. Panizzi, "LHC Missing-Transverse-Energy Constraints on Models with Universal Extra Dimensions," *Phys. Rev.* **D87** no. 7, (2013) 075006, arXiv:1302.4750 [hep-ph].

[230] S. Baek, P. Ko, and P. Wu, "Top-philic Scalar Dark Matter with a Vector-like Fermionic Top Partner," *JHEP* **10** (2016) 117, arXiv:1606.00072 [hep-ph].

[231] T. Gajdosik, R. M. Godbole, and S. Kraml, "Fermion polarization in sfermion decays as a probe of CP phases in the MSSM," *JHEP* **09** (2004) 051, arXiv:hep-ph/0405167 [hep-ph].

[232] Q.-H. Cao, C. S. Li, and C. P. Yuan, "Impact of Single-Top Measurement to Littlest Higgs Model with T-Parity," *Phys. Lett.* **B668** (2008) 24–27, arXiv:hep-ph/0612243 [hep-ph].

[233] M. M. Nojiri and M. Takeuchi, "Study of the top reconstruction in top-partner events at the LHC," *JHEP* **10** (2008) 025, arXiv:0802.4142 [hep-ph].

[234] J. Shelton, "Polarized tops from new physics: signals and observables," *Phys. Rev.* **D79** (2009) 014032, arXiv:0811.0569 [hep-ph].

[235] M. Perelstein and A. Weiler, "Polarized Tops from Stop Decays at the LHC," *JHEP* **03** (2009) 141, arXiv:0811.1024 [hep-ph].

[236] E. L. Berger, Q.-H. Cao, J.-H. Yu, and H. Zhang, "Measuring Top Quark Polarization in Top Pair plus Missing Energy Events," *Phys. Rev. Lett.* **109** (2012) 152004, arXiv:1207.1101 [hep-ph].

[237] C.-Y. Chen, A. Freitas, T. Han, and K. S. M. Lee, "New Physics from the Top at the LHC," *JHEP* **11** (2012) 124, arXiv:1207.4794 [hep-ph].

[238] B. Bhattacherjee, S. K. Mandal, and M. Nojiri, "Top Polarization and Stop Mixing from Boosted Jet Substructure," *JHEP* **03** (2013) 105, arXiv:1211.7261 [hep-ph].

[239] G. Belanger, R. M. Godbole, L. Hartgring, and I. Niessen, "Top Polarization in Stop Production at the LHC," *JHEP* **05** (2013) 167, arXiv:1212.3526 [hep-ph].

[240] I. Low, "Polarized charginos (and top quarks) in scalar top quark decays," *Phys. Rev.* **D88** no. 9, (2013) 095018, arXiv:1304.0491 [hep-ph].

[241] G. Belanger, R. M. Godbole, S. Kraml, and S. Kulkarni, "Top Polarization in Sbottom Decays at the LHC," arXiv:1304.2987 [hep-ph].

[242] K. Wang, L. Wang, T. Xu, and L. Zhang, "Polarization effects in early SUSY searches at the CERN LHC," *Eur. Phys. J.* **C75** no. 6, (2015) 285, arXiv:1312.1527 [hep-ph].

[243] **ATLAS** Collaboration, G. Aad *et al.*, "ATLAS Run 1 searches for direct pair production of third-generation squarks at the Large Hadron Collider," *Eur. Phys. J.* **C75** no. 10, (2015) 510, arXiv:1506.08616 [hep-ex]. [Erratum: Eur. Phys. J.C76,no.3,153(2016)].

[244] **CMS** Collaboration, "Search for top squarks decaying to a charm quark and a neutralino in events with a jet and missing transverse momentum," Tech. Rep. CMS-PAS-SUS-13-009, CERN, Geneva, 2014. http://cds.cern.ch/record/1644584.

[245] **CMS** Collaboration, "Exclusion limits on gluino and top-squark pair production in natural SUSY scenarios with inclusive razor and exclusive single-lepton searches at 8 TeV.," Tech. Rep. CMS-PAS-SUS-14-011, CERN, Geneva, 2014. http://cds.cern.ch/record/1745586.

[246] **CMS** Collaboration, "Search for direct production of top squark pairs decaying to all-hadronic final states in pp collisions at sqrt(s) = 13 TeV," Tech. Rep. CMS-PAS-SUS-16-007, CERN, Geneva, 2016. http://cds.cern.ch/record/2141543.

[247] J. Alwall, M. Herquet, F. Maltoni, O. Mattelaer, and T. Stelzer, "MadGraph 5 : Going Beyond," *JHEP* **1106** (2011) 128, arXiv:1106.0522 [hep-ph].

[248] R. Boughezal and M. Schulze, "$t\bar{t}$+large missing energy from top-quark partners: A comprehensive study at next-to-leading order QCD," *Phys. Rev.* **D88** no. 11, (2013) 114002, arXiv:1309.2316 [hep-ph].

[249] J. Pumplin, D. R. Stump, J. Huston, H. L. Lai, P. M. Nadolsky, and W. K. Tung, "New generation of parton distributions with uncertainties from global QCD analysis," *JHEP* **07** (2002) 012, arXiv:hep-ph/0201195 [hep-ph].

[250] M. Cacciari, M. Czakon, M. Mangano, A. Mitov, and P. Nason, "Top-pair production at hadron colliders with next-to-next-to-leading logarithmic soft-gluon resummation," *Phys. Lett.* **B710** (2012) 612–622, arXiv:1111.5869 [hep-ph].

[251] M. Cacciari and G. P. Salam, "Dispelling the N^3 myth for the k_t jet-finder," *Phys. Lett.* **B641** (2006) 57–61, arXiv:hep-ph/0512210 [hep-ph].

[252] B. Dumont, B. Fuks, and C. Wymant, "MadAnalysis 5 implementation of CMS-SUS-13-011: search for stops in the single lepton final state at 8 TeV,". https://inspirehep.net/record/1301484.

[253] G. Chalons and D. Sengupta, "Madanalysis 5 implementation of the ATLAS multi jet analysis documented in arXiv:1405.7875, JHEP 1409 (2014) 176,".

[254] **ATLAS** Collaboration, G. Aad *et al.*, "Search for direct pair production of the top squark in all-hadronic final states in proton-proton collisions at $\sqrt{s} = 8$ TeV with the ATLAS detector," *JHEP* **09** (2014) 015, arXiv:1406.1122 [hep-ex].

[255] C. Lester and D. Summers, "Measuring masses of semiinvisibly decaying particles pair produced at hadron colliders," *Phys.Lett.* **B463** (1999) 99–103, arXiv:hep-ph/9906349 [hep-ph].

[256] H.-C. Cheng and Z. Han, "Minimal Kinematic Constraints and m_{T2}," *JHEP* **0812** (2008) 063, arXiv:0810.5178 [hep-ph].

[257] Y. Bai, H.-C. Cheng, J. Gallicchio, and J. Gu, "Stop the Top Background of the Stop Search," *JHEP* **1207** (2012) 110, arXiv:1203.4813 [hep-ph].

[258] http://lpsc.in2p3.fr/projects-th/recasting/susy-vs-vlq/ttbarMET.

[259] M. E. Cabrera and J. A. Casas, "Understanding and improving the Effective Mass for LHC searches," arXiv:1207.0435 [hep-ph].

[260] A. Datta, G. L. Kane, and M. Toharia, "Is it SUSY?," arXiv:hep-ph/0510204 [hep-ph].

[261] T. Han, R. Mahbubani, D. G. E. Walker, and L.-T. Wang, "Top Quark Pair plus Large Missing Energy at the LHC," *JHEP* **05** (2009) 117, arXiv:0803.3820 [hep-ph].

[262] J. M. Smillie and B. R. Webber, "Distinguishing spins in supersymmetric and universal extra dimension models at the large hadron collider," *JHEP* **10** (2005) 069, arXiv:hep-ph/0507170 [hep-ph].

[263] A. Datta, K. Kong, and K. T. Matchev, "Discrimination of supersymmetry and universal extra dimensions at hadron colliders," *Phys. Rev.* **D72** (2005) 096006, arXiv:hep-ph/0509246 [hep-ph]. [Erratum: Phys. Rev.D72,119901(2005)].

[264] B. Dumont, "MadAnalysis 5 implementation of ATLAS-SUSY-2013-11: di-leptons plus MET.". DOI: 10.7484/INSPIREHEP.DATA.HLMR.T56W.2.

[265] **ATLAS** Collaboration, G. Aad *et al.*, "Search for direct production of charginos, neutralinos and sleptons in final states with two leptons and missing transverse momentum in pp collisions at $\sqrt{s} = 8$ TeV with the ATLAS detector," *JHEP* **1405** (2014) 071, arXiv:1403.5294 [hep-ex].

[266] F. Domingo and U. Ellwanger, "Updated Constraints from B Physics on the MSSM and the NMSSM," *JHEP* **0712** (2007) 090, arXiv:0710.3714 [hep-ph].

[267] G. Belanger, D. Ghosh, R. Godbole, and S. Kulkarni, "Light stop in the MSSM after LHC Run 1," *JHEP* **09** (2015) 214, arXiv:1506.00665 [hep-ph].

[268] M. Peiro and S. Robles, "Low-mass neutralino dark matter in supergravity scenarios: phenomenology and naturalness," *JCAP* **1705** no. 05, (2017) 010, arXiv:1612.00460 [hep-ph].

[269] T. Cohen, J. Kearney, and M. Luty, "Natural Supersymmetry without Light Higgsinos," *Phys. Rev.* **D91** (2015) 075004, arXiv:1501.01962 [hep-ph].

[270] J. Cao, Y. He, L. Shang, W. Su, and Y. Zhang, "Testing the light dark matter scenario of the MSSM at the LHC," *JHEP* **03** (2016) 207, arXiv:1511.05386 [hep-ph].

[271] http://hepdata.cedar.ac.uk/view/ins1389857.

[272] F. Ambrogi, S. Kraml, S. Kulkarni, U. Laa, A. Lessa, and W. Waltenberger. in preparation.

[273] J. Fan, M. Reece, and J. T. Ruderman, "Stealth Supersymmetry," *JHEP* **1111** (2011) 012, arXiv:1105.5135 [hep-ph].

[274] **ATLAS** Collaboration, G. Aad *et al.*, "Search for pair production of gluinos decaying via stop and sbottom in events with b-jets and large missing transverse momentum in pp collisions at $\sqrt{s} = 13$ TeV with the ATLAS detector," *Phys. Rev.* **D94** no. 3, (2016) 032003, arXiv:1605.09318 [hep-ex].

[275] **CMS** Collaboration, "Search for supersymmetry in pp collisions at $\sqrt{s} = 13$ TeV in the single-lepton final state using the sum of masses of large-radius jets," Tech. Rep. CMS-PAS-SUS-16-037, CERN, Geneva, 2017. http://cds.cern.ch/record/2256652.

[276] B. Dumont, G. Belanger, S. Fichet, S. Kraml, and T. Schwetz, "Mixed sneutrino dark matter in light of the 2011 XENON and LHC results," *JCAP* **1209** (2012) 013, arXiv:1206.1521 [hep-ph].

[277] D. Hooper, J. March-Russell, and S. M. West, "Asymmetric sneutrino dark matter and the Omega(b)/Omega(DM) puzzle," *Phys. Lett.* **B605** (2005) 228–236, hep-ph/0410114.

[278] Z. Thomas, D. Tucker-Smith, and N. Weiner, "Mixed Sneutrinos, Dark Matter and the CERN LHC," *Phys.Rev.* **D77** (2008) 115015, arXiv:0712.4146 [hep-ph].

[279] G. Belanger, S. Kraml, and A. Lessa, "Light Sneutrino Dark Matter at the LHC," *JHEP* **1107** (2011) 083, arXiv:1105.4878 [hep-ph].

[280] C. Arina and M. E. Cabrera, "Multi-lepton signatures at LHC from sneutrino dark matter," *JHEP* **1404** (2014) 100, arXiv:1311.6549 [hep-ph].

[281] P. Bhupal Dev, S. Mondal, B. Mukhopadhyaya, and S. Roy, "Phenomenology of Light Sneutrino Dark Matter in cMSSM/mSUGRA with Inverse Seesaw," *JHEP* **1209** (2012) 110, arXiv:1207.6542 [hep-ph].

[282] J. Guo, Z. Kang, J. Li, T. Li, and Y. Liu, "Simplified Supersymmetry with Sneutrino LSP at 8 TeV LHC," *JHEP* **1410** (2014) 164, arXiv:1312.2821 [hep-ph].

[283] L. A. Harland-Lang, C.-H. Kom, K. Sakurai, and M. Tonini, "Sharpening m_{T2} cusps: the mass determination of semi-invisibly decaying particles from a resonance," *JHEP* **1406** (2014) 175, arXiv:1312.5720 [hep-ph].

[284] **LUX** Collaboration, D. Akerib *et al.*, "First results from the LUX dark matter experiment at the Sanford Underground Research Facility," *Phys.Rev.Lett.* **112** (2014) 091303, arXiv:1310.8214 [astro-ph.CO].

[285] http://smodels.hephy.at.

[286] **CMS** Collaboration, S. Chatrchyan *et al.*, "Observation of a new boson at a mass of 125 GeV with the CMS experiment at the LHC," *Phys. Lett.* **B716** (2012) 30–61, arXiv:1207.7235 [hep-ex].

[287] **LHCb** Collaboration, R. Aaij *et al.*, "First Evidence for the Decay $B_s^0 \to \mu^+\mu^-$," *Phys.Rev.Lett.* **110** (2013) 021801, arXiv:1211.2674 [hep-ex].

[288] **Heavy Flavor Averaging Group** Collaboration, Y. Amhis *et al.*, "Averages of B-Hadron, C-Hadron, and tau-lepton properties as of early 2012," arXiv:1207.1158 [hep-ex].

[289] **Planck** Collaboration, P. Ade *et al.*, "Planck 2013 results. XVI. Cosmological parameters," *Astron.Astrophys.* (2014) , arXiv:1303.5076 [astro-ph.CO].

[290] **Particle Data Group** Collaboration, K. Olive *et al.*, "Review of Particle Physics," *Chin.Phys.* **C38** (2014) 090001.

[291] G. Belanger, B. Dumont, U. Ellwanger, J. Gunion, and S. Kraml, "Global fit to Higgs signal strengths and couplings and implications for extended Higgs sectors," *Phys.Rev.* **D88** (2013) 075008, arXiv:1306.2941 [hep-ph].

[292] **LEPSUSYWG, The ALEPH, DELPHI, L3 and OPAL** Collaborations. http://lepsusy.web.cern.ch/lepsusy/Welcome.html. LEPSUSYWG/04-01.1.

[293] **D0** Collaboration, V. Abazov *et al.*, "Search for squarks and gluinos in events with jets and missing transverse energy using 2.1 fb^{-1} of $p\bar{p}$ collision data at $\sqrt{s}$ = 1.96-TeV," *Phys.Lett.* **B660** (2008) 449–457, arXiv:0712.3805 [hep-ex].

[294] **ATLAS** Collaboration, G. Aad *et al.*, "Observation of a new particle in the search for the Standard Model Higgs boson with the ATLAS detector at the LHC," *Phys.Lett.* **B716** (2012) 1–29, arXiv:1207.7214 [hep-ex].

[295] **CMS** Collaboration, S. Chatrchyan *et al.*, "Observation of a new boson at a mass of 125 GeV with the CMS experiment at the LHC," *Phys.Lett.* **B716** (2012) 30–61, arXiv:1207.7235 [hep-ex].

[296] M. E. Cabrera, J. A. Casas, and R. R. de Austri, "The health of SUSY after the Higgs discovery and the XENON100 data," *JHEP* **1307** (2013) 182, arXiv:1212.4821 [hep-ph].

[297] B. Allanach, A. Djouadi, J. Kneur, W. Porod, and P. Slavich, "Precise determination of the neutral Higgs boson masses in the MSSM," *JHEP* **0409** (2004) 044, arXiv:hep-ph/0406166 [hep-ph].

[298] **ALEPH, DELPHI, L3, OPAL, SLD, LEP Electroweak Working Group, SLD Electroweak Group, SLD Heavy Flavour Group** Collaborations, S. Schael *et al.*, "Precision electroweak measurements on the Z resonance," *Phys.Rept.* **427** (2006) 257–454, arXiv:hep-ex/0509008 [hep-ex].

[299] F. Boudjema, G. Drieu La Rochelle, and S. Kulkarni, "One-loop corrections, uncertainties and approximations in neutralino annihilations: Examples," *Phys.Rev.* **D84** (2011) 116001, arXiv:1108.4291 [hep-ph].

[300] C. Duhr and B. Fuks, "A superspace module for the FeynRules package," *Comput. Phys. Commun.* **182** (2011) 2404–2426, arXiv:1102.4191 [hep-ph].

[301] F. Mahmoudi, "SuperIso v2.3: A Program for calculating flavor physics observables in Supersymmetry," *Comput.Phys.Commun.* **180** (2009) 1579–1613, arXiv:0808.3144 [hep-ph].

[302] F. Feroz and M. Hobson, "Multimodal nested sampling: an efficient and robust alternative to MCMC methods for astronomical data analysis," *Mon.Not.Roy.Astron.Soc.* **384** (2008) 449, arXiv:0704.3704 [astro-ph].

[303] F. Feroz, M. Hobson, and M. Bridges, "MultiNest: an efficient and robust Bayesian inference tool for cosmology and particle physics," *Mon.Not.Roy.Astron.Soc.* **398** (2009) 1601–1614, arXiv:0809.3437 [astro-ph].

[304] F. Feroz, M. P. Hobson, E. Cameron, and A. N. Pettitt, "Importance Nested Sampling and the MultiNest Algorithm," *ArXiv e-prints* (June, 2013) , arXiv:1306.2144 [astro-ph.IM].

[305] **ATLAS** Collaboration, G. Aad *et al.*, "Search for new phenomena in final states with large jet multiplicities and missing transverse momentum at $\sqrt{s}$=8 TeV proton-proton collisions using the ATLAS experiment," *JHEP* **1310** (2013) 130, arXiv:1308.1841 [hep-ex].

[306] "Search for strong production of supersymmetric particles in final states with missing transverse momentum and at least three b-jets using 20.1 fb-1 of pp collisions at sqrt(s) = 8 TeV with the ATLAS Detector.," Tech. Rep. ATLAS-CONF-2013-061, CERN, Geneva, Jun, 2013.

[307] **CMS** Collaboration, S. Chatrchyan *et al.*, "Search for gluino mediated bottom- and top-squark production in multijet final states in pp collisions at 8 TeV," *Phys.Lett.* **B725** (2013) 243–270, arXiv:1305.2390 [hep-ex].

[308] **CMS** Collaboration, S. Chatrchyan *et al.*, "Search for supersymmetry in hadronic final states with missing transverse energy using the variables α_T and b-quark multiplicity in pp collisions at $\sqrt{s} = 8$ TeV," *Eur.Phys.J.* **C73** no. 9, (2013) 2568, arXiv:1303.2985 [hep-ex].

[309] **CMS** Collaboration, S. Chatrchyan *et al.*, "Search for supersymmetry in pp collisions at $\sqrt{s}$=8 TeV in events with a single lepton, large jet multiplicity, and multiple b jets," *Phys.Lett.* **B733** (2014) 328–353, arXiv:1311.4937 [hep-ex].

[310] **CMS** Collaboration, V. Khachatryan *et al.*, "Searches for electroweak production of charginos, neutralinos, and sleptons decaying to leptons and W, Z, and Higgs bosons in pp collisions at 8 TeV," *Eur.Phys.J.* **C74** no. 9, (2014) 3036, arXiv:1405.7570 [hep-ex].

[311] **ATLAS** Collaboration, G. Aad *et al.*, "Search for the direct production of charginos, neutralinos and staus in final states with at least two hadronically decaying taus and missing transverse momentum in pp collisions at $\sqrt{s}$ = 8 TeV with the ATLAS detector," *JHEP* **1410** (2014) 96, arXiv:1407.0350 [hep-ex].

[312] **ATLAS** Collaboration, G. Aad *et al.*, "Search for new particles in events with one lepton and missing transverse momentum in pp collisions at $\sqrt{s}$ = 8 TeV with the ATLAS detector," *JHEP* **1409** (2014) 037, arXiv:1407.7494 [hep-ex].

[313] **CMS** Collaboration, V. Khachatryan *et al.*, "Search for physics beyond the standard model in final states with a lepton and missing transverse energy in proton-proton collisions at sqrt(s) = 8 TeV," *Phys. Rev.* **D91** no. 9, (2015) 092005, arXiv:1408.2745 [hep-ex].

[314] **XENON1T** Collaboration, E. Aprile, "The XENON1T Dark Matter Search Experiment," arXiv:1206.6288 [astro-ph.IM].

[315] J. Billard, L. Strigari, and E. Figueroa-Feliciano, "Implication of neutrino backgrounds on the reach of next generation dark matter direct detection experiments," *Phys.Rev.* **D89** (2014) 023524, arXiv:1307.5458 [hep-ph].

[316] **CMS** Collaboration, S. Chatrchyan *et al.*, "Searches for long-lived charged particles in pp collisions at $\sqrt{s}$=7 and 8 TeV," *JHEP* **1307** (2013) 122, arXiv:1305.0491 [hep-ex].

[317] **ATLAS** Collaboration, G. Aad *et al.*, "Searches for heavy long-lived charged particles with the ATLAS detector in proton-proton collisions at $\sqrt{s} = 8$ TeV," *JHEP* **1501** (2015) 068, arXiv:1411.6795 [hep-ex].

[318] **ATLAS** Collaboration, G. Aad *et al.*, "Search for long-lived stopped R-hadrons decaying out-of-time with pp collisions using the ATLAS detector," *Phys.Rev.* **D88** no. 11, (2013) 112003, arXiv:1310.6584 [hep-ex].

[319] **ATLAS** Collaboration, "Limits on metastable gluinos from ATLAS SUSY searches at 8 TeV," Tech. Rep. ATLAS-CONF-2014-037, CERN, Geneva, Jul, 2014.

[320] A. Arvanitaki, C. Davis, P. W. Graham, A. Pierce, and J. G. Wacker, "Limits on split supersymmetry from gluino cosmology," *Phys.Rev.* **D72** (2005) 075011, arXiv:hep-ph/0504210 [hep-ph].

[321] **CMS** Collaboration, "Search for dark matter in the mono-lepton channel with pp collision events at center-of-mass energy of 8 TeV ," Tech. Rep. CMS-PAS-EXO-13-004, CERN, Geneva, 2013. https://cds.cern.ch/record/1563245.

[322] M. Hirsch, W. Porod, L. Reichert, and F. Staub, "Phenomenology of the minimal supersymmetric $U(1)_{B-L} \times U(1)_R$ extension of the standard model," *Phys. Rev.* **D86** (2012) 093018, arXiv:1206.3516 [hep-ph].

[323] J. Camargo-Molina, B. O'Leary, W. Porod, and F. Staub, "The Stability Of R-Parity In Supersymmetric Models Extended By $U(1)_{B-L}$," *Phys. Rev.* **D88** (2013) 015033, arXiv:1212.4146 [hep-ph].

[324] S. Di Chiara, V. Keus, and O. Lebedev, "Stabilizing the Higgs potential with a Z′," *Phys. Lett.* **B744** (2015) 59–66, arXiv:1412.7036 [hep-ph].

[325] M. A. Ajaib, B. Dutta, T. Ghosh, I. Gogoladze, and Q. Shafi, "Neutralinos and sleptons at the LHC in light of muon $(g-2)_\mu$," *Phys. Rev.* **D92** no. 7, (2015) 075033, arXiv:1505.05896 [hep-ph].

[326] P. Bechtle, O. Brein, S. Heinemeyer, O. Stål, T. Stefaniak, *et al.*, "HiggsBounds $-$ 4: Improved Tests of Extended Higgs Sectors against Exclusion Bounds from LEP, the Tevatron and the LHC," *Eur. Phys. J.* **C74** (2014) 2693, arXiv:1311.0055 [hep-ph].

[327] P. Bechtle, S. Heinemeyer, O. Stål, T. Stefaniak, and G. Weiglein, "$HiggsSignals$: Confronting arbitrary Higgs sectors with measurements at the Tevatron and the LHC," *Eur. Phys. J.* **C74** (2014) 2711, arXiv:1305.1933 [hep-ph].

[328] U. Ellwanger and C. Hugonie, "NMHDECAY 2.0: An Updated program for sparticle masses, Higgs masses, couplings and decay widths in the NMSSM," *Comput. Phys. Commun.* **175** (2006) 290–303, arXiv:hep-ph/0508022 [hep-ph].

[329] **ATLAS** Collaboration, "Search for new high-mass resonances in the dilepton final state using proton-proton collisions at $\sqrt{s}$ = 13 TeV with the ATLAS detector," Tech. Rep. ATLAS-CONF-2016-045, CERN, Geneva, Aug, 2016. http://cds.cern.ch/record/2206127.

[330] E. Accomando, A. Belyaev, J. Fiaschi, K. Mimasu, S. Moretti, and C. Shepherd-Themistocleous, "Forward-backward asymmetry as a discovery tool for Z' bosons at the LHC," *JHEP* **01** (2016) 127, arXiv:1503.02672 [hep-ph].

[331] J. Gunion, L. Roszkowski, and H. Haber, "Z' mass limits, masses and coupling of higgs bosons, and Z' decays in an E_6 superstring based model," *Phys. Lett.* **B189** (1987) 409.

[332] T. Gherghetta, T. A. Kaeding, and G. L. Kane, "Supersymmetric contributions to the decay of an extra Z boson," *Phys. Rev.* **D57** (1998) 3178–3181, arXiv:hep-ph/9701343 [hep-ph].

[333] C.-F. Chang, K. Cheung, and T.-C. Yuan, "Supersymmetric Decays of the Z' Boson," *JHEP* **1109** (2011) 058, arXiv:1107.1133 [hep-ph].

[334] G. Corcella, "Phenomenology of supersymmetric Z' decays at the Large Hadron Collider," *Eur. Phys. J.* **C75** no. 6, (2015) 264, arXiv:1412.6831 [hep-ph].

[335] K. Babu, C. F. Kolda, and J. March-Russell, "Leptophobic U(1)'s and the R(b) - R(c) crisis," *Phys. Rev.* **D54** (1996) 4635–4647, arXiv:hep-ph/9603212 [hep-ph].

[336] **Particle Data Group** Collaboration, K. Olive *et al.*, "Review of Particle Physics," *Chin. Phys.* **C38** (2014) 090001.

[337] G. Belanger, M. Heikinheimo, and V. Sanz, "Model-Independent Bounds on Squarks from Monophoton Searches," *JHEP* **1208** (2012) 151, arXiv:1205.1463 [hep-ph].

[338] **ATLAS** Collaboration, G. Aad *et al.*, "Search for new phenomena in events with a photon and missing transverse momentum in pp collisions at $\sqrt{s} = 8$ TeV with the ATLAS detector," *Phys. Rev.* **D91** no. 1, (2015) 012008, arXiv:1411.1559 [hep-ex].

[339] G. Belanger, F. Boudjema, A. Pukhov, and A. Semenov, "micrOMEGAs4.1: two dark matter candidates," *Comput. Phys. Commun.* **192** (2015) 322–329, arXiv:1407.6129 [hep-ph].

[340] **D0** Collaboration, V. M. Abazov *et al.*, "Search for charged massive long-lived particles at $\sqrt{s} = 1.96$ TeV," *Phys. Rev.* **D87** no. 5, (2013) 052011, arXiv:1211.2466 [hep-ex].

[341] **CMS** Collaboration, V. Khachatryan *et al.*, "Constraints on the pMSSM, AMSB model and on other models from the search for long-lived charged particles in proton-proton collisions at sqrt(s) = 8 TeV," *Eur. Phys. J.* **C75** no. 7, (2015) 325, arXiv:1502.02522 [hep-ex].

[342] **LHCb** Collaboration, R. Aaij *et al.*, "Implications of LHCb measurements and future prospects," *Eur. Phys. J.* **C73** no. 4, (2013) 2373, arXiv:1208.3355 [hep-ex].

[343] N. Bernal, M. Losada, and F. Mahmoudi, "Flavour physics constraints in the BMSSM," *JHEP* **1107** (2011) 074, arXiv:1104.5395 [hep-ph].

[344] A. Arbey, M. Battaglia, F. Mahmoudi, and D. M. Santos, "Supersymmetry confronts $B_s \to \mu^+\mu^-$: Present and future status," *Phys. Rev.* **D87** (2013) 035026, arXiv:1212.4887 [hep-ph].

[345] **Particle Data Group** Collaboration, J. Beringer *et al.*, "Review of Particle Physics (RPP)," *Phys. Rev.* **D86** (2012) 010001.

[346] Heavy Flavor Averaging Group. http://www.slac.stanford.edu/xorg/hfag/rare/2013/radll/OUTPUT/HTML/radll_table7.html.

[347] Heavy Flavor Averaging Group. www.slac.stanford.edu/xorg/hfag/rare/2013/radll/btosg.pdf.

[348] **CMS, LHCb** Collaborations, V. Khachatryan *et al.*, "Observation of the rare $B^0_s \to \mu^+\mu^-$ decay from the combined analysis of CMS and LHCb data," *Nature* (2015) , arXiv:1411.4413 [hep-ex].

[349] Heavy Flavor Averaging Group. www.slac.stanford.edu/xorg/hfag/osc/PDG_2014/#DMS.

[350] Heavy Flavor Averaging Group. www.slac.stanford.edu/xorg/hfag/osc/PDG_2014/#DMD.

[351] T. Aoyama, M. Hayakawa, T. Kinoshita, and M. Nio, "Complete Tenth-Order QED Contribution to the Muon g-2," *Phys. Rev. Lett.* **109** (2012) 111808, arXiv:1205.5370 [hep-ph].

[352] L. J. Hall, K. Jedamzik, J. March-Russell, and S. M. West, "Freeze-In Production of FIMP Dark Matter," *JHEP* **1003** (2010) 080, arXiv:0911.1120 [hep-ph].

[353] X. Chu, T. Hambye, and M. H. Tytgat, "The Four Basic Ways of Creating Dark Matter Through a Portal," *JCAP* **1205** (2012) 034, arXiv:1112.0493 [hep-ph].

[354] F. Franke and S. Hesselbach, "Production of singlino dominated neutralinos in extended supersymmetric models," *Phys. Lett.* **B526** (2002) 370–378, arXiv:hep-ph/0111285 [hep-ph].

[355] D. Suematsu, "Singlino dominated LSP as CDM candidate in supersymmetric models with an extra U(1)," *Phys. Rev.* **D73** (2006) 035010, arXiv:hep-ph/0511299 [hep-ph].

[356] S. Nakamura and D. Suematsu, "Supersymmetric extra U(1) models with a singlino dominated LSP," *Phys. Rev.* **D75** (2007) 055004, arXiv:hep-ph/0609061 [hep-ph].

[357] **ATLAS, CDF, CMS, D0** Collaboration, "First combination of Tevatron and LHC measurements of the top-quark mass," arXiv:1403.4427 [hep-ex].

[358] L. J. Hall, D. Pinner, and J. T. Ruderman, "A Natural SUSY Higgs Near 126 GeV," *JHEP* **1204** (2012) 131, arXiv:1112.2703 [hep-ph].

[359] **CMS** Collaboration, "Search for New Physics in the Multijets and Missing Momentum Final State in Proton-Proton Collisions at 8 TeV,". http://cds.cern.ch/record/1563156. CMS-PAS-SUS-13-012.

[360] **CMS** Collaboration, "Search for supersymmetry in hadronic final states using M_{T2} with the CMS detector at sqrt(s) = 8 TeV,". http://cds.cern.ch/record/1646394. CMS-PAS-SUS-13-019.

[361] **ATLAS** Collaboration, "Search for strongly produced superpartners in final states with two same sign leptons with the ATLAS detector using 21 fb^{-1} of proton-proton collisions at $\sqrt{s}$ = 8 TeV,". http://cds.cern.ch/record/2002212. ATLAS-CONF-2013-007, ATLAS-COM-CONF-2013-006.

[362] **ATLAS** Collaboration, "Search for strong production of supersymmetric particles in final states with missing transverse momentum and at least three b-jets using 20.1 fb^{-1} of pp collisions at $\sqrt{s}$ = 8 TeV with the ATLAS Detector,". https://cds.cern.ch/record/1557778. ATLAS-CONF-2013-061, ATLAS-COM-CONF-2013-071.

[363] **CMS** Collaboration, "Search for supersymmetry in final states with missing transverse energy and 0, 1, 2, 3, or at least 4 b-quark jets in 8 TeV pp collisions using the variable α_T,". http://cds.cern.ch/record/1494483. CMS-PAS-SUS-12-028.

[364] **ATLAS** Collaboration. https://atlas.web.cern.ch/Atlas/GROUPS/PHYSICS/CONFNOTES/ATLAS-s$_\beta$CONF-s$_\beta$2013-s$_\beta$061/fig_12c.png.

[365] **CMS** Collaboration, V. Khachatryan *et al.*, "Search for supersymmetry using razor variables in events with b-tagged jets in pp collisions at $\sqrt{s} = 8$ TeV," *Phys. Rev.* **D91** (2015) 052018, arXiv:1502.00300 [hep-ex].

[366] **CMS** Collaboration, "Search for direct production of bottom squark pairs,". http://cds.cern.ch/record/1693164. CMS-PAS-SUS-13-018.

[367] **ATLAS** Collaboration, G. Aad *et al.*, "Search for direct third-generation squark pair production in final states with missing transverse momentum and two b-jets in $\sqrt{s} =$ 8 TeV pp collisions with the ATLAS detector," *JHEP* **1310** (2013) 189, arXiv:1308.2631 [hep-ex].

[368] G. Bélanger, F. Boudjema, C. Hugonie, A. Pukhov, and A. Semenov, "Relic density of dark matter in the NMSSM," *JCAP* **0509** (2005) 001, arXiv:hep-ph/0505142 [hep-ph].

[369] **ATLAS** Collaboration, "Search for long-lived charginos based on a disappearing-track signature in pp collisions at $\sqrt{s} = 13$ TeV with the ATLAS detector," Tech. Rep. ATLAS-CONF-2017-017, CERN, Geneva, Apr, 2017. https://cds.cern.ch/record/2258131.

[370] **CMS** Collaboration, "Search for new physics in events with two low momentum opposite-sign leptons and missing transverse energy at $\sqrt{s} = 13$ TeV," Tech. Rep. CMS-PAS-SUS-16-048, CERN, Geneva, 2017. https://cds.cern.ch/record/2256640.

[371] **CMS** Collaboration, "Measurements of properties of the Higgs boson in the diphoton decay channel with the full 2016 data set," Tech. Rep. CMS-PAS-HIG-16-040, CERN, Geneva, 2017. http://cds.cern.ch/record/2264515.

[372] **ATLAS** Collaboration, "Measurement of fiducial, differential and production cross sections in the $H \to \gamma\gamma$ decay channel with 13.3 fb^{-1} of 13 TeV proton-proton collision data with the ATLAS detector," Tech. Rep. ATLAS-CONF-2016-067, CERN, Geneva, Aug, 2016. http://cds.cern.ch/record/2206210.

[373] **CMS** Collaboration, S. Chatrchyan *et al.*, "Search for invisible decays of Higgs bosons in the vector boson fusion and associated ZH production modes," *Eur. Phys. J.* **C74** (2014) 2980, arXiv:1404.1344 [hep-ex].

[374] **ATLAS** Collaboration, "Search for an Invisibly Decaying Higgs Boson Produced via Vector Boson Fusion in pp Collisions at $\sqrt{s} = 8$ TeV using the ATLAS Detector at the LHC,". http://cds.cern.ch/record/2002121. ATLAS-CONF-2015-004, ATLAS-COM-CONF-2015-004.

[375] J. Bernon, B. Dumont, and S. Kraml, "Status of Higgs couplings after run 1 of the LHC," *Phys. Rev.* **D90** (2014) 071301, arXiv:1409.1588 [hep-ph].

[376] D. Ghosh, R. Godbole, M. Guchait, K. Mohan, and D. Sengupta, "Looking for an Invisible Higgs Signal at the LHC," *Phys. Lett.* **B725** (2013) 344–351, arXiv:1211.7015 [hep-ph].

[377] A. Djouadi, L. Maiani, A. Polosa, J. Quevillon, and V. Riquer, "Fully covering the MSSM Higgs sector at the LHC," *JHEP* **06** (2015) 168, arXiv:1502.05653 [hep-ph].

[378] M. Bisset, J. Li, N. Kersting, R. Lu, F. Moortgat, *et al.*, "Four-lepton LHC events from MSSM Higgs boson decays into neutralino and chargino pairs," *JHEP* **0908** (2009) 037, arXiv:0709.1029 [hep-ph].

[379] A. J. Williams, C. Boehm, S. M. West, and D. A. Vasquez, "Regenerating WIMPs in the Light of Direct and Indirect Detection," *Phys. Rev.* **D86** (2012) 055018, arXiv:1204.3727 [hep-ph].

[380] T. Cohen, M. Lisanti, A. Pierce, and T. R. Slatyer, "Wino Dark Matter Under Siege," *JCAP* **1310** (2013) 061, arXiv:1307.4082.

[381] G. Belanger, C. Boehm, M. Cirelli, J. Da Silva, and A. Pukhov, "PAMELA and FERMI-LAT limits on the neutralino-chargino mass degeneracy," *JCAP* **1211** (2012) 028, arXiv:1208.5009 [hep-ph].

[382] M. L. Graesser and J. Shelton, "Hunting Mixed Top Squark Decays," *Phys. Rev. Lett.* **111** no. 12, (2013) 121802, arXiv:1212.4495 [hep-ph].

[383] **CMS** Collaboration, "Search for a neutral MSSM Higgs boson decaying into $\tau\tau$ with 12.9 fb^{-1} of data at $\sqrt{s} = 13$ TeV," Tech. Rep. CMS-PAS-HIG-16-037, CERN, Geneva, 2016. https://cds.cern.ch/record/2231507.

[384] **ATLAS** Collaboration, "Search for new phenomena in $t\bar{t}$ final states with additional heavy-flavour jets in pp collisions at $\sqrt{s} = 13$ TeV with the ATLAS detector," Tech. Rep. ATLAS-CONF-2016-104, CERN, Geneva, Sep, 2016. http://cds.cern.ch/record/2220371.

[385] **ATLAS** Collaboration, "Search for Minimal Supersymmetric Standard Model Higgs Bosons H/A in the $\tau\tau$ final state in up to 13.3 fb-1 of pp collisions at $\sqrt{s}$= 13 TeV with the ATLAS Detector," Tech. Rep. ATLAS-CONF-2016-085, CERN, Geneva, Aug, 2016. http://cds.cern.ch/record/2206278.

[386] S. Kraml, U. Laa, K. Mawatari, and K. Yamashita, "Simplified dark matter models with a spin-2 mediator at the LHC," *Eur. Phys. J.* **C77** no. 5, (2017) 326, arXiv:1701.07008 [hep-ph].

[387] H. An, L.-T. Wang, and H. Zhang, "Dark matter with t-channel mediator: a simple step beyond contact interaction," *Phys. Rev.* **D89** no. 11, (2014) 115014, arXiv:1308.0592 [hep-ph].

[388] G. Busoni, A. De Simone, J. Gramling, E. Morgante, and A. Riotto, "On the Validity of the Effective Field Theory for Dark Matter Searches at the LHC, Part II: Complete Analysis for the s-channel," *JCAP* **1406** (2014) 060, arXiv:1402.1275 [hep-ph].

[389] G. Busoni, A. De Simone, T. Jacques, E. Morgante, and A. Riotto, "Making the Most of the Relic Density for Dark Matter Searches at the LHC 14 TeV Run," *JCAP* **1503** no. 03, (2015) 022, arXiv:1410.7409 [hep-ph].

[390] O. Buchmueller, M. J. Dolan, and C. McCabe, "Beyond Effective Field Theory for Dark Matter Searches at the LHC," *JHEP* **01** (2014) 025, arXiv:1308.6799 [hep-ph].

[391] J. Abdallah *et al.*, "Simplified Models for Dark Matter Searches at the LHC," *Phys. Dark Univ.* **9-10** (2015) 8–23, arXiv:1506.03116 [hep-ph].

[392] D. Abercrombie, N. Akchurin, E. Akilli, J. A. Maestre, B. Allen, *et al.*, "Dark Matter Benchmark Models for Early LHC Run-2 Searches: Report of the ATLAS/CMS Dark Matter Forum," arXiv:1507.00966 [hep-ex].

[393] C. Arina *et al.*, "A comprehensive approach to dark matter studies: exploration of simplified top-philic models," *JHEP* **11** (2016) 111, arXiv:1605.09242 [hep-ph].

[394] S. Banerjee, D. Barducci, G. Bélanger, B. Fuks, A. Goudelis, and B. Zaldivar, "Cornering pseudoscalar-mediated dark matter with the LHC and cosmology," arXiv:1705.02327 [hep-ph].

[395] N. F. Bell, G. Busoni, and I. W. Sanderson, "Self-consistent Dark Matter Simplified Models with an s-channel scalar mediator," *JCAP* **1703** no. 03, (2017) 015, arXiv:1612.03475 [hep-ph].

[396] M. Bauer, U. Haisch, and F. Kahlhoefer, "Simplified dark matter models with two Higgs doublets: I. Pseudoscalar mediators," *JHEP* **05** (2017) 1–, arXiv:1701.07427 [hep-ph].

[397] N. F. Bell, Y. Cai, and R. K. Leane, "Impact of mass generation for spin-1 mediator simplified models," *JCAP* **1701** no. 01, (2017) 039, arXiv:1610.03063 [hep-ph].

[398] Y. Cui and F. D'Eramo, "On the Completeness of Vector Portal Theories: New Insights into the Dark Sector and its Interplay with Higgs Physics," arXiv:1705.03897 [hep-ph].

[399] M. Carena, A. Daleo, B. A. Dobrescu, and T. M. P. Tait, "Z' gauge bosons at the Tevatron," *Phys. Rev.* **D70** (2004) 093009, arXiv:hep-ph/0408098 [hep-ph].

[400] A. Albert *et al.*, "Recommendations of the LHC Dark Matter Working Group: Comparing LHC searches for heavy mediators of dark matter production in visible and invisible decay channels," arXiv:1703.05703 [hep-ex].

[401] https://twiki.cern.ch/twiki/bin/view/AtlasPublic/ ExoticsPublicResults.

[402] **CMS** Collaboration, A. M. Sirunyan *et al.*, "Search for dark matter produced with an energetic jet or a hadronically decaying W or Z boson at $\sqrt{s}$ = 13 TeV," arXiv:1703.01651 [hep-ex].

[403] O. Mattelaer and E. Vryonidou, "Dark matter production through loop-induced processes at the LHC: the s-channel mediator case," *Eur. Phys. J.* **C75** no. 9, (2015) 436, arXiv:1508.00564 [hep-ph].

[404] M. Backovic, M. Kraemer, F. Maltoni, A. Martini, K. Mawatari, and M. Pellen, "Higher-order QCD predictions for dark matter production at the LHC in simplified models with s-channel mediators," *Eur. Phys. J.* **C75** no. 10, (2015) 482, arXiv:1508.05327 [hep-ph].

[405] M. Neubert, J. Wang, and C. Zhang, "Higher-Order QCD Predictions for Dark Matter Production in Mono-Z Searches at the LHC," *JHEP* **02** (2016) 082, arXiv:1509.05785 [hep-ph].

[406] G. Belanger, F. Boudjema, A. Pukhov, and A. Semenov, "MicrOMEGAs 2.0: A Program to calculate the relic density of dark matter in a generic model," *Comput. Phys. Commun.* **176** (2007) 367–382, arXiv:hep-ph/0607059 [hep-ph].

[407] H. M. Lee, M. Park, and V. Sanz, "Gravity-mediated (or Composite) Dark Matter Confronts Astrophysical Data," *JHEP* **05** (2014) 063, arXiv:1401.5301 [hep-ph].

[408] C. Garcia-Cely and J. Heeck, "Indirect searches of dark matter via polynomial spectral features," *JCAP* **1608** (2016) 023, arXiv:1605.08049 [hep-ph].

[409] J. Ellis, R. Fok, D. S. Hwang, V. Sanz, and T. You, "Distinguishing 'Higgs' spin hypotheses using $\gamma\gamma$ and WW^* decays," *Eur. Phys. J.* **C73** (2013) 2488, arXiv:1210.5229 [hep-ph].

[410] C. Englert, D. Goncalves-Netto, K. Mawatari, and T. Plehn, "Higgs Quantum Numbers in Weak Boson Fusion," *JHEP* **1301** (2013) 148, arXiv:1212.0843 [hep-ph].

[411] G. Das, C. Degrande, V. Hirschi, F. Maltoni, and H.-S. Shao, "NLO predictions for the production of a spin-two particle at the LHC," *Phys. Lett.* **B770** (2017) 507–513, arXiv:1605.09359 [hep-ph].

[412] K. Agashe, H. Davoudiasl, G. Perez, and A. Soni, "Warped Gravitons at the LHC and Beyond," *Phys. Rev.* **D76** (2007) 036006, arXiv:hep-ph/0701186 [hep-ph].

[413] A. L. Fitzpatrick, J. Kaplan, L. Randall, and L.-T. Wang, "Searching for the Kaluza-Klein Graviton in Bulk RS Models," *JHEP* **09** (2007) 013, arXiv:hep-ph/0701150 [hep-ph].

[414] C. Degrande, "Automatic evaluation of UV and R2 terms for beyond the Standard Model Lagrangians: a proof-of-principle," *Comput. Phys. Commun.* **197** (2015) 239–262, arXiv:1406.3030 [hep-ph].

[415] K. Hagiwara, J. Kanzaki, Q. Li, and K. Mawatari, "HELAS and MadGraph/MadEvent with spin-2 particles," *Eur.Phys.J.* **C56** (2008) 435–447, arXiv:0805.2554 [hep-ph].

[416] P. de Aquino, K. Hagiwara, Q. Li, and F. Maltoni, "Simulating graviton production at hadron colliders," *JHEP* **06** (2011) 132, arXiv:1101.5499 [hep-ph].

[417] P. Artoisenet, P. de Aquino, F. Demartin, R. Frederix, S. Frixione, *et al.*, "A framework for Higgs characterisation," *JHEP* **1311** (2013) 043, arXiv:1306.6464 [hep-ph].

[418] http://feynrules.irmp.ucl.ac.be/wiki/DMsimp.

[419] J. Alwall, C. Duhr, B. Fuks, O. Mattelaer, D. G. Özturk, and C.-H. Shen, "Computing decay rates for new physics theories with FeynRules and MadGraph5_aMC@NLO," *Comput. Phys. Commun.* **197** (2015) 312–323, arXiv:1402.1178 [hep-ph].

[420] B. C. Allanach, K. Odagiri, M. J. Palmer, M. A. Parker, A. Sabetfakhri, and B. R. Webber, "Exploring small extra dimensions at the large hadron collider," *JHEP* **12** (2002) 039, arXiv:hep-ph/0211205 [hep-ph].

[421] R. D. Ball, V. Bertone, S. Carrazza, C. S. Deans, L. Del Debbio, *et al.*, "Parton distributions with LHC data," *Nucl.Phys.* **B867** (2013) 244–289, arXiv:1207.1303 [hep-ph].

[422] D. Abercrombie *et al.*, "Dark Matter Benchmark Models for Early LHC Run-2 Searches: Report of the ATLAS/CMS Dark Matter Forum," arXiv:1507.00966 [hep-ex].

[423] U. Haisch, F. Kahlhoefer, and E. Re, "QCD effects in mono-jet searches for dark matter," *JHEP* **1312** (2013) 007, arXiv:1310.4491 [hep-ph].

[424] O. Buchmueller, S. A. Malik, C. McCabe, and B. Penning, "Constraining Dark Matter Interactions with Pseudoscalar and Scalar Mediators Using Collider Searches for Multijets plus Missing Transverse Energy," *Phys. Rev. Lett.* **115** no. 18, (2015) 181802, arXiv:1505.07826 [hep-ph].

[425] **ATLAS** Collaboration, M. Aaboud *et al.*, "Search for new phenomena in final states with an energetic jet and large missing transverse momentum in pp collisions at $\sqrt{s} = 13$ TeV using the ATLAS detector," *Phys. Rev.* **D94** no. 3, (2016) 032005, arXiv:1604.07773 [hep-ex].

[426] **ATLAS** Collaboration, M. Aaboud *et al.*, "Search for squarks and gluinos in final states with jets and missing transverse momentum at $\sqrt{s} = 13$ TeV with the ATLAS detector," *Eur. Phys. J.* **C76** no. 7, (2016) 392, arXiv:1605.03814 [hep-ex].

[427] D. Sengupta, "Madanalysis5 implementation of the ATLAS monojet and missing transverse momentum search documented in arXiv: 1604.07773." http://doi.org/10.7484/INSPIREHEP.DATA.GTH3.RN26, 2016-07-19.

[428] B. Fuks, S. Banerjee, and B. Zaldivar, "MadAnalysis5 implementation of the multijet analysis of ATLAS (arXiv:1605.03814)." http://doi.org/10.7484/INSPIREHEP.DATA.GTF5.RN03, 2017-01-25.

[429] **CMS** Collaboration, "Search for dark matter and graviton produced in association with a photon in pp collisions at $\sqrt{s} = 13$ TeV with an integrated luminosity of $12.9\ \mathrm{fb}^{-1}$," Tech. Rep. CMS-PAS-EXO-16-039, CERN, Geneva, 2016. https://cds.cern.ch/record/2205148.

[430] **ATLAS** Collaboration, "Search for New Phenomena in Dijet Events with the ATLAS Detector at $\sqrt{s}$=13 TeV with 2015 and 2016 data," Tech. Rep. ATLAS-CONF-2016-069, CERN, Geneva, Aug, 2016. http://cds.cern.ch/record/2206212.

[431] **ATLAS** Collaboration, "Search for diboson resonance production in the $l\nu qq$ final state using pp collisions at $\sqrt{s} = 13$ TeV with the ATLAS detector at the LHC," Tech. Rep. ATLAS-CONF-2016-062, CERN, Geneva, Aug, 2016. http://cds.cern.ch/record/2206199.

[432] **ATLAS** Collaboration, "Search for resonances in the mass distribution of jet pairs with one or two jets identified as b-jets with the ATLAS detector with 2015 and 2016 data," Tech. Rep. ATLAS-CONF-2016-060, CERN, Geneva, Aug, 2016. http://cds.cern.ch/record/2206175.

[433] **CMS** Collaboration, "Search for $t\bar{t}$ resonances in boosted semileptonic final states in pp collisions at $\sqrt{s} = 13$ TeV," Tech. Rep. CMS-PAS-B2G-15-002, CERN, Geneva, 2016. http://cds.cern.ch/record/2138345.

[434] **ATLAS** Collaboration, "Searches for heavy ZZ and ZW resonances in the $llqq$ and $\nu\nu qq$ final states in pp collisions at $\sqrt{s} = 13$ TeV with the ATLAS detector," Tech. Rep. ATLAS-CONF-2016-082, CERN, Geneva, Aug, 2016. http://cds.cern.ch/record/2206275.

[435] **CMS** Collaboration, V. Khachatryan *et al.*, "Search for high-mass diphoton resonances in proton-proton collisions at 13 TeV and combination with 8 TeV search," *Phys. Lett.* **B767** (2017) 147–170, arXiv:1609.02507 [hep-ex].

[436] **ATLAS** Collaboration, "Search for pair production of Higgs bosons in the $b\bar{b}b\bar{b}$ final state using proton−proton collisions at $\sqrt{s} = 13$ TeV with the ATLAS detector," Tech. Rep. ATLAS-CONF-2016-049, CERN, Geneva, Aug, 2016. http://cds.cern.ch/record/2206131.

[437] **ATLAS** Collaboration, G. Aad *et al.*, "Search for Scalar Diphoton Resonances in the Mass Range $65 - 600$ GeV with the ATLAS Detector in pp Collision Data at $\sqrt{s}$ = 8 TeV," *Phys. Rev. Lett.* **113** no. 17, (2014) 171801, arXiv:1407.6583 [hep-ex].

[438] https://hepdata.net/record/ins1307756.

[439] **CMS** Collaboration, V. Khachatryan *et al.*, "Search for diphoton resonances in the mass range from 150 to 850 GeV in pp collisions at $\sqrt{s} = 8$ TeV," *Phys. Lett.* **B750** (2015) 494–519, arXiv:1506.02301 [hep-ex].

[440] **ATLAS** Collaboration, G. Aad *et al.*, "Combination of searches for WW, WZ, and ZZ resonances in pp collisions at $\sqrt{s} = 8$ TeV with the ATLAS detector," *Phys. Lett.* **B755** (2016) 285–305, arXiv:1512.05099 [hep-ex].

[441] M. Chala, F. Kahlhoefer, M. McCullough, G. Nardini, and K. Schmidt-Hoberg, "Constraining Dark Sectors with Monojets and Dijets," *JHEP* **07** (2015) 089, arXiv:1503.05916 [hep-ph].

[442] **CMS** Collaboration, A. M. Sirunyan *et al.*, "Search for dijet resonances in proton-proton collisions at $\sqrt{s} = 13$ TeV and constraints on dark matter and other models," *Phys. Lett.* **B769** (2017) 520–542, arXiv:1611.03568 [hep-ex].

[443] **CMS** Collaboration, "Search for massive resonances decaying into pairs of boosted W and Z bosons at $\sqrt{s}$ = 13 TeV," Tech. Rep. CMS-PAS-EXO-15-002, CERN, Geneva, 2015. https://cds.cern.ch/record/2117062.

[444] **CMS** Collaboration, "Search for a high-mass resonance decaying into a dilepton final state in 13 fb^{-1} of pp collisions at $\sqrt{s} = 13$ TeV," Tech. Rep. CMS-PAS-EXO-16-031, CERN, Geneva, 2016. https://cds.cern.ch/record/2205764.

[445] **CMS** Collaboration, V. Khachatryan *et al.*, "Search for heavy resonances decaying to tau lepton pairs in proton-proton collisions at $\sqrt{s} = 13$ TeV," *JHEP* **02** (2017) 048, arXiv:1611.06594 [hep-ex].

[446] E. Conte, B. Fuks, and G. Serret, "MadAnalysis 5, A User-Friendly Framework for Collider Phenomenology," *Comput.Phys.Commun.* **184** (2013) 222–256, arXiv:1206.1599 [hep-ph].

[447] E. Alvarez, L. Da Rold, J. Mazzitelli, and A. Szynkman, "Graviton resonance phenomenology and a pNGB Higgs at the LHC," arXiv:1610.08451 [hep-ph].

[448] S. Moretti, D. O'Brien, L. Panizzi, and H. Prager, "Production of extra quarks decaying to Dark Matter beyond the Narrow Width Approximation at the LHC," arXiv:1705.07675 [hep-ph].

[449] **CMS Collaboration** Collaboration, "Supersymmetry discovery potential in future LHC and HL-LHC running with the CMS detector," Tech. Rep. CMS-PAS-SUS-14-012, CERN, Geneva, 2015. http://cds.cern.ch/record/1981344.

[450] S. Kraml, B. Allanach, M. Mangano, H. Prosper, S. Sekmen, *et al.*, "Searches for New Physics: Les Houches Recommendations for the Presentation of LHC Results," *Eur.Phys.J.* **C72** (2012) 1976, arXiv:1203.2489 [hep-ph].

[451] https://twiki.cern.ch/twiki/bin/view/LHCPhysics/InterpretingLHCresults.

[452] G. Brooijmans *et al.*, "Les Houches 2015: Physics at TeV colliders - new physics working group report," in *9th Les Houches Workshop on Physics at TeV Colliders (PhysTeV 2015) Les Houches, France, June 1-19, 2015*. 2016. arXiv:1605.02684 [hep-ph]. http://inspirehep.net/record/1456803/files/arXiv:1605.02684.pdf.

[453] P. Bechtle *et al.*, "Killing the cMSSM softly," *Eur. Phys. J.* **C76** no. 2, (2016) 96, arXiv:1508.05951 [hep-ph].

[454] K. J. de Vries *et al.*, "The pMSSM10 after LHC Run 1," *Eur. Phys. J.* **C75** no. 9, (2015) 422, arXiv:1504.03260 [hep-ph].

[455] E. A. Bagnaschi *et al.*, "Supersymmetric Dark Matter after LHC Run 1," *Eur. Phys. J.* **C75** (2015) 500, arXiv:1508.01173 [hep-ph].

[456] **GAMBIT** Collaboration, P. Athron *et al.*, "Global fits of GUT-scale SUSY models with GAMBIT," arXiv:1705.07935 [hep-ph].

[457] **GAMBIT** Collaboration, P. Athron *et al.*, "A global fit of the MSSM with GAMBIT," arXiv:1705.07917 [hep-ph].

[458] **GAMBIT** Collaboration, P. Athron *et al.*, "GAMBIT: The Global and Modular Beyond-the-Standard-Model Inference Tool," arXiv:1705.07908 [hep-ph].

[459] T. Junk, "Confidence level computation for combining searches with small statistics," *Nucl. Instrum. Meth.* **A434** (1999) 435–443, arXiv:hep-ex/9902006 [hep-ex].

[460] A. L. Read, "Presentation of search results: The CL(s) technique," *J.Phys.* **G28** (2002) 2693–2704.

Abstract The recent discovery of the Higgs boson completes the standard model of particle physics, but no compelling signal for physics beyond the standard model has been observed despite the numerous searches performed by experiments at the Large Hadron Collider (LHC). Nevertheless, the hierarchy problem and the observation of dark matter are compelling arguments to study theories predicting new states at the weak scale, and a main effort has been directed towards understanding the negative search results and their implications for such weak scale new physics scenarios. Simplified models have become a standard in the interpretation of LHC searches for supersymmetry (SUSY), aiming at maximal model independence. More recently a similar approach was adopted for the interpretation of dark matter searches. The success of this approach is due to the fact that the small set of free parameters relates to the observables in LHC searches in a clear way, allowing an efficient optimisation of search strategies. Moreover, generic models can be projected on a simplified model description giving an intuitive understanding of the constraints on the parameter space, and providing a fast test against LHC constraints. As the relation between generic model parameters and simplified models is generally not straightforward, sophisticated computational tools are required to facilitate such a projection.
This thesis explores the various aspects of simplified model interpretations of LHC searches and how they can be used to understand the results and bridge the gap between theoretical descriptions and experimental observations. In particular the software tool SModelS is presented, a tool that automates the mapping of generic models onto SUSY-like simplified model components, and that allows direct tests against corresponding experimental limits in the included database. Under certain assumptions SModelS can be used to constrain a wide class of new physics models with a dark matter candidate. These assumptions and some explicit tests are discussed in detail, followed by studies of (non-minimal) supersymmetric models using SModelS for the fast evaluation of constraints from SUSY searches. These studies highlight the capacity as well as the limitations of using simplified model results to study generic models. Finally regarding simplified models for dark matter searches, scenarios with a spin-2 mediator are studied in detail.

Résumé La découverte récente du boson de Higgs complète le Modèle Standard de la physique des particules, mais aucun signal de nouvelle physique n'a été observé en dépit des nombreuses recherches effectuées par les expériences du Large Hadron Collider (LHC). Cependant le problème de hiérarchie et la présence de matière noire sont des motivations importantes pour considérer des théories qui prédisent de nouveaux états à l'échelle électro-faible, de fait, de nombreux travaux ont été initiés sur l'interprétation des résultats négatifs et leurs implications pour de tels scénarios. Les modèles simplifiés sont devenus une norme pour l'interprétation des recherches de supersymétrie (SUSY) au LHC, et plus récemment pour les recherches de matière noire. Le succès de cette approche vient d'un petit nombre de paramètres liés aux observables au LHC de façon claire, ce qui permet une optimisation efficace des stratégies de recherche. De plus, les modèles complets peuvent être projetés sur de tels modèles simplifiés ce qui permet une compréhension intuitive des contraintes sur l'espace des paramètres et un test rapide des contraintes du LHC. Puisque les relations entre les paramètres de modèles généraux et les modèles simplifiés ne sont pas en général directes, des outils numériques sophistiqués sont nécessaires pour faciliter cette projection.
Cette thèse explore de nombreux aspects de l'interprétation des recherches du LHC par les modèles simplifiés et de la façon dont ils sont utilisés pour faire le lien entre les observations expérimentales et les descriptions théoriques. En particulier le code SModelS est présenté, il permet la décomposition automatique de modèles généraux en modèles simplifiés inspirés par la SUSY, et de les tester aux contraintes expérimentales incluses dans une base de données. Sous certaines hypothèses SModelS peut être utilisé pour contraindre une grande classe de modèles comprenant un candidat à la matière noire. Ces hypothèses sont discutées en détail et des études de modèles supersymétriques (non-minimaux) utilisant SModelS pour l'évaluation rapide des contraintes expérimentales sont présentées. Ces études soulignent les avantages ainsi que les limitations de l'utilisation de modèles simplifiés. Finalement, concernant les modèles simplifiés pour la recherche de matière noire, des scénarios avec un médiateur de spin-2 sont étudiés en détail.